AGARD-CP-292

AGARD-CP-292

AGARD

ADVISORY GROUP FOR AEROSPACE RESEARCH & DEVELOPMENT

7 RUE ANCELLE 92200 NEUILLY SUR SEINE FRANCE

AGARD CONFERENCE PROCEEDINGS No. 292

Guidance and Control Aspects of Tactical Air-launched Missiles

NORTH ATLANTIC TREATY ORGANIZATION

DISTRIBUTION AND AVAILABILITY
ON BACK COVER

NORTH ATLANTIC TREATY ORGANIZATION

ADVISORY GROUP FOR AEROSPACE RESEARCH AND DEVELOPMENT

(ORGANISATION DU TRAITE DE L'ATLANTIQUE NORD)

AGARD Conference Proceedings No.292

GUIDANCE AND CONTROL ASPECTS OF TACTICAL AIR-LAUNCHED MISSILES

Papers presented at the Guidance and Control Panel Symposium held at Eglin Air Force Base, Florida, USA - 6,9 May 1980.

THE MISSION OF AGARD

The mission of AGARD is to bring together the leading personalities of the NATO nations in the fields of science and technology relating to aerospace for the following purposes:

- Exchanging of scientific and technical information;
- Continuously stimulating advances in the aerospace sciences relevant to strengthening the common defence posture;
- Improving the co-operation among member nations in aerospace research and development;
- Providing scientific and technical advice and assistance to the North Atlantic Military Committee in the field of aerospace research and development;
- Rendering scientific and technical assistance, as requested, to other NATO bodies and to member nations in connection with research and development problems in the aerospace field;
- Providing assistance to member nations for the purpose of increasing their scientific and technical potential;
- Recommending effective ways for the member nations to use their research and development capabilities for the common benefit of the NATO community.

The highest authority within AGARD is the National Delegates Board consisting of officially appointed senior representatives from each member nation. The mission of AGARD is carried out through the Panels which are composed of experts appointed by the National Delegates, the Consultant and Exchange Programme and the Aerospace Applications Studies Programme. The results of AGARD work are reported to the member nations and the NATO Authorities through the AGARD series of publications of which this is one.

Participation in AGARD activities is by invitation only and is normally limited to citizens of the NATO nations.

Published October 1980

ISBN 92-835-1370-3

Printed by Technical Editing and Reproduction Ltd
Harford House, 7–9 Charlotte St, London, W1P 1HD

THEME

In 1973, the 16th Guidance and Control Panel Symposium on Precision Delivery Systems was held at Eglin Air Force Base, Florida. USA. Many important advances in guidance sensor technology, control system implementation and overall missile design have taken place since that time.

It was timely, therefore, to hold a symposium in 1980 on Tactical Air-Launched Guided Weapons. The symposium treated both air-to-air and air-to-surface missile systems with emphasis on guidance and control technology and its impact over the recent years.

GUIDANCE AND CONTROL PANEL OFFICERS

Panel Chairman:	Mr P.Kant, Ne
Panel Deputy Chairman:	Mr G.C.Howell, UK
Panel Executive:	Colonel J.C. de Chassey, FAF

PROGRAMME COMMITTEE FOR THE 30th GCP SYMPOSIUM

Chairman:	Dr O.C.Williams, Jr, US
Members:	Ing. Principal B.Vandecasteele, Fr Ing. U.Krogmann, Ge Mr G.C.Howell, UK Mr M.A.Ostgaard, US

HOST COORDINATOR

Major L.A.Ankeney, USAF

CONTENTS

* Not available at time of printing.

† Published in CP-292 Supplement (Classified).

† Published in CP-292 Supplement (Classified).

PRECISION FIRE CONTROL FOR SEMIACTIVE TERMINAL HOMING MISSILES

Dr. J. B. Huff
Director, Guidance and Control

and

J. L. Baumann
Research Engineer
US Army Missile Command
Redstone Arsenal, AL 35809

SUMMARY

Since the inception of the laser semiactive terminal homing concept in the early 1960's, much subsystem and system hardware development was required to make the idea feasible for laser guided antitank missiles. Most of the effort was concentrated in the development of "low cost" seekers, reliable laser designators, and test programs to validate the feasibility and accuracy of the concept. In the mid 1960's the US Air Force demonstrated the capability of this combination for bombing with surgical precision which made prime time news in the latter days of the Vietnam War. Since that time, much Tri-Service effort has been concentrated on the development of systems for semiactive laser terminal guidance for armored point targets. This paper concentrates primarily on the US Army Missile Command's technology base for development of the precision pointing and tracking or fire control for laser guidance. General requirements are transformed into specific design parameters for target acquisition and designation; technology hardware and performance are described.

A new target designation performance evaluation method, developed out of a specific need to handle large quantities of data, is discussed.

INTRODUCTION

The fire control for laser semiactive guidance encompasses all the functions required to find targets, track targets, precisely point the laser designator at the target prior to and during missile flight, and to assess the damage following target engagement.

Target acquisition capability is highly dependent on target, scene, atmospheric, and system characteristics. Primary targets under consideration are hard armor, tank-type targets which could be situated in a highly cluttered environment. This type of target will offer a low target to background contrast signature. Also, target engagement could occur during limited atmospheric visibility caused by haze, fog, or obscurants which might be introduced in a typical battlefield environment. Engagement could occur either during day or night time. The problem is compounded by the fact that this engagement will take place from a helicopter flying low altitude nap-of-earth. Low altitude target acquisition introduces its own peculiar set of problems in that the sensor viewing longitudinal footprint tends to infinity, and all the target and scene information is compressed in the display in the vertical direction. The small size target, the low target-to-background signature, the high atmospheric attenuation, and low altitude viewing angle all tend to make target detection a very difficult task.

Target designation performance is more system dependent than acquisition. A measure of designation performance is the ability to point and maintain a laser spot on a vulnerable predetermined target hit point to insure maximum kill probability. The pointing precision of a narrow laser beam is dependent on how well the operator can perceive the desired target hit point, the viewing sensors apparent magnification, the operator's or machine's ability to track the target, the colinearity or boresight between the laser and viewing sensor, the intervening atmosphere, and the stabilizing qualities of the sight. The fact that target acquisition and precision designation must be accomplished in a helicopter vibrational environment makes the design tasks far more difficult. The nature of the helicopter vibrational spectrum is primarily deterministic driven by the well-regulated main rotor frequency. The knowledge of both periodic translational and angular vibrational accelerations at the electro-optical stabilized sight mounting location is helpful to the servo designer, but the large amplitudes of the vibrations strain the ingenuity of the servo designer and the state-of-the-art of theoretical and mechanical stabilized sight design.

REQUIREMENTS

Qualitative operational requirements must be transformed into quantitative values to provide the system designer a starting point. Target acquisition qualitatively involves finding and determining that an object is an engagable target from a given range within specified target, scene, and atmospheric characteristics. The acquisition process involves searching a target sector, detecting, and recognizing military targets.

TARGET ACQUISITION

Recognition is a level of discrimination between specific objects in a class of similar objects. The class of objects may be all vehicles of military interest. The specific objects are tanks, personnel carriers, trucks, etc. The difficulty of the discrimination level varies with the amount of detail needed to make a distinction between targets, which in turn is a function of the number of objects in the class and the similarity of the objects. In typical Army surface-to-surface scenarios, the discrimination usually varies with respect to the front, side, or three-quarters viewing aspect. The following approach to recognition performance is based upon a concept originally proposed by Johnson from the US Army Night Vision Laboratory. This method assumes that target recognition probability is a function of the number of bar pattern cycles which can be resolved across the minimum target dimension. This "target equivalent" bar pattern is one whose bars have a visual contrast or temperature difference equal to that of the target to its background. The relationship between probability of recognition, P_R, and the number of resolution cycles, f_o, must be determined on the basis of field experimentation. Emperical data, sensitive to the aspect or azimuth with which the target is viewed are shown in Table 1.

Detection is a lower order discrimination than recognition. It is defined as the determination that a perceived object is potentially of military interest. A contrasting object is singled out for closer scrutiny when it is detected. Object motion, dust, gunflash, or smoke provide additional cues for target detection and significantly increase the probability and decrease the time to detect. Whatever the reason, detection occurs when the observer's attention is called to a particular object of potential military value. The ability to detect a target in a cluttered background requires a low-order recognition capability. A high level of detail is needed to separate the target from the background if the background clutter has a high degree of structure. Field experience demonstrates that for general medium to low clutter approximately one quarter of the resolution is needed for detection as for recognition (3 to 4 cycles required). Table 2 gives such a relationship between detection probability and number of cycles across the target critical dimension.

TABLE 1. PROBABILITY OF RECOGNITION FOR ARMY VEHICLES

Probability of Recognition (P_R)	Front View Number of Cycles (f_o)	Side View Number of Cycles (f_o)
1.0	12	9
0.95	8	6
0.80	6	4.5
0.50	4	3
0.30	3	2.25
0.10	2	1.5
0.01	1	0.75
0	0	0

TABLE 2. PROBABILITY OF DETECTION FOR ARMY VEHICLES

Probability of Detection (P_D)	Minimum Target Dimension Number of Cycles (f_o)
1.0	3
0.95	2
0.80	1.5
0.50	1
0.30	0.75
0.10	0.50
0.01	0.25
0	0

For quantifiable purposes, the equivalent target can be defined as a flat board, perpendicular to the viewing sensors line-of-sight (LOS). The target board size should be comparable to the minimum target dimension, approximately 2.3 x 2.3 m. The targets contrast between adjacent bars (a line pair) can be specified consistent with the target-to-background contrast in the spectral region of the viewing sensor for the specified military target. For sensors in the visual or near infrared spectrum, the contrast can be defined as the ratio of the target, R_T and background, R_B reflectivities

$$C_o = \left| \frac{R_T - R_B}{R_B} \right|$$

or by the ratio of the target and background temperatures for far infrared viewing sensors. Target motion does not significantly affect the probability of recognition except to the extent that various aspects of the target may be viewed providing more information for recognition.

The viewing sensors contrast as perceived at the aperture is determined by the illumination level incident on the viewed target, the target and background reflectivities, and the contrast losses in the atmosphere. Contrast losses or attenuation through the atmosphere between the target and the sensor aperture can be defined in terms of visibility and sky-to-ground ratio. The atmospheric visibility for a given day (clear, haze, fog) can be approximately defined as the range at which one can perceive a 2% contrast target that is not size limited. The sky-to-ground ratio, H, is just the ratio of the brightness of the sky and ground. When viewing a target from low altitudes with a bright sky (high sky-to-background ratio) in the scene, significant contrast is lost and the target is difficult to discern. The contrast loss due to the atmosphere can be expressed as

$$\frac{C_s}{C_o} = \frac{1}{1 + H\left(\frac{1 - \quad}{\quad}\right)}$$

where C_o is the target-to-background contrast at the target location or zero range, C_S is the target-to-background contrast at the sensor aperture and T_a is the atmospheric transmittance, an exponential function of range to target.

Loss of target-to-background contrast significantly degrades target detection and recognition, whereas resolution loss through the atmosphere primarily degrades target recognition. The primary cause of resolution loss is due to turbulence. The strength of turbulence is defined in terms of a refractive index structure function, C_N^2, which is a strong function of time of day, atmospheric temperature profile, and a weaker function of atmospheric pressure and humidity. Experimental results with electro-optical systems indicate that the effects of turbulence are quite severe at ground level and quickly decrease with altitude of the sensor. High quality LOS stabilization is essential to good image resolution and target recognition.

A typical three spectral system diagram along with performance measurement quantities is shown in Figure 1. It presents the points discussed previously in this section concerning detection/recognition criteria; target size, contrast, and motion; illumination; and atmospheric contrast and resolution losses.

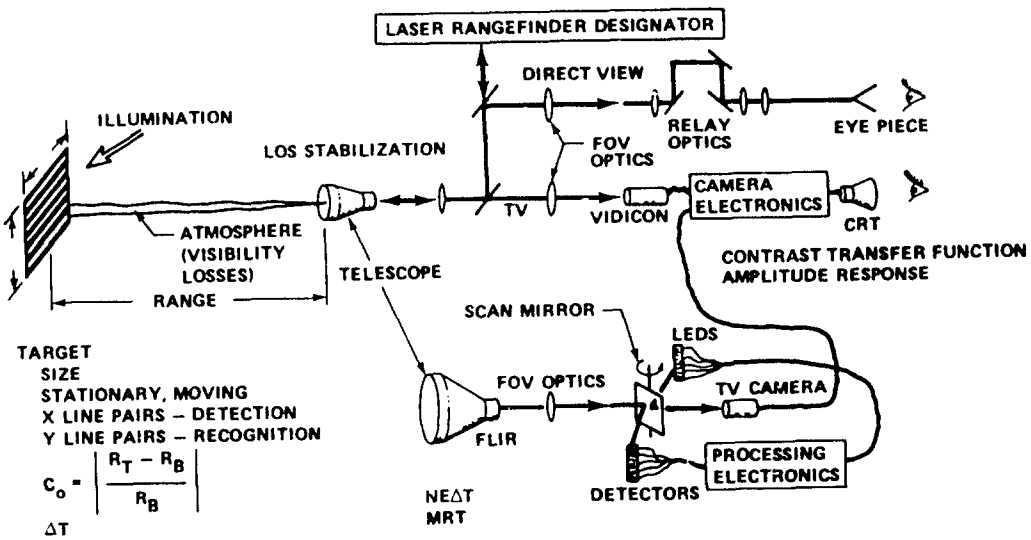

Figure 1. Characterization of target acquisition requirement.

TARGET DESIGNATION

The target designation requirement is totally defined by the behavior of the laser spot on the target required by the missile system. In order to meet the probability of hit specified by the missile system designers, the laser spot which the missile is guiding on must exhibit certain characteristics. First, the spot must be placed on a vulnerable location on the tank. This requires that the target designator operator, detect and recognize the target, place the aimpoint reticle on the desired hit point, and maintain it on the hit point during the duration of missile flight. Electro-optical target designators usually have an automatic tracker feature which allows the operator to lock-on and automatically track the target irrespective of motion as long as the target is visible through the viewing system. The operator then has the capability to minutely perturbate the LOS (reticle crosshair) to achieve better tracking than provided by the autotracker alone. This is especially required for nonsymmetrical targets. The process of selecting and placing the reticle on the desired target hit point by the operator involves some inherent aiming error. The instantaneous alignment between the laser beam and the electro-optical viewing sensor must be adjustable to compensate for manufacturing tolerances and drift. The method of adjusting the alignment or boresight procedure has some inherent error. The alignment is also susceptible to error due to structural drift caused by temperature changes and gradients. This type of boresight drift can, for the most part, be considered slowly varying with time with respect to the time required for a missile flight to target. Both the boresighting procedure error and the boresight drift can be combined and labeled boresight error. The aiming error and boresight error in well-designed target acquisition and designation systems will generally vary slowly with time to the extent that they can be considered time invariant over the short time of missile flight to target.

Equally important as the steady-state aiming and boresight error are the time varying errors. These errors are generally induced into the stabilized sight by helicopter vibration which the sight is not able to stabilize out completely, such as impulses caused by onboard gunfire blast pressure or mechanical shock transmitted through the airframe, man-induced motion into the tracking, or just poor servo or automatic tracker design. These time varying stabilization and tracking errors range from tenths of a Hertz to 50 and 100 Hz. Atmospheric turbulence can also have an affect on beam motion. There is some rationale for spectrally separating this error into stabilization and tracking error since the automatic tracker and any errors induced by the operator would be low frequency, generally below 3 Hz. Further definition of the error categories is contained later in this paper.

The steady-state aiming and boresight error combined with the time varying stabilization and tracking error make up the total pointing error. This total pointing of the laser beam, coupled with the divergence of the laser beam, is what guides the missile to target and ultimately determines the performance of a well-designed missile system. Characterization of a typical precision pointing system is shown in Figure 2. More will be discussed on overall pointing errors and their measurements later in the paper.

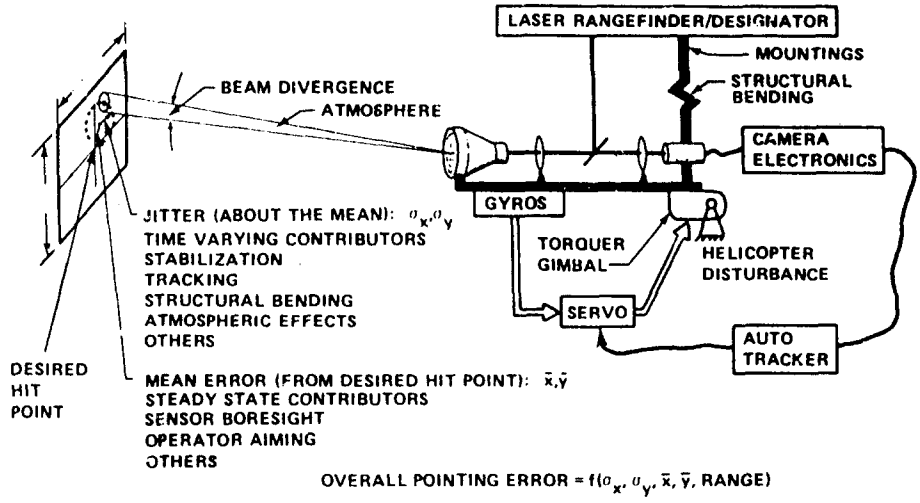

Figure 2. Characterization of target designation requirements.

TECHNOLOGY HARDWARE DEVELOPMENT

The launch and guidance of laser semiactive missiles from helicopter platforms to destroy hard armor at extended ranges is an extremely difficult task which pushed the state-of-art in many areas. The successful accomplishment of this task depends on both the laser seeking missile system and the target acquisition and laser designation system. The burden of accuracy, however, falls squarely on the quality of designation. The target acquisition and designation system is composed of subsystems whose design and development cross many technological areas. As shown in Figures 1 and 2, the laser, long focal length optics, television, and night vision subsystems must all be integrated into the confines of a small turret and structurally maintain in alignment with precision normally associated with optical bench experiments found in laboratories. This delicate equipment must then be stabilized to point at the target with a high degree of accuracy in a severe vibrational environment to meet system overall pointing requirements at extended standoff ranges. The purpose of this section is to describe the hardware technology efforts in the US Army Missile Command's Guidance and Control (G&C) Directorate in Automatic Tracking and Integrated Fire Control for airborne target acquisition and laser designator systems.

Studies were conducted as part of the G&C precision designator technology program to determine the various stabilization and tracking concepts which could be utilized to mechanize a precision airborne laser designator system with the capability to search, identify, acquire, automatically track, and designate targets from long standoff ranges. A survey was made to determine which systems already in existence might be potential candidates to provide this function and concepts of existing systems were modeled and simulated. Based on the studies, surveys, and simulated results, it was determined that two basic concepts for stabilization and many concepts for automatic tracking existed, each concept exhibiting advantages and disadvantages; no concept was clearly superior over the other. As a result, two systems were selected, each with distinctly different approaches to stabilization and automatic tracking.

STABILIZED PLATFORM AIRBORNE LASER (SPAL)

The SPAL is a day-only precision technology airborne laser designator system configured into a pod for helicopter mounting (Figures 3 and 4). The pod is 20 in. high, 11 in. wide, and 60 in. long, with a 20-in. diameter turret. The weight is 326 lb, with an additional 65 lb for the control panel and cabling. The forward turret assembly contains the stabilizing gimbals and sensors, and the aft pod assembly contains power supplies, electronics, and approximately 2 ft^3 of space for future growth. The forward turret assembly may be detached from the aft pod and installed on the nose of an AH-1G Cobra Helicopter. Primary subsystems for SPAL are LOS stabilization, TV viewing, automatic tracker, laser designator/rangefinder, and the laser spot tracker. LOS rate stabilization is provided by a conventional two-axis (azimuth, elevation) gimbal set. The turret assembly contains the optical receiving and transmitting windows and is slaved to the azimuth gimbal axis to decouple wind loads and keep the respective windows in front of the transmitting and receiving optics. The elevation gimbal serves as a one-piece structural platform on which is mounted the optical telescope and vidicons, the laser designator, the laser range receiver, and a laser spot tracker. Target acquisition is provided by a closed circuit 525-line, 2:1 interlace, 1:1 aspect ratio television system consisting of a 2-field-of-view (FOV) catadioptic telescope, silicon vidicons (one each for the wide and narrow field of view), TV electronics (including electronic enhancement circuits), and a heads-up high brightness monitor for operator viewing. The SPAL gimbal angles can be controlled in the manual tracking mode by inputting gimbal slew rate commands as a function of operator control stick displacement or by an automatic tracking mode. The SPAL automatic tracker is a multiple

adaptive gate, area balance, video contrast tracker. By operating on the noncomposite video signal from the TV camera, the tracker gates automatically expand to the edges of the target contrast defined by the target to background contrast ratio. The tracker commands control the servo to track the target centroid automatically.

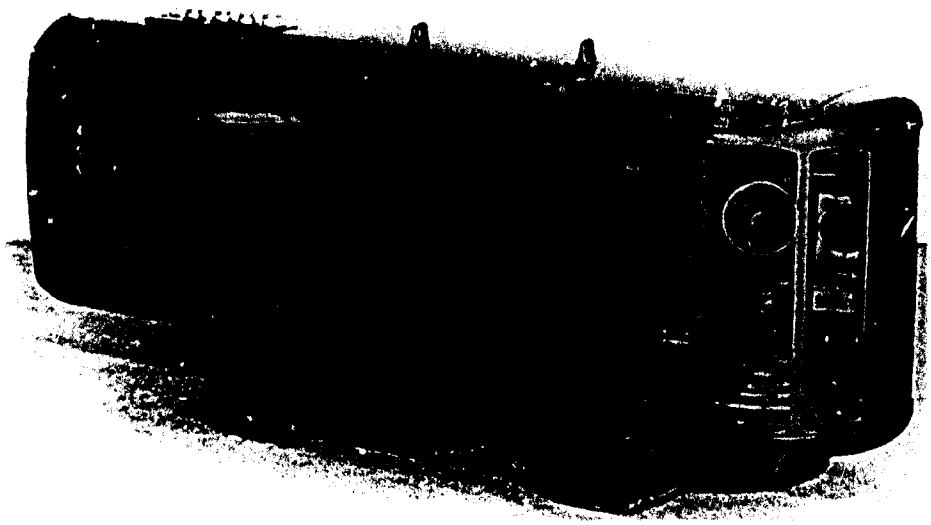

Figure 3. Stabilized Platform Airborne Laser (SPAL).

Figure 4. SPAL, Helicopter mounted.

Significant achievements accomplished with the SPAL were: (1) acquisition and automatic tracking of stationary and moving targets at 9 km, (2) target recognition of various types of vehicles (based on operator's performance), and resolution patterns (based on Johnson's criteria) at 5 to 6 km, (3) laser spot peak-to-peak jitter of 4 in. (measured at the target for designation ranges of 2 to 3 km for automatically tracked targets, (4) laser terminal homing seeker acquisition and lock-on at 4 to 8 km of energy reflected from target designated by SPAL from a range of 4 to 8 km, and (5) laser designation for technology terminal homing missile launches with direct hits.

STABILIZED MIRROR AIRBORNE LASER (SMAL)

The SMAL pod is a day-only technology precision designator pod (Figure 5). Its basic dimensions are 16 x 72 in. and the weight is 265 lb exclusive of cabling and operator's control panel. The primary subsystems which make up the SMAL are the operator's panel with the 875-line high brightness TV monitor, the thumb pressure control stick, the mirror stabilization with azimuth turret, the multispectral tracker, the low light level TV camera with continuous zoom optics, laser, and control electronics. The multispectral tracker does not operate from TV video signals but employs a fixed FOV and a mechanical scan aperture. The tracker collects target and background spectral reflectance information in three-color (green, red, near infrared) regions and computes a composite error signal used to control the servoed stabilized mirror to center the target in the operator's display.

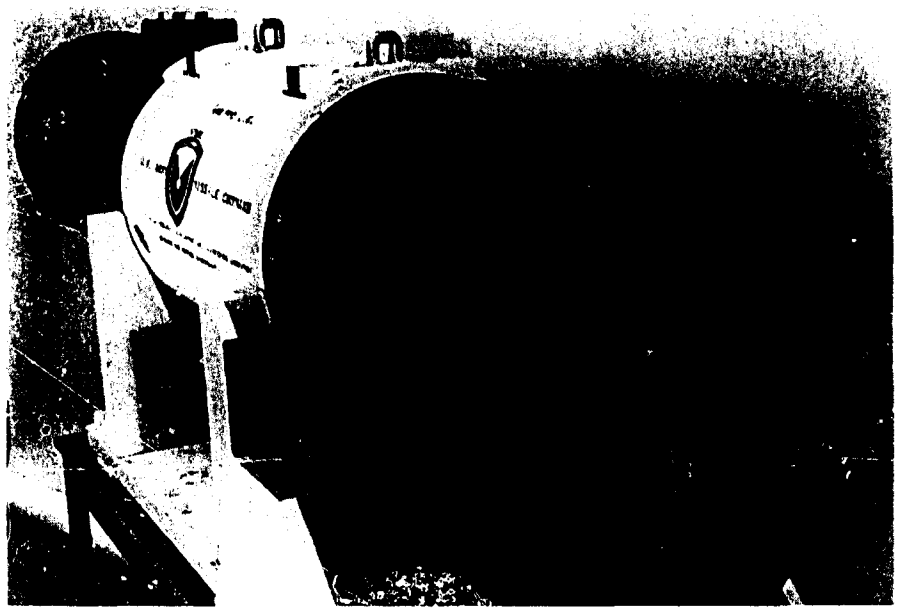

Figure 5. Stabilized Mirror Airborne Laser (SMAL).

The basic mirror stabilization error was less than 20 μrad, well within the LOS error requirements. However, additional image motion was induced by structural bending in the very long optical bed.

TEST PROGRAM AND PERFORMANCE

A well designed test and instrumentation program is essential to assess system performance and potential performance problem areas. It must be remembered that the errors being measured, especially for stabilization, tracking, and overall pointing, are so small that in many cases the instrumentation resolution and test-induced errors are the limiting factors. The performance test program should consist of at least two levels. Major subsystems following fabrication, prior to system integration, should undergo complete laboratory performance tests. The laser should be tested for all key performance parameter especially for boresight drift with respect to its mounting points. If the laser exhibits significant boresight drift in a laboratory environment, overall pointing error will probably exceed the design specification. The day and night sensors should also be tested in a laboratory. For daylight viewing sensors, the Amplitude Response and Contrast Transfer Function should be empirically obtained from the display through the complete subsystem to the objective aperture. For night imaging sensors (FLIR), the Noise Equivalent Temperature Difference (NEΔT) and the Minimum Resolvable Temperature (MRT) should be measured in the laboratory. These laboratory performance measures can be substituted into target acquisition models to predict expected target detection and recognition ranges.

After integration of the subsystems and system integration tests to eliminate subsystem interferences and integration problems, the major subsystem performance tests should be repeated in the laboratory to insure that no system integration problems exist which would reduce target detection, recognition, or overall pointing performance. These test recommendations are the results of design and development cycles on at least three technology systems and will result in identifying potential system and subsystem problems early. Following integration into the helicopter, the flight test is next performed to measure target acquisition and designation performance in a realistic helicopter vibrational environment under conditions which simulate target engagement. The laboratory subsystem and system performance tests, if conducted properly, can be used to predict and correlate with the flight test results.

Target detection and recognition flight tests for the SMAL consisted of a sequence of runs where the helicopter would approach the target array from 9-km standoff range and fly toward the target array with a given speed, altitude, aspect angle, and maneuver. The helicopter would maintain these parameters until

the target array was overflown and then would fly back to the 9-km standoff starting point for the next run. The target array usually consisted of the laser target board, an armored personnel carrier (either stationary or moving) along with stationary resolution boards (Figure 6). A video tape recorder was mounted in the AH-1G Cobra to record system video. In addition, system video was transmitted to the ground test van located near the target array through a modified 12-MHz bandwidth transmitter. IRIG-B reference timing was superimposed on the video signal and recorded.

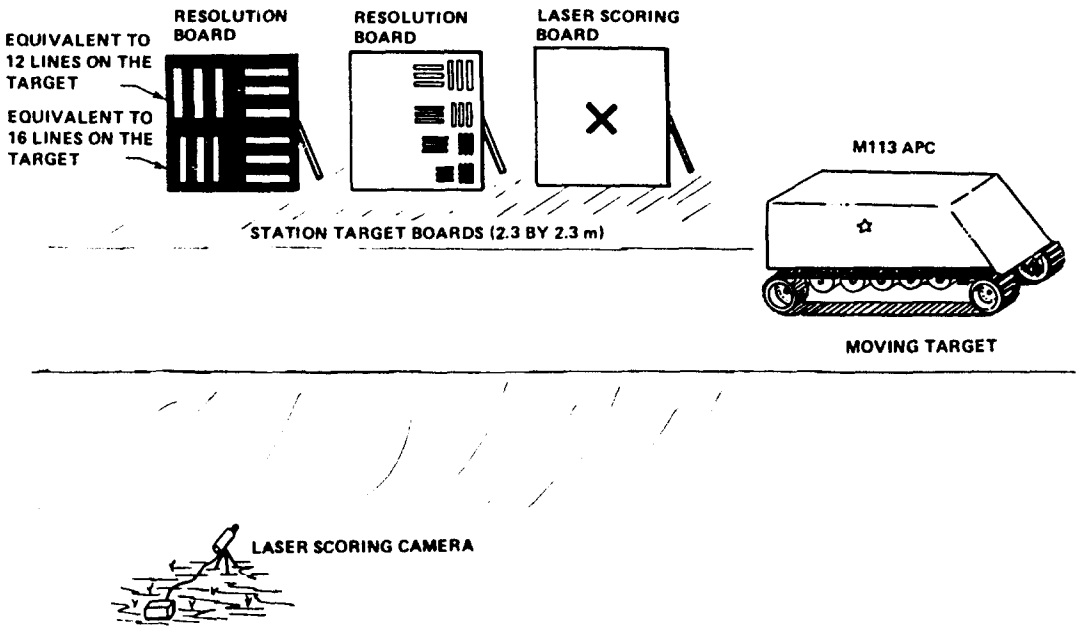

Figure 6. Target array.

A review of the video tapes from the helicopter mounted recorder and transmitted TV video showed that with repeatability, the SPAL system can resolve 6 to 8 cycles on a 2.3- x 2.3-m target board from approximately 5000-m range while flying straight toward the target board at 60 to 100 kt at 100 to 200 ft altitude above ground level. Military personnel (at least 10 observers) viewing the video tapes consistently recognized or identified the moving military vehicle as an M113 armored personnel carrier at a standoff range of 5000 to 7000 m. Most of the observers were able to do this at approximately 7000 m. The SPAL operator (unfamiliar with the test area) had no problems acquiring the target consistently in the wide FOV and tracking (manually or autotrack) in the narrow FOV. Both stationary target boards and moving M113 targets were automatically tracked at various ranges out to 9000-m standoff range. The tracking performance, especially the ability to maintain autotrack, is highly dependent on the amount and type of scene clutter surrounding the target.

The SPAL laser designation flight test was designed to measure the ability of the operator and SPAL system to hold the laser beam on the desired target hitpoint, the laser beam motion around the hitpoint, and the reflected energy from the target. These measured data were gathered as a function of the type of target (target board, armored personnel carrier, or tank); whether the target was moving or stationary; the helicopter speed, altitude, and type of maneuver; and the mode of tracking (manual or automatic) in which the SPAL is being operated. The objective of this phase of testing was not only to obtain accurate data on the pointing, tracking, and stabilization performance of the SPAL system, but also to determine if and at what standoff range the SPAL performance would be sufficient to be used as an airborne laser designator in the technology missile firing program. A test range setup similar to the detection/recognition test was used except that laser scoring cameras and reflected laser energy measurement instrumentation were required. Laser spot data were collected with a silicon vidicon TV laser scoring camera. The coordinates of each laser pulse with respect to the center of the target was calculated on a frame by frame basis from 16 mm film made from the laser scoring camera TV video. Laser spot centroid data were also calculated by another completely independent system using an intensified vidicon which was gated to record each laser pulse. A processor operated on each frame of video to calculate the coordinates of the centroid of each laser pulse. A video threshold (adjustable) level was set to define a contour around the laser spot. Thus, all voltages in the noncomposite video signal greater than the threshold represent imagery of the laser spot. An algorithm in the processor automatically computes the centroid in X and Y coordinates of each laser pulse reflected from the target with respect to a desired preset reference (X = 0, Y = 0) hit point. The process then calculates the statistics (mean and standard deviation) of a sequence of laser pulses over some interval of time. The processor can perform this task in real time or on video recorded with the laser scoring camera. The two methods of computing laser spot centroid coordinate data were used as checks against each other.

The test runs were conducted with the helicopter flying straight toward the laser scoring target board at a nominal altitude of 150 ft at a nominal forward velocity of 100 kt. Some runs were conducted at 60-kt velocity resulting in no noticeable difference in laser spot jitter even though somewhat higher vibration levels were experienced at slower speed flights. A slalom maneuver (fly-in while banking 30° from side to

side) was performed to introduce excessive helicopter tracking motion. During this maneuver, the laser spot jitter did not increase appreciably in the automatic tracking mode, however, the laser spot was off the target scoring board a significant percentage of the time in the manual tracking mode such that statistics of the laser spot could not be calculated. A typical plot of centroids of the laser spot in X and Y coordinates versus time for a 5-sec interval around 3 km for manual tracking is shown in Figure 7. The overall pointing error for manual tracking was in excess of 125 urad and was not categorized as being precision pointing as required by laser terminal homing missiles. A time plot of laser spot centroids for the automatic tracking mode is shown in Figure 8. This plot represents data with "standard deviations" (time varying spot motion - stabilization and tracking) of 10 to 15 urad and "means" (time invariant spot displacement - aiming and boresight) of 25 to 40 urad at 5000-m standoff range. This represents overall pointing accuracies of less than 45 urad.

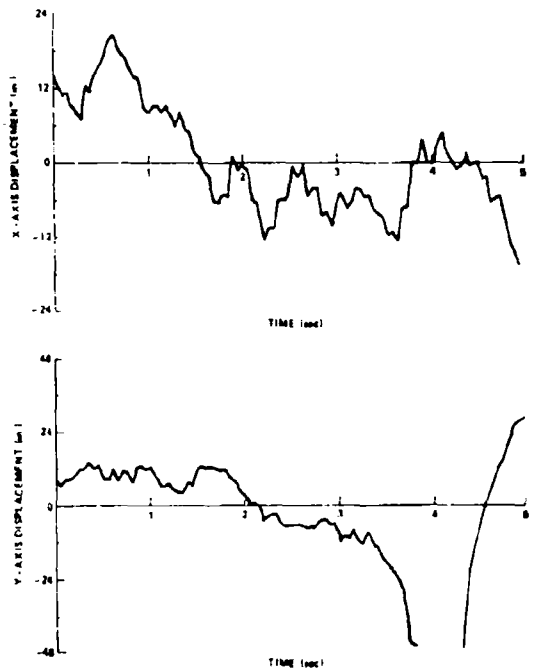

Figure 7. Typical plot of laser spot centroid displacement versus time for a 3-km manual track run.

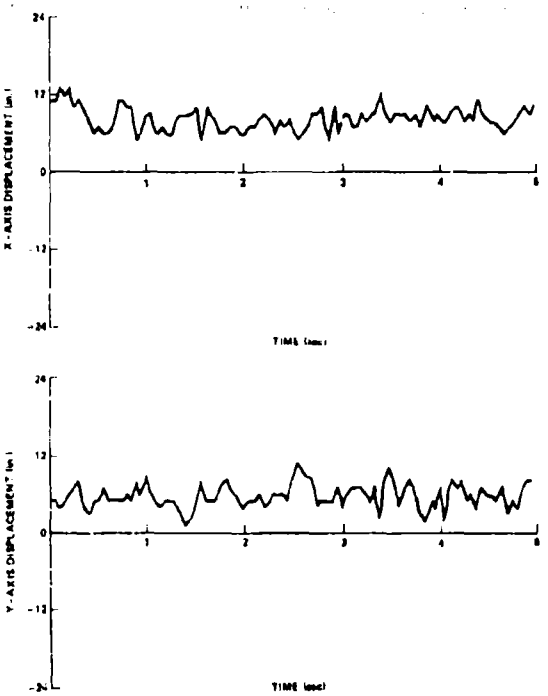

Figure 8. Typical time plot of laser spot centroid at 5-km standoff range.

LASER SPOT CENTROID DATA ANALYSIS

Laser designation flight tests resulted in the accumulation of large amounts of spot centroid data. This clearly pointed out the need for some compact method for data management and the reduction of spot centroid displacement from the desired hit point into a system component error budget. Also, the need for a detailed analysis of the laser designator's overall pointing performance is important from the standpoint of correlating system output performance (laser spot motion) to system operator and internal system hardware error sources (servo rate stabilization, autotracker, gyros, etc.). Two methods have been developed to achieve this. The first method is to record signals from critical test points in the stabilization and pointing servo loops and to instrument the stabilized sight mounting locations with translational and angular accelerometers to determine vibrational input disturbances. Then, for each laser designation run, the laser spot motion frequency and abnormal spot behavior can be correlated with recorded signal levels to identify the source of the anomaly. This method is very time consuming and costly from the instrumentation and data reduction aspect. A second, simpler approach is to make logical assumptions about the behavior of the laser spot motion and to estimate the pointing system error sources from just the laser spot centroid data. This method is much more manageable from the data acquisition/reduction standpoint. Then the first method can be used only on the isolated cases where problems do occur or system performance exceeds specifications. Prior to describing the method of "Estimating Pointing System Errors from Laser Spot Centroid Data," a more descriptive definition must be made of the error categories than previously defined in this text.

ERROR CATEGORIES

Boresight error is likely to be the largest component and is defined as the angular misalignment between the laser beam centroid and the viewing sensor's LOS as defined by a perfect reticle imaged on an ideal target plane. The most common source of boresight error in acquisition and laser designation systems is optical component shifts (translation or tilt) due to thermal gradients. The errors will increase for systems with noncoaxial optics and large physical separations between sensors and the laser. The larger separations imply longer optical lever arms and the likelihood of additional relay optics. The errors will tend to vary monotonically with time or cycle as a function of thermal loading, since equilibrium is never reached. Other sources are errors introduced by the inability to boresight the sensors to the laser

"perfectly" (boresighting procedure), sensor raster drift, and internal laser boresight shifts. Time varying angular misalignment between the laser beam and the viewing sensor LOS induced by structural deformations due to vibration will tend to be periodic and high frequency. Due to the nature and source of the misalignment, this error should be categorized as structural stability error instead of boresight and would be considered part of the stabilization error. It is assumed that boresight error during a run is limited to values which are an order of magnitude smaller than the overall pointing error and can be considered time invariant for this analysis.

Aiming error is the angular misalignment between the viewing sensor's LOS as defined by a perfect reticle imaged on an ideal target plane with respect to an imaginary line from the sensor to the desired hit point on the target. This error tends to be very difficult to measure; the only point at which to make the measurement is the sensor's imagery. Aiming error will most likely be on the order of the sensor's resolution limit, otherwise, the operator would have the information to aim better, thereby reducing the aiming error. This error is caused by imperfect definition of the ideal target point, TV resolution, human/optical resolution, and human actuation limitations coupled with the pointing and tracking system's servo response. Experiences have indicated that aiming error is mainly due to system resolving power limitations when the human is not operating under physiologically stressful conditions. If aiming is required during automatic tracking, then estimation of this new aiming error or estimation of the average aiming error during any target run must separate the manual commands from the purely automatic tracker (machine) commands. Since different operators perform differently, the contribution of the operator to overall pointing error during each test should be estimated to determine a baseline for operator error so that realistic system performance can be predicted. An average aiming error over a run should provide the most reasonable estimate of operator performance. Since the operator is equally likely to aim high as to aim low, etc., the average of the run aiming errors over many runs for that operator should approach zero with the number of runs. Since the estimate of the mean aiming error of an operator will likely be zero, a variance estimate or estimate of the standard deviation provides the only reasonable estimate of (operator) aiming error.

In previous efforts, some attempt has been made to separate stabilization error from tracking error. This can be done in only an approximate way because (1) tracking accuracy depends on the performance of the rate stabilization loop, and (2) the positioning accuracy of a rate stabilization loop can be determined only by using a tracking system (position feedback) to provide pointing. If it is desirable to know precisely how well the stabilization subsystem or the tracking subsystem is performing during flight test, then internal system measurements must be made while laser spot centroid measurements are made at the target. The instantaneous total pointing error is the vector sum of the aiming error, E_A, the stabilization and tracking error, E_S, and the boresight error, E_B.

METHOD OF ESTIMATING ERRORS

Typical data on the coordinates of a laser spot's centroid at the target board as a function of time during a single run are shown in Figure 8. These data give an indication of the typical randomness of centroid movement. If one is limited only to laser spot centroid data, the following random data analysis method can be used to estimate operator error, boresight error, and stabilization and tracking system error.

Let the laser pulse times during a run be denoted by $t = nT_o$ with $n = 1,\ldots,N$ and T_o representing the pulse period. Also, let i, $i = 1,2,\ldots,I$, denote the run number after the j^{th} boresight operation and by the k^{th} operator. If overall aiming error by a population of operators is desired and it is not required to estimate the abilities of individual operators, then the index, k, can be ignored by letting the index, j, include data for all operators. If information about the variance of operator abilities is needed, then the estimation should be done for each operator and the overall operator error computed from the individual error. The latter approach is taken here and the index, k, is used.

The mean estimate for the data of the i^{th} run, j^{th} boresight, and k^{th} operator is

$$\bar{x}_{ijk} = \frac{1}{N}\sum_{n=1}^{N} x_{ijkn}$$

$$\bar{y}_{ijk} = \frac{1}{N}\sum_{n=1}^{N} y_{ijkn} \qquad (1)$$

where x_{ijkn}, y_{ijkn} are coordinates of the laser spot centroid at the pulse time, n, during run number, i, after boresight number, j, performed by operator, k. These mean estimates include both aiming and boresight errors.

Since stabilization with tracking is a regulation control process which attempts to null the error, its error is

$$\epsilon_{sxijk}(t) = x_{ijk}(t) - \bar{x}_{ijk}$$

$$\epsilon_{syijk}(t) = y_{ijk}(t) - \bar{y}_{ijk} \qquad (2)$$

This error is a random variable with zero mean; it might be simply characterized by the variance:

$$\sigma^2_{sxijk} = \frac{1}{N-1} \sum_{n=1}^{N} \epsilon^2_{sxijk}(nT_o)$$

$$\sigma^2_{syijk} = \frac{1}{N-1} \sum_{n=1}^{N} \epsilon^2_{syijk}(nT_o) \quad . \tag{3}$$

Total, single-axis stabilization and tracking error would then be given by one of:

$$\sigma^2_{sx} = \frac{1}{IJK} \sum_{i=1}^{I} \sum_{j=1}^{J} \sum_{k=1}^{K} \sigma^2_{sxijk}$$

$$\sigma^2_{sy} = \frac{1}{IJK} \sum_{i=1}^{I} \sum_{j=1}^{J} \sum_{k=1}^{K} \sigma^2_{syijk} \tag{4}$$

provided stabilization, boresighting, and aiming errors are independent as they are assumed to be. Boresight error should be nearly constant between frequent boresightings. That is, the frequency of boresighting is determined by the assumption that changes in boresight error are small compared to the boresight error itself. Since these changes can only be observed from laser spot data, these data must be processed continuously to determine when to re-boresight. The contribution of aiming error to $\bar{x}_{ijk}$ over all runs should sum to zero; that is, the mean of the aiming error contribution to $\bar{x}_{ijk}$ should be zero. Thus, the boresight error for each boresighting event should be

$$\epsilon_{Bxjk} = \frac{1}{I} \sum_{i=1}^{I} \bar{x}_{ijk} = \frac{1}{I} \sum_{i=1}^{I} (\bar{x}_{Bijk} + \bar{x}_{Aijk})$$

$$\epsilon_{Byjk} = \frac{1}{I} \sum_{i=1}^{I} \bar{y}_{ijk} = \frac{1}{I} \sum_{i=1}^{I} (\bar{y}_{Bijk} + \bar{y}_{Aijk}) \tag{5}$$

wherein $\bar{x}_{Aijk}$ and $\bar{y}_{Aijk}$ are the contributions of aiming error to $\bar{x}_{ijk}$ and $\bar{y}_{ijk}$. The boresight contributions are denoted by $\bar{x}_{Bijk}$ and $\bar{y}_{Bijk}$. As mentioned previously

$$\frac{1}{I} \sum_{i=1}^{I} x_{Aijk} \to 0$$

$$\frac{1}{I} \sum_{i=1}^{I} y_{Aijk} \to 0 \quad .$$

Since the various boresighting events, j=1,2,...J, should not produce a systematic boresight error, a check on the validity of ϵ_{Bxjk} and ϵ_{Byjk} or an indication of no persistent boresight problem is

$$\sum_{j=1}^{J} \epsilon_{Bxjk} \to 0$$

$$\sum_{j=1}^{J} \epsilon_{Byjk} \to 0 \quad .$$

As implicity indicated in Equation (5), the aiming error at each run could be described by

$$\epsilon_{Axijk} = \bar{x}_{Aijk} = \bar{x}_{ijk} - \bar{x}_{Bijk}$$

$$\epsilon_{Ayijk} = \bar{y}_{Aijk} = \bar{y}_{ijk} - \bar{y}_{Bijk} \quad .$$

This error is expressed in terms of the unavailable quantities $\bar{x}_{Bijk}$ and $\bar{y}_{Bijk}$. However, if the boresight error does not change significantly with time, then approximately

$$\bar{X}_{Bijk} = \epsilon_{Bxjk}$$

$$\bar{Y}_{Bijk} = \epsilon_{Byjk}$$

so that

$$\epsilon_{AXijk} = \bar{X}_{ijk} - \epsilon_{Bxjk}$$

$$\epsilon_{Ayijk} = \bar{y}_{ijk} - \epsilon_{Bxjk} \quad . \tag{6}$$

Notice that, and correctly so, over the (many) target runs

$$\sum_{i=1}^{I} \epsilon_{Axijk} = 0$$

$$\sum_{i=1}^{I} \epsilon_{Ayijk} = 0 \quad .$$

If ϵ_{Bxjk} and ϵ_{Byjk} are random variables over many boresighting events, j=1,2,...,J, and if it has zero mean over these events (as assumed and tested previously), then the system boresight error is characterized by

$$\sigma_{Bx}^2 = \frac{1}{JK} \sum_{k=1}^{K} \sum_{j=1}^{J} (\epsilon_{Bxjk})^2$$

$$\sigma_{By}^2 = \frac{1}{JK} \sum_{k=1}^{K} \sum_{j=1}^{J} (\epsilon_{Byjk})^2 \quad . \tag{7}$$

Since the mean of the aiming error is zero over the many runs, the variance is the next best term to use to characterize this error:

$$\sigma_{Ax}^2 = \frac{1}{IJK} \sum_{k=1}^{K} \sum_{j=1}^{J} \sum_{i=1}^{I} (\epsilon_{Axijk})^2$$

$$\sigma_{Ay}^2 = \frac{1}{IJK} \sum_{k=1}^{K} \sum_{j=1}^{J} \sum_{i=1}^{I} (\epsilon_{Ayijk})^2 \quad . \tag{8}$$

The (total) system error over many runs, boresightings, and operators should have zero means so that there are not systematic errors. The variance is the next best way to describe this total error and is defined by

$$\sigma_x^2 = \frac{1}{IJKN} \sum_{i=1}^{I} \sum_{j=1}^{J} \sum_{k=1}^{K} \sum_{n=1}^{N} x_{ijk}^2(nT_o)$$

$$\sigma_y^2 = \frac{1}{IJKN} \sum_{i=1}^{I} \sum_{j=1}^{J} \sum_{k=1}^{K} \sum_{n=1}^{N} y_{ijk}^2(nT_o) \quad . \tag{9}$$

The mean of all data should be zero, otherwise there are not enough samples, or there is a systematic error whose source must be determined by other means. In any case, since systematic errors will become known and can be subtracted out, the following is obtained:

$$\bar{x} = \sum_{i=1}^{I} \sum_{j=1}^{J} \sum_{k=1}^{K} \sum_{n=1}^{N} x_{ijk}(nT_o) \to 0$$

$$\bar{y} = \sum_{i=1}^{I} \sum_{j=1}^{J} \sum_{k=1}^{K} \sum_{n=1}^{N} y_{ijk}(nT_o) \to 0 \quad .$$

Then the total systems error, σ, over many runs, many boresightings, and many operators should be precisely related to the source errors σ_B, σ_A and σ_B by

$$\sigma_x^2 = \sigma_{Sx}^2 + \sigma_{Ax}^2 + \sigma_{Bx}^2$$

$$\sigma_y^2 = \sigma_{Sy}^2 + \sigma_{Ay}^2 + \sigma_{By}^2 \quad .$$

This is seen to be the case by the following analysis shown in the Appendix. The analysis techniques described in this section were applied to a large laser spot data base and found to alleviate the data management problem and provide excellent results.

CONCLUSIONS

Analytical and design techniques have been applied to translate general requirements into hardware design. These techniques have been converted to models that have been validated by laboratory and flight test performance results. Critical design areas have been determined and good (and bad) techniques have identified for both subsystem and system design and integration. Experimental sensor and system hardware has been developed and demonstrated to exceed requirements for target detection, recognition, and laser designation. A number of technology missile firings have confirmed the sufficiency of the designator requirements. Compact mathematical techniques have been developed to alleviate problems with management of large quantities of data and provide excellent estimates of system error budgets.

APPENDIX

$$\sigma_{Sx}^2 + \sigma_{Ax}^2 + \sigma_{Bx}^2 = \sum_{ijkn} \frac{1}{IJKN} (x - \bar{x})^2 + \sum_{ijk} \frac{1}{IJK} (\bar{x} - \epsilon_{Bx})^2 + \sum_{jk} \frac{1}{K..} \epsilon_{Bx}^2$$

$$= \sum_{ijkn} \frac{1}{IJKN} (x^2 - 2x\bar{x} + \bar{x}^2) + \sum_{ijk} \frac{1}{IJK} (\bar{x}^2 - 2\bar{x}\epsilon_{Bx} + \epsilon_{Bx}^2) + \sum_{jk} \frac{1}{JK} \epsilon_{Bx}^2$$

$$= \sigma_x^2 - 2 \sum_{ijk} \frac{1}{IJKN} (N\bar{x}^2) + \sum_{ijk} \frac{1}{IJKN} (N\bar{x}^2) + \sum_{ijk} \frac{1}{IJK} \bar{x}^2$$

$$- 2 \sum_{ijk} \frac{1}{IJK} \bar{x} \epsilon_{Bx} + \sum_{ijk} \frac{1}{IJK} \epsilon_{Bx}^2 + \sum_{jk} \frac{1}{JK} \epsilon_{Bx}^2$$

$$= \sigma_x^2 - 2 \sum_{ijk} \frac{1}{IJK} \bar{x} \epsilon_{Bx} + \sum_{ijk} \frac{1}{IJK} \epsilon_{Bx}^2 + \sum_{jk} \frac{1}{JK} \epsilon_{Bx}^2$$

$$= \sigma_x^2 - 2 \sum_{jk} \frac{1}{JKI} (I\epsilon_{Bx}) \epsilon_{Bx} + \sum_{jk} \frac{1}{IJK} I\epsilon_{Bx}^2 + \sum_{jk} \frac{1}{JK} \epsilon_{Bx}^2$$

$$= \sigma_x^2 \quad .$$

Thus, this allocation method is correct. In these steps, the shorthand notation has been used.

$$\sum_{ijkn} \quad \text{for} \quad \sum_{i=1}^{I} \sum_{j=1}^{J} \sum_{k=1}^{K} \sum_{n=1}^{N}$$

$x \quad$ for $x_{ijk}(=T_o)$

$\bar{x} \quad$ for $\bar{x}_{ijk}$

$\epsilon_{Bx} \quad$ for ϵ_{Bxijk}

and have used the facts that

$$\sum_{i} \bar{x}_{ijk} = I \epsilon_{Bxijk}$$

$$\sum_{ijk} \epsilon_{Bxjk} = I_{jk} \epsilon_{Bxjk} \quad .$$

It should be noted that the estimates of x^2 will be slightly biased unless

$$\frac{1}{N} \sum_{n=1}^{N} \quad \text{is replaced with} \quad \frac{1}{N-1} \sum_{n=1}^{N}$$

in this calculation. This was not done in the preceding development to keep the notation as simple as possible.

STRAPDOWN SEEKER TECHNOLOGY FOR THE TERMINAL GUIDANCE OF TACTICAL WEAPONS

by

R.D.Ehrich
Rockwell International Corporation
4300 East Fifth Avenue
Columbus, Ohio 43216
USA

Lt P.Vergez
Air Force Armament Laboratory
United States Air Force
Eglin AFB, Florida 32548
USA

SUMMARY

Strapdown or body-fixed seekers with sufficient field-of-view for the terminal guidance of many tactical weapons are now approaching state-of-the-art. Such seekers have a number of advantages over gimballed seekers, including increased reliability and unlimited line-of-sight rate capability. The major disadvantage is that inertial line-of-sight rates are not directly available for the implementation of proportional navigation. To form line-of-sight rates, the seeker output must be combined with inertial sensor measurements. This, however, results in a potential instability due to seeker gain errors. This problem has been minimized by a dither adaptive parameter identification approach for the measurement and correction of seeker errors. Simulation studies indicate the performance of such systems can be comparable to that of gimballed seekers. This paper will consider the basic principles and problems involved with mechanizing proportional navigation with strapdown seekers and present performance results for the dither adaptive technique.

1. INTRODUCTION

Most contemporary tactical guided weapons employ inertially stabilized seekers for target tracking and proportional navigation for terminal guidance. These seekers have a narrow instantaneous field-of-view, nominally less than ±3 degrees. In order to increase the seeker's total field-of-view, the target tracking sensor is mounted on a gimballed platform which is stabilized with respect to inertial space. These gimballed seekers have the advantage of providing a direct measurement of inertial line-of-sight (LOS) rate. Therefore, proportional navigation is easily implemented, since it requires body rate or acceleration commands proportional to the measured LOS rate. Proportional navigation is highly accurate for air-to-surface applications, and recent studies have shown it is nearly optimal for minimizing miss distance for these applications. The disadvantages of inertially stabilized seeker systems are that they: (1) require the fabrication, maintenance and calibration of a complex mechanical structure; (2) exhibit tracking rate limits which restrict performance envelopes; and (3) are sensitive to missile accelerations.

Recent advances in seeker technology have increased the field-of-view limits to the point that it is feasible to remove the gimballed platform and fix the seeker to the missile body thus eliminating the major disadvantages of inertially stabilized seekers. Examples of such seekers are optical and radar correlators, laser detectors with a holographic lens, and radar seekers with phased array antennas. These new body-fixed seekers are referred to as strapdown seekers. These seekers have two potential payoffs. First, the elimination of mechanical moving parts would increase the reliability of the system, and second, the removal of the gimbals could provide a cost savings.

One of the disadvantages of strapdown seekers is that the inertial line-of-sight rates needed for proportional navigation are not directly available. This problem could be overcome through the use of a less optimal guidance law, such as pursuit guidance, which does not require line-of-sight rates. Most strapdown seekers provide a direct measurement of line-of-sight error angles in seeker or missile body coordinates. Theoretically, inertial line-of-sight rates can be obtained by taking the derivative of these angles and transforming them into inertial coordinates using inertial sensors such as rate or attitude gyros. Practically, if there are even small errors in the seeker measurements, large miss distances can result or perhaps total system instability. This has been one of the factors, along with limited field-of-view capability, which has prevented the wide scale use of strapdown seekers in the past.

2. BACKGROUND

Beginning in the early 1970's, there has been increasing interest in strapdown seekers as a result of advances in seeker technology. In particular, radar seekers with phased array antennas, electro-optical area correlators, and semi-active laser seekers appeared to be suitable for strapdown applications (References 1, 2). Studies of guidance laws and filtering techniques for implementing strapdown seekers (References 3, 4) yielded concepts which effectively lower the navigation gain to reduce the sensitivity to seeker errors. This attempt to compromise accuracy for stability margin led to combinations of pursuit and proportional navigation. One such concept, Dynamic Lead Guidance, had a navigation gain of unity for low guidance frequencies and a gain of 3 to 6 for higher frequencies. This limited the strapdown seeker to air-to-surface missions and still required relatively high precision seeker elements. This, in turn, kept the cost of strapdown seekers comparable to gimballed seekers with some degradation in accuracy.

Recent advances in microprocessor technology have resulted in low cost computers for tactical weapons with sufficient speed and storage capability to continuously monitor and compensate for strapdown seeker errors, while maintaining a high navigation gain. One such dither adaptive concept was developed by Rockwell International and evaluated under Air Force contract F08635-77-C-0144. This program, completed in April of 1978, indicated the feasibility of strapdown seekers for air-to-surface weapons using this parameter identification approach (Reference 5). Using six degree-of-freedom digital simulations of two typical weapon systems, the dither adaptive concept achieved performance comparable to that of a gimballed seeker. Realistic models of seekers, inertial sensors, and system errors were employed, and relatively low seeker accuracy was required.

A second study, titled Strapdown Seeker Guidance and Control Technology for Tactical Weapons (Contract No. F08635-79-C-0187), was begun in May of 1979 and runs through September of 1980. Its objective is to extend the dither adaptive concept to air-to-air weapons. The concept was refined to handle the higher bandwidths and fields-of-view required for air engagements against maneuvering targets. The performance of the air-to-air weapons with a strapdown seeker compared favorably to that of the same weapon with a gimballed seeker. The refinements in the concept also reduced the accuracy requirements of the strapdown seekers, thus potentially reducing their cost. Although developed for air-to-air applications, the techniques are directly applicable to air-to-surface weapons. During the remainder of the contract, a detailed autopilot design will be developed for an air-to-surface weapon with a particular seeker/airframe combination utilizing the improved dither adaptive concept. This paper will summarize the results of these two studies to date, and will provide insights into the design problems and solutions developed.

3. BASIC CONCEPTS

The major difference between gimballed and strapdown seekers is that those functions performed by a mechanical structure in the gimballed seeker are performed electronically in the strapdown seeker. Examples of these functions are differentiation to yield a rate output, transformation from missile to line-of-sight (LOS) axes, and the removal of body motion from the seeker output. However, in both systems an inertial reference is required, be it rate gyros or an inertial wheel on the inner gimbal of a gimballed seeker, or rate or attitude gyros for the strapdown system. Since the platform of a gimballed seeker must be physically rotated to track the target, there is a limit to LOS rate. This limit is a function of the mechanical torquers and platform mass or angular momentum of the inertial wheel. For strapdown seekers no such limit exists, making the seeker attractive for high performance air-to-air weapons. Another major difference is associated with fields-of-view (FOV). For the gimballed seeker it is possible to have a small instantaneous FOV and a large total FOV corresponding to the maximum gimbal deflection. The small instantaneous FOV has the advantages of low thermal or background noise and good rejection of false targets. For strapdown seekers, two basic types are possible. These are termed "staring" and "beam steered" for the purpose of this discussion. Sketches for each type are presented in Figure 1. The staring type, such as the semi-active laser seeker, has an instantaneous FOV equal to the total FOV. The beam steered type is much like a gimballed seeker, in that it has a small instantaneous FOV or beam which can be moved relative to the missile body. A radar seeker with phased array antenna is an example of beam steering. This comparison of gimballed and strapdown seekers is summarized in Table I. The major sources for error in the line-of-sight rate output are also presented for both seekers. The methods for generating the LOS rates for strapdown seekers are presented in the following section.

3.1 Methods of Generating Line-of-Sight Rates

Two basic methods of generating LOS rate signals from strapdown body fixed seekers have been uncovered which tend to be seeker hardware dependent. These methods are termed "beam steering" and "additive rate compensation" for convenience, although no widely accepted designations seem to exist. They are generally used with "beam steered" and "staring" seekers, respectively, although this is not necessary (as will be shown in a later paragraph). The general forms for each method are shown in Figure 2 for a single seeker channel. Beam steering will be described first since the other method can be considered as a special case with fixed beam or FOV with respect to the missile body. The geometry of the beam steering method is shown in Figure 3. Notice that the center of the beam or FOV can be displaced by an angle θ_{beam} from the missile longitudinal axis. The steering loop (Figure 2) centers the beam on the target by driving the error angle, ϵ_{beam}, to zero. The rate gyro signal, θ_{gyro}, removes body rate information from the seeker output (λ_q) by effectively cancelling the body attitude component in ϵ_{body}. In other words, the gyro adds positive feedback of body attitude (θ_M) to compensate for the existing negative feedback. It will be shown that unless the gain and phase differences in the two paths are small, the system will become unstable.

Therefore, for beaming steering, only the radome effect and the phaser shifter linearity and dynamics affect the stability of the system with respect to cancellation of the two body attitude paths. Thus, the steering loop, which is made up of signal processing and seeker loop compensation, can have less stringent bandwidth and linearity specifications. The integrator in the feedback path performs the function of differentiation of the input signal and also aids in the control of steady state errors. This concept has the advantage of a small instantaneous FOV which results in increased rejection of background noise and false targets over staring seekers. A major drawback is that it can be applied to only certain types of seekers, mainly radars with phased array antennas and optical area

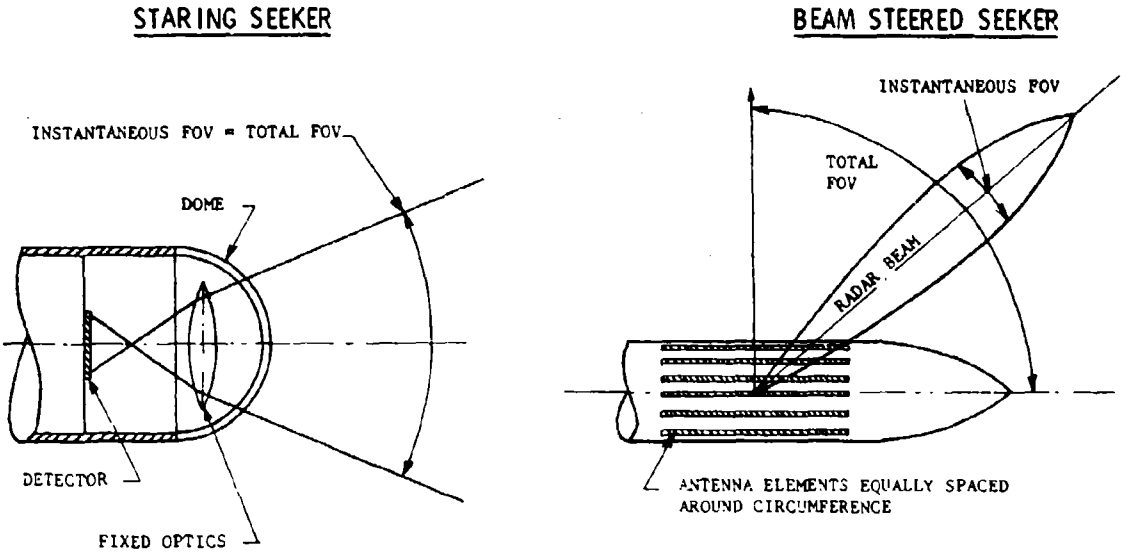

Figure 1. Basic Types of Strapdown Seekers

TABLE I. COMPARISON OF STRAPDOWN AND GIMBALLED SEEKERS

STRAPDOWN	GIMBALLED
Rigidly Mounted to Missile Body	Two-Axis Mechanical Structure with Gryoscopic Stabilization
Output Contains Body Motion, Must be Removed with Gyro	Output Independent of Missile Body Motion (Except for Friction)
Requires Electronic Differentiation	Yields Inertial LOS Rate by Mechanical Differentiation
Requires Electronic Transformation from Missile to LOS	Mechanical Transformation from Missile to Line-of-Sight
LOS Rate Capability Unlimited	LOS Rate Capability Limited by Mechanical Torquers
Staring: Instant FOV = Total FOV Beam Steered: Small Instant FOV, Large Total FOV	Small Instantaneous FOV, Large Total FOV
Major Error Sources: Seeker and Gyro	Major Error Sources: Gyro Drift, Gimbal Friction, Acceleration Sensitivity

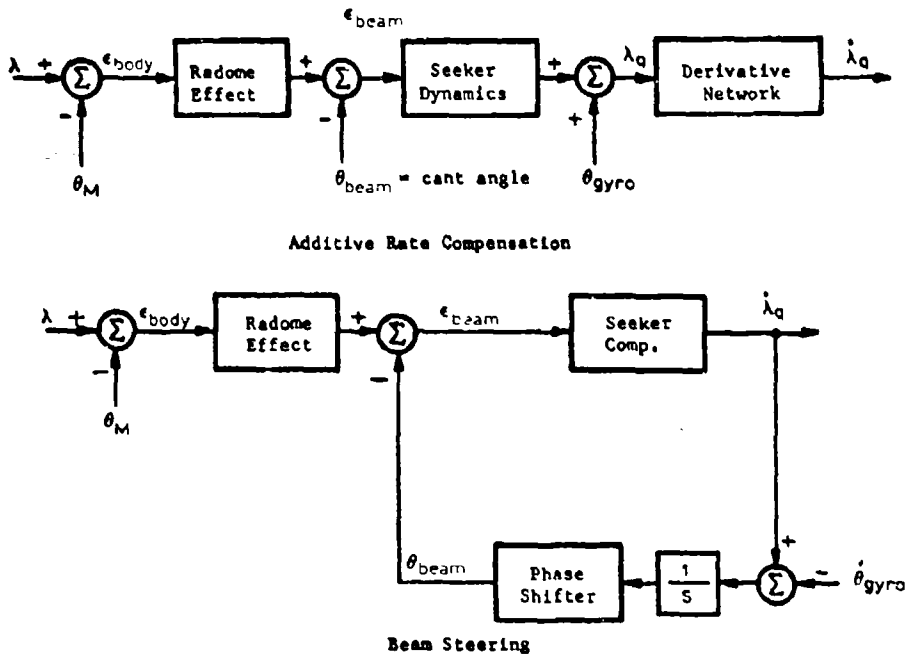

Figure 2. Methods of Generating LOS Rates

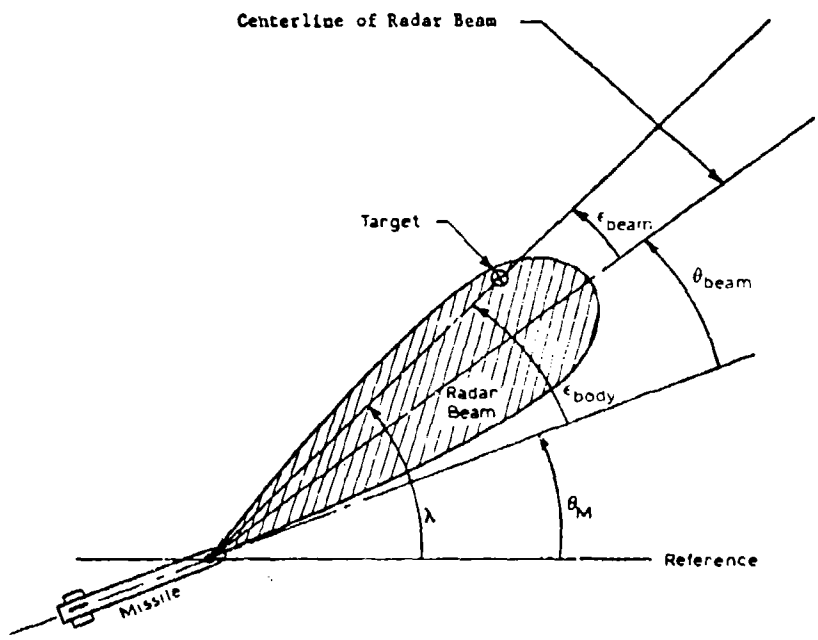

Figure 3. Geometry Definitions

correlators, in which the sensed energy can be displaced with respect to the detector by electromagnetic means.

The "additive rate compensation" technique can be applied to any type of seeker. It can be considered a special case of beam steering in which the angle between the beam and missile centerline (θ_{beam}) is fixed. The angle is normally zero although the beam can be canted down in pitch if necessary to minimize the required FOV. The nominal cant angle is usually the average trim angle of attack. Notice that the radome effect and the seeker dynamics must now be considered in assessing the stability effects of attitude path cancellation. The term "radome effect" will be used in a general sense to denote any distortions of the target energy between target and detector.

In either method the inertial sensor employed can be a rate or attitude gyro. The only difference will be in the errors introduced by the gyro. As previously mentioned, a "beam steered" type of seeker need not generate LOS rates using the beam steering method. If the rate gyro is removed from the beam steering mechanized of Figure 2, and the integrator moved to the forward path, then the beam will be centered on the target. The seeker output will equal θ_{beam} which is approximately ϵ_{body} for a high gain loop. Therefore, the seeker output is the same as for a staring seeker and additive rate compensation can be employed. Since additive rate compensation was a more general configuration which could be used regardless of seeker type, it became part of the dither adaptive concept. Errors in the derived LOS rate result from errors in the seeker and inertial sensor outputs and the processing of these signals. Common types of errors and their approximate magnitudes are the subject of the next section.

3.2 Seeker and Inertial Sensor Models and Errors

The major component errors fall into three broad classes:

(1)	linearity or gain errors:	radome, receiver/detector, phase shifter, gyro scale factor and dynamics
(2)	random errors:	thermal noise, glint or apparent target motion, gyro noise
(3)	offsets:	seeker boresight errors, gyro offsets or drift

The other errors, such as cross-coupling, sampling rate, break-lock or blind range can be shown to be of secondary importance, except in extreme cases. Most of the various seekers studied have common characteristics and errors such that a generalized seeker model could be formed. This model, shown in Figure 4, contains the errors mentioned above along with FOV limits and various models for thermal noise and resolution or radome distortion. Both methods of generating LOS rates, "additive rate compensation" and "beam steering" can be simulated, depending on which is appropriate to the seeker in question. Typical values for the linearity errors of strapdown seekers range from 1.0 milliradian for resolution and phase shifter quantization, 3.0 to 6.0 milliradians for radome distortion at high incidence angles, and gain or scale factor errors of up to 10 percent. The gain errors are often a function of signal level and location of the target within the field-of-view.

For the inertial sensors, the same three types of errors exist except that the offset is in general a function of missile accelerations. The linearity errors are considerably smaller for a gyro than for a typical seeker, and the same is true of noise sources. For example, the magnitudes of these errors for an attitude gyro are: linearity error ($\pm$1%), g-sensitive drift ($\pm$.025 degree per second per g), and noise (0.1 degree rms). The rate gyro has similar characteristics of linearity error ($\pm$1%), offset ($\pm$1% full scale) and noise (1% full scale rms). In addition, rate gyros have frequency characteristics which are usually modelled as second order dynamics. Natural frequencies in the range of 100 to 600 radians/second can generally be assumed, while the damping factors vary widely from unit to unit and also with temperature.

3.3 Errors in the Derived Line-of-Sight Rate

Each of the component errors causes a corresponding error in the derived LOS rate, although the sensitivity to each error source is affected to some degree by the method of generation of the LOS rate. Gain or linearity errors cause components of the missile body rate in the LOS rate, which cause stability problems and errors in the effective navigation gain. Random errors in the seeker and rate gyro cause random errors in the LOS rate with a resulting loss of accuracy. Finally, component offsets or biases can cause offsets in the derived line-of-sight rate depending on their location with respect to the derivative network. Offsets in the LOS rate also result in degradation of miss distance and some increase in required maneuverability.

The stability problem due to gain or linearity errors in the seeker is considered the most serious impediment to mechanizing proportional navigation. For reasonable navigation gains and system bandwidths, seeker gain errors as low as 2 to 4 percent can make some systems completely unstable. The frequency of the instability is often relatively high (e.g., 4 to 8 Hz) making many gain correction or parameter estimation concepts unworkable. The underlying reasons for the stability problem can be explained with the aid of Figure 5. To form an inertial LOS rate from the seeker error angle, ϵ, and rate gyro output, r, the gyro output is integrated and added to ϵ. The resulting LOS angle

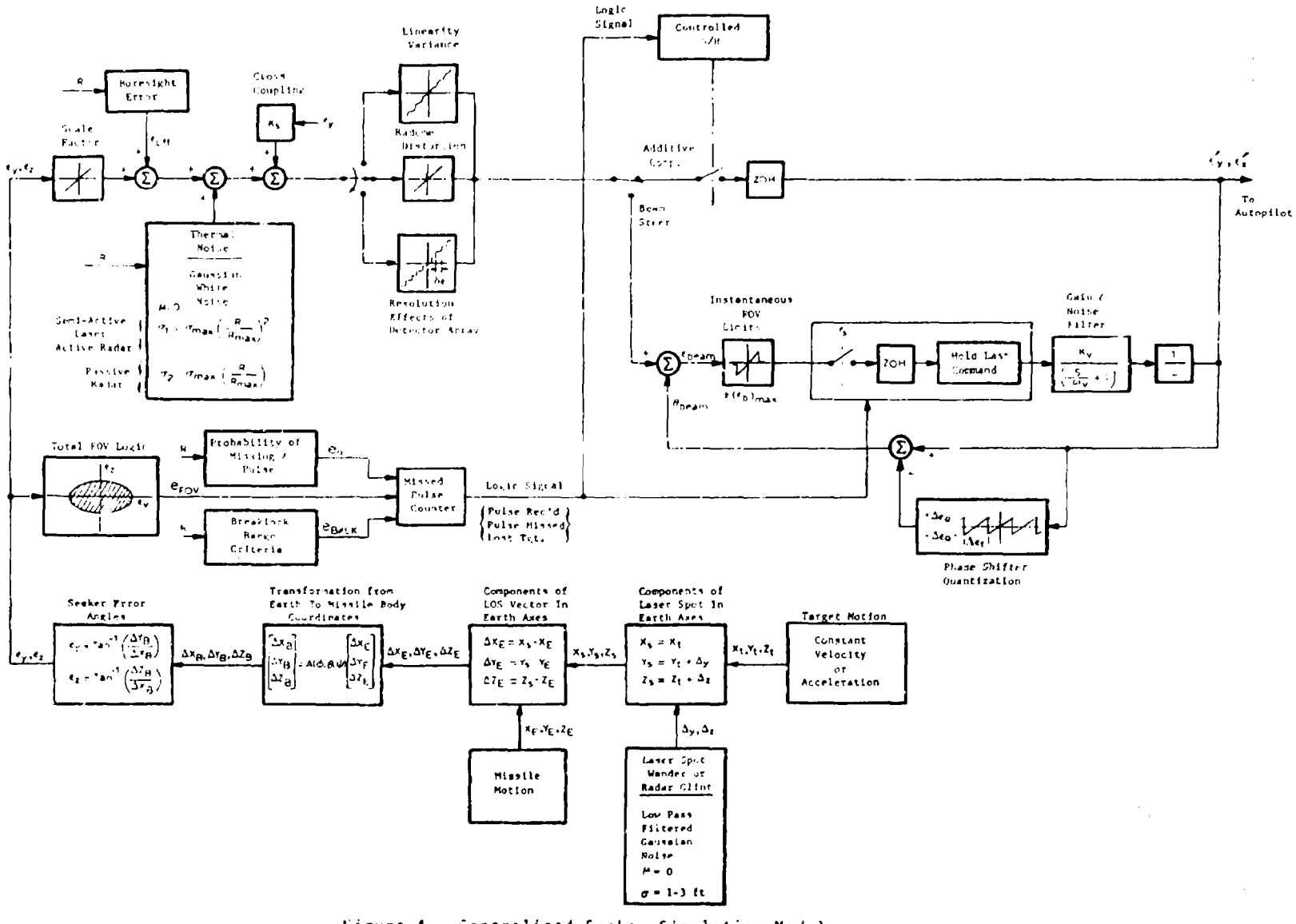

Figure 4. Generalized Seeker Simulation Model

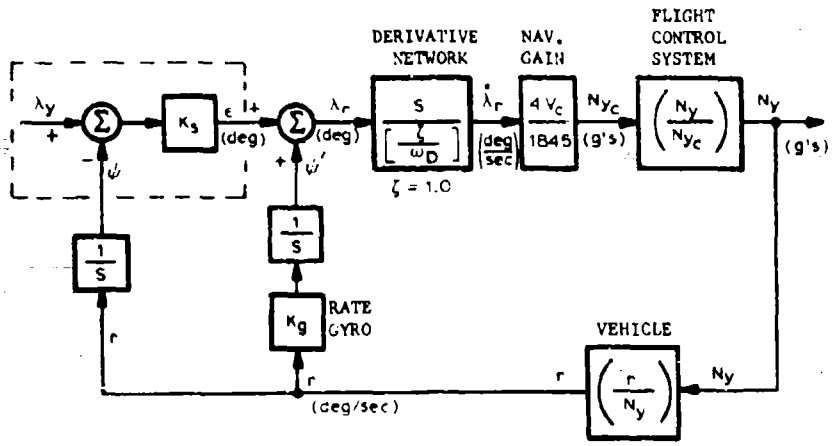

BTT WEAPON: Yaw Channel, $V_c = 1845 = V_m$

$$\left(\frac{r}{N_y}\right) = \left(\frac{r}{\dot{\gamma}}\right)\left(\frac{\dot{\gamma}}{N_y}\right) = \left[\frac{0.868\ (S/0.7835 + 1)}{(S/35.83 + 1)\ (S/(-34.60) + 1)}\right]$$

$$\left(\frac{N_y}{N_{y_c}}\right) = \left[\frac{(S/20 + 1)}{(S/100 + 1)^2}\right] \left[\frac{0.965\ (S/60 + 1)\ (S/35.83 + 1)\ (S/(-34.60) + 1)}{[0.4093/14.98]\ [0.4481/73.27]\ (S/77.8 + 1)}\right]$$

Figure 5. Formation of Yaw LOS Rate with Rate Gyro for BTT Weapon

is then differentiated to yield $\dot{\lambda}_r$. Proportional navigation is implemented by generating an acceleration command proportional to the LOS rate $\dot{\lambda}_r$ using a navigation gain (4Vc/1845). Notice that feedback of body motion, in this case the yaw rate (r), occurs through the seeker and rate gyro paths. If the seeker and gyro are perfect, then: $K_s = K_g = 1.0$ and the two paths exactly cancel. If the seeker gain, K_s, is greater than the gyro gain, K_g, then there will be a net negative feedback of body rate which can have a destabilizing effect on the system. The specific example presented in Figure 5 is for the yaw channel of a bank-to-turn weapon at a nominal flight condition.

To analyze the stability of this system, assume that the homing loop ($\lambda y/N_y$) is open, as is essentially true at long times-to-go before impact. The static open loop gain is a function of the gain difference (K_s-K_g). This represents a stationary target case for air-to-surface weapons or beam aspect in air-to-air engagements. The locus of closed loop poles is shown in Figure 6 as a function of the percent scale factor error, i.e., [K_s-K_g] x 100 percent. Note that the system becomes unstable for scale factor or gain errors of greater than +3.38 percent or less than -1.29 percent, and the frequency of the instability ranges from approximately 10 to 40 radians per second. Even at gain errors somewhat below these critical levels, the system damping may be too low for accurate homing.

This extreme sensitivity is a major problem in view of the fact that seeker hardware exhibiting errors up to 10 percent is not uncommon. The sensitivity can be reduced by increasing the maneuverability of the weapon (e.g., the lift coefficient, C_{L_α}) or by lowering the system bandwidth. Figure 7 indicates that if the bandwidth could be lowered to less than 10 radians/second, significant increases in the tolerance to errors could be realized. The graph indicates the critical seeker scale factor as a function of the derivative network corner frequency (ω_D). But for air-to-air missions, such bandwidths make the missile too sluggish for high accuracy. Even for air-to-surface weapons, lowering the system bandwidth or navigation gain is generally not a satisfactory approach.

Another effect of seeker gain errors is a change in the effective navigation gain from the design value (Figure 8). However, even for seeker scale factor errors as high as ±10 percent, the navigation gain is still in the range of 3 to 6. Clearly this effect is less serious than the stability problem considered above.

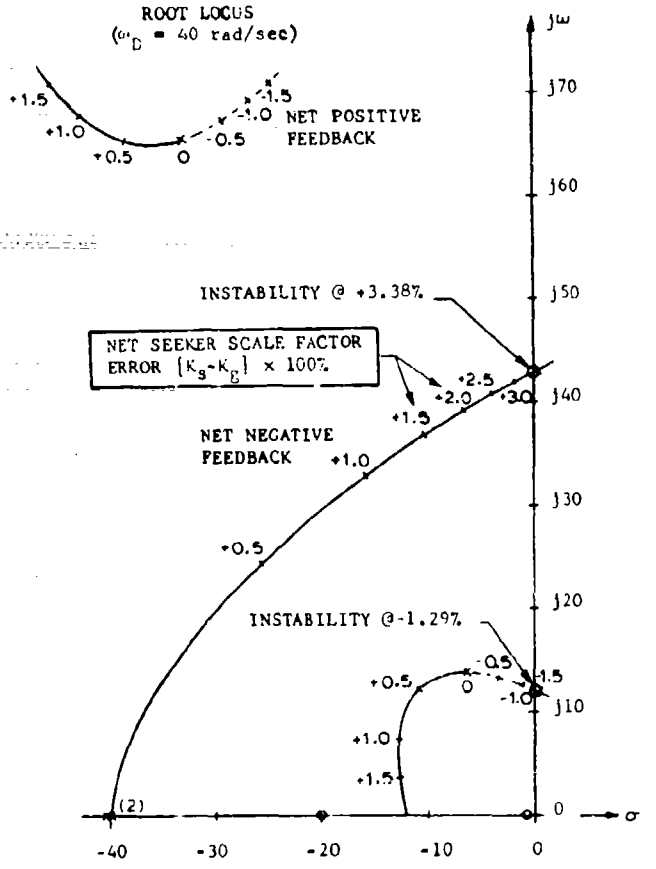

Figure 6. Locus of Closed Loop Poles for Scale Factor Errors

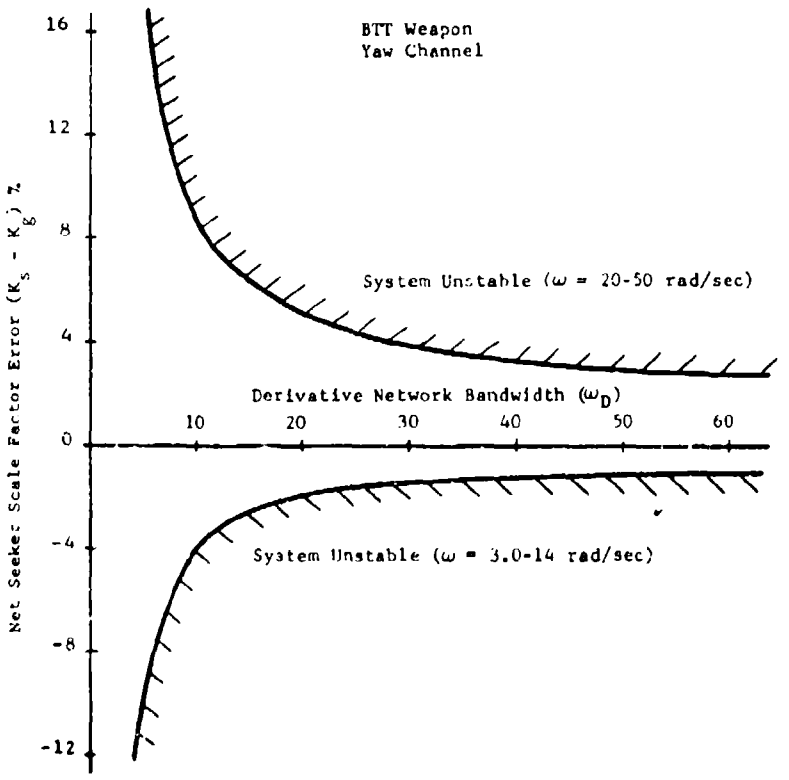

Figure 7. Sensitivity of Critical Seeker Scale Factor Error to System Bandwidth

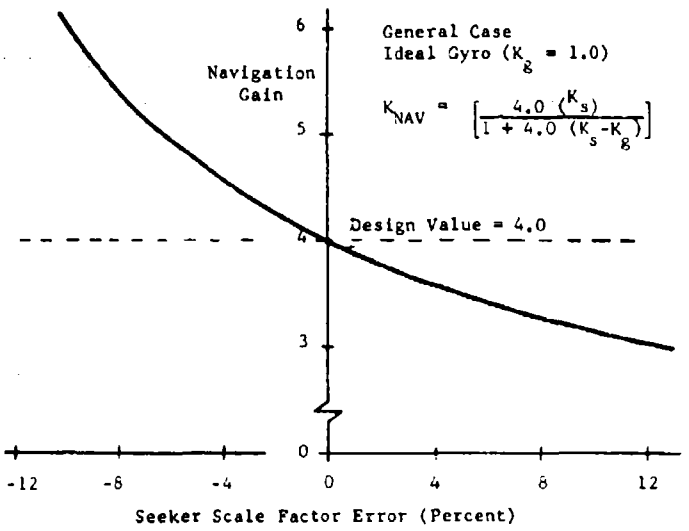

Figure 8. Navigation Gain Sensitivity to Seeker Gain Errors

4. STUDY RESULTS

A solution to these problems is a dither adaptive concept for measuring the seeker transfer function at a particular operating point. This is accomplished by dithering the missile body sinusoidally in both pitch and yaw axes, and comparing the dither components in both the seeker and gyro outputs. The seeker output is then adjusted to compensate for any discrepancies. Simulation evaluation has shown that the system is tolerant to relatively large seeker and gyro errors, such as:

(1) static seeker scale factor errors of ±80 percent
(2) rate gyro scale factor errors of up to ±5 percent
(3) seeker error slopes of up to ±.05 degrees per degree

The use of a geometric transformation based on seeker error angles to transform the rate gyro signals into line-of-sight axes allows the use of fields-of-view approaching ±90 degrees. For air-to-surface weapons with small fields-of-view, this may not be necessary. The dither adaptive concept does require dithering the airframe at frequencies above 20 radians/second (~ 3 Hz) to avoid significant components of dither in the inertial LOS rate. Peak-to-peak amplitudes of 6 to 8 times the resolution or noise levels of the seeker provide sufficient dither signal-to-noise ratio for proper operation of the adaptive system. This translates into a dither amplitude of roughly ±0.25 degree for 1.0 milliradian resolution levels. Missile motion of this amplitude has little effect on maneuverability or range performance and only moderate increases in the actuator rate requirements. The dither adaptive concept makes the use of strapdown seekers feasible for both air-to-surface and air-to-air weapons with accuracy comparable to systems with gimballed seekers. Additional work is needed to apply the concept to bank-to-turn missiles which execute roll maneuvers at high rates. The basic features and operation of the adaptive concept are described below along with the results of the simulation evaluation.

4.1 Features of the Dither Adaptive Concept

The inputs to the adaptive system are the seeker error angles (ϵ_{yb} and ϵ_{zb}) and the missile body rates from rate gyros (p_b, q_b, r_b) as shown in the generalized system block diagram (Figure 9). Alternately, attitude gyros could be employed in place of rate gyros for the inertial reference. The outputs of the adaptive system are the derived or estimated inertial line-of-sight rates ($\dot{\lambda}_{yb}$,$\dot{\lambda}_{zb}$). Missile body rates are transformed into appropriate LOS coordinate systems and then integrated so that they can be compared to and combined with the respective seeker error angle. The transformation matrix is in general seeker hardware dependent. When combined with the seeker angles, the incremental body motion angles ($\Delta\theta_{OA}$,$\Delta\psi_{LOS}$) yield inertial LOS angles in the LOS axes. After passing through the notch filters to remove residual dither components, and the derivative networks to form LOS rates, these signals are transformed back into body coordinates. These inertial LOS rates with respect to body axes ($\dot{\lambda}_{yb}$,$\dot{\lambda}_{zb}$) are then in the proper form for mechanizing proportional navigation with conventional autopilots. This concept has the distinct advantage of requiring minimum changes to existing autopilots designed to utilize gimballed seekers. The most significant element of the block diagram is labelled "Adaptive Networks". It is these networks which compare the sinusoidal dither components present in the seeker and gyro signals and generate the gain correction factors (K_y, K_z).

The operation of the adaptive networks will be explained with the aid of the pitch channel block diagram found in Figure 10. Notice that the two input signals (B_1, B_2) are

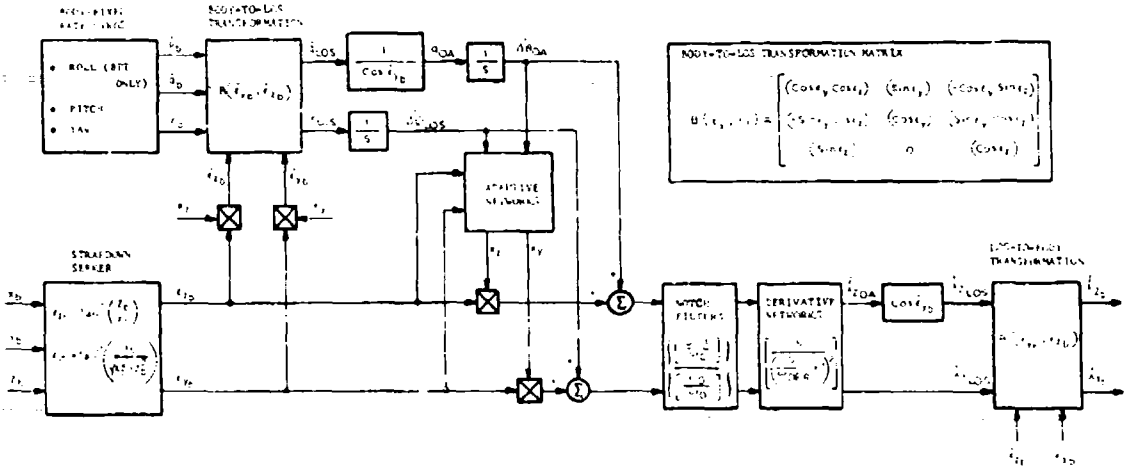

Figure 9. Generalized Block Diagram of Dither Adaptive Concept

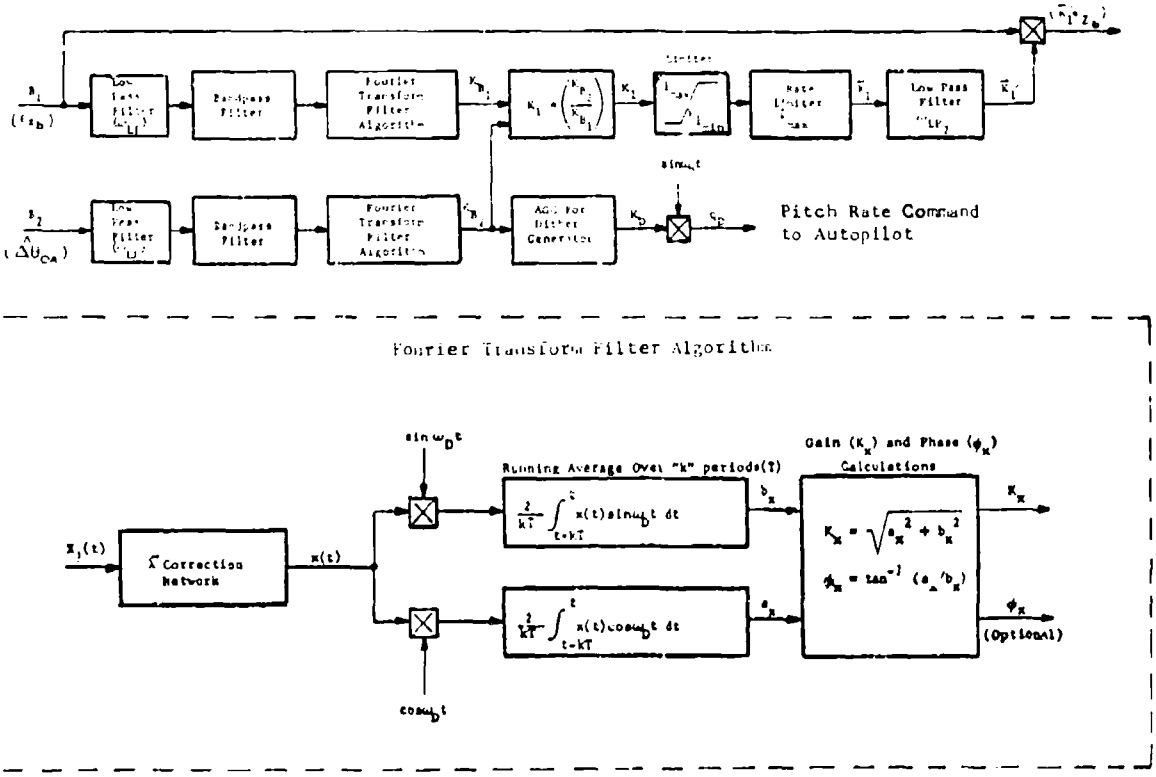

Figure 10. Adaptive Network Block Diagram

filtered identically to form signals K_{B_1} and K_{B_2} which are proportional to the amplitudes of the respective dither components. The ratio of these signals is the gain correction (K_1) required in the seeker output to make the gains of the seeker and gyro paths equal. Therefore, when the two signals are summed, no potentially destabilizing feedback of body rate can occur. The bandpass filters are employed to amplify the dither signal, while the low pass filter (ω_{LP}) rejects the second harmonic of the dither frequency (ω_D). Second harmonics can be generated in the transformation of rate gyro signals from body to LOS axes since these involve multiplications of signals containing dither. Also shown is the dither command signal to the autopilot (q_D). The automatic gain control (AGC) circuits are designed to maintain a constant dither amplitude on the seeker detector by monitoring the dither output of the gyro. By maintaining this constant amplitude, a satisfactory dither signal-to-noise ratio is assured.

To generate a signal proportional to the amplitude of the dither signal from the dither signal itself, a detection concept based on the Fourier Transform of the signal was developed. This Fourier Transform Filter Algorithm is shown in block diagram form in Figure 10. For a periodic input, $x(t)$, of period T, the outputs a_x and b_x are the coefficients for the fundamental or first harmonic of the Fourier series of the input. In this case, the period T will be the period of the dither signal ($T = 2\pi/\omega_D$), since the dither signal is the desired signal and all else is "noise". The gain K_x is then the amplitude of the dither component of the input, and ϕ_x is its phase with respect to the reference dither signal. The phase difference between the seeker and gyro channel could thus be determined by taking the difference between the ϕ_x quantities for the respective channels. However, during the current study, it was assumed that the bandwidths of both seeker and gyro greatly exceed the dither frequency, making the phase correction unnecessary. If the seeker characteristic is essentially nonlinear in nature, the K_x and ϕ_x become the gain and phase of the describing function for that nonlinearity. The running average is shown over "k" periods of the dither, where k = 1 yields the fastest speed of response, but multiple period averaging does provide better rejection of noise and other disturbances.

The line-of-sight acceleration ($\dot{\lambda}$) correction network was made necessary because the Fourier Transform yields a non-zero output for ramp type inputs. But the desired output is zero for any input except a sinusoidal signal at the dither frequency. A ramp type input can result if the seeker error angle (ϵ_{z_b}) has a LOS acceleration component ($\dot{\lambda}_z$), since the bandpass filter in the adaptive network is essentially a derivative network. The correction network measures the slope of the input signal by taking the difference in the average input over two overlapping periods, and adding a ramp of the same slope but opposite sign to offset the ramp component of the input.

The performance of the Fourier filter network is indicated in Figure 11, which shows the filter inputs and outputs during the first second of a simulated flight. Notice that the output is equal to the amplitude of the input as desired, and that the accuracy is particularly good if the amplitude of the input does not change greatly during a single cycle. The performance of the adaptive network for a seeker scale factor error of +10 percent was computed for one second time intervals with various target maneuvers. The theoretical steady state adaptive network output equals (1.0/1.1) = 0.9091. The time history (Figure 12) indicates a rise time to 90 percent of the steady state value in less than one period of the dither, ($\tau \sim .074$ sec), with an error in the steady state of less than 0.5 percent. The steady state performance is independent of LOS accelerations caused by target maneuvers at short range and also independent of missile motion occurring after guidance initiation.

4.2 Performance of the Dither Adaptive System

The most meaningful performance criteria for the adaptive system is the difference between the derived line-of-sight rate and the true inertial LOS rate. These differences in general will degrade the ability of the weapon to impact the target. Therefore, miss distance becomes another useful performance criteria. A comparison of the derived and true LOS rates for a bank-to-turn weapon in a short range engagement is presented in Figure 13. For this tail-on aspect against a 9g aircraft target, the LOS rates begin small and increase as the engagement progresses. Notice that the derived LOS rate is approximately equal to the inertial rate except for a delay caused by the 40 rad/sec bandwidth of the derivative network (i.e., ω_{DER} = 40 rad/sec in Figure 9). The transient which begins shortly after 2.5 seconds of flight is due to the burn-out of the rocket motor. The static seeker scale factor error for this case was +10 percent. However, performance is relatively independent of this error as seen in Figure 14. The accuracy and speed of response of the adaptive networks are not affected by the seeker scale factor (K_S in Figure 5) until this seeker gain becomes so small that the dither signal can no longer be adequately detected. For the case shown, which was for a skid-to-turn weapon, this occurs for scale factors of less than 0.20. This corresponds to a scale factor error of -80 percent. This is almost an order of magnitude greater than the largest expected error.

But seeker gain characteristics are not completely linear and therefore have errors in local slope across the field-of-view. The ability of the adaptive networks to compensate for these errors is a function of missile body rates and the dither frequency, which control the rate of change of the seeker error and the speed of the adaptive process, respectively. The high roll rates of some bank-to-turn weapons makes the application of this concept somewhat more difficult than for skid-to-turn weapons. Therefore, because of the sensitivity to missile body rates, it is difficult to be definitive about the

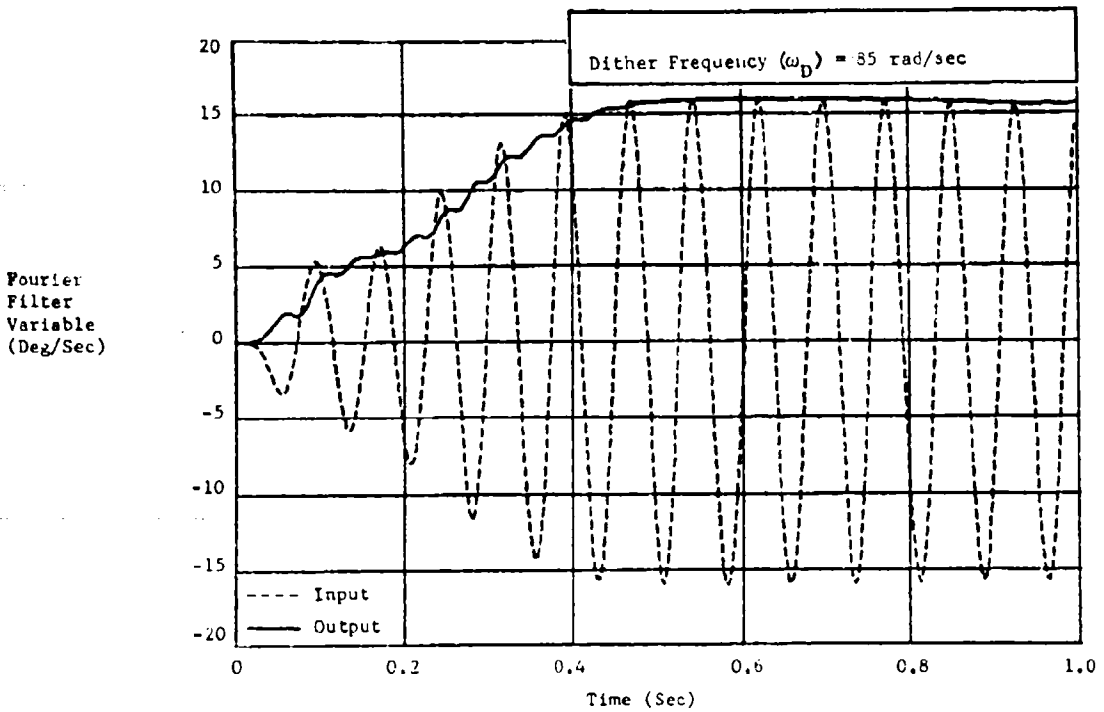

Figure 11. Performance of Fourier Transform Filter Algorithm

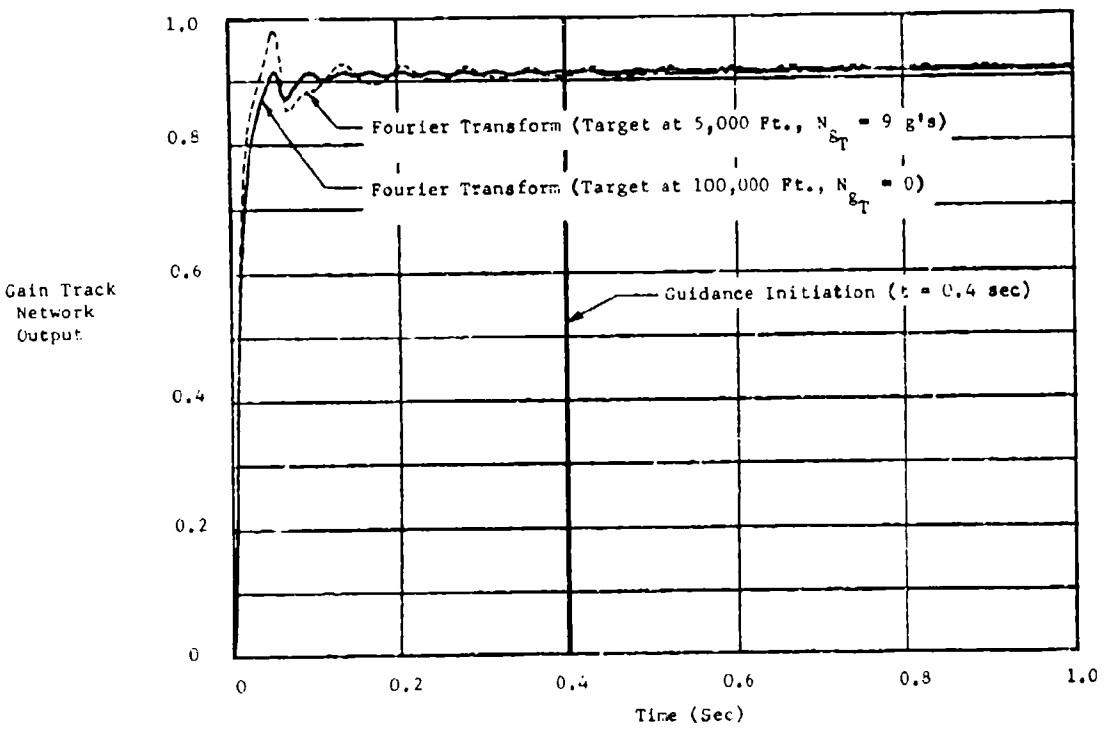

Figure 12. Dither Adaptive Gain Time Histories

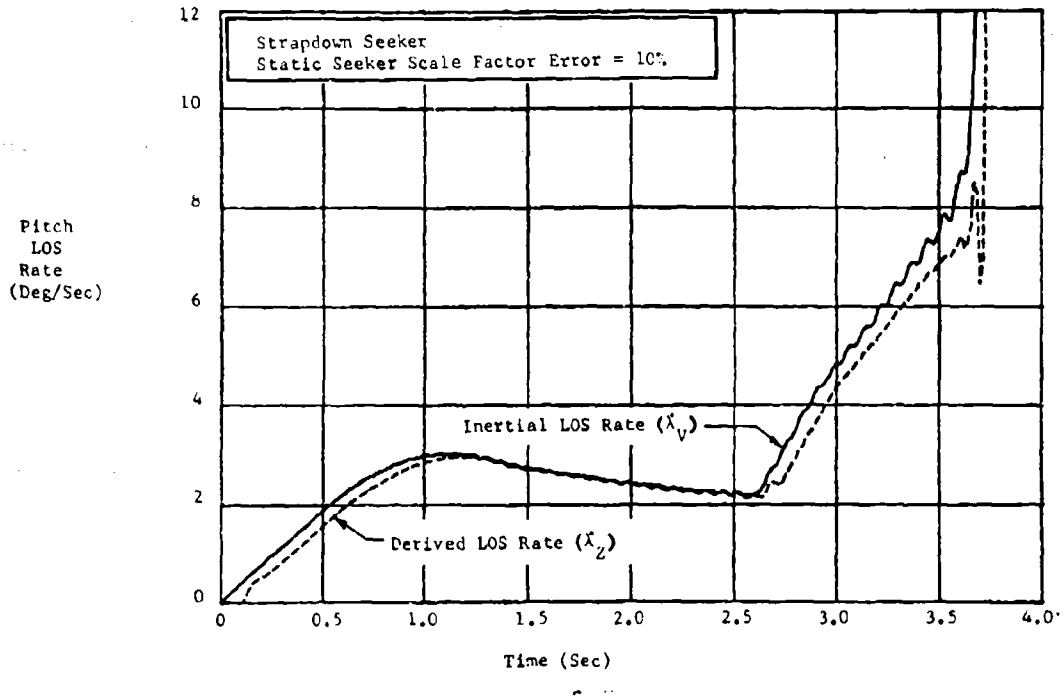

Figure 13. Comparison of Derived and True Line-of-Sight Rates

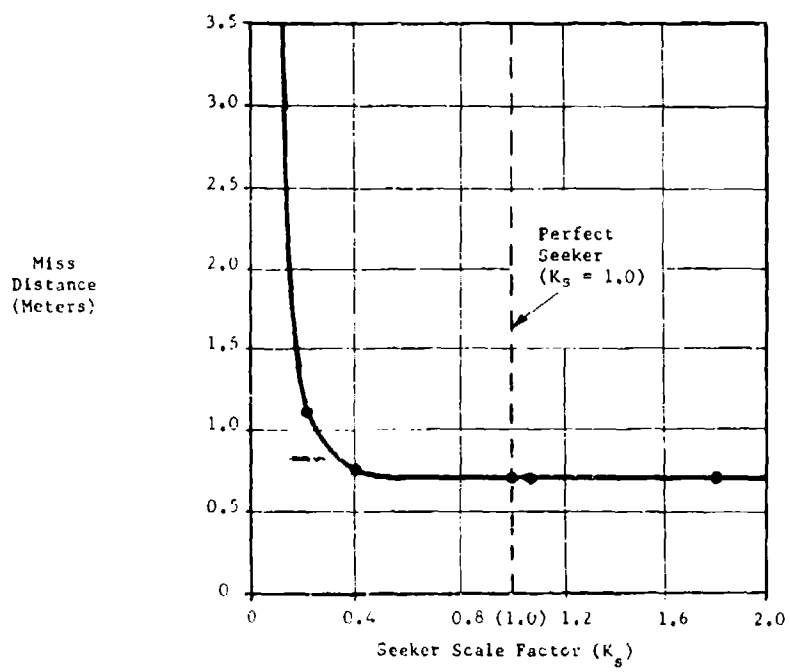

Figure 14. System Sensitivity to Variations of Seeker Scale Factor

ability of the adaptive process to handle nonlinearities, but error slopes on the order of .05 to .20 degree per degree have been successfully employed.

Another basic seeker error source is the effective resolution of the seeker which can be represented by amplitude quantization (Figure 15). This error degrades the capability of the seeker to detect the sinusoidal motion of the missile body. If the peak-to-peak amplitude ($\Delta\theta$) of body motion is divided by the effective resolution ($\delta\epsilon$), then this ratio equals the number of resolution elements averaged in a cycle of the dither. Figure 15 indicates that this ratio must be at least 6 to 10 for satisfactory performance. This plot was generated using a constant dither amplitude ($\Delta\theta$) of 0.40 degree peak-to-peak and varying the seeker resolution. A ratio of 8.0 corresponds to an effective resolution of about 1.0 milliradian, which is within the state of the art for seeker hardware. To produce dither amplitudes of approximately $\pm$.20 degree at a frequency of 40 radians/sec will require body rates of $\pm$8 degrees per second. This, in turn, will increase the required rate capability of the missile actuator system by a modest amount.

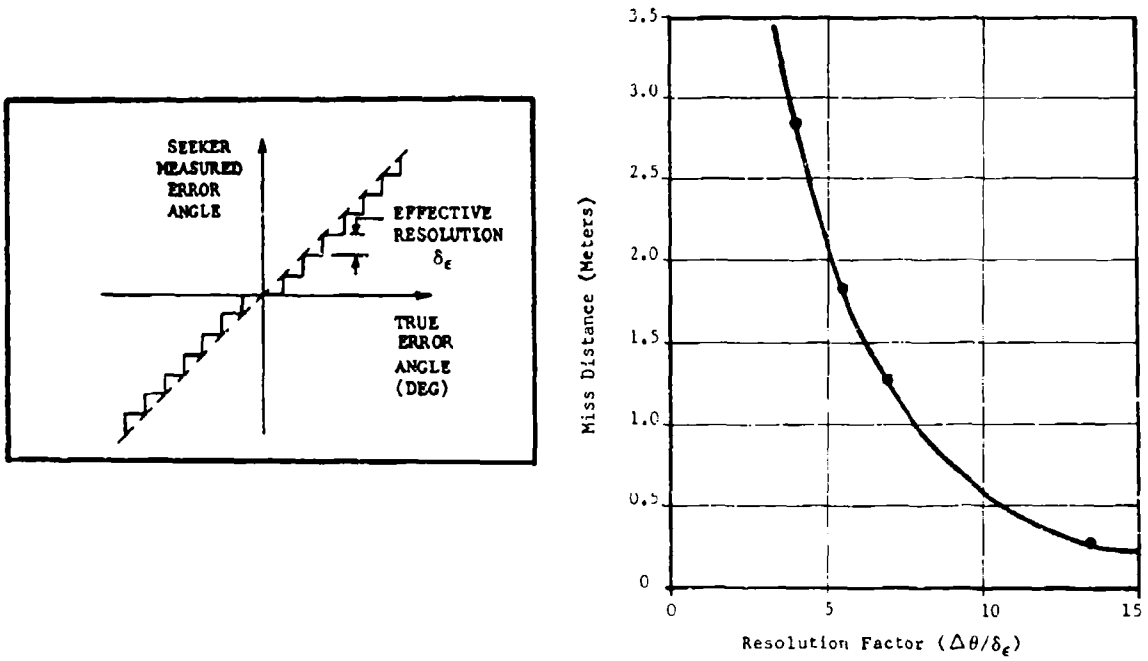

Figure 15. Sensitivity to Seeker Resolution Effects

5. CONCLUSIONS

The results of the two Air Force contracts indicate that a dither adaptive concept makes the use of strapdown seekers feasible for air-to-air and air-to-surface weapons. The accuracy of such systems can be comparable to that of gimballed seekers based on simulations of a number of different types of weapons and seekers. The accuracy required of the strapdown seekers and inertial sensors is moderate and the increase in actuator rates to dither the airframe is not excessive. Digital implementation of the adaptive system appears to be necessary due to the required multiplications, divisions, and geometric transformations. In addition, the required tolerances on dither frequency, notch filter parameters, and system gains precludes analog mechanization. The concept has the advantage of requiring minimum modifications to autopilots designed to employ proportional navigation with gimballed seekers. This is due to the fact that the outputs are inertial line-of-sight rates.

Future studies will include other approaches to solving the problems associated with strapdown seekers, with emphasis on missile performance in high "g" engagements, with current sensor limitations and passive seekers. Modern control and estimation theory, for example, may yield a more flexible solution in the long run.

Existing or near term seeker hardware for air-to-surface missions includes passive radar seekers, correlators, semi-active laser seekers, and imaging infrared seekers. For air-to-air weapons, the active radar seeker with conformal antenna appears to be the most appropriate near term configuration.

The advantages of strapdown seekers over those with two-axis gimbals should make them attractive for many applications. These advantages include increased reliability with the elimination of moving parts, unlimited line-of-sight rate capability, and the elimination

of errors due to gimbal friction and missile accelerations. Strapdown systems could potentially be lower in weight and cost. This would be particularly true in the long term as the cost of electronic components decreases with respect to mechanical components.

REFERENCES

1. Simulator Evaluation of a Strapdown OPTAG Correlation Guidance System, by W. L. Steiner, Goodyear Aerospace Corporation, AFAL-TR-71-142, AD518471L, May 1971.

2. Laser Semiactive Strapdown Seeker Technology, by Dr. C. E. Kulas, Advanced Sensors Directorate, MICOM, AD 530579L, 30 April 1974.

3. Techniques for Generating Guidance Signals from Body-Fixed Sensors, Final Technical Report, by L. D. Holland and R. D. Wetherington, Georgia Institute of Technology, AD 725599, 09 February 1971.

4. Strapdown Laser Seeker Guidance Simulation, Final Report, by R. E. Gallagher, R. D. Ehrich, et.al., Rockwell International, June 1971.

5. Strapdown Seeker Guidance for Tactical Weapons, Final Report, by W. I. Emmert and R. D. Ehrich, Rockwell International, May 1978.

INTEGRATION OF DIGITAL AVIONICS COMPONENTS FOR GUIDED WEAPONS

by
A. M. Henne
Air Force Armament Laboratory (AFATL/DLMM)
Eglin Air Force Base, Florida 32542
USA
AND
D. W. Geyer
General Dynamics Convair Division
San Diego, California 92138
USA

ABSTRACT

The current approach for guided weapon avionics is to use custom digital computational elements connected together with large cables. If these computational tasks can be partitioned into common tasks, and if standard interfaces can be defined, it would promote interchangeable missile guidance and control components and enhance interoperability. The Digital Integrating Subsystem (DIS) Program is a current Air Force Armament Laboratory effort to establish these standards and procedures. The contractor is General Dynamics Convair Division.

In the Digital Integrating Subsystem concept, the total data processing requirements of a typical standoff weapon are met by utilizing a number of individual microcomputers that communicate with each other on a serial multiplex bus - the number of microcomputers being dependent upon the total data processing work load of the weapon. Each microcomputer is tasked to do calculations associated with a particular avionics function. Once the computations are completed, the results are "broadcast" on the multiplex bus. Each computer also listens for only the data it requires on the bus. This serial multiplex bus is referred to as the "Digital Integrating Subsystem Multiplex Bus" or DISMUX Bus.

The protocol and signal levels on the DISMUX Bus are well defined in a draft MIL standard. The draft MIL standard defines the electronic interfaces and also defines the straightforward data structures that are used for inter computer communication. When this standard is adopted, it will allow components built by different manufacturers to operate together with a minimum of interface coordination of either hardware or software.

The sixteen bit DIS computers have up to 64K words of memory, four standard interface cards, and are housed in 150 cubic inches. As the maturity of the various avionics subsystems develops, these computers could become embedded within the subsystem themselves and no longer exist as individual components.

Connection to the aircraft store's management bus is via a MIL-STD-1553B interface. Where the carrier aircraft is not equipped with a MIL Standard 1553B interface, a set of analog/discrete/digital interfaces peculiar to the signal and data protocol of the host aircraft can be easily implemented in a single input/output card of one of the DIS computers. This single DIS computer then transmits any of the aircraft interface data to any of the other DIS processors which may require information from the host aircraft.

All operational software is being written in the Air Force Standard High Order Language, JOVIAL J73.

This paper presents system design, details on the interface characteristics, and a progress report on the construction of brassboard units.

1. INTRODUCTION

Conventional standoff missiles suffer from many of the same problems which are present in today's aircraft. These problems relate to the large number of cables and wires which are required to transmit the various guidance signals about the vehicle, and the proliferation of custom computers with their programs written in many different assembly languages. This situation has caused a situation where it is almost impossible to have meaningful competition in missile modification contracts. Software maintenance is extremely difficult and it severely hampers the ability to integrate components from various NATO countries. The Air Force aircraft avionics community has addressed these areas by the adoption of several MIL standards; namely: MIL-STD-1553B, MIL-STD-1589A, and MIL-STD-1750. The basic concepts presented in these aircraft avionics standards can be used as guides by missile avionics designers in many common areas of concern.

There are, however, significant differences between the aircraft and tactical missiles which would prevent the complete adoption of the aircraft standards by the missile designers. The Digital Integrating Subsystem (DIS) Program has evaluated these aircraft standards and adapted MIL-STD-1553, which describes the aircraft time division command/response Multiplex Data Bus, for missile use. MIL-STD-1589A, which describes the JOVIAL language, is appropriate and has been adopted in its entirety.

MIL-STD-1750, which describes a government-owned instruction set architecture, was evaluated in detail. However, at the time the Digital Integrating Subsystem contract was let, no contractor found it technically feasible to be able to implement the MIL-STD-1750 instruction architecture in the small amount of space available for a federated processor. The use of custom hybrids was deemed inappropriate to the ultimate development of a very low cost, easy to compete, federated processor. For that reason, our selected approach utilized a commercial microprocessor chip that would ultimately be available in a military version with appropriate quality levels. At the point in time the MIL-STD-1750 instruction architecture becomes

vailable on a single microprocessor chip, the adaptation of the chip into the DIS processors would be a reasonably straightforward task. When that chip is available, it will be evaluated for missile use.

2. COMPUTATIONAL REQUIREMENTS

Tactical standoff missiles being designed today have surprising computational requirements. In fact, it is easy to find missile designs where the tasks to be done exceed those of the central computer on an aircraft. This is due to the tasks such as navigation, target location and classification, guidance, homing, and fusing which must be done without the aid of a pilot. Early attempts at standoff missile computer design used a single computer to control and monitor the function of several analog subsystems. As the advantages of all-digital systems became obvious, manufacturers expanded and sped up their central computers to handle more functions.

The ownership of a complex and ultra-fast central computer provides significant benefits for its manufacturer at a much higher ultimate cost to the government. These machines usually are custom built for a particular missile. Therefore, spare parts, expansions, and modifications to the computer must be sole sourced to the designer. Also, it is unlikely that a high order programming language (HOL) compiler is available for this custom computer. If no HOL compiler exists, then it is mandatory to program the computer in its custom assembly language. It is very difficult to maintain or modify someone else's assembly language program. If that assembly language is not common or familiar to those maintaining or modifying the weapon software, then any change must be sole sourced to the original programmer. Even though it is undesirable from a customer's viewpoint to use assembly language, the use of a central computer may also necessitate the use of assembly language programming due to the limited amount of available processor time when compared to the large processing load.

A typical central computer may be required to run at two million operations per second or more. To reach this speed today requires a bit-slice or similar design approach. Most assembly languages developed for commercial computers of this type are copyrighted and not available for competitive procurements. Another problem is that a high order language compiler that is within 10% of being as speed and memory efficient as an assembly language program is usually very expensive and beyond the capability of either the government or the industrial contractor to fund for a custom central computer application. Since different manufacturers are prohibited, from the copyright infringement point of view, from using each others instruction sets, each manufacturer attempts to build his own unique architecture. This proliferation of architectures would also require a proliferation of compilers if the Air Force attempted to program these multiple architectures in the same high order language. Maintenance of these many compilers would also be a prohibitive task.

An alternative to the use of a central computer is to distribute the tasks to several independent computers which may operate at lower speeds. These computers may be tightly coupled where they share memory or some other component and carry out program tasks in full knowledge of the activity of the other tasks involved, or they can be loosely coupled over some input or output port and have little knowledge of the activity, or even the existence of other tasks.

Loosely coupled or federated computers have the advantage of modular programs which are not affected by programs in the other computers. A program need only know what inputs to expect and what outputs to provide. With this modular arrangement, one program can be changed without affecting the other programs. This separation may be implemented with a central command computer, or it may be implemented with a round-robin protocol.

Size, weight, power, and cost are critical concerns to a missile which must be designed within the constraints of range, number carried on the host aircraft, autonomous operation, and the eventual destruction of the vehicle. For this reason the addition of a command computer with its rather large command-response program is not economically justified. Therefore, the federated approach was selected.

One goal of the DIS Program is to provide standards and specifications for modular computers and their interfaces to promote the interchangeability and interoperability of the subsystems used in future tactical missiles. If a computer has standard hardware and software interfaces, then a new subsystem meeting these standards can easily be exchanged for an existing subsystem.

3. ADVANTAGES OF DIS

By using the DIS approach to standard interfaces and standard interconnection of federated computers we can achieve significant benefits of modularity and interchangeability of components. This allows us the opportunity to use components from one manufacturer in a missile built by another. Thus, we can have full partnership with our NATO neighbors, with each country able to contribute the technology it best knows. For instance, a terminal seeker with a DIS interface built in Europe can be easily electrically and data structure compatible with a missile built in the USA. If a new technology then makes it possible to significantly increase the seekers accuracy, new seekers, built by a manufacturer in a third country could be easily interchanged for the previous ones.

The DIS approach allows components previously used in a missile to be used in the design of a new missile. This can significantly reduce the cost and the time required for the new design.

Figure 1 shows a configuration of the guidance electronics of a typical long range standoff weapon. Here we have shown five computers; the number and their function depend upon systems engineering decisions made at the time the missile is designed. One of the required concept design studies of the weapon will determine the number of tasks to be done and the logical grouping of those tasks. This study also determines the partitioning of the required tasks considering the partitioning of other similar sized missiles so that advantage can be taken of existing components and programs. The partitioning of the tasks shown below assumes the following activities in each computer. (A key point to remember when reading each of the tasks is that, in the DIS concept, the operating system in every computer is the same - only the application software is dependent upon the task assignment of a particular processor).

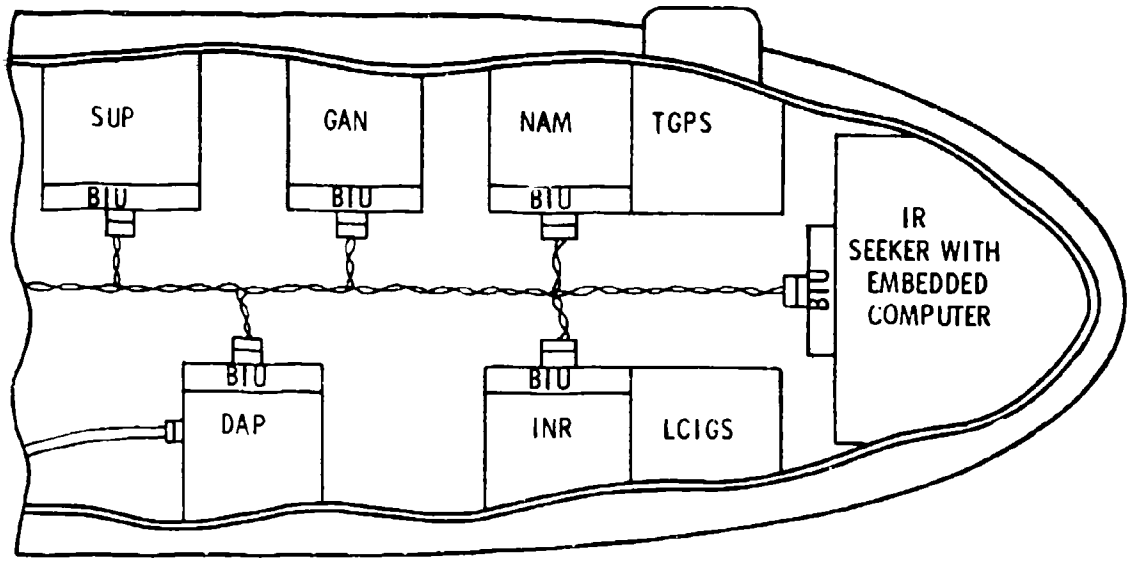

Figure 1

SUP - Supervisor Computer - This computer is tasked with communicating with the host aircraft and translating messages going to or from it. The SUP computer also handles engine controls, telemetry (if applicable) and fusing functions. In the DIS concept, each airborne computer contains an operating system that can drive many independent software tasks. These tasks can be set into execution either based on time, event, or data supplied to the processor. The software in the SUP computer just described would include all of the software necessary to interface the signal protocol of the host aircraft (usually one task) and rebroadcast any data needed by other computers on the bus. Other individual software tasks would then handle the other functions mentioned. In most missiles this computer may be combined with the Digital Autopilot Computer.

INR - Inertial Reference Computer - This computer interfaces to the inertial measurement unit (IMU) and performs the calculations necessary for the strapdown algorithm. The INR computer operates in conjunction with the guidance and navigation computer when operating in the Unaided Tactical Guidance (UTG) mode which is being discussed in another paper. The software in the INR and GAN computer are dependent upon the IMU and the mission type.

GAN - Guidance and Navigation Computer - This unit is responsible for giving the commands to alter the missile's direction so that a predetermined flight path is made to the target. This computer also performs the calculations necessary for the Kalman filter used with UTG. In addition to the software dependencies shown above, this software must contain mission dependent parameters.

NAM - Navigation Aiding Management Computer - This computer is included when there is an update source to correct the inertial position. If no update source is to be used, this unit can be removed from the bus. The NAM computer is used to perform those calculations which are required by the update source, such as calculating the position from time delay inputs from a Global Positioning System (GPS) or correlating inputs with TERCOM maps. The NAM software is mission and source dependent.

DAP - Digital Autopilot - This device is simply another computer or a task in the SUP programmed to issue FIN commands to cause the desired vehicle motion. The DAP software is dependent upon the dynamic characteristics of the missile.

Each of these devices is shown as a separate computer. If a subsystem has its own computational capability and can connect directly to the bus, this is not necessary. In the figure we have the terminal seeker connected that way. Each subsystem communicates over the DISMUX bus in exactly the same manner.

Let us now consider s ral alternative subsysters and their connection to the DISMUX bus.

If we replace the previous terminal seeker with a new one which also has an update capability, we simply disconnect the old update device and terminal seeker and connect the new device. When the new software is loaded, we are ready to begin checkout of the new configuration.

If we have a requirement to change the type of inertial measurement unit to one which also has its own computer, it need only have a DIS bus interface unit (BIU).

Probably one of the most significant advantages is the ability to change interface cards and software to interface to a new type of aircraft. Thus, if the required information is available at the missile connector, there is a powerful computer already on board to perform the necessary protocol transformation. This flexibility allows rapid transfers of a new weapon to existing aircraft.

A major advantage of the bus concept not immediately apparent is the ease of testing of a vehicle built around this concept. The ground checkout equipment is simply connected to the bus as one more computer terminal. If particular functions are missing during the test sequence, then the ground checkout system can be programmed to emulate more than one terminal on the bus and place the missing messages on the bus to facilitate the checkout of the remaining portions of the vehicle. The test set can also be programmed to operate in a totally listening mode simply monitoring the output messages on the bus and relating the state of the vehicle to the operator.

During test flights, the telemetry system can be easily connected to the DISMUX bus and not only telemeter the various analog and digital commands within the vehicle but also the data sets from the multiple digital processors as they put their "answers" on the bus.

4. DIS COMPUTERS

To validate the DIS specifications, a brassboard computer has been developed. The original goal of the DIS project was not to develop a standard computer, but the synergistic combination of the requirements and advances in the state-of-the-microprocessor-art have produced a computer which is very near to the leading edge of technology.

The DIS computer described here is a 150 cu. inch (2460 CC) unit (see Figure 2) which, if necessary, could be repackaged to a smaller size for production use in a mini missile. In its present design, which has no hybrids or custom devices, it can be used for intermediate and cruise-type missiles, remotely piloted vehicles, and aircraft.

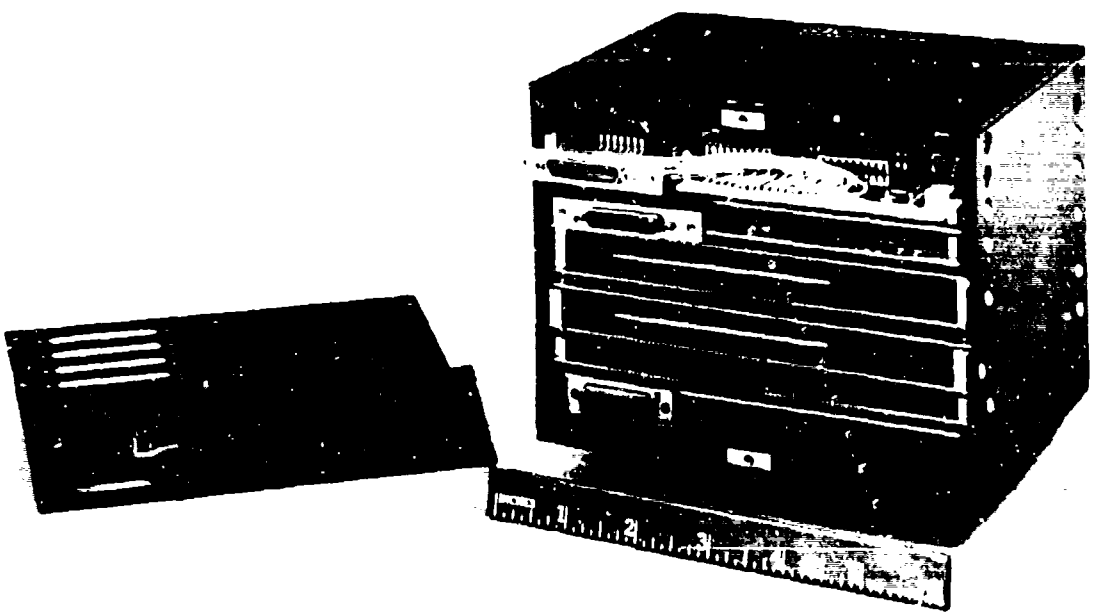

Figure 2

The driving force behind the design has been the use of commercially available parts which meet military specifications. The selection of all parts was based on their availability from at least two commercial sources.

The computer is based on the Zilog Z8002, 16 bit, single chip micro-computer. It can address up to 65K words of memory. The DIS computer volume, including case, power supply, 4 input/output (I/O) cards, CPU and full memory is 150 cu. in. (2460 CC). Standard I/O cards include parallel, serial, DMA, MIL-STD-1553B and DIS multiplex bus (BIU). Any combination of these cards, including 4 DMA cards, may be placed in the 4 I/O slots. An analog to digital and digital to analog card will be available soon. The complete unit

dissipates 50 watts of 28 volt power.

When executing a mix of instructions which are typical of missile guidance, its throughput is 350K operations per second. Zilog has committed to produce a 6 MHz and possibly a 10 MHz CPU chip. In fact, laboratory tests of the DIS computer have been run in excess of 6 MHz at a temperature of 80 degrees C. When using a 6 MHz chip, the DIS computer runs at 524K operations per second.

The Z8002 advantages stem from an expected production of more than one million devices per year, an additional US manufacturer (AMD), a European manufacturer (SGS), and a Japanese manufacturer (Sharp), a wide user base, many existing and planned support chips, and a large instruction set (416 instructions) designed for HOL use. At the time of this writing a free license agreement is about to be signed which will grant the US Department of Defense the right to use the Z8001 and Z8002 instruction set for weapon systems and their support systems. This significant agreement will allow other manufacturers to build Z8000 copies for weapons systems. This means that a common instruction set can be used for the range of computers from simple 4 or 5 chip devices to the very high speed bit-slice multiprocessors.

5. ALTERNATIVE CONFIGURATIONS

The missile shown in the previous figure appears fairly complicated when compared with many designs. The question then is, "Is DIS advantageous for smaller designs?" Our answer to that question is yes. Even if only one or two computers are required, the advantages of standard interfaces to subsystems and familiar program modules are very significant.

The DIS concept has been extended to a Class 0 machine for just such uses. Where the DIS computer described in this paper is expected to cost about $5,000.00 each, in production, the Class 0 computer is designed to cost less than $2,000.00. This type machine would be used in vehicles such as dispensers, smart bombs, and very small missiles. The Class 0 machine does not initially have the complete interface flexibility of a Class I or Class II DIS computer, but the interfaces it does have are of standard format. With only one computer in a vehicle, it is not necessary to have a DIS BIU for communication with other computers. However, a special internal connection allows a Class 0 computer to be attached to a BIU or 1553 Bus and thus communicate with any other subsystem or launch aircraft. Even though we have stripped down our Class 0 computer to its bare essentials, it is still able to be made totally compatible with other guidance subsystems.

The Class 0 computer uses the same CPU and is completely software compatible with the DIS Class I and Class II computers.

6. STANDARD INTERFACES

In order to facilitate the interchange of subsystems and computers, the DIS project is also developing standard interface specifications. The following represents an outline of these interfaces. Copies of the specifications may be obtained from the authors.

The parallel interface allows the transmission of 16 bits of information to or from the computer in parallel transfers. Handshake signals allow the peripheral device to notify the computer of the need to transmit data and signals which allow the computer or the peripheral device to indicate data reception. Data transfers can proceed at the rate of up to 250,000 transfers per second.

The serial transfer interface has similar handshake signals to the parallel interface, but data is transferred as a serial bit stream. This transfer of 16 data bits and a parity bit may proceed at a rate of up to 400,000 bits per second.

The direct memory access (DMA) interface allows transfer of 16 bit data words directly to or from memory, without processor intervention after initial setup. These transfers can occur at a rate of up to 500,000 transfers per second.

The MIL-STD-1553B interface is intended for use in data transfer to and from the carrier aircraft. This existing MIL Standard is mandated for use in all future US military aircraft. It is also contained in the proposed MIL-STD-1760 for aircraft store's management interfaces. Data transfers through this interface take the form of 16 bit data words with 3 synchronization bits and one parity bit. Serial transfers occur at a 1 MHz rate. There is extensive handshaking and command-response protocol.

The DIS serial multiplex interface is similar in word structure to that of MIL-STD-1553B, but the protocol is different. Each unit on the bus follows the end of transmission from the preceding known unit. In effect, each bus interface unit (BIU) knows who it follows (see Figure 3). When a BIU decodes the end of transmission from its predecessor, it then transmits. Each BIU's order of transmission consists of a beginning of message word, up to 32 data words, and an end of transmission word. If a given BIU has messages from more than one task, (each task normally has its own beginning of message word) then a new beginning of message word may be embedded in the string of data words. When the BIU has completed the transmission of all its messages or the maximum of 32 words, it sends an end of transmission (EOT) message. A part of this EOT is the number of the BIU which sent it. Each BIU connected to the bus is programmed to respond to the preceding BIU number. When a BIU receives its preceding EOT it is triggered to respond. If it does not have data to send, it simply transmits an EOT with its number in it, thus triggering the next BIU. By this scheme each BIU connected to the bus is given an opportunity to transmit during each round of the connected units. Since the data transmitted on the bus is already processed, the bus is normally lighted loaded (<5%) in every application analyzed to date.

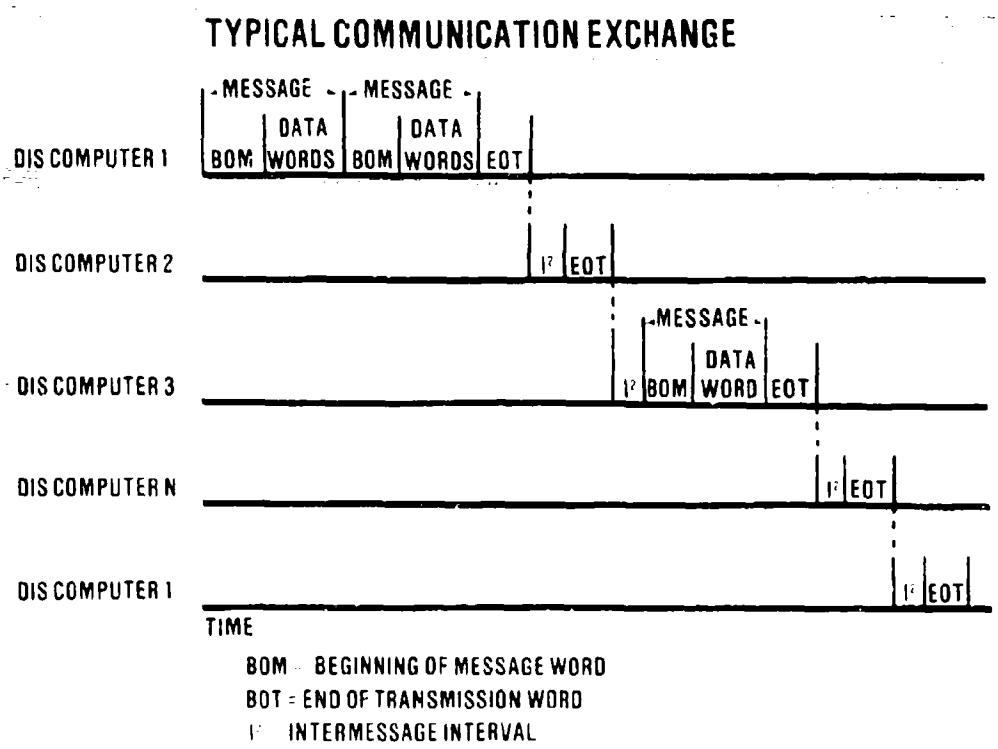

Figure 3

A message transmitted by one BIU may be captured by any of the computers on the bus (see Figure 4). When a program or subsystem is changed, other programs need not be changed so long as the new program requires and produces the same types of data. For example, the midcourse update subsystem may be changed from tactical TERCOM to GPS so long as both systems require inertial reference inputs and both output geographic position.

In the present laboratory and brassboard systems, a firmware program on one mux interface card (not CPU interactive) checks to determine if each BIU on the bus transmits in sequence. If one BIU does not respond for any reason, then this supervisory BIU restarts the loop. Each BIU performs without processor intervention to place desired messages in memory before interrupting the CPU.

This scheme, referred to as round-robin-passing-protocol, was developed through a joint effort of the Armament Laboratory and the Charles Stark Draper Labs. It has been validated in laboratory tests at Eglin AFB, and is now being tested in flightworthy units by the contractor, General Dynamics Convair Division. General Dynamics has found the implementation of the DIS round robin passing protocol to be extremely straightforward and easy to learn. The implementation of the bus interface unit takes only about 30 electronic components. Tests to date indicate an essentially error free environment is easily achieved on the direct coupled DISMUX bus (early BIU logic designs exhibited a bit error rate of less than one in ten to the eleventh transmitted bits).

Round-robin protocol has been shown to be more efficient than command response. This is important when navigation data are being transferred. More efficiency is also achieved by eliminating the need for a computer to run the executive program. Round-robin protocol is also more advantageous than contention schemes because of its near 100 percent probability of message reception.

An even more relevant point regarding the round-robin passing protocol is that the housekeeping and timing problems associated with developing bus controller software are completely eliminated. Since each processor outputs answers, when computed, onto the bus for reception by any desired user, the using program always has access to the latest possible data since it will usually be in a "wait" state awaiting receipt of the latest data set. The operating systems in each individual computer provide the double buffering between the bus interface unit message decoding function and the application program using function. No task in any computer has to be interrupted to transmit data to, or to receive data from, another application task. This is a significant software development (and missile integration) advantage.

DIS INTER-COMPUTER COMMUNICATION CONCEPT

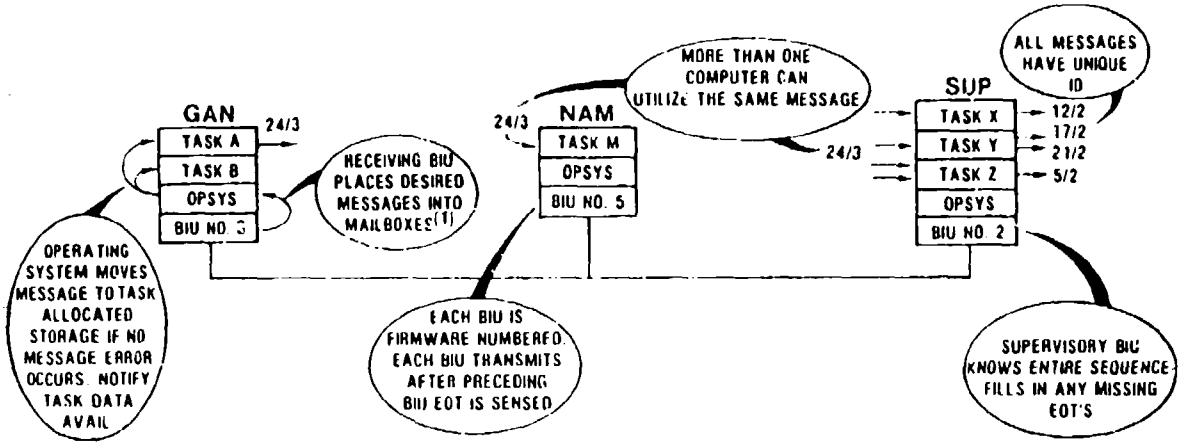

(1) Desired messages firmware programmed. 64 mailboxes per computer total for all I/O cards. EOT interrupt to operating system at message end

Figure 4

7. SOFTWARE

All the software for the DIS computer is being written in JOVIAL J73 according to MIL-STD-1589A. This includes a JOCIT compiler hosted on an IBM 360/370 and the operating system in the DIS computers. The linking loader and assembler are hosted on a diagnostic station based on the PDP 11/34. A JOCIT code generator for the 11/34 (RSX-11M) is also provided. A code generator option produces Z8000 code which can be loaded through a commercial Z8000 development station.

The DIS project is closely following the development of ADA, the new standard HOL. The DIS computer is one of the first targets for the Air Force ADA compiler.

The operating system of the DIS computers is as relevant to the federated computer concept as are the other elements mentioned previously. The operating system for the DIS computers handles all interrupts, processes all data requests (both intra computer and inter computer), schedules the multiple tasks within a computer (up to 256 separate tasks), and formats all of the input/output messages going to and from the input/output cards. The operating system also includes the software necessary to interface with the monitor software resident on the ground checkout station so that, while an airborne task is in the process of executing, memory calls can be observed and/or modified, a capability which is absolutely necessary when developing real time operational software. The monitor software in the DDS in conjunction with the operating system can also start, stop, single step, and observe any of the registers in the Z8000 microprocessor.

8. STATUS

The Air Force is now under contract to General Dynamics to produce 25 flight qualified DIS computers for use in a flight demonstration test program. Units are also being procured to use in hardware-in-the-loop simulations in the Armament Laboratory's simulation lab. Two complete diagnostic stations will also be delivered. These units are scheduled to be delivered over a seven month period starting in July 1980.

The contract also includes JOVIAL code generators for the DIS computers and diagnostic station to be delivered in November, and a complete operating system and linking loader to be delivered at the same time.

The specifications for the standard interfaces, the DIS system and the DIS computers have been published.

9. CONCLUSION

The Digital Integrating Subsystem is attempting to facilitate the modularity of tactical guided weapon electronics through the use of standard interfaces. These concepts are now being tested. This project should simplify future design and modifications of missile electronics, and promote interoperability of subsystem components.

INDUSTRY LOW-COST INERTIAL GUIDANCE SYSTEM DEVELOPMENT

by
Warren K. Stob
Lear Siegler Inc, Grand Rapids Mich
and
Dr. Thomas K. Wu
U.S. Air Force Armament Test Laboratory, Eglin AFB, Florida

SUMMARY

The necessity for an adverse weather, standoff launch and leave capability in both powered and unpowered guided weapons has led to development programs for a low cost inertial guidance subsystem by the United States Air Force (USAF). The subsystem, initialized via a prelaunch maneuver sequence to permit transfer alignment and inertial sensor calibration, is used to provide midcourse inertial guidance to a terminal acquisition basket or it can be used with periodic updates provided by other subsystems such as Global Positioning System (GPS), Radiometric Area Correlator (RAC), or Terrain Contour Matching (TERCOM) for improved accuracy on extended range missions.

This paper describes the history of the Low Cost Inertial Guidance System (LCIGS) concept development and the design features of the Industry LCIGS configuration.

HISTORY AND INTRODUCTION

Two programs were initiated by the Air Force Armament Test Laboratory (AFTAL) in 1976 after previous surveys revealed that, although many missile guidance systems were available, none met the USAF performance and cost goals required for the next generation of standoff tactical weapons.

The first program, Tactical Inertial Performance Requirements Analysis (TIPRA), identified the requirements for a variety of tactical missions and quantified the inertial sensor performance requirements for a Low Cost Inertial Guidance System (LCIGS). [1, 2] The second program was the award of a contract to the Charles Stark Draper Laboratory (CSDL) to provide a nonproprietary baseline LCIGS design incorporating low-cost modular concepts with a Production Unit Cost (PUC) goal of $10,000 in F.Y.'76 dollars. CSDL also provided a baseline design for test equipment which permits rapid factory calibration and simplified depot level repair of the LCIGS.

CSDL chose to implement the LCIGS in a strapdown system configuration using mature single-degree-of-freedom rate integrating gyros and force rebalanced accelerometers of modest performance characteristics (1-to-5 deg/hr and 100-to-200ug turn-on to turn-on repeatability). The key feature of this baseline design included the utilization of imbedded microprocessors for sensor control, modeling, and data processing. This feature permits the use of multi-sourced sensors in the same system without impacting either electronic or mechanical interfaces or data processing. Thus, each proprietary instrument is specified to meet a normalized sensor module interface so that the highest cost elements in the system may be procured competitively.

The CSDL LCIGS Program was completed in 1979. The results of the program included a complete set of design specifications, a brassboard system configured for the GBU-15 glide bomb, and a set of Peculiar Support Equipment (PSE). [3, 4]

In 1979, AFATL initiated a program to demonstrate digital weapon guidance technology. The core of this demonstration is the Midcourse Guidance Demonstration (MGD) Program which will demonstrate an all-digital weapon concept. Within this context, LCIGS represents a central avionic subsystem providing basic functions for an integrated weapon system. The various associated AFATL subsystem developments and studies that include elements of this overall weapon concept are: Digital Integrating Subsystem (DIS), Radiometric Area Correlation Guidance (RACG), Tactical Global Positioning System Guidance (TGPSG), and Unaided Tactical Guidance (UTG).

To support MGD, the LCIGS Program entered the second phase of development in 1979 with the award of a competitively determined contract to Lear Siegler, Inc. (LSI) to validate the CSDL baseline concepts and deliver five systems for laboratory and flight testing.

Successful transition of the CSDL LCIGS technology and its aggressive PUC goals to the Industry LCIGS Program required the retention of several design concepts. These included use of digital gyro torquing; inertial sensor interchangeability; use of mature, low risk inertial sensors; sensor control and compensation via microprocessors; and compatibility with rapid system test and calibration features via the CSDL-developed PSE.

The transition was accomplished by a complete review of the design specifications and drawings for both hardware and software provided by the CSDL contract and by close coordination with the Industry LCIGS Associate Contractors for the UTG and DIS Programs (McDonnell Douglas Astronautics - St Louis, and General Dynamics/Convair - San Diego, respectively).

The transition also included added considerations to provide a modular design applicable to multiple weapons, use of MIL-approved parts, inclusion of a totally integral power supply and parallel autopilot output, incorporation of current technology microprocessors, a strong emphasis on low cost through application of advanced but demonstrated production techniques, and increased multiple source procurement of inertial sensors. A system design is now complete which maintains all features of the brassboard configuration in 25% less volume and 30% less weight while incorporating the integral 28 VDC power supply. A comparison of the basic design features are provided in Table 1; a functional block diagram of the Industry LCIGS is shown in Figure 1.

This block diagram illustrates that the Industry LCIGS retains a distributed processing architecture in two basic module functions. Within the gyro loop, angular rate is sensed, digitized, and preprocessed by the gyro processors imbedded in each of the three gyro channels. The gyro channel output, partially compensated $\Delta\theta$s, is transmitted to the service processor via a two-way parallel bus structure where the data is additionally corrected, formatted, and transmitted serially to the external DIS or PSE. In the accelerometer loop the acceleration is sensed, digitized via the analog-to-frequency (A/F) converters, stored in accumulators, and transmitted directly to the service processor for processing similar to that of the gyro channel.

The service processor, as the second basic processing module function, collects the inertial sensor data, and provides corrections to this data based on sensed temperatures and on electronics thermal characterization information stored in Electrically Alterable Read-Only Memory (EAROM). The corrected $\Delta\theta$s and ΔVs are output at a 100-Hz rate over the serial data channel. Additionally, the service processor outputs uncorrected $\Delta\theta$s and ΔVs at a 400-Hz rate for autopilot use, communicates with the gyro processors to initialize the system at power turn-on or reset, interprets and implements commands from the DIS or Peculiar Support Equipment (PSE), and controls sensor heaters for optimum warm-up and thermal stabilization.

The EAROM data base permits use of multi-sourced, moderate performance inertial sensors by allowing storage of specific correction terms and error coefficients for design parameters and empirically determined performance characteristics. This key feature of the LCIGS development provides system performance accuracy previously unobtainable from inertial systems utilizing sensors of this cost and performance classification.

The Industry LCIGS which has been designed for production is shown in Figure 2; a typical complement of inertial sensors which may be used are shown with it.

Table 1 - LCIGS Configurations

Item	CSDL LCIGS	LSI LCIGS
Volume	506 in^3 (8.3ℓ)	375 in^3 (6.1ℓ)
Weight	23.25 lbs. (10.5Kg)	16 lbs. (7.3Kg)
Power - Heaters - Operating	115V, 400 Hz: 1000 Watts Missile Inv.: 80 Watts	115V, 400 Hz: 500 Watts +28 VDC: 75 Watts
Thermal Design	Forced Air Convection and Conduction	Conduction
Angular Rate Input	±150 deg/sec.	±150 deg/sec.
Acceleration Input	±10g	±10g
Output Resolution		
Serial @ 100 Hz	$\Delta\theta$: 3 $\overline{sec.}$ ΔV: 1 cm/sec.	$\Delta\theta$: 3.3 $\overline{sec.}$ ΔV: 1 cm/sec.
Parallel @ 400 Hz	None	$\Delta\theta$: 3.3 $\overline{sec.}$ ΔV: 0.25 cm/sec.
Circuit Cards	13	8

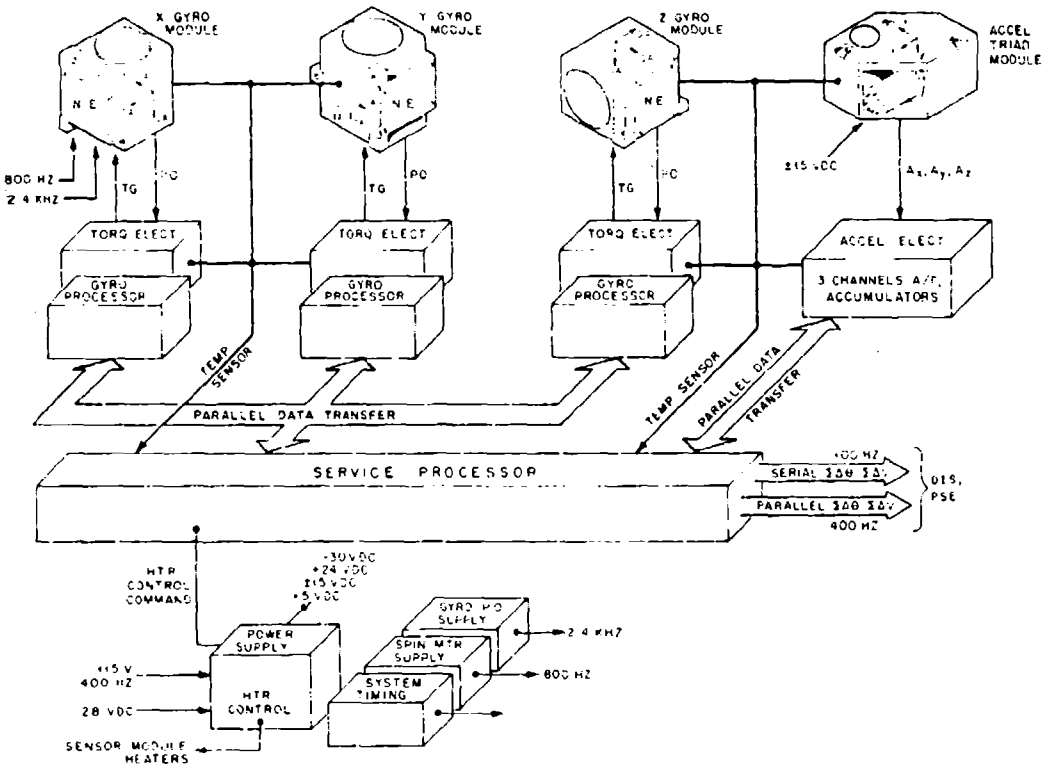

Figure 1 - Industry LCIGS Block Diagram

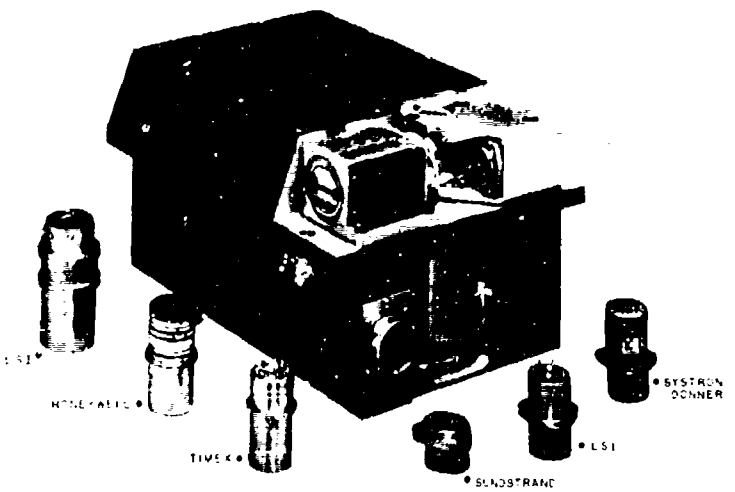

Figure 2 - LCIGS with Typical Inertial Sensors

MECHANICAL DESIGN DETAILS

CHASSIS DESIGN

The structural design provides maximum sensor performance during dynamic environments while maintaining functional modularity. The achievement of the desired high degree of modularity in the design is illustrated in Figure 3. A rigid aluminum casting with an integral mounting flange provides the primary structural element. The inertial

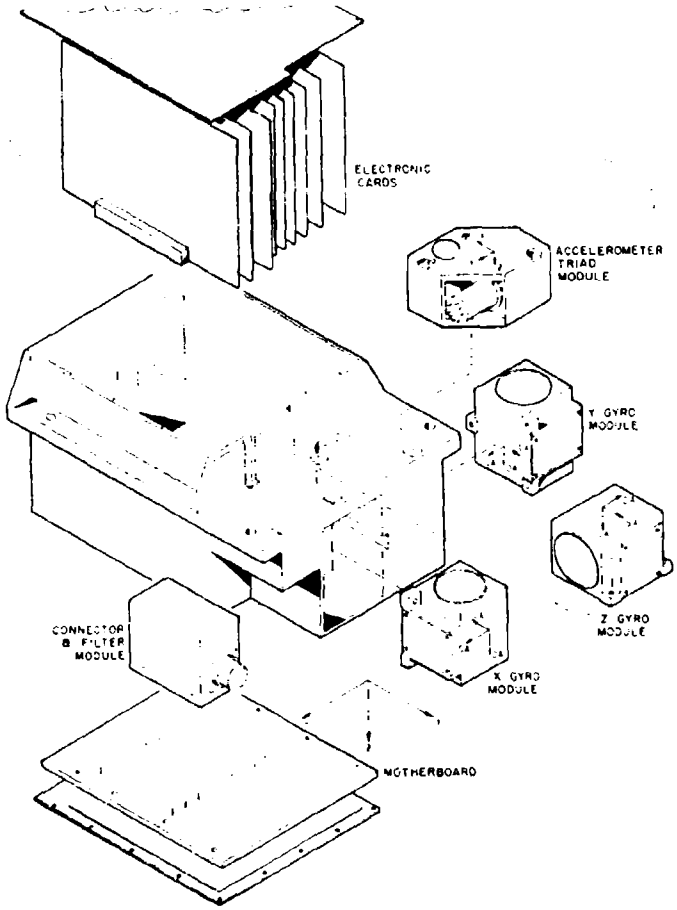

Figure 3 - LCIGS Structural Explosion

sensor modules are attached on one end of the structure; the electronic cards are contained within the structure as illustrated. Minimum repair and assembly time is accomplished by utilization of the plug-in assemblies.

Each of the three interchangeable gyro modules contains a rate integrating gyroscope, a thermal sensor, a module heater, and normalization electronics required to provide a standard electronic interface to the system.

The accelerometer triad module contains an orthogonal set of linear force-rebalanced accelerometers, thermal sensors, and a heater. It is installed on the structure adjacent to the Z gyro module.

The LCIGS electronics are packaged on eight printed circuit cards. The circuit allocation for each card was selected to optimize overall system size, functionality, and cost. The cards contain integral heat sinks and use either glass-epoxy or laminated aluminum core construction as dictated by thermal and reliability design criteria. The cards are interconnected with other system modules via a mother board located in the bottom of the electronic compartment. The card functional description is provided in Table 2.

THERMAL DESIGN

Key elements in the attainment of system performance goals include pre-launch thermal control for optimum inertial sensor error estimation and post-launch compensation of sensor outputs via the microprocessor. Ambient of -54°C to +71°C are specified for LCIGS with significant changes during a single period of operation. Most missiles have no environmental control system and limited power available during the free flight phase. These factors dictated the design of a fast warm-up mode with heaters using aircraft power during captive flight.

Table 2 - Circuit Card Function Allocation

Card	Function
A1	Gyro Torquer Electronics (2 Gyros)
A2	Gyro Torquer Electronics (1 Gyro), Torquer Common Logic, Gyro Pick-off Excitation and Output Sample/ Hold (3 Gyros).
A3	Gyro Processor (3 Gyros)
A4	Service Processor, Parallel I/O.
A5	Service Processor, Serial I/O, EAROM
A6	Accelerometer A/F Converter (3 Accels.), Converter Accumulators.
A7	System Timing, Spin Motor Supply, Temperature Sensor Multiplexer.
PSI	Power Supply

To optimize the system warm-up characteristics, a 234-node thermal model was generated. By simulation, using this model, the optimum size and placement of heaters was determined and the cooling characteristics during the post-launch period were defined. As a result, the heaters on the inertial sensors are controlled by the service processor to obtain a nominal 60°C LCIGS temperature within 15 minutes in a -54°C ambient. In high temperature environments, adequate cooling is provided conductively through the primary structure. Use of only MIL-approved parts provides adequate thermal margin for system reliability over all temperature extremes. Several features of the thermal design concept are noteworthy.

a. Elimination of a cooling fan. The selected mechanical configuration and the use of aluminum-cored electronic cards as determined by the thermal model permitted increased capability for conductive cooling of the electronic assemblies. In a +55°C ambient, the maximum circuit card temperature at the time of missile launch will not exceed +85°C.

b. Multimode heater control. Optimization of the transient response of the system is obtained by incorporating low range (-54°C to -20°C), mid-range (-20°C to +20°C), and high range (+20°C to +55°C) heater control algorithms in the service processor. The processor samples the actual temperature of the X gyro and the system ambient at approximately 10-second intervals and uses a predictor algorithm to control the power applied to the sensor heaters. This concept minimizes power consumption and provides both coarse and fine thermal control of the critical elements without the use of trim heaters previously employed. Provisions are also included to allow application of heater power without operation of the inertial sensors. This feature allows improved thermal stabilization of the LCIGS prior to initiating the transfer alignment sequence.

Even with this improved thermal control technique for limiting the dynamic range of operational temperatures, precision temperature compensation of the inertial sensor outputs is applied continuously to achieve the ultimate performance.

The service processor, using temperature data from each inertial sensor and it's corresponding electronics, and the measured inertial sensor thermal sensitivities, computes the bias, scale factor and loop gain corrections. These corrections are updated every 10 seconds. No correction algorithms are valid for the complete LCIGS operating temperature range but maximum compensation accuracy is obtained when the sensor and electronic temperature is between +10°C and +65°C.

INERTIAL SENSOR CHARACTERISTICS

Charles Stark Draper Labs (CSDL) prepared a generic procurement specification for the LCIGS inertial sensors. The specifications were based on the performance requirements determined in the TIPRA program, and were compiled by a survey of vendor-supplied data on available components that demonstrated both performance and a volume production cost history. These generic specifications are summarized in Tables 3 and 4.

Table 3 - Gyro Specification Summary

Characteristic	Units
Weight	10.5 oz (300 grams)
Input Power	26 VAC, 800 Hz, 2Ø Mtr, 8 VAC, 2.4 KHz PO
Drift Rates	
G-Insensitive: Absolute	100°/h
G-Insensitive: Turn-on Repeatability	4°/h
G-Sensitive: Absolute	25°/h/g
G-Sensitive: Turn-on Repeatability	4°/h/g
Random	0.15°/h (1σ)
Command Rate	
Continuous	80°/s
Maximum (2 Sec.)	150°/s
Accuracy: Turn-on Repeatability	300 ppm
Run-Up Time	30 Seconds (Max.)
Warm-Up Time	5 Minutes (Max.)
Environmental	
Temperature (Operating)	-20°C to +100°C
Temperature (Non-operating)	-62°C to +95°C
Vibration	MIL-E-5400, Figure 2 MIL-STD-810, 0.04 g^2/Hz
Shock	30 g's, 11 ms
Magnetic Fields	10 Gauss

Table 4 - Accelerometer Specification Summary

Characteristic	Units
Weight	3.5 oz (100 grams) (Max.)
Input Power	±15 VDC
Bias: Absolute	5 mg
Bias: Turn-on Repeatability	300 ug
Scale Factor Accuracy (Turn-On Repeatability)	300 ppm
Warm-Up Time	1 Minute (Max.)
Environmental	
Temperature (Operating)	-20°C to +90°C
Temperature (Non-operating)	-62°C to +90°C
Vibration	MIL-E-5400, Figure 2; MIL-STD-810, 0.04 g^2/Hz
Shock	30 g's, 11 ms
Magnetic Fields	10 Gauss

Within a basic class of sensors, however, design details of the various vendors result in small but significant variations in both cost and specific performance characteristics. To demonstrate sensor interchangeability, the Industry LCIGS will be tested with sensors from three different established vendors:

Gyroscopes: Lear Siegler, Honeywell, Timex
Accelerometers: Lear Siegler, Sundstrand, Systron-Donner

Extensive testing is in progress on the sensors from these vendors. The purpose of these tests is:

a. To establish the degree to which the sensors meet the specified performance and reliability requirements

b. To determine the parameter coefficients to be utilized by the LCIGS processors

c. To identify any significant performance differences which may allow selective procurement for the most cost effective solution to future mission requirements within the framework of the LCIGS configuration

d. To provide a standardized method to evaluate available sensors. For this purpose relevant tests such as gyro drift are being conducted in both analog and digital closure loops to establish correlation. This will allow analog mode acceptance tests by various vendors that will assure specified performance when the gyros are operated in the digital rebalance mode.

The testing of a large number of sensors over a long period of time is being accomplished by using commercially available Data Acquisition Systems (DAS). The systems, with specially prepared software programs, allow simultaneous tests of multiple sensors, automatic data reduction, printout of test results, and automatic control over the test equipment. A DAS and rate table for gyroscope evaluation is shown in Figure 4. The tests being performed on a minimum of three sensors from each vendor are shown in Tables 5 and 6.

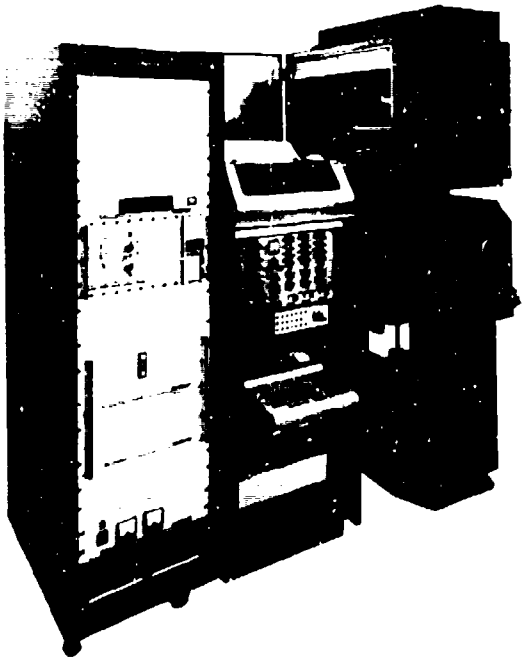

Figure 4 - Gyroscope Test Station

Table 5 - Gyroscope Tests

ITEM	MEASUREMENT
1. Mechanical Inspection	Dimensions, weight, seal integrity.
2. Electrical Inspection	Torquer, Pick-off and spin motor impedance, circuit DC resistance, insulation resistance, dielectric, magnetic flux leakage.
3. Warm-up Characteristics	Record output each 90 seconds for 1 hour at +30°C.
4. Spin Motor Tests	Starting and running power, run-up and coast times.
5. Polar Axis Tumble	Record gyro output at 1 degree intervals at an input rate of ±90 deg/min; plot output and calculate bias, mass unbalance, and σ of deviations from curve fit.
6. Cog Test	Determine drift repeatability after multiple controlled (± displacement) inputs are applied.
7. Torquer Scale Factor (TSF)	Record at rates between ±1 and ±150 deg/sec; compute TSF and second and third order non-linearity coefficients.
8. Drift Rates	Determine bias and mass unbalance values and repeatability using standard 6-position tumbles.
9. Drift Randomness	Record output once/sec for up to 5 hours; compute $\bar{X}$, σ, best fit trend line and σ of departures therefrom; compute power spectral density.
10. Temperature Coefficients	Perform selected tests at 9 temperatures between -20°C and +90°C; calculate scale factor, bias, mass unbalance, and axis alignment coefficients.
11. Vibration Sensitivity	Sinusoidal inputs at 5g, 20-2000 Hz; Random inputs @0.04 g^2/Hz, 20-2000 Hz; determine g^2 coefficient and overall vibration sensitivity.
12. Magnetic Sensitivity	Determine magnetic sensitivity to external fields of 10, 50, and 100 gauss.
13. Shock	Verify retention of performance stability after 18 shocks (30 g, 11 msec).
14. Long Term Stability	Determine performance stability of primary parameters over a 4-month period.

Table 6 - Accelerometer Tests

TEST	MEASUREMENT
1. Mechanical Inspection	Dimensions, weight, seal integrity.
2. Electrical Inspection	Insulation resistance, dielectric, magnetic flux leakage.
3. Warm-up Characteristics	Record output in 1 g position each 30 seconds for 1 hour.
4. Two-Position Tumble	Compute bias and scale factor from multiple tumbles at 15 VDC, 15.75 VDC and 14.25 VDC.
5. Threshold & Resolution	Determine input required to produce 50% of predicted output at both 0 g and 0.707 g, nominal.
6. 36-Position Tumble	Compute bias, scale factor and second and third order non-linearity coefficients.
7. Temperature Coefficients	Perform selected tests at temperatures between -20°C and +90°C, compute temperature coefficients.
8. Hysteresis	Compute scale factor and bias hysteresis after various temperature exposures in non-operating mode.
9. Vibration Sensitivity	Sinusoidal inputs at 5g, 20-2000 Hz; Random inputs at .04 g^2/Hz, 20-2000 Hz; determine overall vibration sensitivity including vibropendulousity coefficient.
10. Magnetic Sensitivity	Determine magnetic sensitivity to eternal fields of 10, 50 and 100 gauss.
11. Input Range	Apply ±10 g via centrifuge.
12. Shock	Verify retention of performance stability after 18 shocks (30 g, 11 msec.)
13. Long Term Stability	Determine performance stability of primary terms over a 4-month period.

ELECTRONIC DESIGN DETAILS

Design of the Industry LCIGS electronics was initiated after a review of the CSDL drawings, and an analysis of the deficiencies recorded during brassboard testing was completed [5]. Design changes were made to incorporate military-grade components, microprocessor capability unavailable to LCIGS at the time of brassboard design, an integral power supply, and an autopilot output. A simplified electronics block diagram with electronic card allocation is shown in Figure 5.

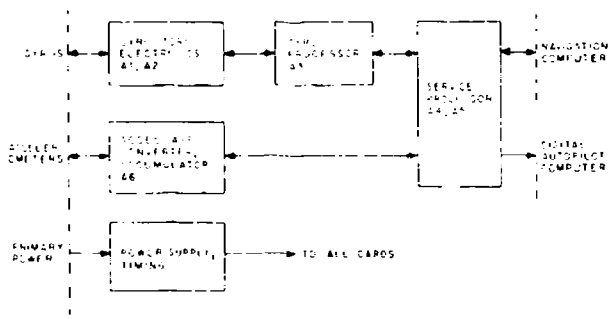

Figure 5 - LCIGS Electronics Diagram

Power Supply

The new self-contained power supply is a switching mode driven inverter type with an operating frequency of 50 KHz. The input section receives +28 VDC from an external source, provides filtering, and contains four-power field effect transistors (FETs) to switch the input voltage through the primary of a power transformer. The output section consists of multiple secondaries on a power transformer to provide the necessary internal operating voltages. Each output is full wave rectified and filtered. A separate bifilar wound secondary on the +15V output winding provides power and feedback for the power supply control section. The control section generates the pulse width modulation signals for the input section power FETs. The control circuitry also monitors the input line and makes instantaneous pulse width corrections to minimize output voltage variations.

The power supply also contains overcurrent shutdown circuitry to prevent damage during integration and testing with other subsystems.

Tests on the power supply breadboard confirm operation to specified limits over the complete temperature range with input voltages of +18 VDC to +35 VDC. Operation at higher input voltages is limited by power dissipation and attendent thermal considerations.

System Timing

The system timing electronics uses an 8.448 MHz crystal oscillator and low power Schottky-type logic to provide various timing and synchronization signals required within the system. The timing diagram is illustrated in Figure 6.

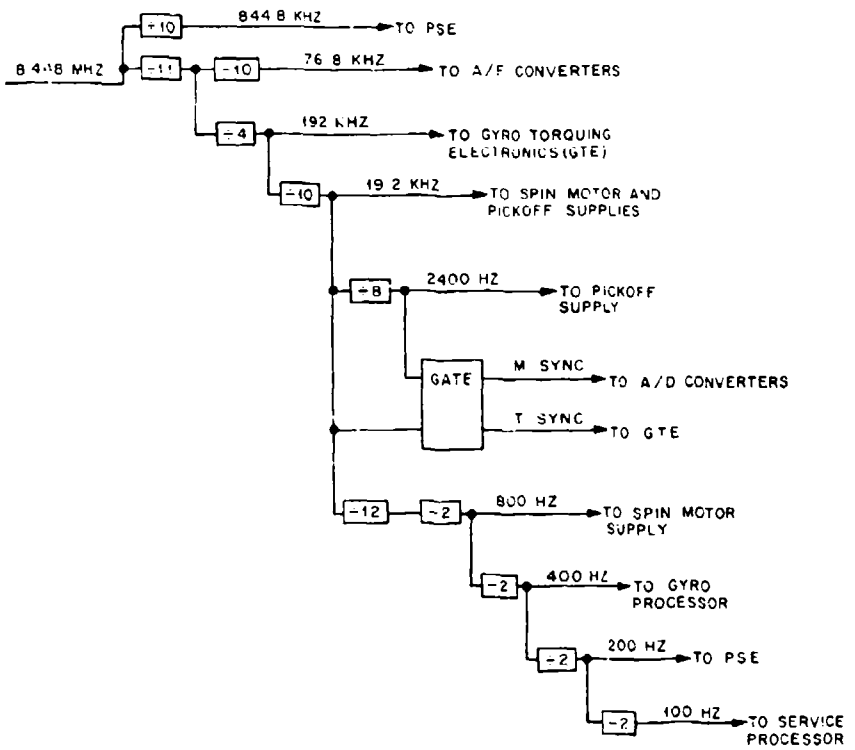

Figure 6 - LCIGS Timing Diagram

Spin Motor Supply, Temperature Multiplexing

The gyro spin motor supply operates directly from the LCIGS power supply rather than the missile inverter/converter. The spin motor supply is a push-pull driven transformercoupled inverter providing an 800-Hz, 26-volt square wave source for the three gyro spin motors. The supply also includes circuitry which, when externally commanded, determines motor operability by sensing back EMF during a 10 ms interruption of the motor excitation.

Temperature sensors are located on each inertial sensor, on each gyro torquer electronics assembly, and on the accelerometer electronics assembly. These provide 10 inputs to a 16-channel analog multiplexer and a current to the voltage buffer conditioner. Other inputs include power supply voltages and various built-in-test (BIT) responses.

The multiplexer output is fed to a 10-bit analog-to-digital (A/D) converter which is a part of the service processor. The converter outputs are used in conjunction with the EAROM stored coefficients to provide temperature corrections to the inertial sensor outputs, and as BIT to determine operational status.

Accelerometer A/F Converter

The three accelerometer analog-to-frequency (A/F) converters and respective accumulators are contained on a single circuit card. The design retains the basic features of the CSDL brassboard but mechanization with a nonproprietary hyrid constant current source allowed a 40% reduction in the physical size.

The converter, illustrated in Figure 7, is a pulse-rebalanced integrator in which the integrator output is maintained within pre-set limits by application of precise rebalance pulses to the summing point of the integrator. The rebalance pulses, which are precise in current and duration, represent the true integral of the accelerometer analog output. The pulses are accumulated in an 8-bit up/down counter which is read by the service processor.

An A/F inhibit command which disables the rebalance circuits is issued by the service processor during the counter read period to ensure that all pulses are read. The channel scale factor is 0.25 cm/sec/pulse.

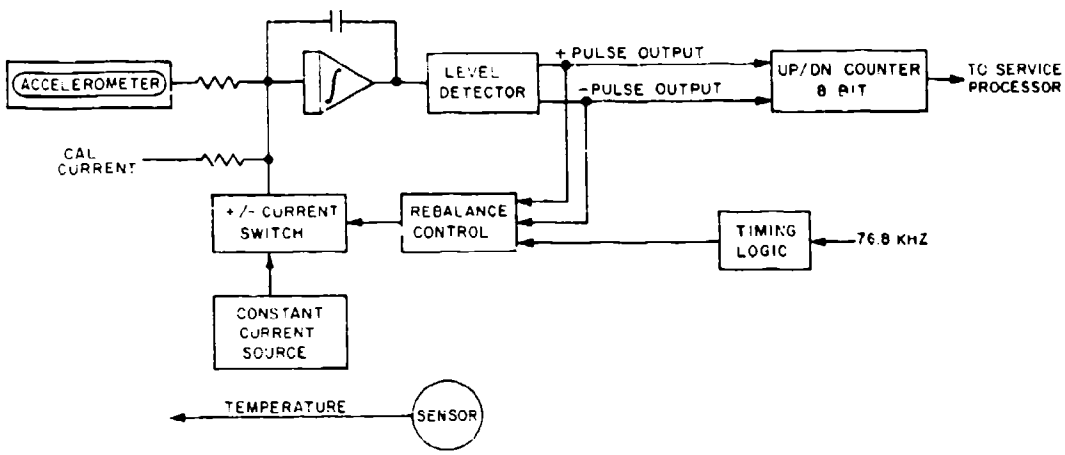

Figure 7 - A/F CONVERTER

Gyro Torquing Electronics (GTE)

The gyro torquing electronics (GTE), illustrated in Figure 8, filters, amplifies, and digitizes the gyroscope pickoff output at a 2.4 KHz rate. The digitized signal, a 10-bit A/D output, is read by the gyro processor which computes an 8-bit torque command each sampling period. The GTE, in response to this torque command, selects one of the two current rebalance modes, steers an H-bridge switching circuit, and applies precise rebalance current pulses to the gyroscope torquer.

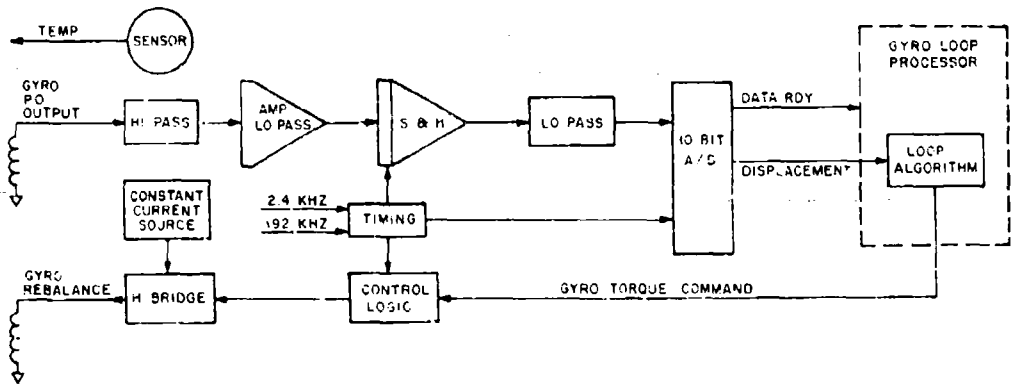

Figure 8 - Gyro Torquing Electronics

Review of the CSDL GTE design, including brassboard test data and its performance analysis [5] revealed gyro scale factor linearity errors of 80 to 800 ppm in the range of 30 to 120 deg/sec. Tests on a breadboard version of this design concept by LSI confirmed these errors, which are due to the effect of pulse rise and fall times. Even larger errors exist at the lower input rates typical of those encountered in Scorsby-type motion. One potential solution to this problem, within existing processor capability, would be to characterize the scale factor of each gyro module. This solution would, however, require extensive and costly testing of a gyro module with a specific GTE over temperature, and it would inhibit sensor interchangeability since the non-linearity is dependent on precise matching of the gyro normalization electronics and GTE to a specific gyroscope.

The LSI GTE design utilizes a precision dual-level (8:1) constant current source operating in a Pulse Width Ternary (PWT) mode. The design minimizes the sensitivity of gyroscope and electronics matching and eliminates the need for temperature characterization to maintain scale factor errors within acceptable limits.

In the design, each 416.7 μs torquing cycle is divided into 80 increments of 5.208 μs duration. Since a 1 ns equivalent error in pulse rise and fall time during a 5 μs pulse represents a large scale factor error, the gyro processor algorithm commands lower current (1X) and extended duration (41.66 μs) pulses. This reduces the error from the pulse rise and fall time to approximately 25 ppm. At input rates up to approximately 16 deg/sec, the low current extended duration pulses are commanded. At higher rates, the processor commands the higher current (8X) for the standard 5.208 μs pulse duration.

The gyro processor, by the gyro torque command word, controls the number of time increments the constant current source is gated to the gyro torquer, the current polarity, and the current level of 1X or 8X.

The GTE uses components with very low temperature coefficients for precision reference and current sensing and drives a dummy resistive load, located in the normalization electronics, during periods when the gyroscope is not being torqued.

Gyro Processor (GP)

The Gyro Processor (GP) card contains three separate and independent microprocessors which share a common clock driver and a parallel bus for communication with the service processor. The gyro loop functional block diagram, shown previously in Figure 8, illustrated that the gyro processor is integral to the closing of the total gyro loop. A functional diagram of the GP is shown in Figure 9.

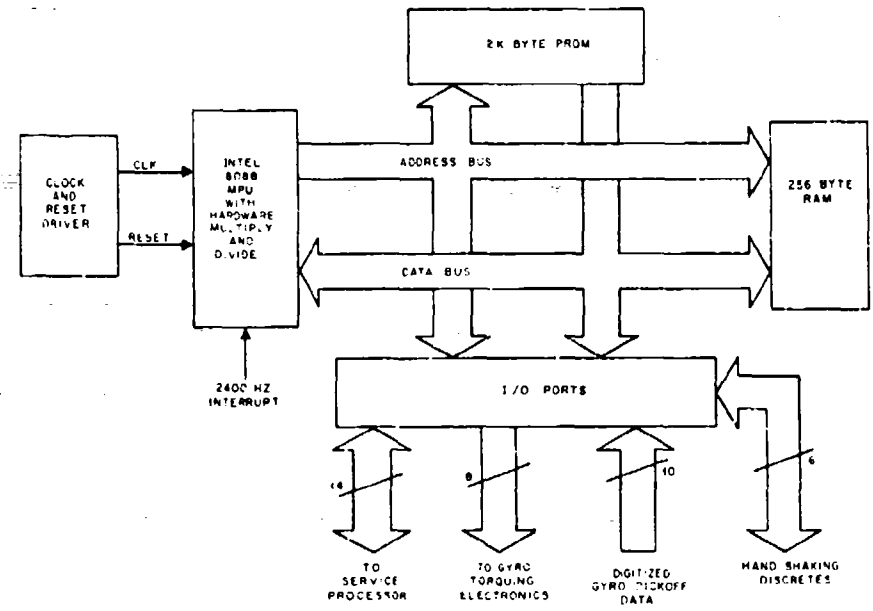

Figure 9 - Gyro Processor

The GP, in conjunction with mode commands and loop response data from the service processor, establishes the mode of operation and loop response characteristics. Inputs to the GP include the digitized gyro pickoff information from the torquer electronics card at a 2.4 KHz rate and loop gain coefficients from the service processor sampled at 10-seconds intervals.

Upon command from the service processor, the gyro processor operates the gyro loop in one of three modes: initialization, self-test (BIT), or the normal operating mode.

In the operating mode the control loop implements the same processing equation as that used in the brassboard [3]. The equation is:

$$T = K_1\theta + K_2\dot{\theta} + K_3\int \theta \, dt$$

where T = the torque command to the gyro torquing electronics;
and K_1, K_2, and K_3 are the proportional, rate, and integral gain coefficients.
The rate gain coefficient, K_2, is temperature compensated by the service processor. This compensation reduces limit cycling which was a problem in the brassboard LCIGS when gyroscopes from different vendors were used. The control loop has been implemented with an 80-Hz bandwidth with a damping factor of 0.3-0.6. The torquing command is an 8-bit word transmitted to the gyro torquing electronics at a 2.4 KHz rate.

The design is based on the use of the INTEL 8088 microprocessor which has a 16-bit internal architecture and an 8-bit bus structure. The processor also contains a 2K byte Programmable Read-Only Memory (PROM) for program storage and constants, and 256 bytes of Random Access Memory (RAM) for variables and scratch pad memory. The memory capacity and existing processor utilization levels are shown in Table 7.

Table 7 - Gyro Processor Utilization

MEMORY	CAPACITY	UTILIZATION
RAM	256	135
PROM	2048	1200
Time available is utilized 75%		

Service Processor

The service processor communicates with the missile system navigation processor across a bi-directional serial data interface (500-KHz bit rate). The output I/O structure is shown in Figure 10.

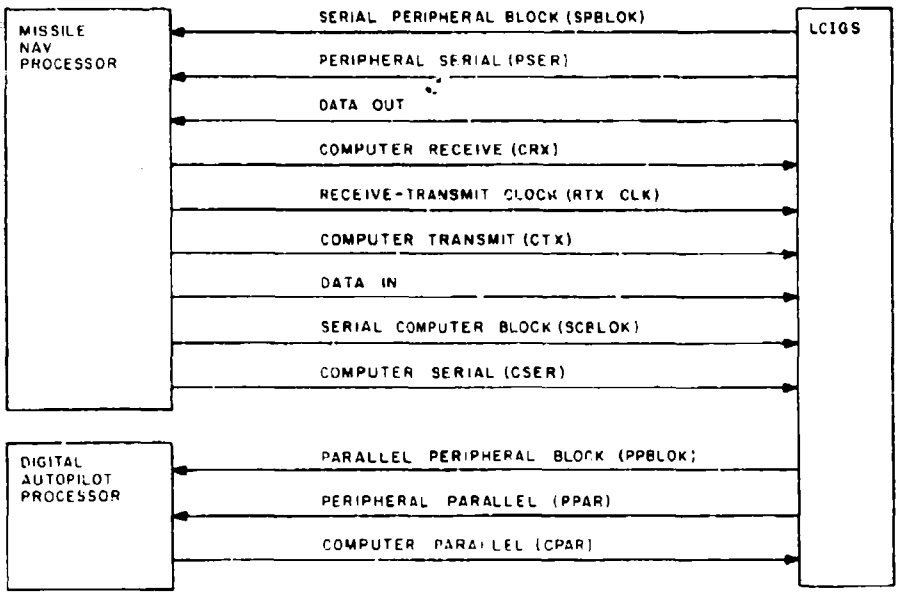

Figure 10 - LCIGS/Missile Processor Interface

A variable length block transfer protocol is used. The discrete SPBLOK (see Figure 10) and the pulse PSER signal that the LCIGS output must have priority servicing. The missile processor must respond after each PSER by clocking out two bytes of data plus parity using the CRX discrete and the RTX-CLK clock signal.

The missile navigation processor sequences block transmissions to LCIGS by signaling the SCBLOK discrete and pulsing the CSER signal. When the LCIGS is ready to accept the data transmission, PSER will be pulsed with the SPBLOK discrete reset. The missile processor will then clock two bytes of data plus parity to the LCIGS with the CTX discrete and the RTX-CLK clock signal.

The service processor communicates with the Digital Autopilot Processor (DAP) across an 8-bit parallel data interface. The service processor signals the DAP with the PPBLOK discrete and pulses the CPAR signal when data is ready for transmission. The DAP can then clock out raw sensor data ($\Delta\theta$ x,y,z and ΔV x,y,z) using the CPAR discrete. This data transfer occurs at a 400-Hz rate. This high rate parallel output is required for stability of the inner loop missile control system.

Output transmissions from LCIGS include the preprocessed and formatted sensor data ($\Delta\theta$ x,y,z and ΔV x,y,z) at a 100-Hz rate. Other output data includes gyro g-sensitive drifts, output axis coupling, anisoinertia, and alignment parameters, as required. The missile processor may also request specific LCIGS data (e.g., memory status), commands the start-up sequence, and initiates BIT functions.

The PSE functions through this I/O to implement test and calibration of the LCIGS. After calibration, the PSE can command the service processor to load the EAROM with all of the new characterization data used to model the sensor errors.

The service processor, illustrated in functional form in Figure 11, is also mechanized with the INTEL 8088 microprocessor. Programmable read-only memory and random access memory are also used.

Remaining hardware components include serial I/O, parallel I/O (autopilot), EAROM, and a 10-bit A/D converter.

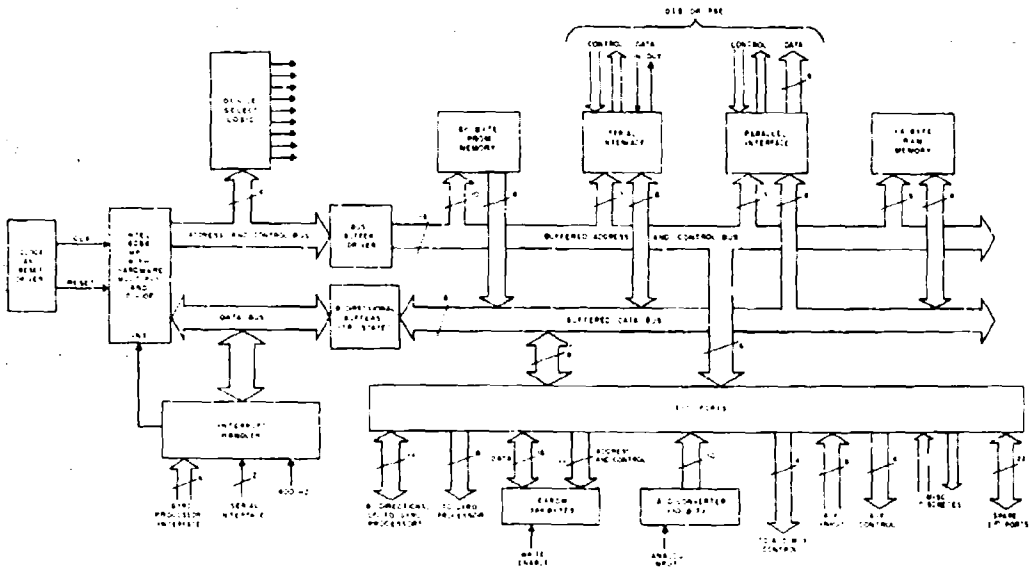

Figure 11 - Service Processor Functional Diagram

The memory capacity and existing processor utilization levels are shown in Table 8.

Table 8 - Service Processor Utilization

MEMORY	CAPACITY	UTILIZATION
RAM	1024	750
PROM	6144	3500
EAROM	384	300
Time available is utilized 70%		

PECULIAR SUPPORT EQUIPMENT (PSE)

System level test equipment for LCIGS, designated PSE, was developed by CSDL in parallel with the brassboard LCIGS design. The PSE is designed to provide stand-alone capability to support factory calibration, factory acceptance, and field maintenance requirements. The design of the Industry LCIGS PSE maintained all features of the CSDL PSE. Limited physical and electrical modifications were necessitated by changes in the interface (integral power supply, and parallel output).

The new LCIGS PSE hardware configuration is shown in Figure 12. The magnetic tape system is a Digi-Data 1730 MAXIDEX featuring 9 tracks with a 45-inch-per-second tape speed and 800-bytes-per-inch packing density. It provides a mass storage media for all PSE test programs and LCIGS test data. The Burroughs SII 1240-200 Display is a microprocessor-based flat gas plasma panel featuring 480 alpha-numeric characters in 12 rows with a maximum data rate of 1000 characters per second. This display and the keyboard are used interactively by the operator to initiate and progress through the test sequences. A DECWRITER, the master control device for the RSX-11S operating system, can also be used to initiate test programs and provide a hard copy of the test results.

A PDP-11/34A-ME computer provides execution and control of the PSE test programs and LCIGS data reduction programs. It also controls the PSE/LCIGS data interface, keyboard, Burroughs display and the magnetic stripe reader/writer. The computer is a floating point processor with 64K words of core memory and 1K words of cache memory. Cycle time is 1 us and 250 ns for the core and cache memories respectively. All computer software has been coded in Fortran using the RSX-11S operating system. The software includes algorithms to provide LCIGS performance testing in both attitude and pseudo-navigation modes.

The magnetic stripe reader/writer provides the interface to a 1024 byte magnetic stripe card which contains the system identification and inertial sensor characterization data. These data, essentially the same as that contained in the LCIGS EAROM, are used by the PSE to verify the EAROM contents and are updated by the PSE at each LCIGS calibration or repair. Card information includes a system identifier, a vendor identifier and serial number for each inertial sensor, calibration and thermal characterization data, and sensor dynamic compensation parameter.

The LCIGS calibration software developed by CSDL, emphasizing minimum demand on operator skills, has been retained in this PSE configuration. The program uses the LCIGS interactively by using six-position accelerometer data to establish the reference frame for gyro calibration. Additional positions are used for the entire system calibration with a goal of obtaining accuracies of 0.1 deg/hr and 100/ ug in 30 minutes. Diagnostic programs are also included that monitor LCIGS self-tests or initiate special tests to enhance fault isolation to a replaceable module.

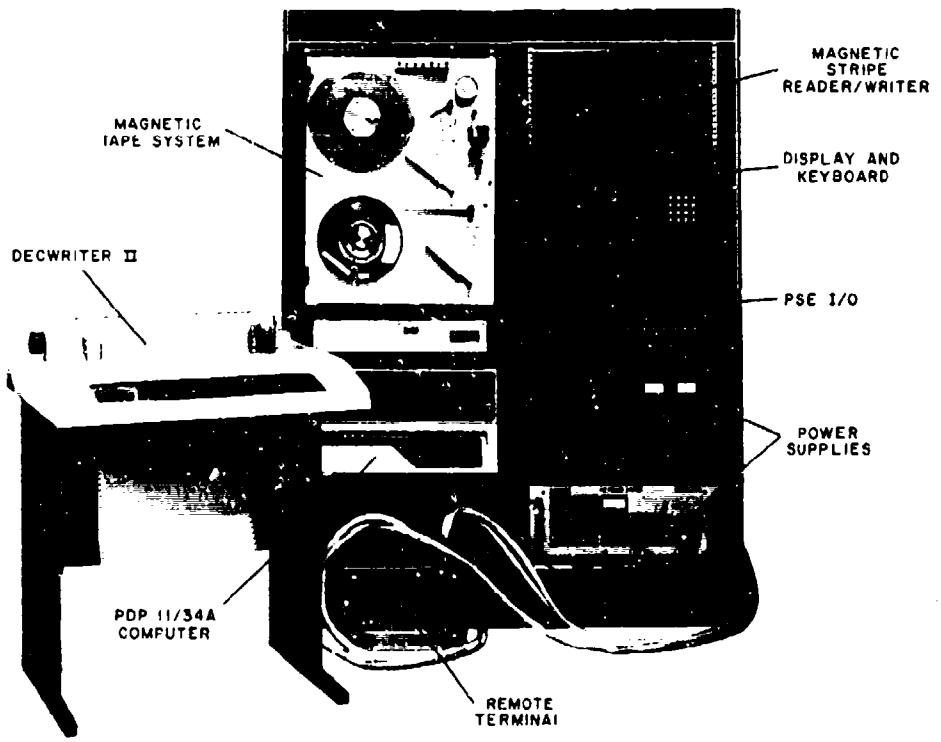

Figure 12 - LCIGS Peculiar Support Equipment

LIFE CYCLE COSTS (LCC)

USAF studies have shown that the decisions made during conceptual and advanced development programs basically define the Life Cycle Cost (LCC) of equipment [3]. Essential to the successful transition of the brassboard LCIGS concept to Industry was the retention of the Production Unit Cost (PUC) goal. The PUC goal of $10,000 in FY '76 dollars for a 2000-unit production run at 1000 units per year was a key factor in defining the basic design concepts. The PUC factors used in the CSDL brassboard design were thoroughly reviewed by LSI to determine if current technology allowed cost changes within the framework of the LCIGS concept. The review validated the significant contribution of the inertial sensors to the overall system cost and re-emphasized the necessity to procure only those sensors with proven performance and cost history. Multiple source procurement of these sensors provides PUC credibility by using price information on a normalized specification from established vendors. Additional cost factors, which are limited to the Industry LCIGS, include design changes to improve system applicability to a broader range of missiles (integral power supply and elimination of a form factor necessary for the CBU-15 Glide Bomb), and elimination of commerical grade electronic components.

In the design evaluation phase, the basic system modules were identified and cost targets were established to provide each designer a tool for evaluating alternate approaches. The Design-To-Cost (DTC) and LCC disciplines were combined to emphasize the reality of "total cost" considerations. The design review of each Industry LCIGS module considered contributions from Reliability, Maintainability, Logistics, Packaging, Manufacturing, Quality Control, as well as the actual Module Design Engineer, to assure that design trade-offs were accomplished and that the design selected represented an optimum balance between cost and performance. As the system design matured, previous cost targets were updated as necessary to attain the system PUC.

The current PUC estimate for the LCIGS configuration is summarized in Table 9 by major categories. The values shown for the CSDL brassboard are obtained from Reference [5] and include costs of military grade components. All values are adjusted to FY '79 dollars.

Table 9 - Category Cost Allocation FY '79 Dollars

	CSDL LCIGS	INDUSTRY LCIGS	
		PRESENT	GOAL
Gyro Modules (3)	$6,002	$5,900	$5,480
Accelerometer Module	$3,915	$2,860	$2,700
Electronics	$3,936	$4,600	$4,260
Assembly & Test	$1,879	$2,560	$2,040
	$15,732	$15,920	$14,480

The evaluation of Life Cycle Costs must include consideration of Reliability and Maintainability factors so that the Operation and Support (O & S) costs can be determined. The Industry LCIGS reliability prediction based on MIL-HDBK-217B and Ref [6] is shown in Table 10. This prediction was used with other necessary acquisition and deployment parameters in the Air Force Logistics Command Life Cycle Cost Model. The model for the LCIGS program assumes an all-up-round maintenance concept with missiles returned to a Depot for repair, and a quantity of 18,000 missiles for a 10-year period. The results show that O & S costs are less than 4% of the initial acquisition costs.

The Industry LCIGS is also required to have a Mission Completion Success Probability (MCSP) of 0.9800 under environmental conditions of a +55°C ambient, one year storage, and mission operating time of 1.6 hours. The predicted MCSP is 0.9859.

Table 10 - LCIGS Reliability Prediction

SUBASSEMBLIES	NON-OPERATING FAILURE RATE (x 10^{-9})	OPERATING FAILURE RATE (x 10^{-6})
Gyro Torquing Elec. (A1/A2)	273.727	25.068
Gyro Processor (A3)	80.604	72.890
Service Processor (A4/A5)	214.947	109.742
Accel. A/F (A6)	122.625	9.559
Timing (A7)	133.185	9.0106
Power Supply (PS1)	82.844	5.915
Gyros	435.513	155.0934
Accelerometers	89.820	25.860
Misc. System	105.150	40.064
Total	1,538.415	453.202
		$MTBF_O$ = 2207 Hrs.

PERFORMANCE

The LCIGS performance requirements have been established by a series of Air Force-funded studies to determine the lowest cost inertial guidance system that will provide sufficient missile guidance accuracy in an aided-inertial midcourse guidance mode. The Tactical Inertial Performance Requirements Analysis (TIPRA) programs performed by MDAC and Honeywell quantified the inertial sensor performance requirements for planar-wing and cruciform-wing GBU-15 Glide Bombs, and for a powered standoff missile. A prelaunch transfer alignment and calibration maneuver consisting of 5.5 minutes of level flight with half-S turns was used. Post-launch configurations using updates from Radiometric Area Correlation (RAC), Global Positioning System (GPS) as well as autonomous strapdown inertial were analyzed with inertial sensor performance ranges of 0.01 mg to 100 mg and 0.01 deg/hr-to-10 deg/hr turn-on-to-turn-on repeatability for accelerometers and gyros respectively. A Kalman filter was used to estimate the missile strapdown inertial tilt errors, azimuth errors, velocity errors, and sensor errors. The conclusions reached included the following [1,2]:

1) A 3.5-deg/hr gyro and a 1 mg accelerometer are adequate for all RAC missions, the shorter range cruciform-wing GBU-15 mission, and GPS-aided missions with break-lock ranges less than 10 nm.

2) Gyros in the 0.1-to-0.5 deg/hr range with a 1 mg accelerometer are adequate for longer range missions and GPS aided missions with early break-lock.

3) Higher quality accelerometers (0.2 mg) are required if significant lateral maneuvers are anticipated.

4) Key sensor parameters are: Gyro g-sensitive drift, gyro random drift, gyro scale factor error, gyro dynamic rectification error, and accelerometer bias.

5) For unaided missions a precision aircraft navigation system such as GPS/INS is needed: a 1 nm/hr INS is adequate for RAC missions with a pre-launch RAC fix.

Additional studies [7] conducted by MDAC optimized alignment and calibration techniques for LCIGS considering other powered and unpowered missiles with ranges up to 250 nm. Various transfer alignment maneuvers were analyzed by covariance analysis techniques and a 39-state variable real-world model. The conclusions of this study included:

1) A 5.5-minute axial acceleration aircraft maneuver, illustrated in Figure 13, provided the best transfer alignment and calibration accuracy.

2) A 15-state Kalman filter provides performance nearly the same as a 39-state optimal filter and is recommended with the axial acceleration maneuver.

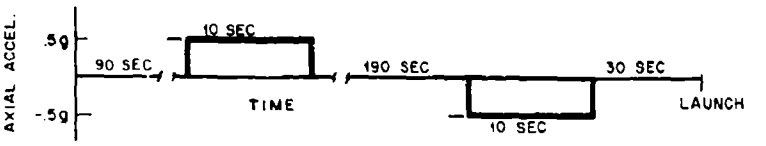

Figure 13 - Aircraft Axial Acceleration Maneuver

LSI is currently performing studies to determine the LCIGS autonomous navigation performance due to the effects of a cruise missile flight profile, flight times exceeding 10 minutes, fast reaction alignment and calibration, and low ambient temperatures. Table 11 reflects the error model being used to characterize the system for these studies.

Table 11 - LCIGS Error Model

ERROR TERM	STATISTICAL MODEL	1σ VALUE
Gyro		
Fixed Bias (turn-on) (deg/hr)	Random Constant	2.0
Random Bias (OA ↑) (deg/hr @ 1 hr)	Random Walk (rate)	0.15
Random Bias (IA ↑) (deg/hr @ 1 hr)	Random Walk (rate)	0.38
Random Bias (OA ↑) (deg @ 1 hr)	Random Walk (angle)	0.0042
Random Bias (IA ↑) (deg @ 1 hr)	Random Walk (angle)	0.0072
Scale Factor Error (ppm)	Random Constant	150.
g-Sens. Drift (along IA) (deg/hr/g)	Random Constant	2.0
g-Sens. Drift (along SA) (deg/hr/g)	Random Constant	2.0
Nonorthogonality ($\widehat{sec}$)	Random Constant	60.
Accelerometer		
Fixed Bias (1 g')	Random Constant	100.
Random Bias (1 g's; τ = 1 h)	1st Order Gauss-Markov	15.
Scale Factor Error (ppm)	Random Constant	150.
Nonorthogonality ($\widehat{sec}$)	Random Constant	20.

The launch aircraft navigation system is a GPS/INS with 20 feet (6.1 m) 1σ position accuracy and 0.2 ft/sec (0.06 m/s) 1σ velocity accuracy. The alignment profile is the axial acceleration maneuver of Figure 13; the missile post-launch profile consists of a flight at 800 ft/sec (244 m/s) with a 60-degree turn at 560 seconds. A 16-state Kalman filter was used with covariance analysis techniques to obtain the expected performance.

Figure 14 illustrates the anticipated LCIGS performance for a 10-minute flight.

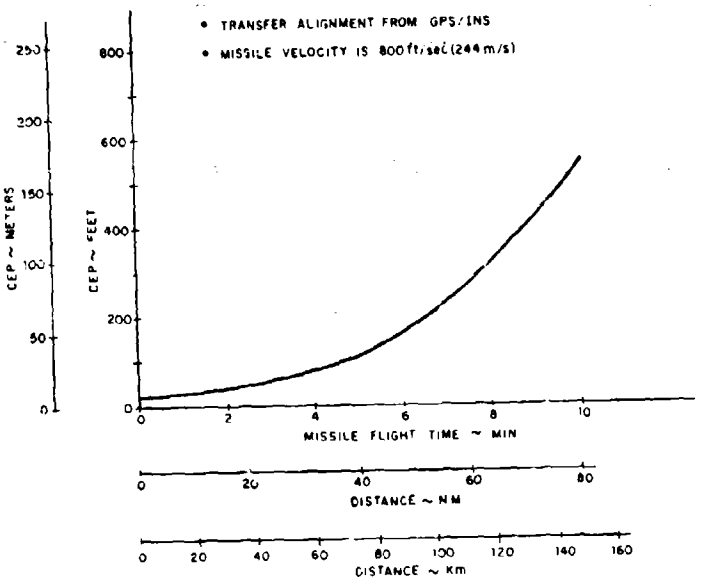

Figure 14 - LCIGS 10-Minute Flight Performance

The figure shows that excellent performance can be obtained from the basic LCIGS configuration. Performance over extended flight times, shown in Figure 15, shows that the Industry LCIGS thermal design and inertial sensor characterization provides essentially the same LCIGS performance for external ambient temperatures as low as -54°C for flight times less than 25 minutes.

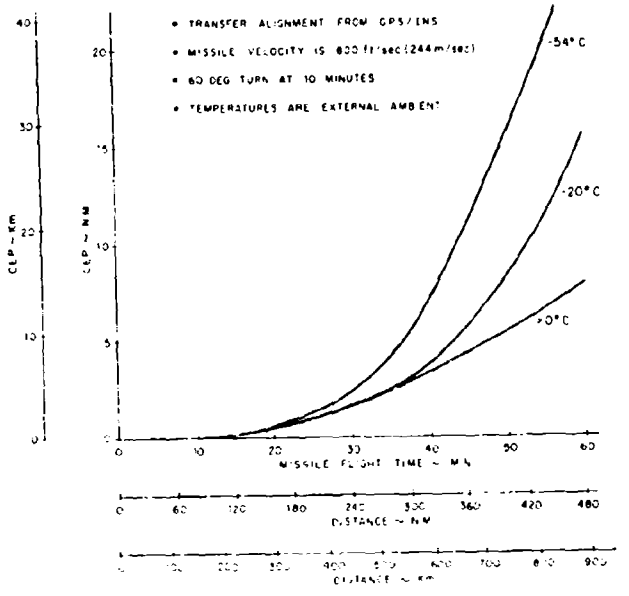

Figure 15 - LCIGS Performance - Extended Flight Time

Figure 16 shows the anticipated performance when a fast reaction missile launch is necessary. The alignment profile is 10 seconds of +0.5-g axial acceleration followed by 10 seconds of unaccelerated flight; no calibration of sensors is accomplished because of the very short maneuver time. The transfer alignment is accomplished with a GPS/INS and the alignment accuracies obtained are shown in Table 12.

Table 12 - LCIGS Fast Reaction Alignment Accuracy

Tilt:	1.5 and 1.0 $\overline{\text{min.}}$
Azimuth:	6.7 $\overline{\text{min.}}$
Velocity:	0.07 ft/s (0.02 m/s)
Position	20.0 ft (6.1 m)

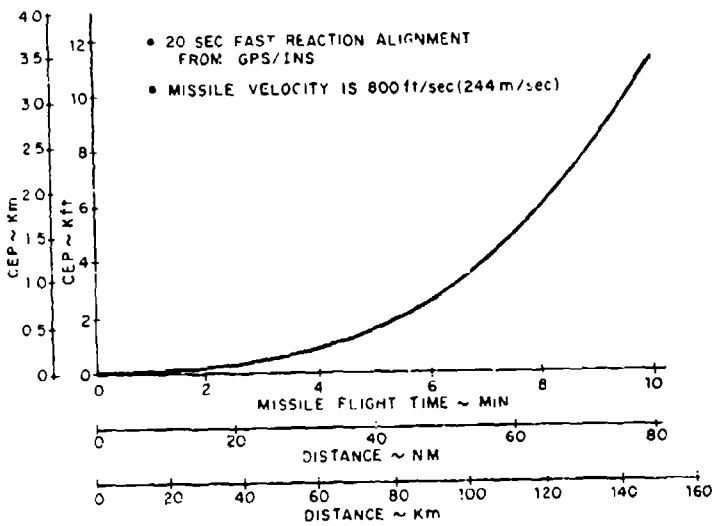

Figure 16 - Fast Reaction Missile Accuracy With LCIGS

Additional simulations are being performed using the USAF Standard (F^3) INS as the launch aircraft reference system. The LCIGS performance over more complex profiles with various aiding system accuracies during missile flight is similarly being analyzed. Laboratory tests by LSI and subsequent laboratory and flight tests in the UTG and MGD programs will complement these simulations and demonstrate that LCIGS yields highly accurate missile guidance at a very low cost.

REFERENCES

(1) Perlmutter, L. D., J. W. Kraemer, N. J. Roessler, MDAC-East, "Strapdown Inertial Sensor Requirements for Tactical Guidance"; NAECON '77 RECORD.

(2) Mueller, C., R. K. Phelps, R. Scheidenhelm; Honeywell; "Tactical Guidance Requirements for Strapdown Inertial"; NAECON '77 RECORD.

(3) Wu, Dr. T., Maj. T. Filiatreau, J. P. Gilmore; "A Design Concept for Low Cost Inertial Guidance of Tactical Weapons".

(4) Gilmore, J. P.; "Modular Strapdown Guidance Unit with Embedded Microprocessors"; Journal of Guidance and Control, Jan.-Feb. 1980.

(5) "Low Cost Inertial Guidance Subsystem Final Report", R-1295, The Charles Stark Draper Laboratory, Inc., Jan. 1980.

(6) U. S. Army Missile Research and Development Command, "Storage Reliability Summary Report.", LC-78-2.

(7) McDonnell Douglas Astronautics Co. - St. Louis Division, "Unaided Tactical Guidance", AFATL-TR-78-49, April 1978.

ACKNOWLEDGEMENT

The work in this paper is sponsored by the U.S. Air Force Armament Test Laboratory under Contract F08635-79-C-0196. Publication of this paper does not constitute approval of the U.S. Air Force of the findings or conclusions herein.

UNAIDED TACTICAL GUIDANCE FLIGHT TEST

by
Lawrence D. Perlmutter
McDonnell Douglas Astronautics Company
St. Louis, Missouri 63141
USA
AND
C. Keith Fitschen, Major, USAF
Air Force Armament Laboratory (AFATL/DLMM)
Eglin Air Force Base, Florida 32542
USA

SUMMARY

The Air Force Armament Laboratory has developed a low-cost midcourse guidance technique suitable for standoff tactical weapons. The technique uses the launch aircraft navigation system and Kalman filtering to align and calibrate a weapon-contained, low-cost strapdown navigation system. Post-launch, the strapdown system provides unaided inertial guidance along the midcourse trajectory. The strapdown inertial sensor chosen to implement this form of guidance is the Low Cost Inertial Guidance Subsystem (LCIGS). LCIGS is a modular strapdown package which uses embedded microprocessors, single-degree-of-freedom gyroscopes, and pendulous mass accelerometers. LCIGS has been designed and built for use in tactical weapons and features digital torque loops for the gyros and temperature compensation of all six sensors. Studies have been conducted to project system performance, and the results indicate that through the alignment and calibration process the predominant LCIGS sensor errors can be reduced by an order of magnitude. A flight test program has been structured to demonstrate performance. The first system to be tested consists of a brassboard LCIGS, a McDonnell Douglas Model 771 computer which serves as the guidance processor, and the Completely Integrated Range Instrumentation System (CIRIS) which performs the aircraft precision navigation function for transfer alignment. In a second series of flight tests the brassboard LCIGS will be replaced with an Engineering Model LCIGS built for the Air Force by Lear Siegler, Inc. The Central Inertial Guidance Test Facility (CIGTF) at Holloman Air Force Base is the responsible test organization providing ground test facilities and a C-141 aircraft. This paper describes the Unaided Tactical Guidance concept, the system hardware and software to be tested, the LCIGS and the pre-flight calibration features incorporated into its support equipment, unique laboratory testing to be performed on the system, and the planned flight tests.

1. INTRODUCTION

A requirement exists for an autonomous, all-weather, jam-proof, quickly targeted midcourse guidance capability for use in tactical standoff weapons. Many forms of midcourse guidance have been forwarded as viable candidates for meeting this requirement, but each has one or more operational limitations. Pure inertial guidance has always been an attractive option for midcourse guidance, but the cost of high accuracy gimballed inertial navigators has precluded their use in "throw-away" tactical weapons, and the inaccuracy of low-cost strapdown inertial navigators has prohibited their use unless position-aided by some external source. The primary cause of the inaccuracy in these strapdown navigators is gyroscope and accelerometer sensor errors. Recent studies indicate that through a careful inflight alignment and calibration process the predominant sensor errors can be reduced by an order of magnitude. This performance when coupled with a precise position and velocity initialization, projected to be available from the tactical weapon-carrying aircraft through hybrid LORAN or GPS inertial systems, makes unaided strapdown inertial navigation a viable midcourse guidance candidate for tactical weapons.

The Air Force Armament Laboratory initiated a series of programs in 1976 to investigate the potential of low-cost strapdown inertial guidance.[1] The Tactical Inertial Performance Requirements Analysis (TIPRA) studies[2,3] determined the gyroscope and accelerometer sensor quality necessary in a strapdown navigator to perform tactical weapon guidance when the navigator was position aided (Radiometric Area Correlation or Global Positioning System position aiding), or unaided. The Low-Cost Inertial Guidance Subsystem (LCIGS) program[4,5] with Charles Stark Draper Laboratory (CSDL) produced a design and brassboard hardware for a low-cost, non-proprietary, strapdown inertial sensor that uses single-degree-of-freedom gyros, pendulous mass accelerometers, and current microprocessor technology. The performance specification for the gyros and accelerometers was established through the TIPRA studies.

The CSDL non-proprietary design formed the baseline for a follow-on LCIGS program with industry. This program, Industry LCIGS[6], is an on-going effort to build five engineering model LCIGS' for captive and free-flight purposes.

In parallel with the LCIGS effort, the Unaided Tactical Guidance (UTG) studies[7,8] were conducted to determine the optimum airborne alignment and sensor calibration technique for LCIGS. An LCIGS sensor error model, developed by CSDL from their testing, was used in the work. These studies formed the basis for the Unaided Tactical Guidance Validation (UTGV) flight test program which is an on-going effort to demonstrate unaided inertial guidance in a realistic manner. This flight test program and the system hardware and software implementation will be described in detail in this paper.

In another Armament Laboratory program, Digital Integrating Subsystem (DIS)[9], the processing capability for a weapon system is being developed. This program will produce the specification for a federated set of microprocessors communicating together through a multiplex bus; the hardware implementation of the specification will also be a program output. In 1981, the DIS, LCIGS, and software necessary to perform unaided tactical guidance will be integrated into a testbed missile and free-flown in a midcourse guidance demonstration.

2. Unaided Tactical Guidance Concept

The cost of high-quality gimballed inertial navigators may preclude their use in tactical weapons. Strapdown navigators with low-cost sensors are an attractive alternative provided the desired performance can be attained. As low-cost sensors typically have large turnon-to-turnon bias shifts a significant performance benefit can be attained by inflight sensor calibration. The in-flight initialization, alignment, and calibration technique is illustrated in Figure 1.

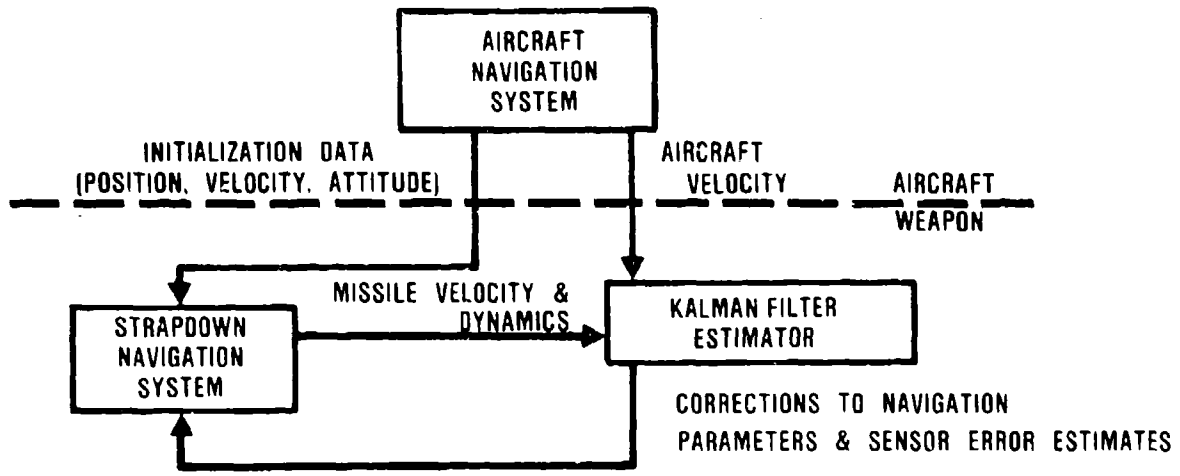

FIGURE 1. Airborne Alignment/Calibration Concept

The strapdown navigator is initialized with current position, velocity, and body attitude information from the aircraft navigation system. Thereafter the system keeps current its own navigation solution. The Kalman filter estimator contains an error model for the missile navigator which mathematically describes critical strapdown gyro and accelerometer error terms. This error model is driven by the trajectory dynamics as sensed by the strapdown system. Periodically during the mated flight the Kalman filter samples aircraft and missile velocity and computes velocity, alignment, and sensor corrections to the strapdown system. These corrections are fed back to the navigation processor and incorporated. The estimation process is iterated until weapon release. To enhance observability of dominant errors, aircraft maneuvers can be performed.

The Unaided Tactical Guidance studies were performed to determine the optimum transfer alignment and calibration technique for a specific strapdown inertial measurement unit, the LCIGS. The sensor error model used for the studies was provided by Draper Laboratory. Gyroscope errors included: bias - .5 DEG/HR, random walk in rate - .1 DEG/HR at 1 hour for the level gyros and .25 DEG/HR at 1 hour for the vertical gyro, scale factor - 150 PPM, gravity sensitive drift - 1 DEG/HR/G for the input axis and .8 DEG/HR/G for the spin axis, and non-orthogonality - 100 sec. Accelerometer errors included: bias - 100 μG, scale factor - 150 PPM, and non-orthogonality - 20 sec. The launch aircraft was assumed to be equipped with approximately a one nautical mile per hour navigator augmented with a Global Positioning System. This hybrid navigator provides a smoothed accuracy of 20 feet (6.1 m) 1σ in position and .2 ft/sec (.06 m/sec) 1σ in velocity. The purpose of the GPS augmentation was to provide accurate missile position and velocity initialization at launch. Three planar postlaunch trajectories, approximately 10 minutes in length, were used to determine system CEP. Study variables were the Kalman filter error state and the launch aircraft maneuvers during the alignment/calibration phase. Side issues studied included the effects of wing flexure on measurement error, the effects of time delay uncertainties in missile and aircraft velocities, and gravity anomaly effects. Covariance analyses was the major study tool.

The studies determined that for missions with relatively benign post-launch trajectories, i.e., minimum turning, the most effective aircraft calibration maneuver was straight and level flight with two periods of acceleration; specifically,

90 seconds wings level

.5g axial acceleration for 10 to 20 seconds

210 seconds wings level

.5g axial deceleration for 10 to 20 seconds

launch

The velocity increment provided by the acceleration is important, but the shape of the pulses or duration is not critical. This maneuver allows good estimation of level-gyro bias during the periods of wings level flight. The velocity changes are made primarily to allow azimuth calibration. Also observable during the acceleration parts of the profile are certain gyro g-sensitive drift terms.

The suboptimal Kalman filter that provided overall best performance for the study scenario was composed of 15 states: 3 velocities, 3 tilts, 3 gyro biases, 2 gyro g-sensitive biases, 3 accelerometer biases, and one accelerometer scale factor. Measurements were made using 3 axes of velocity and a 5-second measurement interval. The simulations indicate that using the chosen aircraft maneuver and the 15-state filter, gyro bias errors can be reduced by an order of magnitude. The CEP for planar trajectories approximately 10-minutes in length is 500-700 feet (152-213 m).

3. LCIGS and Support Equipment

The brassboard Low-Cost Inertial Guidance Subsystem (LCIGS), built by CSDL, is described in detail in References 4 and 5. LCIGS is a modular strapdown inertial sensor subsystem which features the use of embedded microprocessors and low-cost single-degree-of-freedom (SDF) gyroscopes and accelerometers (repeatability 1-5 deg/hr and 100-200 micro-g). The block diagram of the system is shown in Figure 2, and a picture of the hardware is provided in Figure 3. Five microprocessors (Motorola M6800) are used, one each per gyro module, one per accelerometer triad (velocity reference module) and one in the service module. The service module processor's electrically alterable read only memory (EAROM) provides storage for the LCIGS system data base. EAROM is updated via the PSE following system calibration.

The gyro modules each consist of a gyro block assembly, a gyro torque electronics (GTE) card, and an instrument processor card. The low-cost SDF integrating gyros used in the brassboard are Timex IG-10s. The GTE conditions the gyro signal-generator output and provides the digitized signal to the gyro instrument processor. This processor implements a third-order control loop algorithm and returns the torque command to the GTE. The GTE applies a precisely controlled constant-amplitude current to the gyro magnetic torquer. The GTE has been configured in a ternary pulse width rebalance mode for most of the work to date; however, the logic is reconfigurable for other modes via an instruction from the processor. The gyro processor also compensates the accumulated ±θ torque count with temperatured-compensated bias and scale factor increments provided by the service processor.

FIGURE 2. LCIGS System Mechanization

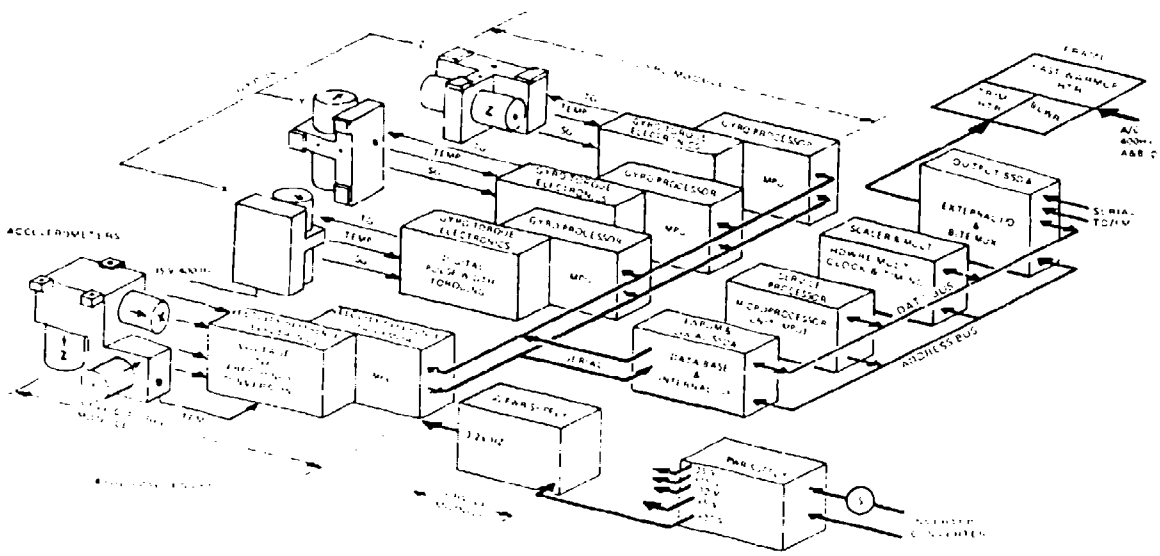

The velocity reference module (VRM) consists of an accelerometer triad, a velocity reference electronics (VRE) assembly, and an instrument processor. The accelerometers in the LCIGS brassboard are the Sundstrand QA 1200 units which are gas-filled, quartz-hinged pendulum instruments. An analog torque-to-balance loop is integral to the unit. The accelerometer output voltage, which is proportional to acceleration, is an input to the voltage-to-frequency (V/F) converter in the VRE. The V/F output frequency is proportional to acceleration. The VRM processor accumulates the V/F counts and applies temperature-compensated bias and scale factor increments provided by the service processor. (Separate compensation coefficients are maintained for the accelerometers and the V/F).

The service module processor performs system executive functions, outputs on-off commands to a trim heater and blower to effect temperature control, and implements sensor compensation processing functions. The service processor's EAROM memory stores the following items: sensor bias and scale factor compensation data including temperature sensitivity coefficients, sensor alignment angles, gyro g-sensitive drift, gyro dynamic coupling terms (gyro output axis coupling and anisoinertial drift), and temperature control law parameters. The service processor computes the temperature-compensated bias and scale factor corrections that are applied in the instrument processors. These computations, based upon EAROM coefficients and sensed temperature data, are executed using the hardware multiply capability of the service module. The

coefficients for the cross-axis type compensation (e.g., g-sensitive drift, alignments, and dynamic coupling) are passed to the navigation processor where the compensation is implemented using the appropriate $\Delta\theta$s and ΔVs.

The brassboard LCIGS will be flight-tested in the first phase of a two part test program. Following this set of tests the brassboard LCIGS will be laced with an engineering model LCIGS, described in reference 6, and further flight tests conducted The configuration discussed in this paper uses the brassboard.

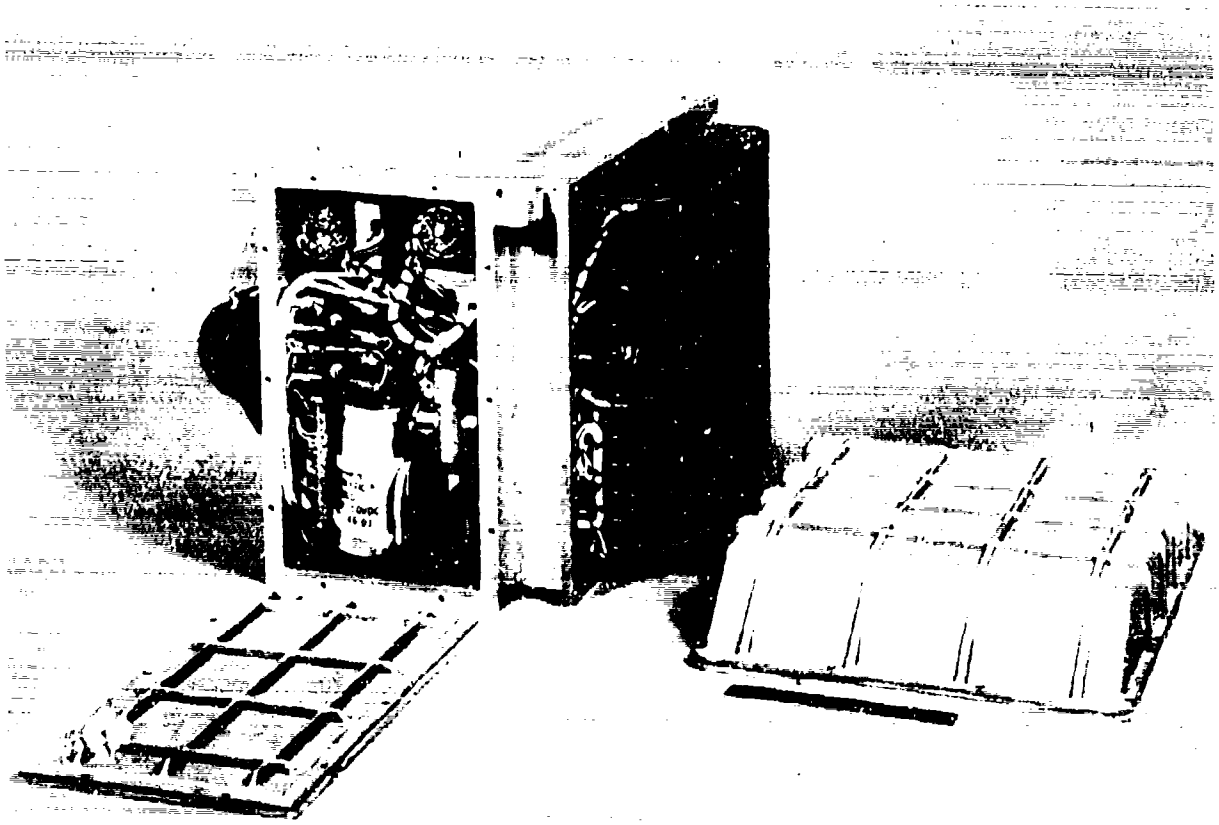

FIGURE 3. LCIGS Hardware (Covers Removed)

3.1 Support Equipment Test Capability

The Peculiar Support Equipment (PSE), developed by the Draper Laboratory, provides the stand alone capability to support LCIGS navigation performance tests, calibration functions, and diagnostic tests. One objective of the UTGV program is to determine the effectiveness of the PSE in performing pre-flight sensor calibration. Accordingly, PSE test capabilities are described in this section and the planned PSE-effectiveness tests are described under TEST PLANS.

The Factory Selloff tests are navigation performance tests using a simplified alignment and navigation mechanization. These laboratory tests consist of a 3-position alignment mode (Autocal) followed by navigation under static conditions or discrete attitude changes. For navigation under Scorsby motion, a 4-position Autocal mode is used for alignment. The autocal program estimates inertial sensor errors using least-squares curve fits of system-level velocity outputs of a simplified local-level navigation algorithm. The inertial error estimates (gyro bias and g-sensitive drift, accelerometer bias and scale factor) are applied as sensor compensation during the navigation phase. The resulting navigation performance provides a measure of the effectiveness of the sensor compensation. A two-part, non-realtime data processing procedure is used for both the calibration and navigation phases. First, the 100 Hz inertial data ($\Delta\theta$s and ΔVs) are stored on magnetic tape. Then, the tape is processed through the Autocal and navigation programs.

The Traditional Calibration procedure provides the capability to determine the following parameters: gyro bias, g-sensitive drift, scale factor, and misalignments; and accelerometer bias, scale factor, and misalignment. For the full calibration procedure, raw sensor data is accumulated in each of twelve static positions and three dynamic positions. The dynamic sequence employs constant rates about each axis, in turn, in order to determine gyro scale factor and misalignment. The software also supports partial calibration procedures. Nine static positions can be used (instead of twelve) if accelerometer module inter-axis alignment is available from VRM module-level calibration. Also, a five-position (static only) procedure can be used if only gyro bias and g-sensitive drift terms need to be re-calibrated.

The Field Calibration procedure permits the calibration of gyro static and dynamic error parameters using test equipment with very loose tolerances. The test procedure assumes that the LCIGS accelerometer misalignments have already been accurately determined using conventional techniques. The gyro parameters determined by Field Calibration are bias, g-sensitive drifts, scale factor, and misalignment. The PSE collects and stores inertial sensor data during eleven static positions and during six 90-degree rotations. The tape containing the inertial data is then processed via uncoupled Kalman estimators to obtain the polynomial coefficients of the sensor output data. These coefficients are used in an algorithm that determines the gyro static and dynamic parameters using two or more passes.

4. Software

As part of the Unaided Tactical Guidance Validation (UTGV) flight test program, the software necessary for navigation and transfer alignment had to be developed. McDonnell Douglas (MDAC), the UTGV contractor, chose to use FORTRAN for all applications software and some portions of the executive software. The Higher Order Language (HOL) applications software is organized into strapdown, navigation, and filter modules as shown in Figure 4. This structure is designed to minimize control logic and inter-module data communications and to facilitate the extension of this software to distributed processing system (e.g., the Air Force Digital Integrating Subsystem). All three applications modules contain an initialization section and a computational loop. The computational loops contain at least one buffered data input request which queues on data availability. Control is passed among these modules by the scheduler as a function of priority and current data availability. The strapdown module has top priority; it queues on LCIGS inertial input data at 100 Hz. The navigation module has second priority; it queues on the transformed inertial data output by the strapdown task at 10 Hz. The Kalman filter module has lowest priority; it queues on navigation data output and CIRIS reference navigation data at 1 Hz. Buffered feedback data consists of: navigation frame rates sent from navigation to strapdown at 10 Hz; position and velocity corrections sent from the Kalman filter to navigation at 0.25 Hz (nominal); and biases and tilts sent from the Kalman filter to strapdown at 0.25 Hz (nominal).

4.1 Executive Software

The executive software provides multi-task scheduling services, inter-task communications services, data input/output and formatting, clock maintenance, and operating system services required by the HOL. The task scheduling system provides for priority-based multi-tasking (i.e., time sharing). Tasks are scheduled by interrupt handlers or executing tasks upon occurrence of a significant event. Typical external events are LCIGS inertial data input and CIRIS reference data input, whereas typical internal events are transformed inertial data available and filter corrections available. A ready task is scheduled by being added to that queue appropriate to the task priority level. Each queue operates on a first-in-first-out (FIFO) basis. If the task being added is higher priority, the current active task is preempted, and the new task is initiated. This provides for fast response to time-critical processing requirements. The executive preserves the necessary operating environment of the task being preempted (e.g., the current location counter, registers, and status word), and restores the operating environment of a task being restarted.

FIGURE 4. Software Mechanization

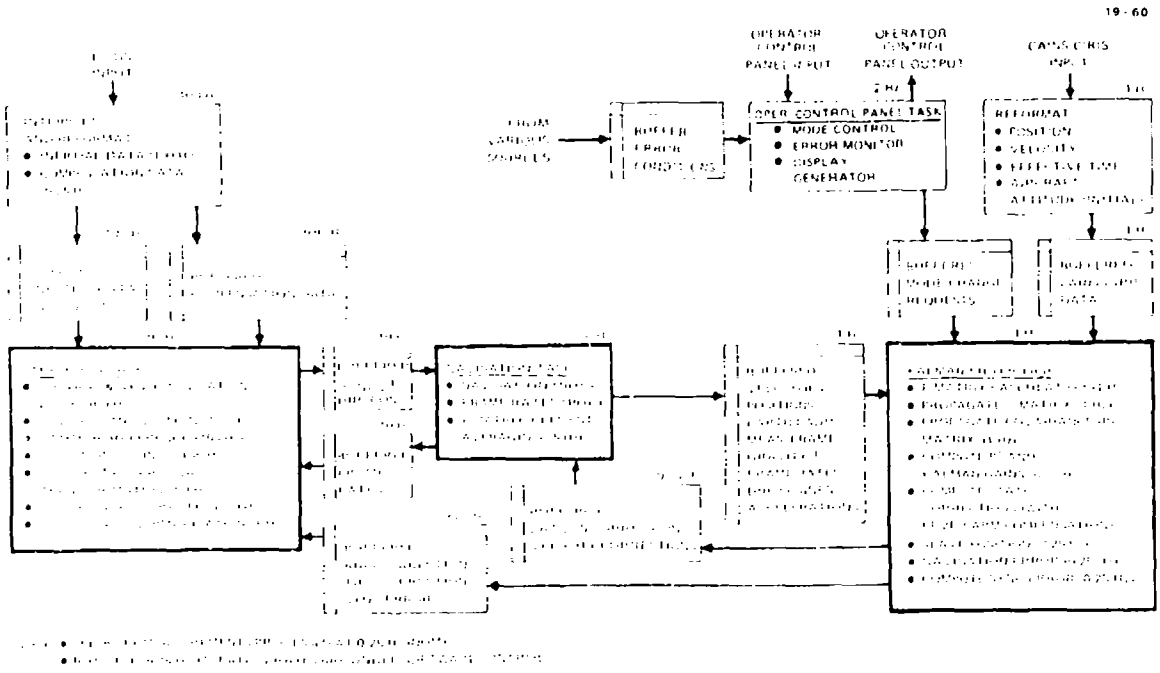

The task communication services provide for buffered data message passing between two tasks, or between an interrupt handler and a task. This approach eliminates most of the real-time data interlock problems associated with asynchronous processing. The buffering technique insures the time consistency of data within a message, and allows the "stacking" of inputs to a task to eliminate short-term real-time constraints. Two service functions are provided: SEND and RECV. SEND physically moves the message buffer from the sending task to either: 1) the receiving task input buffer, if the receiving task has been queued on receipt of the message, or 2) dynamically allocated system storage in memory. RECV transfers messages from dynamic storage to the receiving task input buffer (if the message had already been sent), or enables the direct transfer by a subsequent SEND (this is referred to as message receipt queueing). If an input message is unavailable at RECV time, the receiving task has the option of: 1) an immediate return with a status parameter indicating the unavailability, or 2) of being preempted until the message becomes available. This option is a parameter of RECV calling sequence. SEND is responsible for rescheduling any receiving task waiting on the message sent.

The input/output interface software performs the following functions: data input and output, data conversion to and from MDAC Model 771 internal format, measurement of arrival times, and the calculation of "effective" times of input data. The I/O interface software utilizes the task communication services to SEND input data to the appropriate processing functions and to RECV data for output from various processing functions. The I/O functions provided are LCIGS I/O, CIRIS input, OCP I/O, and DAS output.

The executive software also includes system service functions. Clock maintenance service is provided to support a programmable count-down clock which measures current time within 10 microceconds; a FORTRAN run-time library is provided; and various supervisor calls are implemented to provide linkages between the executive and the applications software.

Built-in test functions are included for flight readiness checks. These tests include: LCIGS test, CIRIS test, OCP controls and displays tests, and the DAS test. For the LCIGS tests, each gyro is sequentially torqued to a programmed null offset position and then back to a null position; whereas accelerometers are checked passively by monitoring reasonableness of the measured accelerometer outputs.

4.2 Strapdown Module

The strapdown module performs dynamic compensation of the LCIGS inertial data, implements a quaternion algorithm to determine attitude, and transforms acceleration data to a local-level navigation frame (East, North, Up). LCIGS inertial data compensation is performed for the following coupling-type terms: g-sensitive gyro drifts, anisoinertial gyro drift, gyro drift due to output-axis angular acceleration, and misalignments of gyro and accelerometer axes. These terms are computed at a 100 Hz rate using pre-flight error coefficients stored in the LCIGS EAROM memory. (Note - LCIGS inertial data is compensated within LCIGS for temperature effects on bias and scale factor prior to transmission). The inertial data is also compensated for error terms determined by the Kalman filter during the in-flight transfer alignment/calibration maneuver sequence.

A quaternion representation is used to define body attitude relative to the navigation frame,

$$\dot{q} = \tfrac{1}{2} q \omega_B - \tfrac{1}{2} \gamma_N q$$

where

ω_B = inertial attitude rate (in body axes)

γ_N = navigation frame rate (in navigation axes)

The navigation frame rate consists of earth-rate terms plus vehicle transport terms (i.e., velocity divided by earth radii). The inertial attitude rate (ω_B), sensed by LCIGS gyros, is highly dynamic; whereas the navigation frame rate (γ_N), computed in the navigation module, is a relatively small, slowly changing variable. Therefore, a generalized third-order 100 Hz quaternion algorithm is used to compute

$$\dot{q} = \tfrac{1}{2} q \omega_B$$

and a first-order 10 Hz update is used for the frame rate term,

$$q' = q - \tfrac{1}{2} \gamma_N q \Delta t$$

The 100 Hz LCIGS velocity increments are transformed to the navigation frame at 50 Hz using the transformation matrix computed from the quaternions at the midpoint of the interval. The navigation frame velocity increments are accumulated over a 0.1 second interval and then sent to the navigation module.

4.3 Navigation Module

The navigation module computes current position and velocity using a geodetic earth model. Velocity is integrated into position at 10 Hz using trapezoidal integration. Navigation frame rates (γ_N) are computed and fed back to the strapdown module.

The navigation module also performs special support functions for the Kalman filter. This module computes those elements of the Kalman filter system dynamics matrix (F-matrix) that vary rapidly with vehicle attitude motion. These elements, which involve terms containing accelerations (A_E, A_N, A_U) and the direction cosine matrix (T), are accumulated at a 5 Hz rate and averaged over a one-second interval.

4.4 Filter Module

A conventional 15-state Kalman filter is employed to process three-axis CIRIS velocity measurements at a nominal rate of 0.25 Hz during a transfer alignment/calibration maneuver sequence. The Kalman filter code has been optimized via sparse-matrix techniques, partitioning, and symmetry considerations and is compatible with single-precision floating-point processing. The filter mechanization, based on the UTG study[7], includes the following states: velocity (3), attitude (3), gyro bias (3), g-sensitive drift (2), accelerometer bias (3), and axial accelerometer scale factor (1). During the navigation phase, the filter is augmented with three position states. These states facilitate flight test navigation performance analysis (i.e., compare actual position errors to filter variances), and provide a growth capability for midcourse position update systems.

The state transition matrix (ϕ) is propagated using the system dynamics matrix (F) as follows,

$$\phi' = (I + F\,\Delta t)\phi$$

where the time interval is nominally one second. The covariance matrix propagation algorithm is,

$$P' = \phi P \phi^T + Q\,\Delta t$$

where Q is the driving noise matrix. For LCIGS, driving noise must be added to the attitude states (3) and gyro bias states (3) to reflect the random characteristics of the low-cost gyros (i.e., random walk on attitude and random walk of gyro drift).

A filter tuning feature called "turn compensation" is included to enhance filter performance during alignment turns without impacting wings-level performance. (Note - a wings-level axial acceleration alignment maneuver was recommended in the UTG studies). Additional driving noise is added to the attitude states during turns to compensate for unmodelled gyro scale factor and nonorthogonality errors. The compensation algorithm is,

$$\Delta Q\ (\text{attitude}) = C_1 \omega_X^2 + C_2 \left(\frac{\sin\phi}{V}\right)^2$$

where

C_1, C_2 = constants

ω_X = x-gyro (axial) output

ϕ = roll angle

V = vehicle velocity

A delayed observable mechanization is used to incorporate Kalman updates. The Kalman gain (K), computed at the effective measurement time, is propagated to the measurement-incorporation time via the appropriate state transition matrix,

$$K' = \phi K$$

This feature permits Kalman corrections to be efficiently incorporated into the state long after the effective measurement time and minimizes processor throughput requirements by permitting Kalman operations to be spread out. It also provides growth capability for midcourse update applications (e.g., terrain contour matching) where the measurement is delayed.

5. System Test Configurations

The UTGV test configurations consist of a flight configuration for operation in the C-141 aircraft and a laboratory configuration for interface and software development. The flight configuration consists of the LCIGS, guidance processor, an operator control panel, and a power control and conditioning unit. It interfaces with the Completely Integrated Range Instrumentation System (CIRIS) for transfer alignment and with a data acquisition system.

5.1 Flight Configuration

The flight configuration is shown in Figure 5. The LCIGS strapdown inertial package provides incremental sensor data, ΔV's and $\Delta\theta$'s to the MDAC Model 771 navigation processor in response to a command from the navigation processor to initialize and start the transfer of inertial data. The LCIGS data is compensated via temperature-corrected bias and scale factor coefficients prior to transmission. Sensor data compensation is completed in the navigation processor which incorporates the coupling-type terms, e.g., g-sensitive drift, anisoinertial coupling, output-axis coupling, and misalignments. The coefficients for these terms are transmitted from the LCIGS EAROM memory during initialization. The navigation processor performs executive functions and implements strapdown navigation and Kalman filter algorithms to effect transfer alignment and unaided navigation. The navigation processor also performs system integration functions via digital interfaces with LCIGS, the CIRIS reference navigator, the operator control panel (OCP), the CIGTF data acquisition system, and the Silent 700 printing terminal. The CIRIS serves a dual function: (1) performs the function of a precision aircraft navigation system which is required for UTG missions, and (2) provides the scoring reference for flight data performance analysis. CIRIS transmits a data block containing attitude, position, and velocity reference data. The complete data set is used by the navigation processor to initialize the strapdown navigation system, whereas a velocity match is used for transfer alignment. The OCP applies power to the system and sequences the navigation processor through program loading (from a Tektronix tape cartridge), alignment, navigation, and test modes. Displays are provided for monitoring

system performance data, failure conditions, and the operating mode. The CIGTF Data Acquisition System (DAS) is the primary means of recording flight data, however the Silent 700 printing terminal will be used for quick-look data output during all ground tests and during C-141 flight tests. The power control unit (PCU) conditions aircraft power for the LCIGS and the 771 processor, routes unconditioned power to the LCIGS heaters and blower and to a blower for the 771, and converts single-ended LCIGS signals into double-ended signals for interfacing with the 771. A picture of the flight hardware is provided in Figure 6.

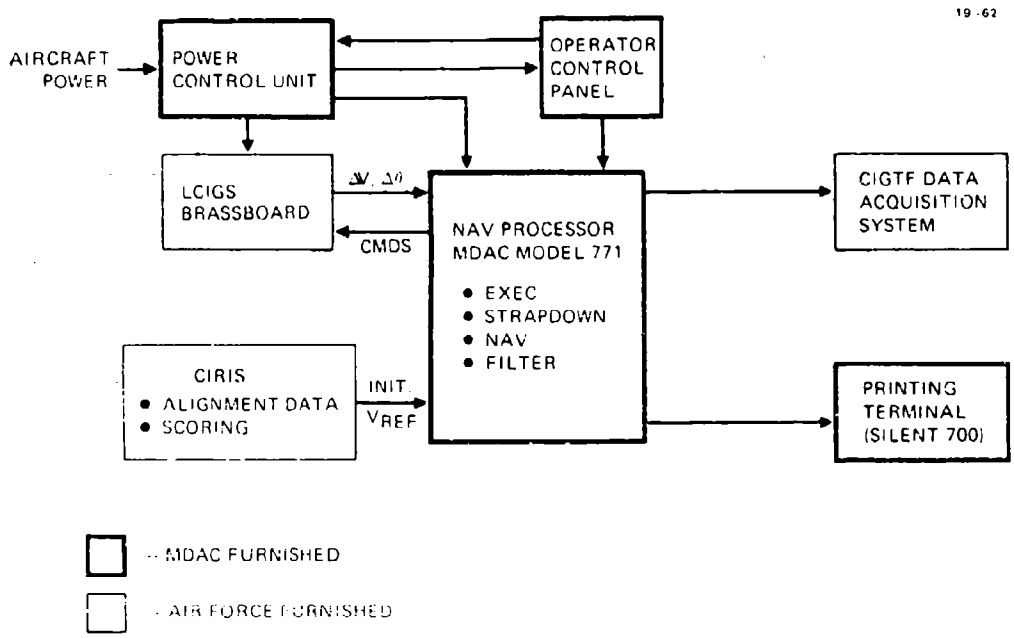

FIGURE 5. UTGV Flight Configuration

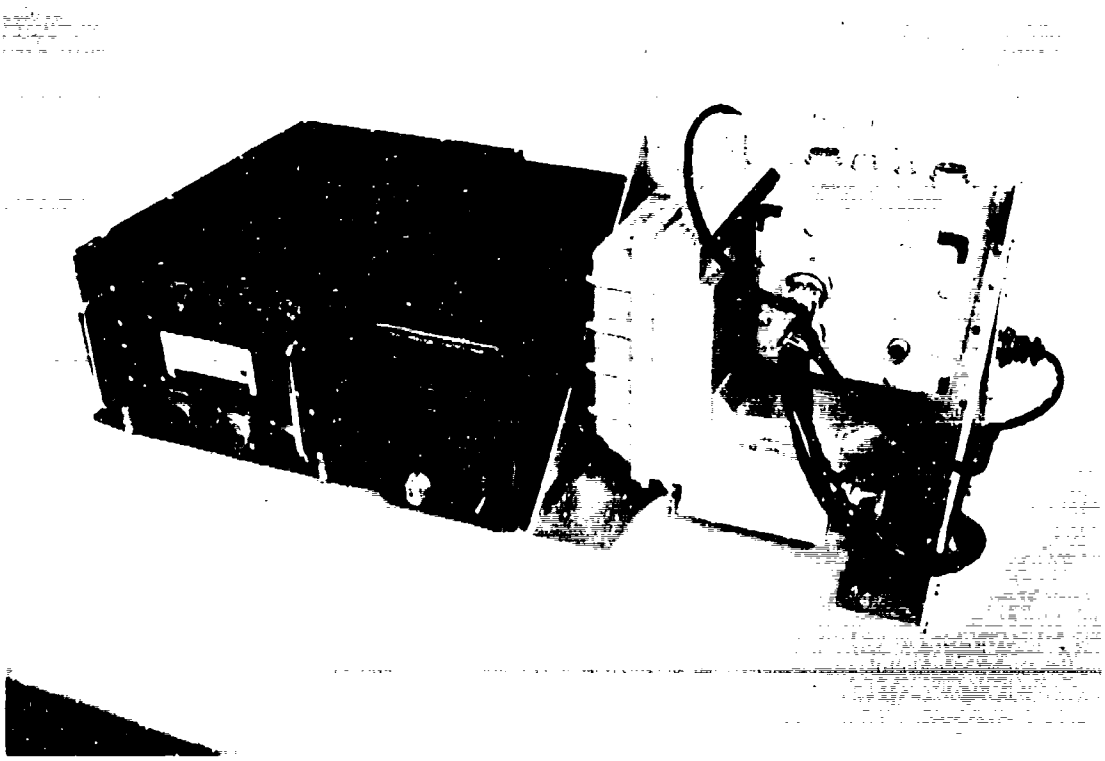

FIGURE 6. UTGV Flight Hardware

5.2 Laboratory Configuration

The laboratory configuration provides the basis for navigation equipment interface development and navigation software testing. The laboratory configuration features a switch box to provide the capability to switch LCIGS data signals from the CSDL Peculiar Support Equipment to the Model 771 processor without gyro power interruption. This capability facilitates software development and PSE-effectiveness evaluations.

The laboratory configuration is shown in Figure 7. The MDAC-built equipment (heavy lines) operates in conjunction with the CSDL-built LCIGS, PSE, and remote terminal. The PSE provides a stand-alone system level test capability. For stand-alone operation, LCIGS is connected to the PSE via the remote terminal which routes power to LCIGS and converts LCIGS output data from single ended to double-ended signals. This conversion to double-ended signals is required to allow transmission over long laboratory interconnect cables. The PSE, described in Reference 4, consists of a Norden PDP 11/34 minicomputer, digital I/O, a DEC-writer hard copy console terminal, and a magnetic tape for mass storage of both PSE test programs and system test data. The minicomputer implements the following functions: 1) navigation performance tests using a simplified alignment/navigation mechanization, 2) three calibration procedures (Traditional Calibration, Field Calibration, and Autocal) along with EAROM data base management, and 3) diagnostic testing for fault isolation of LCIGS hardware and software.

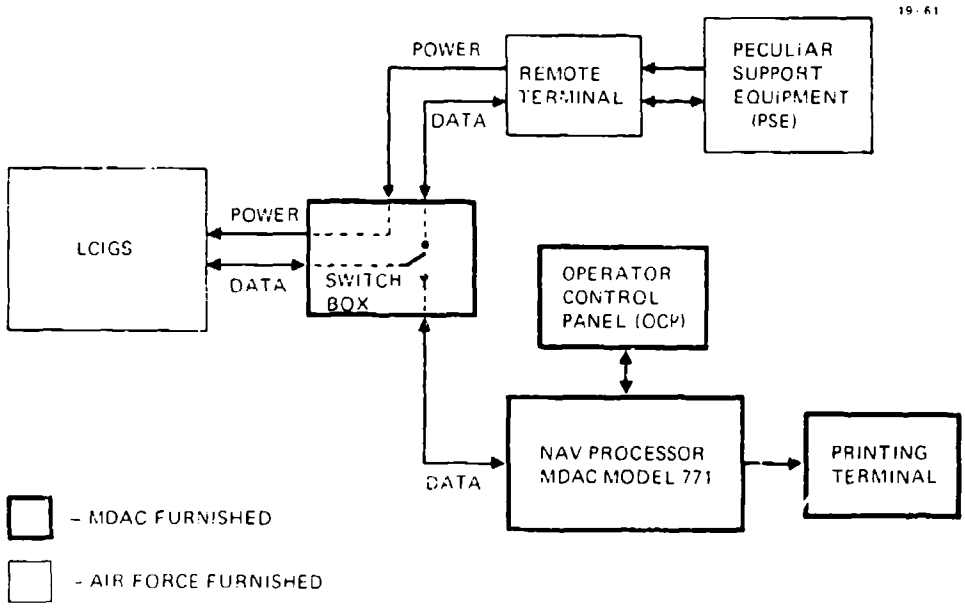

FIGURE 7. UTGV Laboratory Configuration

The MDAC switch box provides the capability to electronically switch LCIGS data signals from the PSE to the MDAC Model 771 navigation processor without interruption of the PSE-supplied power to LCIGS. This allows a comparison of LCIGS inertial navigation operation with either the PSE or Model 771 without turning off the LCIGS gyros and introducing large gyro bias shifts. This provides a cross check of processor hardware, interfaces, and software. It facilitates the evaluation of PSE effectiveness, an objective of the UTGV program.

6. Test Peculiar Hardware

As discussed in the system test configuration section, the UTGV test program will interface the LCIGS, a guidance processor, operator control panel, and a power control unit into a system. This section describes the processor, digital interfaces, and operator control panel used for the test program. Eventually the LCIGS will be interfaced with the Digital Integrating Subsystem (DIS). The software developed for the UTGV program will be implemented in DIS and a free-flight midcourse guidance demonstration program conducted.

6.1 Navigation Processor

The MDAC Model 771 is a ruggedized, high-speed, 16-bit general purpose processor built by McDonnell Douglas Astronautics-Huntington Beach (MDAC-HB). The model 771 is currently being applied to the Joint Tactical Information Distribution System (JTIDS) terminal processor where flight tests in an F-4 pod are planned. It is also the selected processor for the MDAC-HB Advanced Lightweight Torpedo (ALWT) program.

The Model 771 is based upon the AMD 2900 logic family and emulates the popular Perkin-Elmer (Interdata) 8/16 commercial minicomputer. It provides a large instruction set, including fixed and single-precision floating point arithmetic, and instructions for byte, logical, shift and input/output operations. A hardware

implementation is used to provide the capability for high-speed single-precision floating point operations. This capability is highly desirable for executing the HOL code in general and the Kalman filter code in particular. The single-precision floating point word is 32 bits (21-24 bits of mantissa depending on the data). The 771 has 16 general purpose registers (15 useable as index registers), and eight single-precision floating point registers. Input/output is based on a unibus-type architecture, and 16 hardware priority interrupts are provided (expandable to 64). A 32K 16-bit word memory is used.

The 771 has a cycle time of no more than 267 nanoseconds. RAM memory, with an access time of 240 nanoseconds, is used. Approximate instruction timing with this fast memory is as follows:

Floating Point -	Add/subtract	3.0 microsec.
	Multiply	8.0 microsec.
	Divide	15.0 microsec.
	Load	2.8 microsec.
	Store	1.2 microsec.
Fixed-Point (memory to register)		
	Add/subtract	0.72 microsec.
	Multiply	5.04 microsec.
	Divide	8.83 microsec.
	Load/Store/Logical	0.72 microsec.

Double precision floating point arithmetic is emulated in the software. Its use is restricted, for efficiency, to adds and subtracts, and is only used where necessary (e.g., in quaternion, velocity, and position integrations).

6.2 Digital Interfaces

The LCIGS/771 interface provides for bidirectional serial data transfer between LCIGS and the Model 771 at a 250 KHz bit rate. A variable length block transfer protocol is implemented with hand shaking in both directions. The line protocol allows LCIGS to interrupt any incoming transmission from the Model 771 in order to transmit time critical inertial data to the 771. The 771 interface provides interrupts to the software for each word received from or transmitted to LCIGS.

The CIRIS/771 interface is a one-way serial communications from CIRIS to the 771 at a 2.4 MHz bit rate, in 1 Hz data blocks of 24 16-bit words. The data blocks are surrounded by a data envelope signal line. The clock is provided in the CIRIS UART (Universal Asynchronous Receiver-Transmitter). Due to the high transmission rate and lack of inter-computer handshaking, incoming CIRIS data is buffered in FIFOs in the 771 interface electronics. Interrupts to the 771 software are therefore provided only at start and end of block.

The OCP/771 interface provides bidirectional serial communications at a 250 KHz bit rate. The 771 interface, under software control, initiates transfer in both directions. Input from the OCP is one 16-bit word containing the current positions of all switches and controls. Output to the OCP consists of three 16-bit words to drive all lights and displays. The OCP lights and displays are held constant to the data last received from the 771. The 771 software will service both input and output at 2 Hz, although input and output does not occur at the same time. The transmission clock and all shift counters are provided from the 771 interface side.

The 771/DAS interface provides a one-way 16-bit parallel data path, with handshaking to allo- each processor (771 and DAS) to operate at its own convenient speed according to current processing demands. Provisions are made for the DAS to signal recording problems back to the 771 (e.g., end-of-tape reached). When the DAS is not connected, the 771 interface will automatically provide the problem signal to the 771 software.

6.3 Operator Control Panel

The Operator Control Panel, shown in Figure 8, provides controls for program load, mode select, reference navigator select, and test/display select. Displays are provided for monitoring system performance data, failure conditions, and operating mode. The OCP mode select rotary switch controls system power to the 771 processor and LCIGS (removed when in the OFF position), enables computer program loading, and the selection of system operating mode. Operating modes consist of TEST, standby (STBY), transfer alignment (ALN), and unaided navigation (NAV). TEST mode provides five built-in-tests which are individually selectable via the test/display select thumbwheel. The tests are intended to verify system flight readiness and supplement fault isolation to the module level. Standby mode provides a nonoperational state which effectively reinitializes filter parameters between runs and disables flight recording. ALN mode can be entered either from STBY or NAV mode. In the latter case, filter parameters (e.g., biases) are not reinitialized. This capability is provided to allow multiposition static lab alignments (NAV mode can be selected during repositioning in order to avoid faulty measurement data). The reference navigator select switch is used by the 771 software to determine which reference data to use, CIRIS or constant laboratory (LAB mode) data. Flight recording is automatically started in ALN and NAV modes.

The six-digit system performance display is controlled by the test/display select thumbwheel in all but TEST mode. (In TEST mode, the display is controlled by specific test requirements.) Examples of selectable parameters are: mode time, position, velocity, and navigation errors.

Extensive and continuous error condition monitoring is provided to supplement the built-in-tests. An error light is provided, along with a two-digit error code display. The following are examples of monitored error conditions: LCIGS overheated, LCIGS and/or CIRIS transmissions overdue, navigation errors exceed tolerance, and LCIGS sensor failures.

FIGURE 8. Operator Control Panel

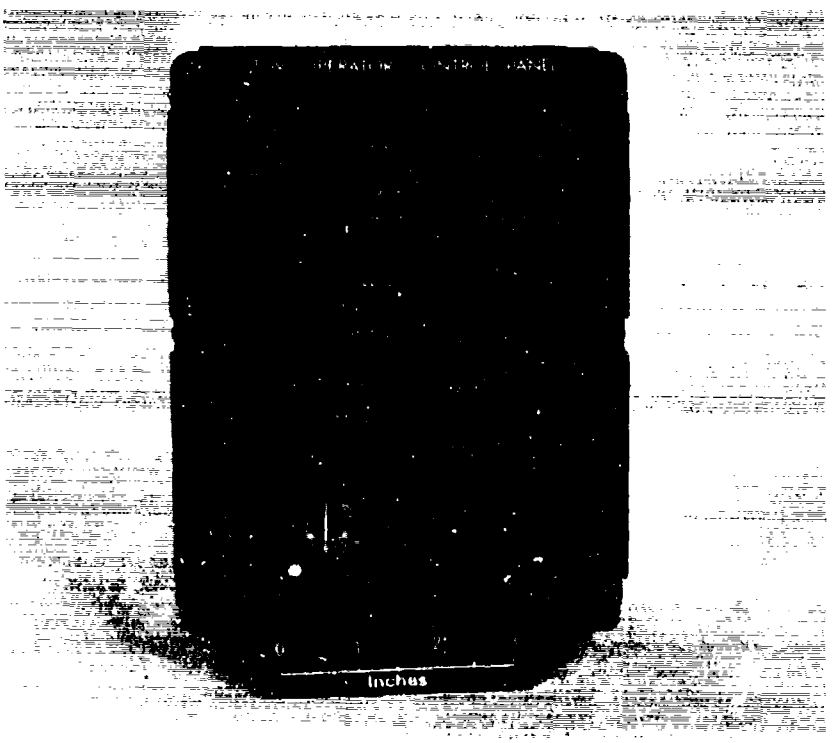

7. Test Plan

The test objectives of the UTGV program are:

1) A determination, through system level testing, of the magnitude of LCIGS sensor errors.

2) A determination of the effectiveness of the peculiar support equipment (PSE) designed for LCIGS in performing pre-flight sensor calibration.

3) A determination of the effectiveness of the 15-state Kalman filter in initializing and aligning the system and calibrating the LCIGS' sensor errors.

4) A determination of the most effective aircraft maneuver for making the LCIGS sensor errors observable.

5) A determination of system accuracy over tactical weapon trajectories up to ten minutes in length.

The test plan calls for an in-house laboratory test phase at MDAC and a Holloman AFB (HAFB) flight test phase. The in-house tests are primarily concerned with system validation and special PSE Effectiveness tests using the switch box capability of the lab test configuration. The Holloman test plans include laboratory tests and C-141 flight tests. Flight testing will emulate as closely as possible the Unaided Tactical Guidance study scenario. The CIRIS is very similar in accuracy to the GPS/Inertial system used in the studies. Benign weapon-like trajectories will be flown by the C-141 to simulate post-launch dynamics and a variety of alignment maneuvers will be tried to determine which allows best sensor calibration.

7.1 Laboratory Tests

Following system integration and software debugging, in-house testing will be conducted at MDAC to validate system navigation performance and initially assess PSE effectiveness. These tests will employ both the laboratory test configuration and the flight test configuration previously discussed (Section 5). The laboratory configuration will be used for software validation and PSE effectiveness testing because the switch box feature allows the processing of LCIGS outputs to be done in either the PSE or the 771 which is useful for comparative analysis.

The LCIGS navigation system performance will be validated in-house through multiposition transfer alignment and navigation runs using lab reference (e.g., zero velocity) as the alignment measurement. The tests will be performed on a two-axis tilt/index table with five minutes allotted for each position in a transfer alignment sequence and 10 minutes for the navigation phase. The following is a listing of the tests:

a. Static transfer alignment and static navigation

b. Static transfer alignment and two-azimuth navigation

c. Two-azimuth transfer alignment and two-azimuth navigation

d. Static transfer alignment followed by navigation with the LCIGS dipped from the alignment position.

e. Transfer alignment with dip and navigation with dip

f. Static transfer alignment and navigation with Scorsby motion

During these tests, position, velocity, attitude, and sensor bias estimates are printed on the Silent 700 terminal for data analysis.

PSE effectiveness will be determined by a series of in-house tests utilizing the switch box capability of the laboratory configuration (Figure 7). These tests consist of a PSE calibration/navigation sequence followed by a transfer alignment/navigation sequence using the Model 771 processor. The gyros will remain powered throughout the entire test so that gyro error estimates and navigation results from the PSE and 771 processor are comparable. The following specific tests will be accomplished.

a. A PSE 1-position Autocal will be followed by a 10-minute PSE static navigation run. A static transfer alignment and navigation will immediately follow. The navigation results and filter estimates of gyro bias will be compared with the PSE navigation results and PSE estimate of gyro bias.

b. A PSE 3-position Autocal test followed by a 10-minute PSE navigation run with a 5-degree dip will be performed. PSE gyro error estimates and position and velocity results will be recorded. A transfer alignment with dip followed by navigation with dip will then be performed and the results compared with PSE results.

c. A PSE 1-position autocal test followed by a 10-minute PSE navigation with Scorsby motion will be performed followed by a static transfer alignment and navigation with Scorsby motion. The gyro estimates and position and velocity errors will be compared.

d. Gyro bias and the three acceleration-sensitive drifts will be determined for each gyro using the 5-position PSE traditional calibration. A test will then be conducted using a series of transfer alignments to provide estimates of gyro bias and output and spin axis acceleration-sensitive drifts. The results will be compared.

7.2 UTG Flight Testing

System performance tests will be conducted by CIGTF at Holloman AFB. Three types of testing are planned: laboratory, ground, and flight. During laboratory testing, the navigation system and the PSE will be evaluated using tables with 3-axis and rate capability. Ground tests will be used to revalidate the system prior to flight tests and to evaluate the system under Scorsby motion. During flight tests, the system will be installed in a C-141 aircraft equipped with CIRIS to evaluate navigation performance in a flight environment.

Laboratory tests will be used to determine the effectiveness of the PSE in calibrating LCIGS and to determine, through system level testing, the characteristics and magnitudes of LCIGS sensor errors. Figure 9 shows the laboratory tests planned and the objective of each test.

Ground testing will be performed to validate system operation prior to flight testing and to collect additional performance data. Tests include: static alignment and static navigation, two-azimuth alignment and two-azimuth navigation, and static alignment followed by navigation with Scorsby motion.

A summary of the planned C-141 flight tests is presented in Figure 10. Transfer alignment maneuvers include acceleration/deceleration, half-S turn, and rudder-only turn maneuvers. The 10-minute navigation profiles consist of straight and level, turn, acceleration, and descending trajectories. Transfer alignment sequences are repeated at least six times, and the navigation profile, with a specific alignment, are repeated at least three times for statistical evaluation purposes. From the data collected on these flights, a determination of the effectiveness of the Kalman filter in initializing and aligning the system and calibrating LCIGS sensor errors can be made. Additionally, the most effective aircraft maneuver for a given post-launch navigation profile and overall system CEP over various tactical weapon trajectories can be determined. Data analysis will be performed independently by both MDAC and CIGTF personnel. The CIRIS position and velocity outputs, time-tagged and recorded during flight, will serve as the absolute reference for the analyses.

LABORATORY TEST	TEST OBJECTIVE
PSE TRADITIONAL CALIBRATION VERSUS PSE FIELD CALIBRATION	DETERMINE EFFECTIVENESS OF PSE FIELD CALIBRATION IN DETERMINING • GYRO BIAS (EACH AXIS) • GYRO INPUT, OUTPUT, AND SPIN AXIS ACCELERATION-SENSITIVE DRIFTS • GYRO SCALE FACTOR
LABORATORY REFERENCE TRANSFER ALIGNMENT AND NAVIGATION A. STATIC ALIGNMENT, STATIC NAVIGATION B. STATIC ALIGNMENT, TWO AZIMUTH NAVIGATION C. TWO AZIMUTH ALIGNMENT, TWO AZIMUTH NAVIGATION D. STATIC ALIGNMENT, NAVIGATION WITH DIP E. ALIGNMENT WITH DIP NAVIGATION WITH DIP	DETERMINE SENSOR ERRORS FROM SYSTEM LEVEL TESTING • GYRO BIAS ERRORS • ACCELEROMETER ERRORS • ACCELERATION SENSITIVE DRIFTS
MULTIPOSITION LEVEL GYRO CALIBRATION	DETERMINE SENSOR ERRORS • GYRO BIAS • GYRO OUTPUT AND SPIN AXIS ACCELERATION SENSITIVE DRIFTS
RATE SENSITIVITY TESTS (RATES FROM 1 TO 100 DEG SEC	DETERMINE SENSOR CHARACTERISTICS • GYRO PLUS AND MINUS SCALE FACTOR • INPUT AXIS MISALIGNMENTS • GYRO RATE SENSITIVITY
THERMAL TESTS A. 10°C COOLDOWN TESTS B. CONSTANT TEMPERATURE TESTS	DETERMINE SENSOR CHARACTERISTICS • GYRO TEMPERATURE SENSITIVITY AND STABILITY

FIGURE 9. CIGTF Laboratory Tests

FIGURE 10. CIGTF C-141 Flight Tests

TRANSFER ALIGNMENT (6 MINUTES)	NAVIGATION PROFILE (10 MINUTES)
ACCELERATION/DECELERATION • STRAIGHT AND LEVEL FOR 3 MIN AT 250 KTAS (463 km/hr) • AT 3 MIN ACCELERATE TO 350 KTAS (649 km/hr) • AT 3.5 MIN DECELERATE TO 250 KTAS (463 km/hr) • STRAIGHT AND LEVEL AT 250 KTAS (463 km/hr)	1. STRAIGHT AND LEVEL 2. TURN (60° TURN AT 30° BANK AT 1 min) 3. ACCELERATION (ACCELERATE TO 350 KTAS AT 1 MIN) 4. DESCEND AT 1000 FT/MIN (305m/min)
ACCELERATION/DECELERATION • SAME MANEUVER SEQUENCE AS ABOVE • CIRIS AIDING OF AIRCRAFT NAVIGATOR TURNED OFF	1. TURN (60° TURN AT 30° BANK AT 1 MIN) 2. ACCELERATION (ACCELERATE TO 350 KTAS AT 1 MIN)
COORDINATED HALF S TURN • STRAIGHT AND LEVEL FOR 3 MIN AT 350 KTAS (649 km/hr) • 45° TURN AT 30° BANK (0.5 MIN) • −90° TURN AT −30° BANK (1 MIN) • 45° TURN AT 30° BANK (0.5 MIN) • STRAIGHT AND LEVEL (1 MIN)	1. STRAIGHT AND LEVEL 2. TURN (60° TURN AT 30° BANK AT 1 MIN)
COORDINATED HALF S TURN • SAME MANEUVER SEQUENCE AS ABOVE • TURN COMPENSATION INHIBITED	1. STRAIGHT AND LEVEL 2. TURN (60° TURN AT 30° BANK AT 1 MIN)
EXCESS RUDDER TURN • STRAIGHT AND LEVEL FOR 3 MIN AT 350 KTAS (649 km/hr) • 45° TURN AT 1.5 DEG/SEC HEADING RATE WITH EXCESS RUDDER • −90° TURN WITH RUDDER • 45° TURN WITH RUDDER • STRAIGHT AND LEVEL (1 MIN)	1. STRAIGHT AND LEVEL 2. TURN (60° TURN AT 30° BANK AT 1 MIN)

8. Conclusion

The hardware and software described has been integrated to form a flight-ready system. The Laboratory testing described in Section 7 will commence in May 80 and the system sent to Holloman AFB in mid-June 80 for flight test. The flight testing of the brassboard LCIGS system will be completed in October 80 with engineering model LCIGS system flight test to follow shortly thereafter. In October 81 the UTG concept will be free-flown in a midcourse guidance demonstration.

REFERENCES

1. Cox, J. W., "Low Cost Inertial Guidance with GPS Update for Tactical Weapons," NAECON 1976 RECORD", pp 623-626, May 1976

2. Perlmutter, L. C., Kraemer, J. W., and Roessler, N. J., "Strapdown Inertial Sensor Requirements for Tactical Guidance", NAECON 1977 RECORD, pp 424-432, May 1977

3. Mueller, C. E., Phelps, R. K., and Scheidenhelm, R., "Tactical Guidance Requirements for Strapdown Inertial", NAECON 1977 RECORD, pp 433-440, May 1977

4. Wu, T. K., Filiatreau, T. R., and Gilmore, J. P., "A Design Concept for Low Cost Inertial Guidance of Tactical Weapons", NAECON 1978 RECORD, p 405, May 1978

5. Gilmore, J. P., "Modular Strapdown Guidance Unit With Embedded Microprocessors", Journal of Guidance and Control, Vol. 3, pp 3-10, Jan-Feb 1980

6. Stob, W. K., Wu, T. K., "Industry Low Cost Inertial Guidance Subsystem Development", AGARD RECORD, 30th Guidance and Control Panel Symposium

7. Kraemer, J. W., Roessler, J. J., and Brandin, D. M., "In-Flight Alignment/Calibration Techniques for Unaided Tactical Guidance", NAECON 1978 RECORD, pp 705-711, May 1978

8. Ignagni, M. B., and Mueller, C. E., "Optimal Tactical Guidance Requirements for Unaided Strapdown Inertial", NAECON 1978 RECORD, p 415, May 1978

9. Henne, A. M., and Geyer, D. W., "Integration of Digital Avionics Components For Guided Weapons", AGARD RECORD, 30th Guidance and Control Symposium

ACKNOWLEDGMENT

The work reported in this paper was sponsored by the Air Force Armament Laboratory of the Air Force Systems Command under Contract F08635-79-C-0175. Publication of this paper does not constitute approval by the U. S. Air Force of the findings or conclusions contained herein. It is published for the exchange and stimulation of ideas.

The authors acknowledge the contributions of the MDAC team to the UTGV program. The UTGV documentation (i.e., design definition, software development specification, and test plan) provided the basis for this paper.

APPLICATION OF MODERN CONTROL THEORY TO THE GUIDANCE OF AN AIR TO AIR DOGFIGHT MISSILE

By

M. MIRANDE
Chef du Département des Missiles Courte Portée
de la Société MATRA

M. LEMOINE
Chef du Groupe de Pilotage Guidage
de la Société MATRA

E. DOREY
Ingénieur du Groupe Pilotage Guidage
de la Société MATRA

37, Av. Louis Bréguet
78140 Vélizy - FRANCE

ABSTRACT

The optimal guidance laws proposed for air to air missiles are generally based upon a criterium involving the miss distance and sometimes the energy consumed for manoeuvering.

These guidance laws lead, assuming a linearization around the collision course, to proportional navigation in the simplest case, and to the well known four state law, if additional refinements are introduced.

However, these results assume implicitely small perturbations around the collision course, or a relatively long range firing ; this is not the case with air to air dogfight missiles, specially with large off-boresight launch conditions and short firing ranges.

The aim of the study which has been undertaken was to derive an "optimal" guidance law (taking into account the flight time and the consumed energy in the "cost" function), without having to assume linearization, i.e low off-boresight conditions with respect to the collision path. A condition on miss distance is set by imposing a constraint on the final state missile to target range. The study has been conducted assuming a constant speed missile, which has led to a closed forme analytical expression for the guidance law.

However, this solution imposes to know the final state ; in order to solve difficulty, we have developped an algoritbm to mechanize the guidance law.

The results obtained with the optimal guidance law have been compared to the ones obtained with conventional proportional navigations (true P.N and pure P.N).

The results show that the optimal guidance law derived in this study is always convergent, even in firing conditions where T.P.N. fails (large off boresight) ; however, it seems that P.P.N. leads to very comparable results, provided the gain is adequately adjusted, without the complication of needing the final state knowledge.

1. INTRODUCTION

Les lois de guidage optimales classiques, (four state law, par exemple), supposent que le missile est tiré au voisinage des conditions de collision.

Or, dans de nombreux cas, les missiles de combat rapproché futurs seront tirés avec un fort depointage initial par rapport à ces conditions.

Pour tenter de résoudre ce problème, nous avons étudié une loi de navigation "optimale" pour un missile évoluant dans un plan, à vitesse constante, mais sans hypothèse simplificatrice sur la direction de son vecteur vitesse.

Le critère d'optimisation choisi concerne le temps de vol et la consommation d'énergie.

Dans le cas d'un missile évoluant à vitesse constante et disposant d'un temps de réponse en accélération latérale infiniment court, une formulation analytique de cette loi de guidage optimale a pu être explicitée.

Nous avons ensuite défini un algorithme de résolution en vue d'une mécanisation de la loi. On peut ainsi utiliser cette loi sur un modèle plan plus réaliste (missile présentant des saturations de manoeuvrabilité, cible manoeuvrante).

2. CINEMATIQUE ET EQUATIONS D'ETAT

Supposant que la cible et le missile évoluent dans un plan, la géométrie relative de ces deux mobiles est définie par la figure suivante :

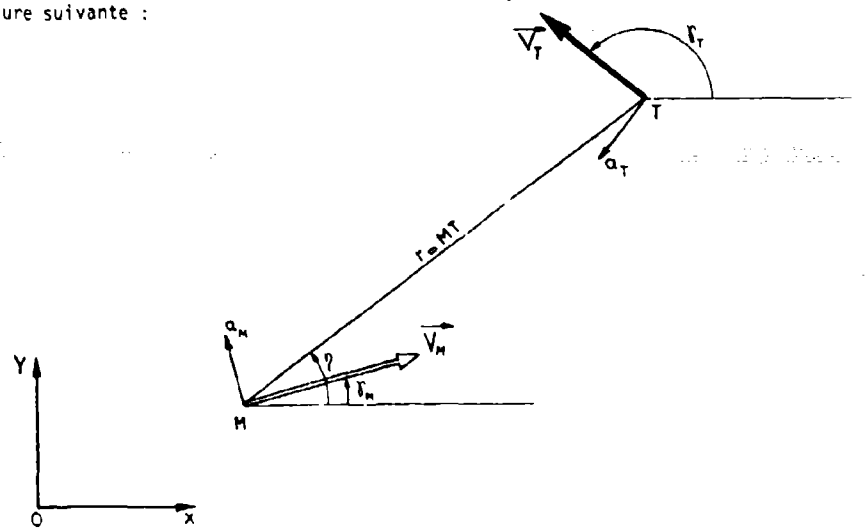

Avec :

OXY repère inertiel de référence

T position de la cible

$\vec{V_T}$ vecteur vitesse de la cible

V_T module de la vitesse de la cible

γ_T angle $(\vec{OX}, \vec{V_T})$ définissant la direction de la vitesse de la cible par rapport au repère inertiel.

a_T accélération de la cible normale au vecteur vitesse

M position du missile

x_M, y_M coordonnées du missile dans le repère OXY

$\vec{V_M}$ vecteur vitesse du missile

V_M module de la vitesse du missile

γ_M angle $(\vec{OX}, \vec{V_M})$ définissant la direction de la vitesse du missile par rapport au repère inertiel.

a_M accélération du missile, normale au vecteur vitesse.

r=MT distance missile - cible

η angle $(\vec{OX}, \vec{MT})$ définissant la direction de la droite missile - but par rapport au repère inertiel.

En supposant que :

. La vitesse V_M du missile est une constante

. Le missile est commandé en accélération perpendiculairement à sa vitesse

. Le temps de réponse du missile à cette commande est nul.

Les équations d'état du système peuvent s'écrire :

$$\begin{cases} \dot{\eta} = \frac{1}{r}\left[V_M \sin(\eta - \gamma_M) - V_T \sin(\eta - \gamma_T)\right] \\ \dot{r} = V_T \cos(\eta - \gamma_T) - V_M \cos(\eta - \gamma_M) \\ \dot{\gamma}_M = \frac{a_M}{V_M} \end{cases}$$

3. POSITION DU PROBLEME ET SOLUTION

Compte tenu des hypothèses effectuées, l'état initial du système est défini par :

$$r_o \ , \ \eta_o \ , \gamma_{m_o}$$

Cet état initial étant défini, on se propose d'atteindre la cible en minimisant le critère

$$J = t_f + k \int_{t_o}^{t_f} a_m^2 . d\tau$$

en s'imposant une contrainte sur la distance missile-cible finale :

$$r(t_f) = r_f = \ell$$

Cette distance pouvant être choisie aussi petite qu'on le désire, on s'impose donc d'atteindre la cible.

On peut noter que la minimisation du temps de vol est particulièrement importante pour la survie du tireur alors que la distance de passage n'influe pratiquement pas sur la trajectoire du missile lorsqu'il est tiré avec un fort dépointage initial et à une distance raisonnable de la cible : il nous semble donc particulièrement judicieux d'imposer la distance de passage tout en minimisant le temps de vol.

Le problème posé est classique : la commande s'obtient en résolvant les équations de Pontriaguine.

Cette résolution a été menée à bien dans le cas où la vitesse du missile est constante.

Cette commande optimale satisfait l'équation :

$$\boxed{a_m = \varepsilon \sqrt{\frac{2 V_m}{-k . \dot{r}_f} . \left[\cos^2\left(\frac{\eta_f - \gamma_{m_f}}{2} \right) - \cos^2\left(\frac{\eta_f - \gamma_m}{2} \right) \right]}}$$

avec

$$\varepsilon = \operatorname{sgn}\left[\sin(\eta_f - \gamma_{m_f}) \right]$$

On peut remarquer que cette commande s'exprime en fonction de l'état final, ce qui pose le problème particulièrement délicat d'exprimer l'état final en fonction de l'état initial.

4. MECANISATION DE LA LOI

4.1 Position du problème

Afin d'utiliser la loi de guidage précédemment définie, il convient de calculer l'état final en fonction de l'état initial.

La derobade de la cible étant difficilement mesurable à bord d'un missile, nous avons supposé que la cible volait en ligne droite à vitesse constante.

Dans ce cas, les directions finales de la droite missile but (η_f) et de la vitesse du missile (γ_{m_f}) sont définies par les deux équations implicites suivantes :

$$\begin{cases} x_{m_f} - x_{m_o} - V_T \cos\gamma_T \, t_f + r_f \cos\eta_f - r_o \cos\eta_o = 0 \\ y_{m_f} - y_{m_o} - V_T \sin\gamma_T \, t_f + r_f \sin\eta_f - r_o \sin\eta_o = 0 \end{cases}$$

avec

r_f : distance finale imposée

$$t_f = \sqrt{\quad} + V_m^2 \quad (r_o - r_f)$$

$$K_1 = \int \frac{du}{\sqrt{\quad}} \qquad \psi_f = \frac{\eta_f - \gamma_{m_f}}{2}$$

$$K_2 = \int \frac{du}{\sqrt{\quad}}$$

$$u = \text{Arc sin}\,\frac{\cos\psi}{\cos\psi_f} \qquad \psi = \frac{\eta_f - \gamma_M}{2}$$

$$\alpha_f = \text{Arc sin}\,\frac{\cos\psi_o}{\cos\psi_f}$$

$$x_{M_f} = V_M^2 \sqrt{\frac{-2k\dot{r}_f}{V_M}}\,.\,(A.\cos\eta_f + \varepsilon.B.\sin\eta_f) + x_{M_o}$$

$$A = K_1 - K_2 - 2\,(E_1 - E_2)$$

$$B = 2.\sqrt{\cos^2\psi_f - \cos^2\psi_o}$$

$$\varepsilon = \text{sgn}\left[\sin(\eta_f - \gamma_{M_f})\right]$$

$$E_1 = \int_0^{\pi/2} \sqrt{1 - \cos^2\psi_f \sin^2 u}\;.du$$

$$E_2 = \int_0^{\alpha_f} \sqrt{1 - \cos^2\psi_f \sin^2 u}\;.du$$

$$y_{M_f} = V_M^2 \sqrt{\frac{-2k\dot{r}_f}{V_M}}\,.\,(A.\sin\eta_f - \varepsilon\,B.\cos\eta_f) + y_{M_o}$$

On note que :

K_1 est une fonction elliptique complète de 1ère espèce

K_2 une fonction elliptique incomplète de 1ère espèce

E_1 une fonction elliptique complète de 2ème espèce

E_2 une fonction elliptique incomplète de 2ème espèce

Dans ces conditions, le système des deux équations prend la forme :

$$\begin{cases} F(r_o, \eta_o, \gamma_{M_o}, \gamma_{M_f}, \eta_f) = 0 \\ G(r_o, \eta_o, \gamma_{M_o}, \gamma_{M_f}, \eta_f) = 0 \end{cases}$$

Ce qui permet théoriquement de calculer, en fonction des conditions initiales, γ_{M_f}, η_f, et donc la commande.

En pratique, ce calcul nécessite un algorithme assez complexe, et ce d'autant plus, que le système précédemment obtenu peut avoir plusieurs solutions.

4 - Algorithme de calcul de l'état final en fonction de l'état initial.

On propose tout d'abord de localiser les solutions. Dans ce but, on effectue un balayage préliminaire sur les conditions finales en respectant les contraintes suivantes :

. La vitesse de rapprochement finale doit être positive :

$$\dot{r}_f < 0 \longrightarrow V_M \cos(\eta_f - \gamma_{M_f}) > V_T \cos(\eta_f - \gamma_T)$$

. Le carré de la distance finale doit également être positif :

$$\ldots \longrightarrow \left|\cos\left(\frac{\eta_f - \gamma_{M_o}}{2}\right)\right| \leq \left|\cos\left(\frac{\eta_f - \gamma_{M_f}}{2}\right)\right|$$

Une fois l'ensemble des solutions localisé, la convergence vers chacune des solutions s'obtient grâce à un classique algorithme de Newton.

On calcule alors le critère J pour chacune des solutions par la formule :

$$J = \sqrt{-\dot{r}_f . k . V_M} \cdot \left\{ (K_1 - K_2) . \left[1 + \frac{V_M}{\dot{r}_f} . (1 - \cos 2\psi_f) \right] - \frac{2 V_M}{\dot{r}_f} . (E_1 - E_2) \right\}$$

La comparaison des différentes valeurs obtenues pour le critère permet alors de sélectionner l'état final correspondant à la commande optimale.

4.3 Guidage en boucle fermée

Dans le cas où des perturbations non prises en compte dans la loi de guidage interviennent (saturation de la commande, dérobade de la cible ...), les conditions finales correspondant à la commande optimale changent : il faut donc calculer l'état final au cours du vol à intervalles réguliers.

Dans ce but, on utilise l'algorithme de Newton en résolvant le système ayant pour conditions initiales les conditions de l'instant courant et en utilisant comme solution approchée, celle obtenue au pas précédent.

5. SIMULATION

5.1 Introduction

Afin de comparer la loi de guidage précédemment définie aux lois de navigation classiques, un modèle cinématique plan a été programmé sur calculateur numérique.

Les lois de guidage utilisées pour la comparaison sont :

. La navigation proportionnelle "pure" (P.P.N.) :

$$a_M = A . V_M . \dot{\eta}$$

. La navigation proportionnelle "vraie" (T.P.N.) :

$$a_M = - \frac{a . \dot{r}}{\cos(\eta - \gamma_M)} . \dot{\eta}$$

Les comparaisons ont été effectuées sur des cas de tir

anti-parallèles : $\gamma_{T_0} = 180°$ et $\gamma_{M_0} = 0$

avec vitesse cible : $V_T = 400\ m/s$

et une vitesse missile : $V_M = 600\ m/s$

Par ailleurs, afin de tester la loi de guidage optimale face à des perturbations non prises en compte au niveau de la définition de la loi, les phénomènes suivants on été introduits dans le modèle :

. Saturation de la commande

. Dérobade de la cible

5.2 Résultats de simulation

5.2.1 Comparaison de la loi de guidage optimale avec des lois classiques (P.P.N. et T.P.N.)

Supposant une cible non manoeuvrante et un temps de réponse nul pour le missile, on démontre que la navigation proportionnelle, avec un coefficient réduit de 3, est optimale du point de vue minimisation de la distance de passage et de l'énergie dépensée lorsqu'on annule le coefficient de pondération affectant l'énergie dépensée.

Cette démonstration supposant que le missile soit tiré au voisinage de la collision, il nous a semblé intéressant de comparer notre loi de guidage optimale à la navigation proportionnelle vraie (T.P.N.) pour un cas de tir ne s'éloignant pas trop de la collision moyenne (cf planche n° 1).

Pour un coefficient de pondération $k = 10^{-4}$, les trajectoires de la loi de guidage optimale (O.G.L.) et de la navigation proportionnelle sont confondues (cf planche n° 1).

Les commandes sont par ailleurs très voisines (cf planche n° 1) de même que les temps de vol (8,09 s pour l'O.G.L. contre 8,08 s pour la T.P.N.) et les critères (18,5 s pour les deux lois).

Ce résultat montre, du moins à notre avis, la qualité de la loi de guidage proposée et nous autorise à poursuivre son étude.

Lorsque l'on s'éloigne un peu plus des conditions de collision (cf planche n° 2), la commande de la loi de guidage optimale , obtenue avec un coefficient de pondération $k = 10^{-4}$, s'éloigne de celle obtenue avec une loi de guidage en navigation proportionnelle "vraie" dotée d'un coefficient réduit $a = 3$ (cf planche n° 2).

Par contre, en utilisant une loi de guidage en navigation proportionnelle "pure" avec un coefficient $A = 4$, on obtient une trajectoire et une commande très voisines de celles de la loi de guidage optimale.

Lorsque l'angle initial entre la vitesse du missile et la droite missile - but dépasse 90° (cf planche n° 3) la loi de guidage en navigation proportionnelle "vraie" est mise en défaut.

Utilisant toujours un critère pondéré par un coefficient $k = 10^{-4}$ et pour le cas de tir présenté sur la planche n° 4, on obtient un temps de vol de 30.8 s et un critère de 61.1 s.

Des résultats très voisins en ce qui concerne la trajectoire, la commande (cf planche n° 3), le temps de vol (31.6 s) et le critère (61.1 s) sont obtenus en utilisant une loi de guidage en navigation proportionnelle "pure" de gain $A = 2$.

En utilisant un gain $A = 6$, on obtient une trajectoire beaucoup plus tendue ($t_f = 16.5$ s) dont on peut se demander si elle correspond à une trajectoire optimale.

Utilisant un coefficient de pondération de 10^{-5}, on obtient en effet une trajectoire optimale très voisine de la trajectoire obtenue avec un gain $A = 6$ (cf planche n° 4).

En fait, la trajectoire optimale est encadrée par les courbes obtenues pour $A = 4$ et $A = 6$.

Il semble donc bien que la loi de guidage optimale soit très voisine d'une loi de navigation proportionnelle pure dont on saurait adapter le gain A au cas de tir si on veut garder l'équivalence avec une loi optimisée pour un coefficient de pondération k constant.

5.2. Sensibilité de la loi de guidage optimale à des perturbations

On peut se poser le problème de la sensibilité de la loi de guidage optimale à certaines perturbations.

Nous avons donc introduit dans le modèle une saturation de la commande à 400 m/s2 et une dérobade de la cible de 30 m/s2.

On peut rappeler à ce sujet que la loi de guidage a été mécanisée en supposant une cible volant en ligne droite.

On constate encore une fois sur la planche n° 5 que les lois de guidage optimales et de navigation proportionnelle "pure" sont très voisines et qu'elles réagissent toutes les deux très bien aux perturbations introduites.

6. CONCLUSION

Par rapport aux lois de guidage optimales classiques, celle que nous proposons ici est donc originale à plus d'un titre :

. Elle ne suppose pas que le missile vole au voisinage des conditions de collision.

. Elle fait intervenir dans son critère d'optimisation le temps de vol du missile et l'énergie dépensée.

. La distance de passage est imposée comme une contrainte sur les conditions finales.

Ces particularités semblent, à priori, particulièrement intéressantes pour le guidage des missiles de combat rapproché.

A posteriori, nous avons vérifié l'intérêt de cette loi qui donne des résultats très voisins de la navigation proportionnelle "vraie" lorsqu'on est au voisinage des conditions de collision.

Lorsque l'on s'écarte de ces conditions, la navigation proportionnelle "vraie" peut être mise en défaut et l'intérêt de la loi étudiée apparaît clairement.

Cette loi est malheureusement très difficile à mécaniser puisque la commande s'exprime en fonction de l'état final. On est donc conduit à chercher une loi simple se rapprochant de la loi de guidage optimale étudiée ici.

Les résultats que nous avons obtenus semblent montrer que la loi de guidage optimale se rapproche d'une loi de navigation proportionnelle "pure", à condition, toutefois, de savoir choisir son gain A en fonction des conditions de tir.

Une exploitation systématique de la mécanisation que nous avons mise au point devrait permettre d'atteindre ce résultat.

Cette étude devrait se poursuivre par la recherche d'une loi sub-optimale dérivée de la loi trouvée, mais plus simple à mécaniser et par l'étude des performances sur la limite courte d'un domaine de tir.

PLANCHE N° 1

$\eta_0 =$ [illegible] $r_0 =$ 7000 m

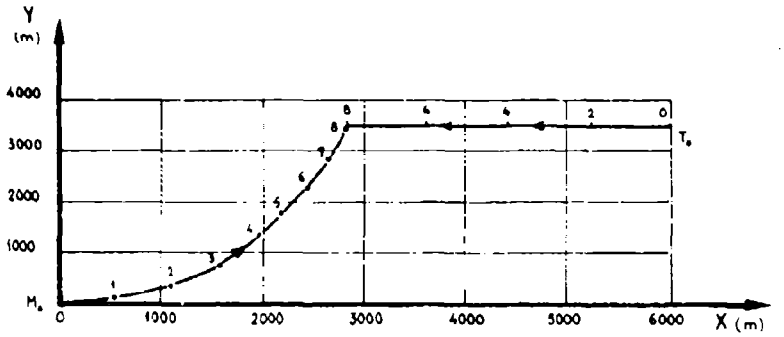

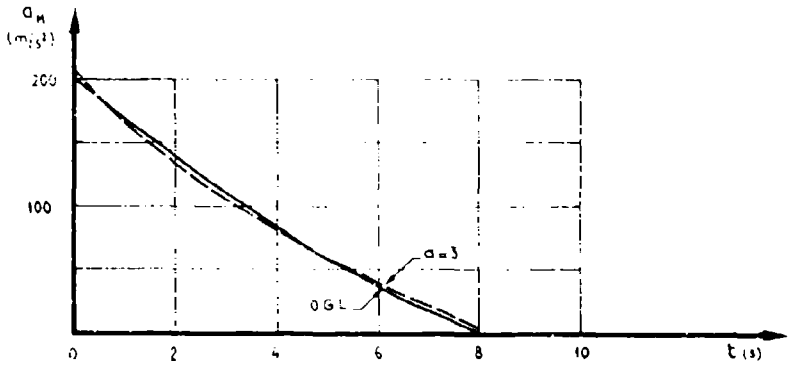

[illegible]

	t_f (s)	J (S)
[illegible]	[illegible]	[illegible]
	[illegible]	[illegible]

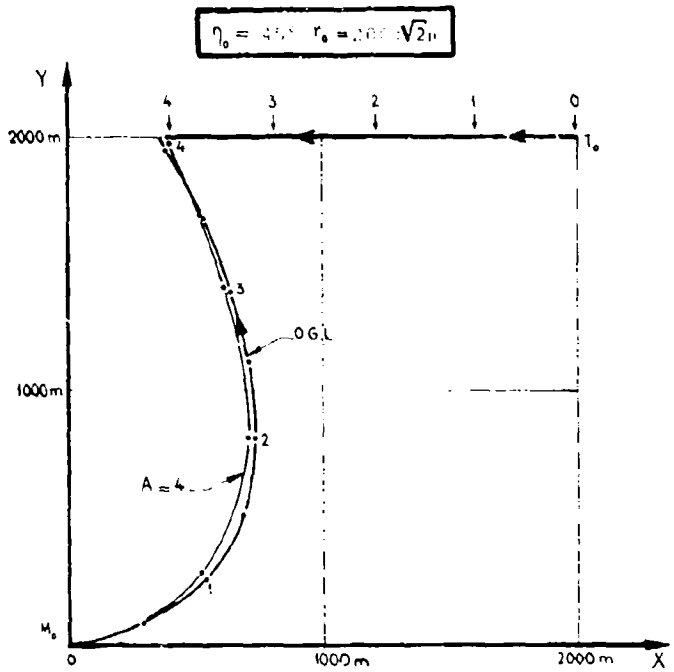
Y
2000 m
1000 m
M_0
0
1000 m
2000 m
X
4
3
2
1
0
T_0
O.G.L
A = 4

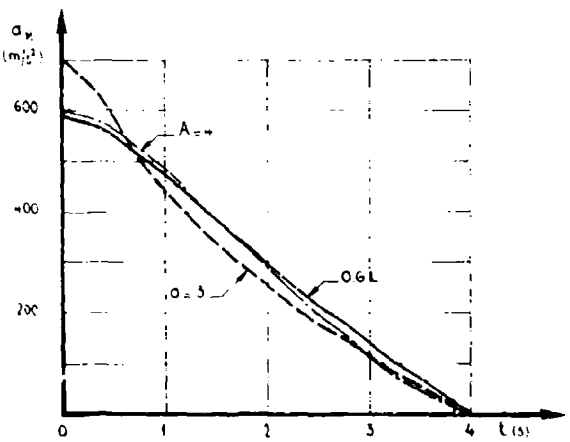
600
400
200
A = ∞
O.G.L
0
1
2
3
4
t (s)

	t_f (s)	J (s)

PLANCHE N° 3

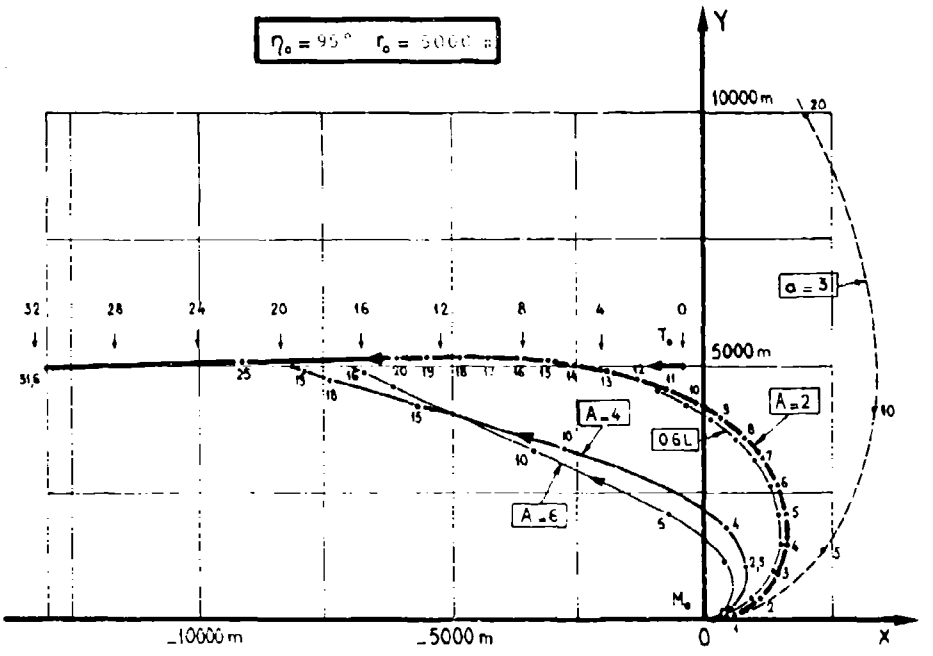

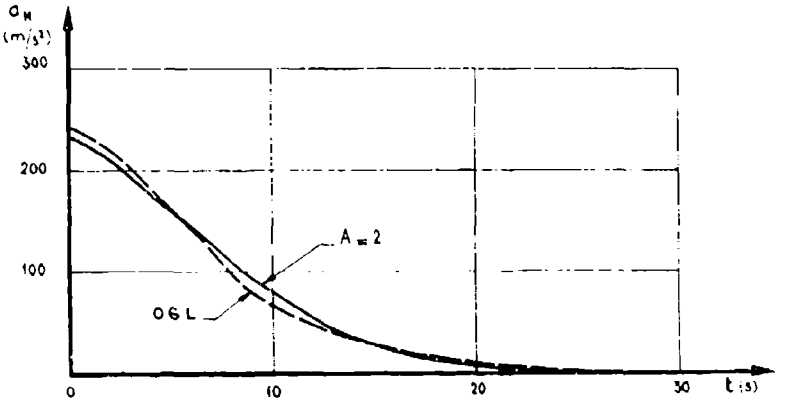

	t_f (s)	J (s)

PLANCHE N° 4

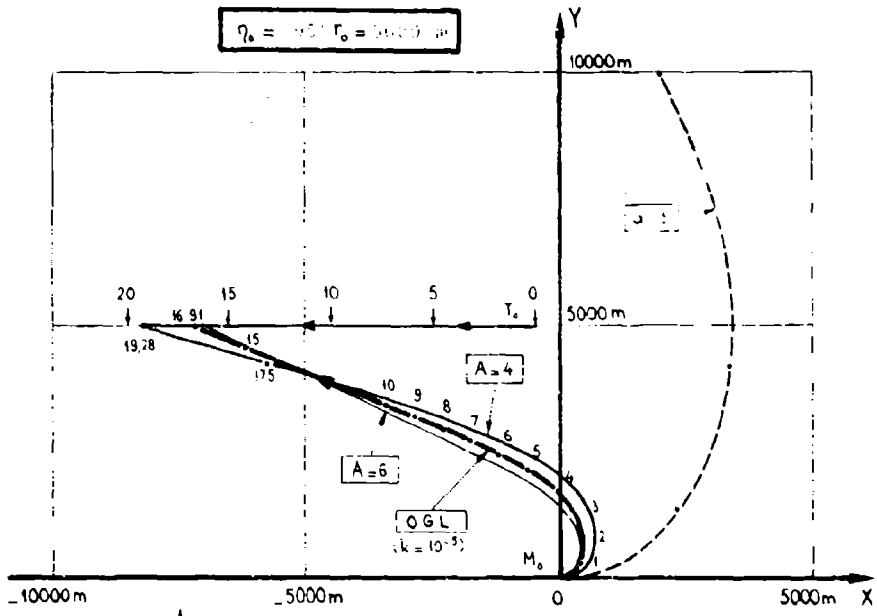

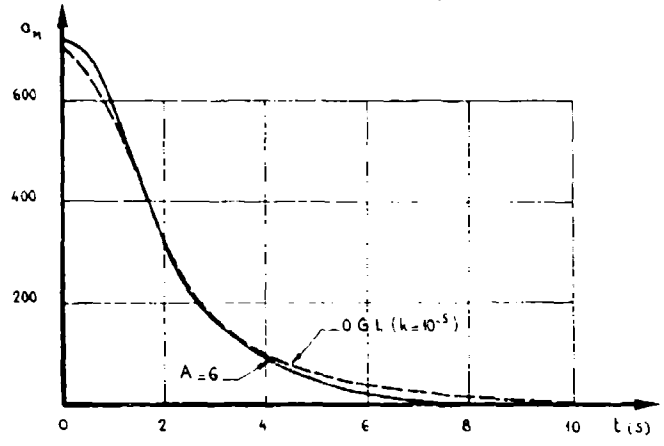

	t_f (s)	J (s)

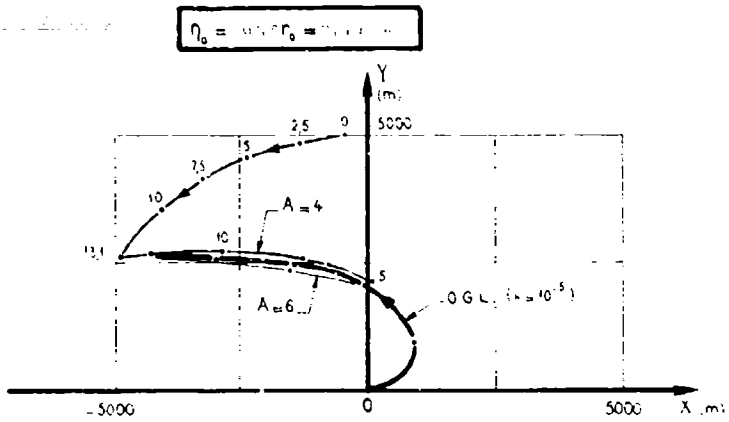
Y
(m)
5000
2,5
0
5
7,5
10
A = 4
10
12,5
5
A = 6
OGL
-5000
0
5000
X (m)

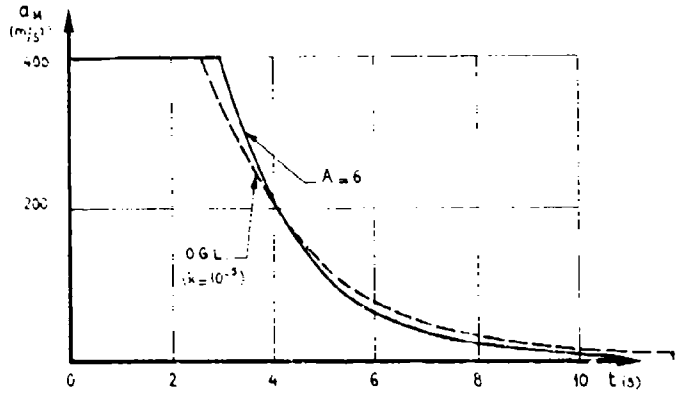
400
200
A = 6
OGL
0
2
4
6
8
10
t (s)

CLASSICAL VERSUS MODERN HOMING MISSILE GUIDANCE

F. William Nesline and Paul Zarchan
Raytheon Company, Missile Systems Division
Bedford, Massachusetts 01730

ABSTRACT

Modern guidance systems are generally accepted to yield better performance than classical proportional navigation systems. However, it is not always recognized that this better performance carries with it certain costs in improved components or additional instruments. This paper compares a modern guidance system, MGS, to a classical proportional navigational, PN, homing missile guidance system in terms of performance, robustness, and ease of implementation. Quantitative first order miss distances are compared to show that MGS has the smallest miss if component tolerances can be met, but as component tolerances or measurement errors degrade, MGS degrades faster than PN until, at relatively large component or measurement errors, PN has less miss distance than MGS.

INTRODUCTION

During the 1960's modern control theory was used in theoretical studies of closed form guidance laws for intercepter missiles. It was shown that PN was an optimal solution to the linear guidance problem in the sense of producing zero miss distance for the least integral square control effort with a zero lag guidance system in the absence of target maneuver.[1] This important result gave credibility to the use of modern control theory as a tool that many analysts have used to derive missile guidance laws.[2, 3, 4] Although much has been written concerning the mathematics of guidance, little, if any, has appeared in the open literature concerning the practical implementation of a modern guidance system, MGS.

Proportional navigation has been in use for over three decades on radar, TV, and IR homing missile systems because of its effectiveness.[5, 6] Although PN was apparently known by the German scientists at Peenemünde, no application using PN was reported.[7] It was first studies by C. Yuan and others during World War II at the RCA Laboratories under the auspices of the U.S. Navy[8], it was extensively studied by Bennett and Matthews at Hughes Aircraft and implemented in a pulse radar system[9], and it was fully developed by H. Rosen and M. Fossier for a continuous wave radar system at Raytheon Company. The latter development included a closing velocity multiplier to compensate the guidance law dynamically in flight for changing engagement geometry. After World War II, the U.S. work on PN was declassified and first appeared in the Journal of Applied Physics.[10]

The purpose of this paper is to compare both classical and modern methods of guidance in terms of performance and implementation. Both guidance philosophies are reviewed and typical implementations are discussed. Finally both methods of guidance are compared in terms of performance and sensitivity to errors in implementation.

Proportional Navigation

Proportional navigation, PN, is a method of guidance in which the missile acceleration is made proportional to the line of sight rate. The geometry of an idealized intercept in which the missile and target are closing on each other at constant speed is shown in Figure 1. Here movement of the missile and target cause the line of sight to rotate through a small angle, λ, indicating a differential displacement, y, between target and missile perpendicular to the reference. The PN guidance law is an attempt to mechanize an acceleration command, n_c, perpendicular to the line of sight according to

$$n_c = N' V_c \dot{\lambda} \tag{1}$$

where N' is the effective navigation ratio, V_c is the closing velocity, and $\dot{\lambda}$ is the line of sight rate.

The effective navigation ratio determines both the trajectory and acceleration history of the missile. For a zero lag guidance system, PN will result in zero miss distance ($y(t_F)=0$) due to heading error or target maneuver for any N' (assuming infinite missile acceleration capability). This phenomenon is clearly demonstrated for the head-on case in the normalized trajectories shown in Figure 2. Although relative target-missile displacement during the flight increases with decreasing N', all flights result in zero miss distance. The effective navigation ratio influences the accelerations needed to produce zero miss distance. Normalized missile acceleration histories due to both disturbances are shown in Figure 3. Here missile acceleration is monotonically decreasing (except for $N'=2$) for a heading error disturbance and monotonically increasing for a target maneuver distrubance. Figure 3 also shows that increasing N' minimizes the maximum acceleration due to target maneuver but maximizes the maximum acceleration due to heading error. In practice the navigation ratio is held fixed with acceptable values ($3 \le N' \le 5$) determined by noise, radome and target maneuver considerations.

A typical implementation of a PN guidance system is shown in Figure 4 where an inertially stabilized seeker is used to measure the boresight error, ϵ. This signal, which is proportional to the line of sight rate, is low pass filtered to obtain an estimate of the line of sight rate. The time constant, T_N, of the noise filter can be fixed, as in this implementation, or time-varying to account for the range dependence of the measurement noise. The closing velocity can either be estimated, as in IR applications, or measured by a doppler radar, as in radar homing applications. The resulting acceleration command which is proportional to the line of sight rate estimate is applied to an acceleration autopilot that moves wing or tail control surfaces so as to develop the commanded acceleration.

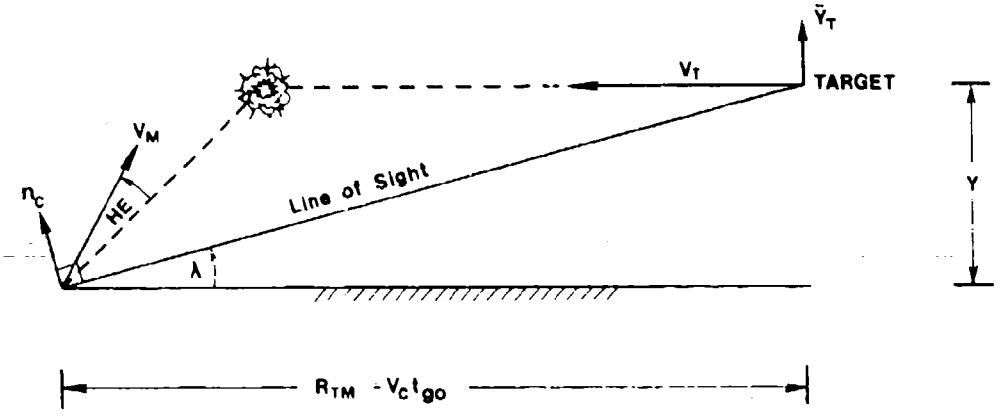

λ - Line of Sight Angle
V_M Missile Velocity
V_T - Target Velocity
n_C - Missile Acceleration
$\bar{Y}_T$ Target Acceleration
V_C - Closing Velocity
HE - Heading Error
Y = Relative Missile - Target Separation

Figure 1 - Intercept Geometry

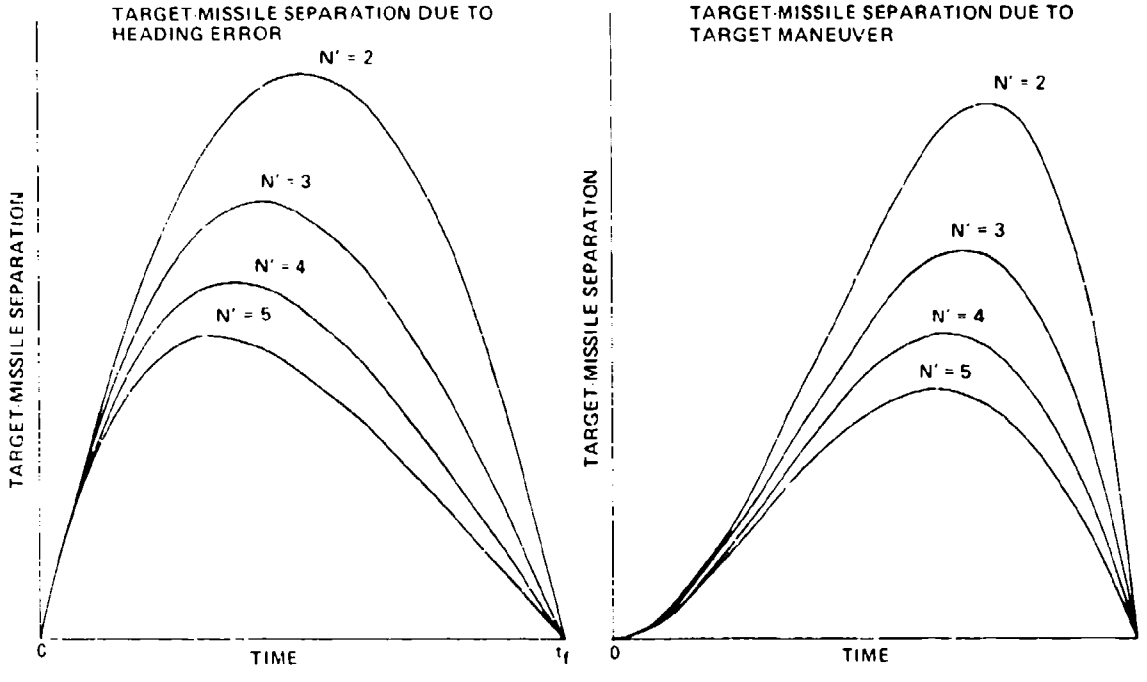

Figure 2 - Typical Proportional Navigation Trajectories

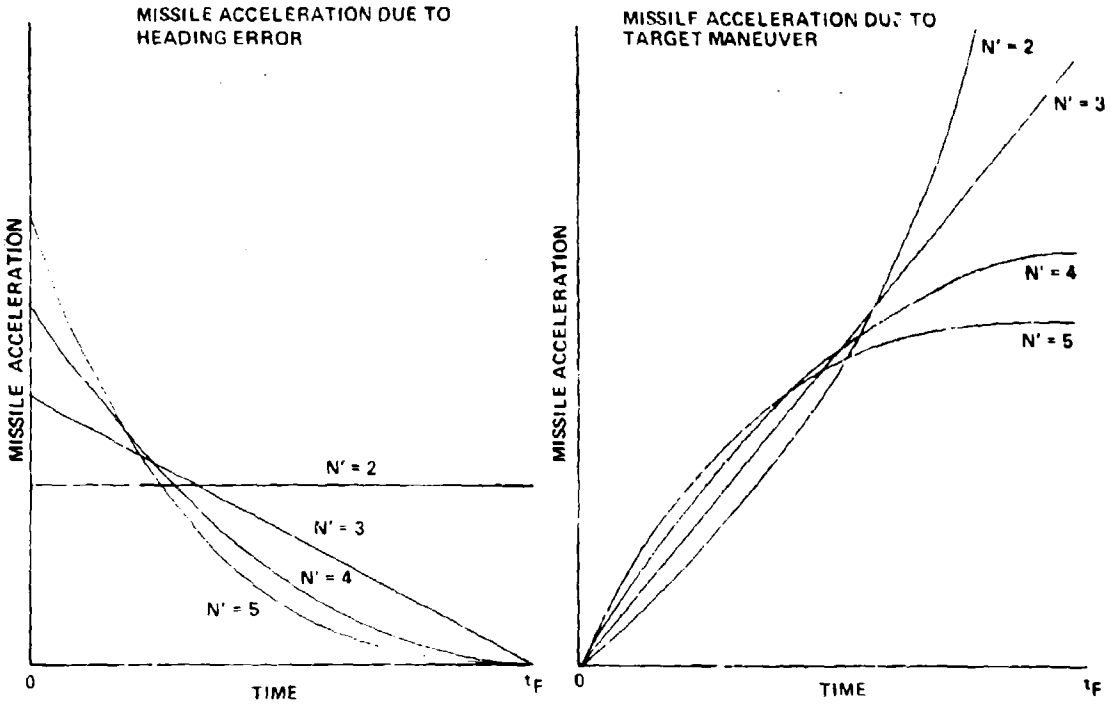

Figure 3 - Typical Proportional Navigation Acceleration Histories

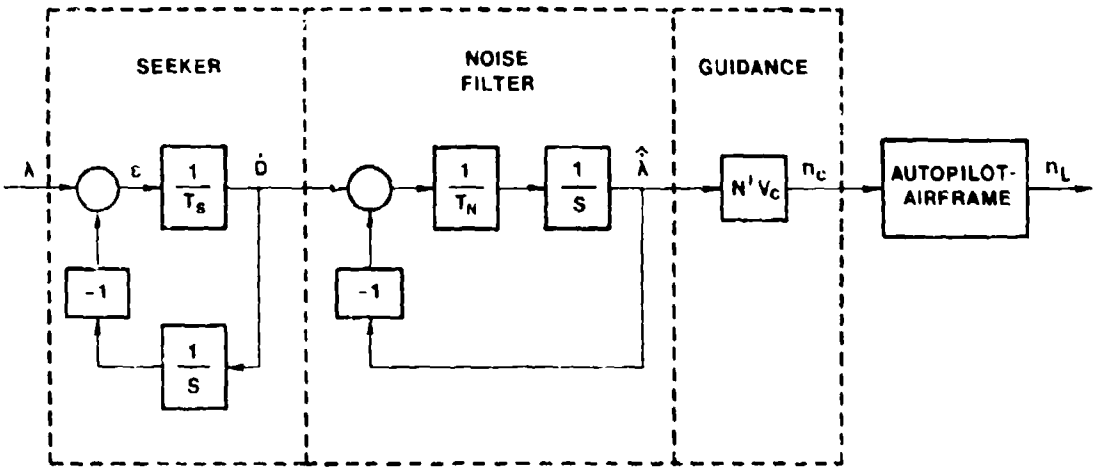

Figure 4 - Proportional Navigation Guidance System - PN

Augmented Proportional Navigation

Other guidance concepts such as those used in modern guidance systems can best be understood by studying proportional navigation. It can be observed from Figure 1 that PN is mathematically equivalent to

$$n_c = N'V_c\dot{\lambda} = N'V_c \frac{d}{dt}\left(\frac{y}{V_c t_{go}}\right) = \frac{N'}{t_{go}^2}\left[y + \dot{y}\, t_{go}\right] \qquad (2)$$

The expression in the brackets of Eq. (2) represents the miss distance that would result in the absence of target maneuvers if the missile made no further corrective accelerations and is referred to as the zero effort miss, ZEM. Therefore PN can be thought of as a guidance law in which acceleration commands are issued inversely proportional to the square of time-to-go and directly proportional to the ZEM. If target maneuver, n_T, is considered, the ZEM changes and a new guidance law knows augmented proportional navigation, APN, results

$$n_c = \frac{N'}{t_{go}^2}\left[y + \dot{y}\, t_{go} + \frac{1}{2} n_T t_{go}^2\right] \qquad (3)$$

This guidance law is compared to PN, in terms of trajectory and acceleration histories, for the case of a maneuvering target with the results displayed in Figure 5. Although both guidance laws achieve zero miss distance, the trajectory and acceleration histories are vastly different. The information concerning target maneuver enables APN guidance to use up less acceleration capability than PN while keeping it closer to an intercept course. In addition the APN acceleration history is monotonically decreasing unlike the monotonically increasing history of PN. It can be shown that for $N'=3$ APN is optimal in the sense that it achieves zero miss distance utilizing the least integral square control effort (see Appendix C).

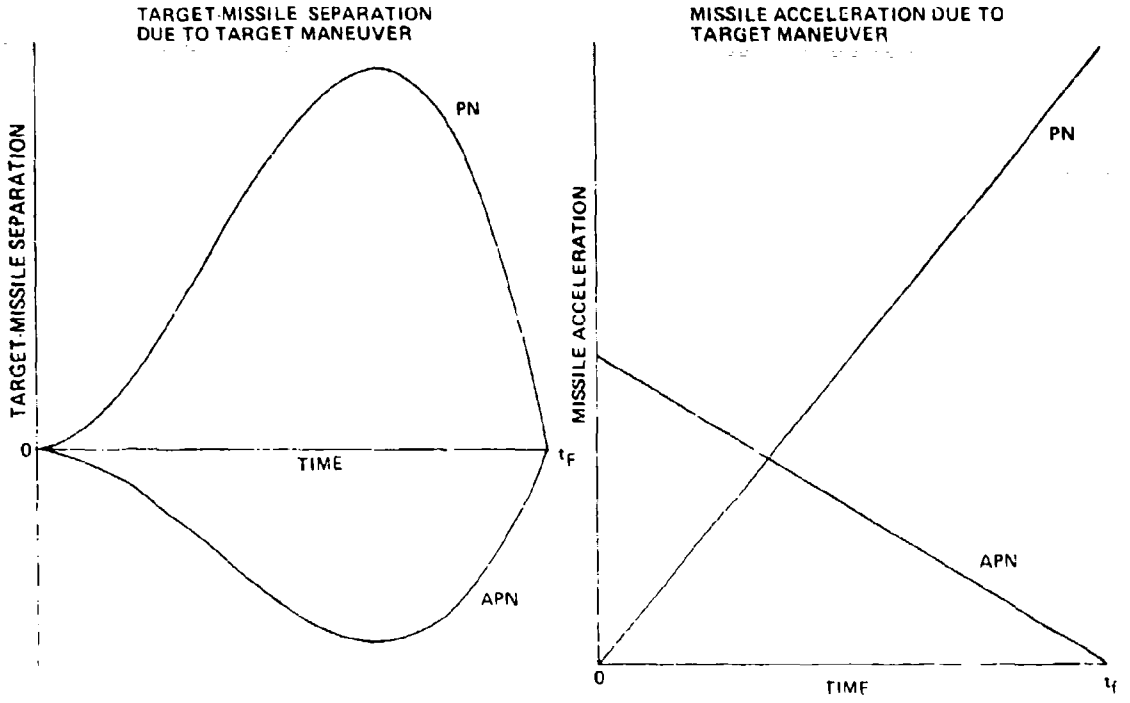

Figure 5 - Guidance Method Comparison

Modern Guidance

In a modern guidance system, the ZEM is modified to take into account target maneuver and missile guidance system dynamics. If the guidance system dynamics can be represented by a first order transfer function, with bandwidth ω, either modern control theory [11] or the Schwartz Inequality (see Appendix D) can be used in deriving a guidance law which drives the miss distance to zero while minimizing the integral of the square of the acceleration, $\left[y(t_F)=0 \text{ subject to minimizing } \int_{t_0}^{t_F} n_c^2 dt\right]$. This law can be written as

$$n_c = \frac{N'}{t_{go}^2}\left[y + \dot{y}t_{go} + \frac{1}{2}n_T t_{go}^2 - n_L\frac{(e^{-T}-1+T)}{\omega^2}\right] \tag{4}$$

where

$$T = \omega t_{go} \tag{5}$$

$$N' = \frac{6T^2(e^{-T}-1+T)}{2T^3+3+6T-6T^2-12Te^{-T}-3e^{-2T}} \tag{6}$$

The expression within the brackets of Eq. (4) is the ZEM and Eq. (6) shows that the effective navigation ratio is time-varying. Therefore this guidance law is a form of APN with an extra term to account for guidance system dynamics and a time-varying navigation ratio.

This guidance law, unlike PN, requires information concerning time-to-go, t_{go}, guidance system bandwidth, ω, and achieved missile acceleration, n_L. Range measurements and additional filtering are required to estimate t_{go} and accelerometer measurements must now be fed into the guidance system. The states required for the implementation of this guidance law (y, $\dot{y}$, n_T) can not be obtained from a simple low pass filter as was done with PN, but must be estimated.

A simple form of a Kalman estimator can be derived by considering the two most important stochastic distrubances in a guidance system, random target maneuver and glint noise. The resulting Kalman filter is stationary and represented by transfer function

$$\frac{\hat{y}}{y^*} = \frac{1 + 2s/\omega_o + 2s^2/\omega_o^2}{1 + 2s/\omega_o + 2s^2/\omega_o^2 + s^3/\omega_o^3} \tag{7}$$

with characteristic frequency, ω_o, given by

$$\omega_o = (\Phi_s/\Phi_N)^{1/6} \tag{8}$$

where Φ_s and Φ_N are estimates of the spectral density levels of the target maneuver process noise and glint measurement noise respectively (See Appendices A and B for derivations via Wiener and Kalman filter formulations). Thus the characteristic frequency of the filter increases with increasing process noise and decreases with increasing measurement noise.

A typical implementation of a modern guidance system appears in Figure 6. Here the line of sight angle is reconstructed from a seeker measurement of the boresight error and by integrating the rate gyro measurement of the secker dish rate. This angle is then converted to relative target-missile position, y^*, by the multiplication of the range measurement. The signal is then sent through the Kalman filter in order to obtain estimates of the necessary states for the implementation of the modern guidance law. These states are multiplied by control gains, which are functions of the estimated time to go and autopilot bandwidth, in order to generate an acceleration command. This command is applied to an acceleration autopilot in order to develop the commanded acceleration.

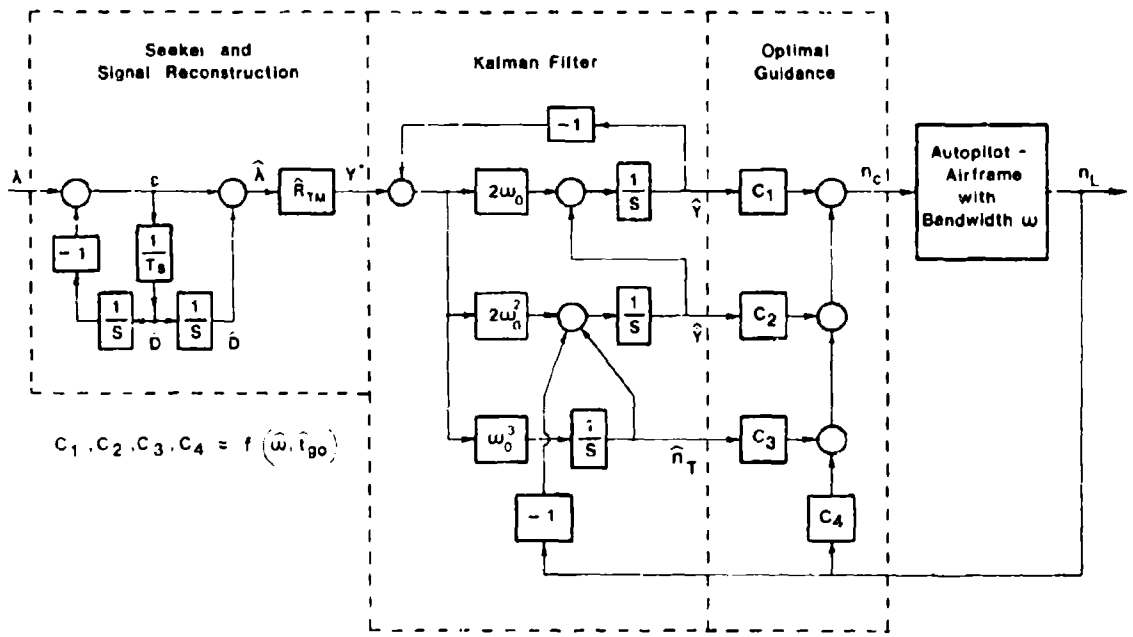

Figure 6 - Modern Guidance System - MGS

In summary the implementation of MGS requires some additional information which is not required by a classical PN guidance system. Estimates of range, measurement and process noise statistics are needed for the implementation of the Kalman filter while estimates of time-to-go, guidance system bandwidth and missile acceleration are needed for the implementation of the guidance law.

Performance Comparison

Both classical and modern guidance methods are now compared in terms of performance as measured by the rms (root mean square) miss distance. The comparison is made utilizing the linearized, but realistic model of the kinematic homing loop shown in Figure 7. Here autopilot dynamics are represented by a first order transfer function and only the two most important stochastic error sources are considered, namely glint noise and random target maneuver. The seeker, noise filter and guidance dynamics have been previously presented in Figures 4 and 6. In this case the Kalman filter of MGS is optimal since it is perfectly matched to the "real world" in that it has an exact dynamical model of the system along with perfect knowledge of the measurement and process noise statistics. With this methodology any deterioration in MGS performance will be caused solely by the guidance law.

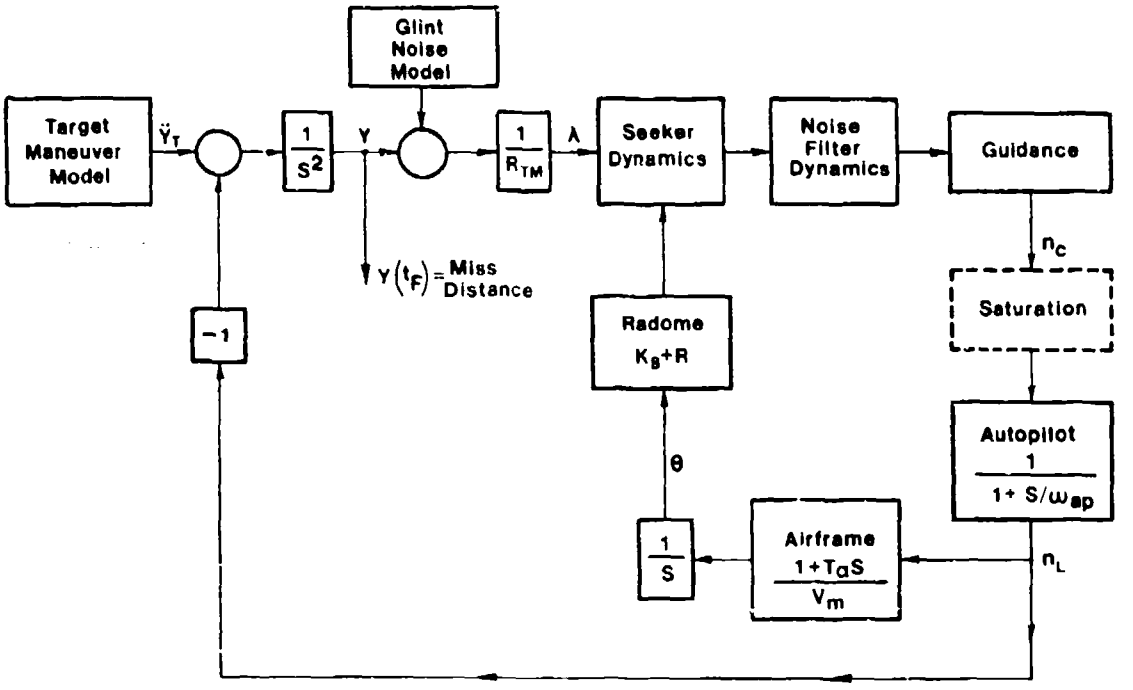

Figure 7 - Kinematic Homing Loop

Imbedded in the MGS guidance law is a dynamical model of the actual system. If this model is inaccurate or if the t_{go} estimate is lacking or inaccurate, MGS performance degrades. If the estimated time to go, $\hat{t}_{go}$, is considered to be a simple function of t_{go} as shown in Eq. (9),

$$\hat{t}_{go} = At_{go} + B \tag{9}$$

then the influence of bias errors, B, and scale factor errors, A, on MGS system performance can be investigated. Typical miss distance results, shown in Figure 8, indicate that errors in $\hat{t}_{go}$ result in rapid performance degradation of MGS. In fact, negative bias errors lead to guidance system instabilities of MGS. PN performance, superimposed on Figure 8 is not sensitive to these errors. For this example PN achieves a miss of 4.3 ft. Therefore if the required miss distance was less than 4.3 ft, only MGS could meet that specification and then only if bias errors could be kept below 0.2 s and scale factor errors were between 0.68 and 1.35. If the required miss were greater than 4.3 ft, PN could meet the specification, but MGS could only meet the specification if bias and scale factor errors could be kept below the values of the curves in Figure 8. Of course, PN does not use these quantities at all and therefore is not sensitive to such errors. In summary, the implementation of MGS places requirements not only the algorithm for calculating t_{go}, but also on the special filtering needed to estimate range and range rate.

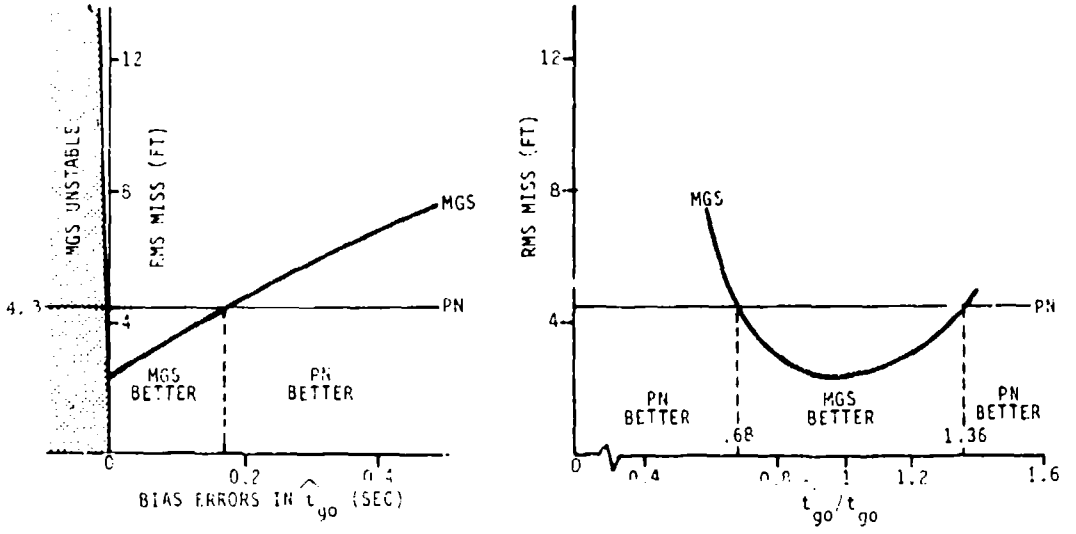

Figure 8 - Errors in Estimating Time to Go Seriously Degrade MGS Performance

Modern Guidance System, unlike Proportional Navigation, attempts to compensate for autopilot dynamics by the use of a dynamic lead term in the missile acceleration command. In order to implement this concept, MGS requires an accurate measurement of the achieved missile acceleration and an estimate of the autopilot bandwidth, W_{AP}. If this measurement is perfect and if the dynamic model within MGS is perfectly matched to the "real world", optimum performance can be obtained. However, if for example, we assume that missile acceleration is measured perfectly, but the estimate of autopilot bandwidth is in error according to Eq. (10)

$$\hat{W}_{AP} = CW_{AP} \tag{10}$$

then the influence of scale factor errors, C, on MGS system performance can be investigated. Figure 9 shows that system instabilities result if the scale factor falls below 0.6. As before, PN performance is not sensitive to this error source. In this example, for miss distances below 4.3 ft, only MGS can meet the requirements if the scale factor is greater than 0.6. If the required miss distance is greater than 4.3 ft, PN can always meet the requirement, but MGS can only meet the specification if the scale factor is greater than 0.6. In summary, the implementation of MGS places requirements on allowable errors in dynamic modeling.

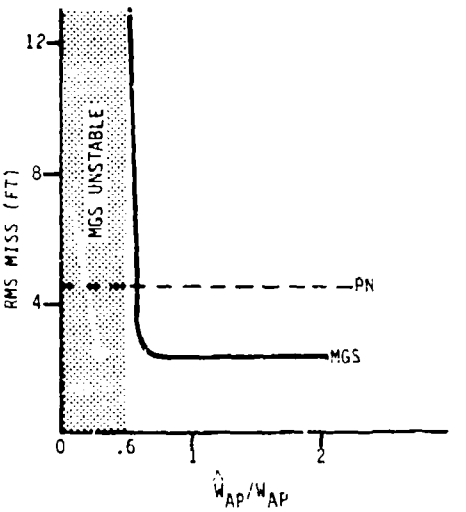

Figure 9 - Errors in Estimating System Dynamics Can Lead to MGS Instability

The nonhemispherical shape of the missile radome causes distortion of the incoming radar beam. As the radar beam passes through the radome a refraction effect takes place and the net result is an error in the angle of the apparent target. The radome error slope, R, is a measure of the distortion taking place and is a function of the gimbal angle, among other things.[6] The guidance system designer attempts to specify the manufacturing tolerances and the limits on the permissible variations of R. This error source is particularly important at high altitudes where the missile turning rate time constant, $T_{\dot{\theta}}$, is large. This time constant in conjunction with large radome refraction slopes can cause guidance system instability. It is, therefore, of considerable practical importance to see how PN and MGS performance degrade in the presence of radome slope errors. Typical high altitude performance results for both guidance systems are shown in Figure 10. The results indicate that the PN guidance system has more of a tolerance to radome errors than does MGS. In this regard PN is more robust.

Figure 10 indicates that the MGS implementation is more sensitive to negative radome slopes than positive slopes. In a practical design, the seeker stabilization loop gain could be adjusted to bias the radome, thus insuring only positive slopes. It is for this reason that the allowable radome slope is more of an important measure than the average radome slope. In fact, the allowable radome slope range is one important measure used in guidance system design to specify manufacturing tolerances on the radome. The average rms miss distance due to a radome slope range can be calculated from the information provided in Figure 10. Typical results showing the sensitivity of both guidance systems to radome slope range is displayed in Figure 11. This figure shows that when the radome is taken into consideration, MGS can only offer superior miss distance performance if the allowable radome slope range is less than 0.075. Otherwise PN yields smaller average rms miss distances. Nevertheless, if a radome slope range less than 0.075 can be met, MGS yields less miss distance.

Finally, missile acceleration saturation, one of the most important guidance system nonlinearities in the performance comparison, is considered. Since MGS predicts intercept using estimates of target acceleration and measurements of missile acceleration, it requires less acceleration than PN to hit a maneuvering target. In Figure 12, where rms miss is plotted versus the missile-to-target acceleration ratio for both guidance system implementations, it is evident that PN requires a larger acceleration advantage over the target than MGS to achieve a specific miss distance. For example, to achieve an RMS miss of less than 7 ft, PN requires a 5 to 1 acceleration advantage over the target whereas MGS requires only a 2.3 to 1 advantage. This reduced acceleration requirements extends the missile's zone of effectiveness against maneuvering targets and is the major advantage of MGS over PN.

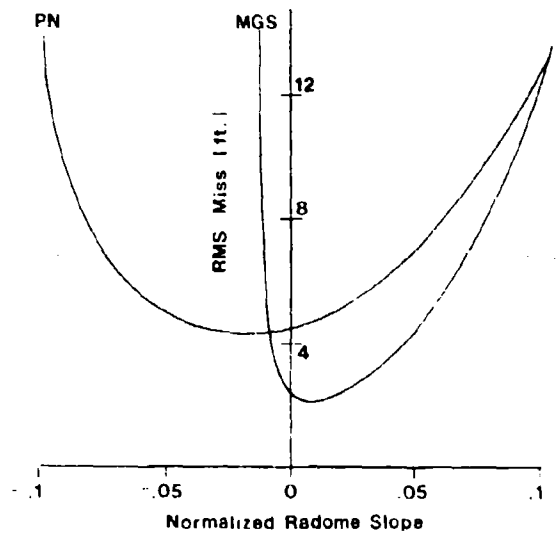

Figure 10 - Radome Errors Influence System Performance

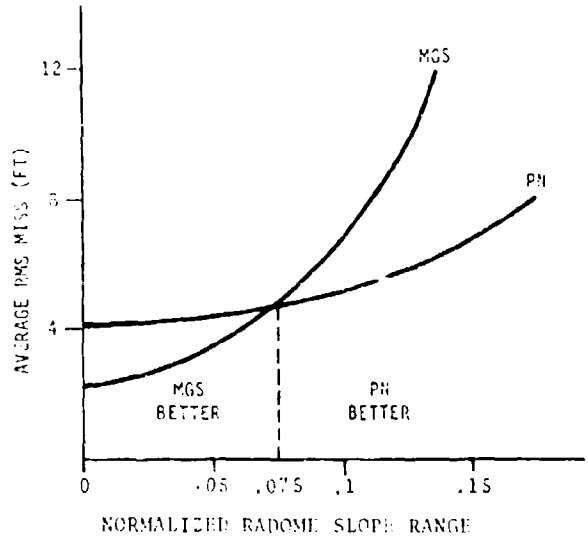

Figure 11 - PN Allows Greater Flexibility in Radome Design

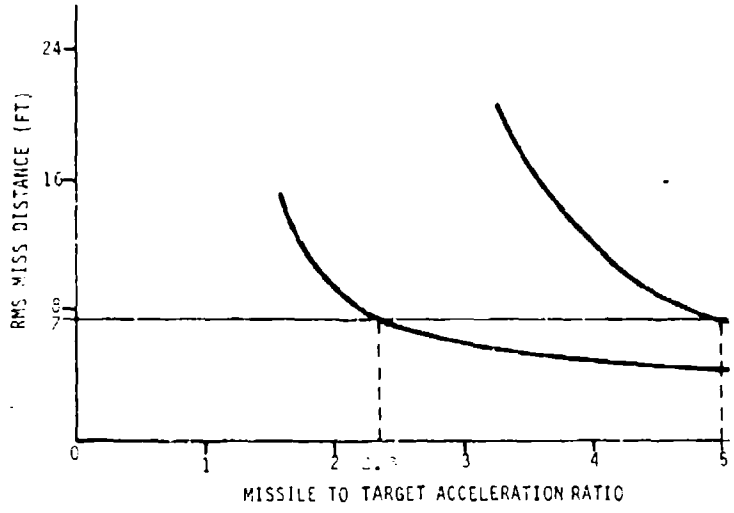

Figure 12 - MGS Requires Less Acceleration Due to Target Maneuver

SUMMARY

A modern guidance system and a proportional navigation guidance system designed to meet the same miss distance specification yield different implementation of subsystems, and each subsystem must meet a different set of requirements. A modern guidance system imposes more severe requirements on radome refraction slope and on knowledge of the system dynamics, but it does not require as much maximum missile normal acceleration to intercept an accelerating target. If the miss distance specification is extremely small, only MGS can do the job. Thus the additional instrumentation and subsystem requirements is the price that must be paid to meet severe miss distance requirements. If the miss distance specification is such that both MGS and PN can do the job, then instrumentation specifications can be relaxed in favor of more missile normal acceleration capability. When sufficient missile acceleration is available, PN offers the least stringent instrumentation requirements. Thus, if component tolerances can be met, MGS has the smallest miss distance, but as component tolerances or measurement errors degrade, the performance of MGS degrades faster than that of PN until at relatively large component or measurement errors, PN has less miss distance than MGS.

REFERENCES

1) Bryson, A. E. and Ho, Y. C., "Applied Optimal Control," Blaisdell Publishing Company, Waltham, Massachusetts 1969.

2) Willems, G., "Optimal Controllers for Homing Missiles," U. S. Army Missile Command, Report No. RE-TR-68-15, Redstone Arsenal, Alabama, September 1968.

3) Willems, G., "Optimal Controllers for Homing Missiles with Two Time Constants," U. S. Army Missile Command, Report No. RE-TR-69-20, Redstone Arsenal, Alabama, October 1969.

4) Price, C. F., "Optimal Stochastic Guidance Laws for Tactical Missiles", The Analytical Sciences Corporation, Report No. TR-170-2, Reading, Massachusetts, September 1971.

5) Phillips, T. L., "Anti-Aircraft Missile Guidance", Electronic Progress published by Raytheon Co., March-April 1958, pp 1-5.

6) Nesline, F. W., "Missile Guidance for Low Altitude Air Defense", AIAA Guidance and Control Conference, Palo Alto, California, August 1978.

7) Benecke, T. and Quick, A. W. (Eds), "History of German Guided Missiles Development", AGARD First Guided Missiles Seminar, Munich, Germany, April 1956.

8) Yuan, C. L., "Homing and Navigational Courses of Automatic Target-Seeking Devices", RCA Laboratories, Report No. PTR-12C, Princeton, New Jersey, December 1943.

9) Bennett, R. R. and Mathews, W. E., "Analytical Determination of Miss Distances for Linear Homing Navigation Systems", Technical Memorandum No. 260, Hughes Aircraft Company, Culver City, California, March 1952.

10) Yuan, C. L., "Homing and Navigational Courses of Automatic Target-Seeking Devices", Journal of Applied Physics, December 1948.

11) Cottrell, R. G., "Optimal Intercept Guidance for Short-Range Tactical Missiles", AIAA Journal, Vol. 9, July 1971, pp 1414-1415.

12) Fitzgerald, R. J. and Zarchan, P., "Shaping Filters for Randomly Initiated Target Maneuvers", AIAA Guidance and Control Conference, Palo Alto, California, August 1978.

13) Wiener, N., "Extrapolation, Interpolation and Smoothing of Stationary Time Series", MIT Press, Cambridge, Massachusetts 1949.

14) Newton, G. C., Gould, L. A., and Kaiser, J. F., "Analytical Design of Linear Feedback Controls", John Wiley and Sons, Inc., New York, 1957.

15) Kalman, R. E., and Bucy, R., "New Results in Linear Filtering and Prediction," Journal of Basic Engineering (ASME), Vol. 83D, 1961, pp 95-108.

16) Gelb, A., ed., "Applied Optimal Estimation", MIT Press, Cambridge, Massachusetts, 1974.

APPENDIX A
WIENER OPTIMAL FILTER

The disturbances entering the guidance system are considered to be white glint noise with spectral density Φ_N and random target maneuver. In this paper the maneuver is considered to be a step function whose initiation time is uniformly distributed over the flight time. It can be shown[12] that integrated white noise has the same autocorrelation function as this maneuver process. The optimal filter with transfer function, H_o, can be derived by either Wiener or Kalman filter theory.

The Wiener filter formulation is based upon the diagram of Figure A-1. The problem is to find H_o which will minimize the integral of the mean square error signal minimize $\int_0^\infty e^2\,dt$.

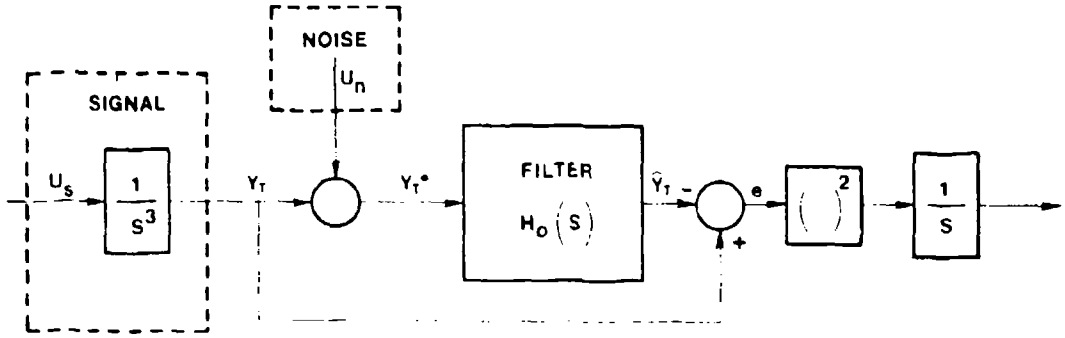

U_S - White Noise with Power Spectral Density $\dot{\phi}_S$
U_n = White Noise with Power Spectral Density $\dot{\phi}_N$
Y_T = Actual Target Position
Y_T^* = Measured Target Position
$\hat{Y}_T$ = Estimated Target Position
e = Error in Estimate

Figure A-1 - Wiener Filter Formulation

The optimal transfer function, H_o, can be found from the explicit solution of the Wiener-Hopf integral equation

$$H_o = \frac{1}{(W_S+W_N)^+}\left[\frac{W_S}{(W_S+W_N)^-}\right]_+ \qquad \text{(A-1)}$$

where W_S and W_N are the spectral densities of the signal and noise, $(W_S+W_N)^+$ represents that part which has all its poles and zeroes in the left half plane, $(W_S+W_N)^-$ represents that part which has all its poles and zeroes in the right half plane. The expression $[\cdot]_+$ is the component of $[\cdot]$ which has all its poles in the left half plane. In order to obtain $[\cdot]_+$ we expand $[\cdot]$ in partial fractions and throw away all the terms corresponding to poles in the right half plane. From Figure A-1 the output spectral densities of the signal and noise, W_S and W_N, can be expressed in terms of the input spectral densities, Φ_S and Φ_N, and the shaping network transfer function as

$$W_S = \frac{\Phi_S}{-S^6} \qquad \text{(A-2)}$$

$$W_N = \Phi_N \qquad \text{(A-3)}$$

Therefore

$$W_S+W_N = \frac{\Phi_S}{-S^6} + \Phi_N = \frac{\Phi_S\left(1-\frac{\Phi_N S^6}{\Phi_S}\right)}{-S^6} \qquad \text{(A-4)}$$

If we define

$$\omega_o = (\Phi_S/\Phi_N)^{1/6} \tag{A-5}$$

then Eq. (A-4) can be factored

$$W_S+W_N = \frac{\Phi_S(1-S^6/\omega_o^6)}{-S^6} = \Phi_S \frac{(1+2S/\omega_o+2S^2/\omega_o^2+S^3/\omega_o^3)\,(1-2S/\omega_o+2S^2/\omega_o^2-S^3/\omega_o^3)}{(-S^3)\,(-S^3)} \tag{A-6}$$

Therefore

$$(W_S+W_N)^+ = \Phi_S \frac{(1+2S/\omega_o+2S^2/\omega_o^2+S^3/\omega_o^3)}{S^3} \tag{A-7}$$

$$(W_S+W_N)^- = \frac{(1-2S/\omega_o+2S^2/\omega_o^2-S^3/\omega_o^3)}{-S^3} \tag{A-8}$$

Substitution of Eqs. (A-2), (A-7) and (A-8) into (A-1) yields

$$H_O = \frac{S^3}{\Phi_S(1+2S/\omega_o+2S^2/\omega_o^2+S^3/\omega_o^3)} \times \left[\frac{\Phi_S}{S^3(1-2S/\omega_o+2S^2/\omega_o^2-S^3/\omega_o^3)}\right]_+ \tag{A-9}$$

The expression in the brackets of Eq. (A-9) can be expanded by partial fractions yielding

$$[\cdot]_+ = \left[\Phi_S\left(\frac{1}{S^3}+\frac{2/\omega_o}{S^2}+\frac{2/\omega_o^2}{S}+\frac{1/\omega_o^3}{1-S/\omega_o}-\frac{1/\omega_o+S}{1-S/\omega_o+S^2/\omega_o^2}\right)\right]_+ \tag{A-10}$$

Eliminating these terms with poles in the right half plane leaves

$$[\cdot]_+ = \Phi_S\left(\frac{1}{S^3}+\frac{2/\omega_o}{S^2}+\frac{2/\omega_o^2}{S}\right) \tag{A-11}$$

which simplifies to

$$[\cdot]_+ = \Phi_S\left(\frac{1+2S/\omega_o+2S^2/\omega_o^2}{S^3}\right) \tag{A-12}$$

Substitution of Eq. (A-12) into (A-9) yields the optimal transfer function

$$H_o = \frac{1+2S/\omega_o+2S^2/\omega_o^2}{1+2S/\omega_o+2S^2/\omega_o^2+S^3/\omega_o^3} \tag{A-13}$$

APPENDIX B
KALMAN OPTIMAL FILTER

The same transfer function can also be obtained by the Kalman formulation. The state and measurement equations can be derived from the plant, shown in Figure B-1, and are

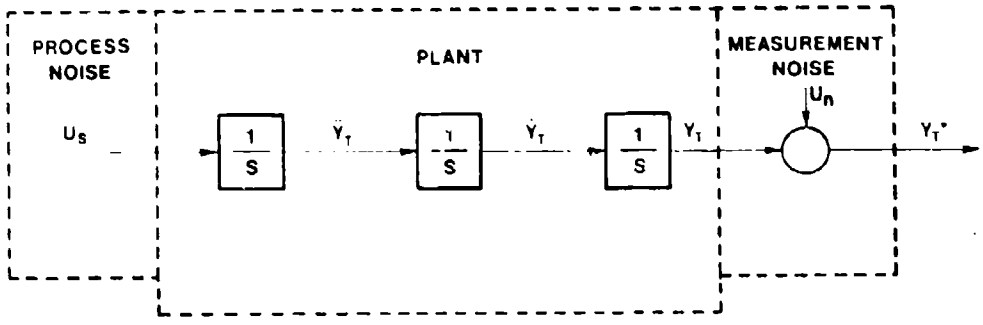

U_S · White Noise with Power Spectral Density Φ_S

U_n · White Noise with Power Spectral Density Φ_N

$\ddot{Y}_T$ Target Acceleration

$\dot{Y}_T$ Target Rate

Y_T Target Position

Y_T^* Measured Target Position

Figure B-1 - Kalman Filter Formulation

$$\begin{bmatrix} \dot{y}_T \\ \ddot{y}_T \\ \dddot{y}_T \end{bmatrix} = \begin{bmatrix} 0 & 1 & 0 \\ 0 & 0 & 1 \\ 0 & 0 & 0 \end{bmatrix} \cdot \begin{bmatrix} y_T \\ \dot{y}_T \\ \ddot{y}_T \end{bmatrix} + \begin{bmatrix} 0 \\ 0 \\ u_S \end{bmatrix} \tag{B-1}$$

$$\dot{\underline{X}} = \underline{F} \cdot \underline{X} + \underline{U}$$

$$Y_T^* = \{1\ 0\ 0\} \cdot \begin{bmatrix} y_T \\ \dot{y}_T \\ \ddot{y}_T \end{bmatrix} + u_N \tag{B-2}$$

$$\underline{z} = \underline{H} \cdot \underline{X} + V$$

The Kalman filter equation is

$$\dot{\hat{\underline{X}}} = \underline{F} \cdot \hat{\underline{X}} + \underline{K}\,[\underline{Z} - \underline{H}\,\hat{\underline{X}}] \tag{B-3}$$

where the Kalman gains, $\underline{K}$, are determined from the following matrix Riccati equations

$$\dot{\underline{P}} = \underline{F}\,\underline{P} + \underline{P}\,\underline{F}^T - \underline{P}\,\underline{H}^T\,\underline{I}^{-1}\,\underline{H}\,\underline{P} + \underline{Q} \tag{B-4}$$

$$\underline{K} = \underline{P}\,\underline{H}^T\,\underline{R}^{-1} \tag{B-5}$$

where

$$Q = \begin{bmatrix} 0 & 0 & 0 \\ 0 & 0 & 0 \\ 0 & 0 & \Phi_S \end{bmatrix} \text{ and } \underline{R} = \Phi_N \tag{B-6}$$

Recognizing that the covariance matrix, $\dot{P}$, is symmetric, the scalar equations representing the steady state solution ($\dot{\underline{P}} = \underline{0}$) can be written from (B-4) as

$$\begin{aligned} P_{11}^2 &= 2 P_{12} \Phi_N \\ P_{12}^2 &= 2 P_{23} \Phi_N \\ P_{13}^2 &= \Phi_S \Phi_N \\ P_{11} P_{12} &= \Phi_N (P_{22} + P_{13}) \\ P_{11} P_{13} &= P_{23} \Phi_N \\ P_{12} P_{13} &= P_{33} \Phi_N \end{aligned} \tag{B-7}$$

After some algebra, the solutions to Eq. (B-7) can be substituted into Eq. (B-5) yielding the steady state Kalman gains

$$\underline{K} = \begin{bmatrix} K_1 \\ K_2 \\ K_3 \end{bmatrix} = \begin{bmatrix} 2(\Phi_S/\Phi_N)^{1/6} \\ 2(\Phi_S/\Phi_N)^{1/3} \\ (\Phi_S/\Phi_N)^{1/2} \end{bmatrix} \tag{B-8}$$

Defining

$$\omega_o = (\Phi_S/\Phi_N)^{1/6} \tag{B-9}$$

the gain matrix becomes

$$\underline{K} = \begin{bmatrix} 2\omega_o \\ 2\omega_o^2 \\ \omega_o^3 \end{bmatrix} \tag{B-10}$$

The filter equations are obtained by substituting Eq. (B-10) into Eq. (B-3) yielding

$$\begin{bmatrix} \dot{\hat{y}}_T \\ \dot{\hat{y}}_T \\ \dot{\hat{y}}_T \end{bmatrix} = \begin{bmatrix} 0 & 1 & 0 \\ 0 & 0 & 1 \\ 0 & 0 & 0 \end{bmatrix} \begin{bmatrix} \hat{y}_T \\ \hat{y}_T \\ \hat{y}_T \end{bmatrix} + \begin{bmatrix} 2\omega_o \\ 2\omega_o^2 \\ \omega_o^3 \end{bmatrix} \cdot [y_T^* - \hat{y}_T] \tag{B-11}$$

The transfer function between the position estimate output and the position measurement input can easily be obtained from Eq. (B-11) as

$$\frac{\hat{y}_T}{y_T^*} = \frac{1 + 2S/\omega_o + 2S^2/\omega_o 2}{1 + 2S/\omega_o + 2S^2/\omega_o 2 + S^3/\omega_o^3} \tag{B-12}$$

(B-12)

This is identical to the transfer function obtained by the Wiener filter approach.

APPENDIX C
MATRIX APPROACH TO MODERN GUIDANCE

Optimal guidance laws are generally derived on the basis of modern control theory. The linear model of Figure C-1, in which missile dynamics are represented by a single lag, is used for the application of modern control theory to the guidance problem. In this case we are interested in deriving a guidance law which will achieve zero miss distance while minimizing the integral of the square of the guidance commands [minimize $\int_0^{t_f} n_c^2\, dt$ subject to $y(t_F)=0$].

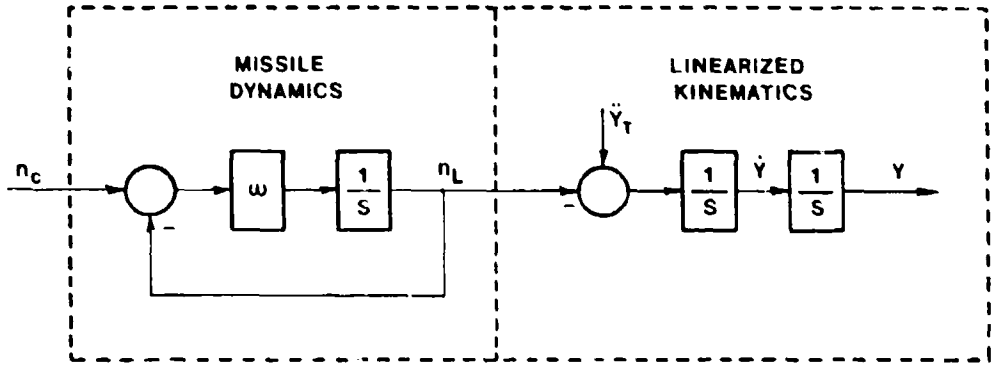

n_c = Commanded Missile Acceleration
n_L = Achieved Missile Acceleration
$\ddot{Y}_T$ = Target Acceleration
$\dot{Y}$ = Relative Target - Missile Rate
Y = Relative Target - Missile Separation

Figure C-1 - Guidance Problem Formulation

The solution to minimizing the quadratic performance index

$$J = \frac{1}{2}\int_0^{t_F} n_c^2\, dt \tag{C-1}$$

subject to the linear differential equation

$$\dot{\underline{x}} = \underline{F}\,\underline{x} + \underline{G}\, n_c \tag{C-2}$$

with zero miss distance [$y(t_F)=0$] is well known[1] and is given by

$$n_c = \frac{\underline{G}^T \underline{R}\,\underline{R}^T \underline{x}}{\int_t^{t_F} (\underline{R}^T \underline{G}\,\underline{G}^T \underline{R})\, dt} \tag{C-3}$$

where $\underline{R}$ is obtained from the differential equation

$$\dot{\underline{R}} + \underline{F}^T \underline{R} = 0 \; ; \; R(t_F) = \begin{bmatrix} 1 \\ 0 \\ 0 \\ 0 \end{bmatrix} \tag{C-4}$$

$$\underline{x} = \begin{bmatrix} y \\ \dot{y} \\ \ddot{Y}_T \\ n_L \end{bmatrix} \; ; \; \underline{F} = \begin{bmatrix} 0 & 1 & 0 & 0 \\ 0 & 0 & 1 & -1 \\ 0 & 0 & 0 & 0 \\ 0 & 0 & 0 & -\omega \end{bmatrix} \; ; \; G = \begin{bmatrix} 0 \\ 0 \\ 0 \\ \omega \end{bmatrix} \tag{C-5}$$

The solution to Eq. (C-4) is

$$\underline{R} = \begin{bmatrix} 1 \\ t_{go} \\ t_{go}^2/2 \\ \frac{1}{\omega^2}(e^{-T} + T - 1) \end{bmatrix} \tag{C-6}$$

where T is the normalized time to go until intercept given by

$$T = \omega(t_F - t) = \omega t_{go} \tag{C-7}$$

The integral appearing in Eq. (C-3) therefore becomes

$$-\int_t^{t_f} (\underline{R}^T \underline{G}\underline{G}^T \underline{R})\, dt = -\frac{1}{\omega^3}\left[\frac{1}{5} - \frac{1}{2}e^{-2T} - 2Te^{-T} - T^2 + T + \frac{1}{3}T^3\right] \tag{C-8}$$

Substituting Eq. (C-8) into Eq. (C-3) yields the optimal closed loop guidance law

$$n_c = \frac{N'}{t_{go}^2}\left[y + \dot{y}t_{go} + \frac{1}{2}\ddot{y}_T t_{go}^2 + \frac{n_L}{\omega^2}(e^{-T} + T - 1)\right] \tag{C-9}$$

where

$$N' = \frac{6T^2(e^{-T} - 1 + T)}{2T^3 + 3 + 6T - 6T^2 - 12Te^{-T} - 3e^{-2T}} \tag{C-10}$$

If missile guidance dynamics are neglected ($\omega \to \infty$), application of L'Hopital's Rule reduces the guidance law to

$$\lim_{\omega \to \infty} n_c = \frac{3}{t_{go}^2}\left[y + \dot{y}t_{go} + \frac{1}{2}\ddot{y}_T t_{go}^2\right]$$

This guidance law is augmented proportional navigation with an effective navigation ratio of three.

APPENDIX D

SCALAR APPROACH TO MODERN GUIDANCE

The Schwartz Inequality can also be used in the derivation of optimal guidance laws. For the same problem considered in Appendix C, we can express the system state vector of Eq. (C-2) at the terminal time according to the matrix superposition integral

$$\underline{x}(t_F) = \underline{\Phi}(t_F - t)\underline{x}(t) + \int_t^{t_F} \Phi(t_F - \lambda)\underline{G}(\lambda) n_c(\lambda)\, d\lambda \tag{D-1}$$

where Φ is the fundamental matrix. Eq. (D-1) actually represents a set of scalar equations for each of the different states. For the guidance problem, the first state is the object of our control and can be expressed as

$$y(t_F) = f_1(t_F - t) - \int_t^{t_F} h_1(t_F - \lambda) n_c(\lambda)\, d\lambda \tag{D-2}$$

For zero miss distance Eq. (D-2) can be rewritten as

$$f_1(t_F - t) = \int_t^{t_F} h_1(t_F - \lambda) n_c(\lambda)\, d\lambda \tag{D-3}$$

Application of the Schwartz Inequality yields

$$f_1^2(t_F - t) \leq \int_t^{t_F} h_1^2(t_F - \lambda)\, d\lambda \int_t^{t_F} n_c^2(\lambda)\, d\lambda \tag{D-4}$$

or

$$\int_t^{t_F} n_c^2(\lambda)\, d\lambda \geq \frac{f_1^2(t_F - t)}{\int_t^{t_F} h_1^2(t_F - \lambda)\, d\lambda} \tag{D-5}$$

The integral of the square of the acceleration can be minimized by insuring that the equality sign of Eq. (D-5) holds. According to the Schwartz Inequality, this occurs when

$$n_c(\lambda) = k h_1(t_F - \lambda) \tag{D-6}$$

Substitution of Eq. (D-6) into Eq. (D-3) yields

$$k = \frac{f_1(t_F - t)}{\int_t^{t_F} h_1^2(t_F - \lambda)\, d\lambda} \tag{D-7}$$

Therefore the acceleration is given by

$$n_c(t) = \left[\frac{f_1(t_F - t)}{\int_t^{t_F} h_1^2(t_F - \lambda)\, d\lambda} \right] h_1(t_F - t) \tag{D-8}$$

In order to demonstrate the power of Eq. (D-8) in solving for optimal guidance laws the example of Appendix C is reconsidered. The fundamental matrix can be found from Eq. (C-5) to be

$$\Phi(t) = \begin{bmatrix} 1 & t & t^2/2 & -t/\omega + 1/\omega^2(1 - e^{-\omega t}) \\ 0 & 1 & t & -1/\omega(1 - e^{-\omega t}) \\ 0 & 0 & 1 & 0 \\ 0 & 0 & 0 & e^{-\omega t} \end{bmatrix} \tag{D-9}$$

and

$$f_1(t_F-t) = y + \dot{y}\, t_{go} + \ddot{y}_T \frac{t_{go}^2}{2} + \frac{n_L}{\omega^2}\left(e^{-\omega t_{go}} + \omega t_{go} - 1\right) \tag{D-10}$$

$$h_1(t_F-\lambda) = t_F - \lambda - \frac{1}{\omega}\left[1 - e^{-\omega(t_F-\lambda)}\right] \tag{D-11}$$

where

$$t_{go} = t_F - t \tag{D-12}$$

The integral of Eq. (D-5) becomes

$$\int_t^{t_F} h_1^2(t_F-\lambda)d\lambda = \frac{1}{\omega^3}\left(\frac{1}{2} - \frac{1}{2}e^{-2\omega t_{go}} - 2\omega t_{go}e^{-\omega t_{go}} - \omega^2 t_{go}^2 + \omega t_{go} + \frac{1}{3}\omega^3 t_{go}^3\right] \tag{D-13}$$

Substitution of Eq. (D-13) into Eq. (D-8) yields

$$n_c = \frac{N'}{t_{go}^2}\left[y + \dot{y}\, t_{go} + \frac{1}{2}\ddot{y}_T t_{go}^2 + \frac{n_L}{\omega^2}(e^{-T} + T - 1)\right] \tag{D-14}$$

where

$$T = \omega t_{go}$$

and

$$N' = \frac{6T^2(e^{-T} - 1 + T)}{2T^3 + 3 + 6T - 6T^2 - 12Te^{-T} - 3e^{-2T}} \tag{D-15}$$

Here modern control theory and the Schwartz inequality can be used in the derivation of certain types of guidance laws. The mathematical solutions of both approaches are in fact equivalent as can be seen by rewriting Eq. (C-3) and (D-8).

$$n_c = \frac{\underline{G}^T \underline{R}\underline{R}^T \underline{x}}{-\int_t^{t_F} \underline{R}^T \underline{G}\underline{G}^T \underline{R}\, dt} = \frac{h_1(t_F-t)\, f_1(t_F-t)}{\int_t^{t_F} h_1^2(t_F-\lambda)d\lambda} \tag{D-16}$$

A careful examination of the example used in both approaches shows the following equivalences

$$\underline{G}^T \underline{R} = h_1(t_F-t) \tag{D-17}$$

$$\underline{R}^T \underline{x} = f_1(t_F-t) \tag{D-18}$$

$$-\int_t^{t_F} (\underline{R}^T \underline{G}\underline{G}^T \underline{R})\, dt = \int_t^{t_F} h_1^2(t_F-\lambda)d\lambda \tag{D-19}$$

OPTIMAL CONTROL AND ESTIMATION FOR TERMINAL GUIDANCE OF TACTICAL MISSILES

Tom L. Riggs, Jr., 1Lt, USAF

Air Force Armament Laboratory
United States Air Force
Eglin Air Force Base, Florida

SUMMARY To help meet the demanding requirements of the modern air-to-air engagement, the U.S. Air Force is conducting basic research to develop advanced guidance laws and estimation techniques for application in future tactical weapons. This research has developed numerous candidate high performance guidance and estimation techniques. In addition to providing an overview of the program, this paper will present an example of the most simplistic guidance technique developed and compare its performance to proportional navigation.

INTRODUCTION

The modern air-to-air missile engagement is the most demanding tactical weapon scenario from the viewpoint of the terminal guidance law. This is due to a number of factors including short engagement times (nominally, 2-5 seconds) and rapid, drastic changes in the kinematics of the scenario. Further, trends in operational requirements indicate that future air-to-air missiles will have to have a high probability of kill under total sphere launch engagement conditions and a launch and leave capability when employed against a wide variety of highly maneuverable, intelligent targets. Present day air-to-air missiles employ proportional navigation (pro-nav) guidance laws in the terminal mode. In fact, this class of missiles has employed variations of pro-nav for more than twenty-five years. There are several reasons for pro-nav's tenure. First, pro-nav is very effective in guiding missiles that are launched under restricted conditions and are intercepting low maneuverability type aircraft. Second, pro-nav is relatively easy to implement on-board the missile using off-the-shelf hardware. Third, until recently, it was not feasible to incorporate the on-board computers that would be required to implement more complex guidance laws. However, proportional navigation's effectiveness in modern air-to-air engagements is limited and cannot meet the demanding operational requirements of the future. In order to satisfy these requirements, future air-to-air missiles will require more sophisticated guidance algorithms. Additionally, in order to implement these guidance algorithms, more information about the missile and target dynamic states will have to be accurately measured or estimated on-board the missile. The very nature of this problem lends itself to the use of Optimal Control and Estimation Theory to develop the required advanced guidance and estimation algorithms.

In October 1976, the Air Force Armament Laboratory initiated a basic research program to investigate and extend those modern control and estimation techniques that have potential application for improving the state-of-the-art in missile guidance for air-to-air missiles. Specific emphasis was placed on the short range mission (launch ranges less than five miles) because this is the most demanding phase in missile guidance and it is a common mission phase to all air-to-air missiles. The research topics that this program is investigating can be classified into three main areas, (1) Guidance and Control Theory, (2) Estimation Theory, and (3) the combination of (1) and (2). The first area is directed at the derivation of advanced guidance and control laws using a broad spectrum of modern control theories. The second area will investigate and develop modern nonlinear estimation techniques that can be used to filter the available sensor information and use that information to estimate the state/parameters needed by the guidance laws. The third area addresses the interdependence between the control and estimation problem and will develop the theory and methodology to be used to solve the combined problem.

PROBLEM FORMULATION

The optimal guidance formulation is a complex process involving many engineering decisions which ultimately impact complexity, validity, and technical quality (performance) of the resulting guidance algorithm. The key ingredients of the optimal guidance formulation are the performance index, system/state constraints, missile math model, the methodology or theory used to solve the problem and the estimation requirements. These ingredients are all interrelated, making the selection or construction of each ingredient difficult because of the possible ramifications on the other ingredients. Figure 1 summarizes these ingredients and depicts their interrelationships. Before dwelling on the interrelationships of these ingredients it will be useful to describe the function of each of these ingredients.

The performance index is a mathematical equation or set of equations that explicitly define the parameters or states to be minimized. Thus the performance index provides a measure of optimality or cost. (Because of this the performance index is often called the cost functional and in this paper the two terms will be used interchangeably.) Since often the minimization of the desired parameters lead to conflicting strategies (i.e., minimum fuel, minimum time) weighting terms are employed in the cost functional to define the degree of minimization for each parameter. Thus in constructing the cost functional not only must the parameters to be minimized be defined but the relative degree of minimization must also be defined. Ideally, the

determination of the parameters to be minimized is a direct result of the mission requirements; however, in certain cases a literal translation of mission requirements to the performance index leads to unrealizable or non-unique guidance strategies. In this situation the design engineer must add additional terms (secondary mission requirements) to the cost functional. Care must be taken in selecting and weighting the additional performance criteria such that the primary criteria are not significantly deemphasized. Often the additional parameters are selected to implicitly enforce system constraints such as maximum acceleration limits. This will be discussed further in modelling system constraints. The last factor that must be considered in the design of the performance index is its form, i.e., quadratic or generalized. This factor is driven by the parameters to be minimized and by the theory or methodology that will be used to solve the problem.

System/state constraints can be handled explicitly or implicitly by optimal control formulations. In the missile control problem these constraints may be factors such as acceleration limits, seeker angle or rate limits, terminal constraints (zero miss distance, terminal aspect angle) and other state constraints that may limit the system's performance. However, inclusion of explicit constraints virtually always leads to a difficult two-point-boundary-value-problem that can only be solved by iterative numerical techniques, making on-line real-time solutions via microprocessors difficult at best. Further, solutions of this type are quite sensitive to modeling and measurement errors. Because of these reasons, explicit constraints are generally avoided in the missile guidance problem. An alternative approach to handling system constraints is by implicit enforcement via the cost functional. In this approach the constrained factors are minimized rather than explicitly bounded. This minimization can lead to unnecessary or undesirable conditions if extreme care is not taken in weighting the parameters to be constrained.

The missile math model construction, as in the performance index definition requires a large degree of engineering judgement. The accuracy of the math model translates directly into the optimality of the solution. Unfortunately the accuracy of the math model also translates directly into the complexity of the solution. This conflicting situation of optimality versus complexity, forces the design engineer to make engineering trade-offs. This is not as great a problem as it appears since the near term goal is not to derive "The Optimal Guidance Law" but rather to derive a guidance law that performs better than what currently exists, is realizable, and exhibits "good" control qualities such as stability and insensitivity to modeling errors and noise. For the missile guidance problem, there is a multitude of math models that can be selected, ranging from a simple point mass linear kinematic engagement model to approximately a sixty state (the actual number of states is system dependent) nonlinear dynamic missile/target model. Practical models are normally closer to lower range of complexity. As will be shown in this paper, even the use of simplistic models can realize extremely good performing guidance laws.

Central to all the factors in the optimal control formulation is the selected theory or methodology. The theory interrelates the key ingredients by dictating the mathematical form of the major formulation factors. For instance, if linear quadratic theory is the chosen methodology, then the cost functional must be quadratic in form, the missile math model must be restricted to a linear model and in general the system constraints can dictate the methodology that should be selected. For instance, if the missile math model is nonlinear or if the system constraints must be explicitly enforced or if the cost functional cannot be constructed as a quadratic equation then a generalized methodology must be used to solve the problem.

The decisions made by the design engineer in the guidance law formulation will ultimately translate into the effectiveness of the resulting guidance algorithm. The effectiveness of the resulting guidance law involves two issues, first, how well the guidance law meets the original mission requirements when applied to real world situations and second, is the guidance law realizable with on-board sensors and within real-time computational constraints? In terms of realizability, the ultimate goal is that the guidance law be in closed form, requiring only information that is directly available from on-board sensors. Short range air-to-air missiles normally employ passive seekers. The most effective guidance for missiles using passive seeker information directly is proportional navigation with a fixed navigational gain. As previously mentioned, proportional navigation performs inadequately in the modern air-to-air arena. This situation presents a dilemma in missile guidance design. In order to employ more effective guidance laws more information about the missile and target must be known; however, if measurement devices are added to the missile to obtain this information then the complexity and cost increase. The solution to this dilemma is to use optimal estimation techniques to estimate the additional information. This can be done without increasing the number of on-board sensors.

Optimal estimation techniques offer the potential for improvement in filtering noise from measurements over classical filtering techniques and more importantly provide the ability to estimate mathematically observable but unmeasured system states. This is possible because the theory used in designing the estimator provides explicit use of the system dynamic model, the system measurement model, and knowledge of the measurement noise characteristics. The optimal state estimation problem is at least equal to the optimal guidance problem in both magnitude and complexity. Regardless of the theoretical technique used to develop the estimation algorithm, there are two ways in which it can be related to the optimal guidance law. These relationships occur from (1) the missile

model can contain unknown or uncertain parameters which ultimately appear in the guidance law (i.e., lift and drag coefficients) and (2) the guidance law will be a function of dynamic states which are either unmeasurable or corrupted by noise. In order to adequately estimate unmeasured states, the states must be mathematically observable. Simply stated, this means that the estimated states must be a function, at least indirectly, of the measurements. This is the case in the missile guidance problem allowing the estimation of extremely important state information such as range, range rate, and target acceleration from passive seeker and missile accelerometer measurements.

RESEARCH FINDINGS

This program has investigated a broad spectrum of modern control and estimation theories. The major control theories that have yielded good results are:

a. Linear Quadratic Theory (1)

b. Linear Quadratic Guassian Theory (2)

c. Singular Perturbation Theory (3)

d. Reachable Set Theory (3)

e. Differential Game Theory (4)

All the guidance laws that were derived using these theories perform better than proportional navigation, however, all of the guidance laws require more information that proportional navigation does. This problem can be solved by (1) increasing the number of sensors on-board the missile or (2) utilizing modern estimation techniques to estimate the required information from existing sensor measurements. Since the latter approach offers the highest pay-off and the greatest challenge it was the selected approach on this research program.

The objective was to derive the estimation algorithms that would provide the information required by the advanced guidance laws, utilizing the following sensor information:

a. Passive Seeker Information (line-of-sight angle and line-of-sight rate).

b. Missile body accelerations (axial, lateral, and normal).

c. Missile body angular rates (p, q, and r).

d. Initial range and range-rate (assumed available from launch aircraft).

The main estimation theory used to solve this problem was extended Kalman Filtering Theory. A number of different approaches was taken in deriving the estimators. Each of the approaches resulted in different filters which varied in performance and complexity. Once derived, each filter was analyzed to determine the best (performance vs complexity) approach in deriving the estimation algorithm. It was determined that the filter that utilized a linear kinematic state model with a nonlinear measurement model yielded the best performance with the least complexity (5).

One of the most important findings in this research was that the performance of the guidance laws is extremely dependent on knowledge of time remaining till intercept, commonly referred to as time-to-go. It was determined that even the most simplistic guidance laws derived using Optimal Control Theory yielded significant performance improvement over proportional navigation if a good method for estimating time-to-go was employed in the guidance algorithm. (6).

CANDIDATE ADVANCED GUIDANCE ALGORITHM

The research has resulted in the development of nearly thirty different advanced guidance and estimation algorithms. Obviously, all cannot be presented in this paper. However, to dramatize the significance of this research, the most simplistic algorithm will be presented and compared to proportional navigation. This guidance law was derived using Linear Quadratic Guassian Theory. The derivation of the guidance law is given below.

STATE MODEL

Consider the engagement scenario depicted in Figure 1. Let M be the missile and T be the target and

$\vec{r}_M$ $\vec{v}_M$ $\vec{a}_M$ - Missiles position, velocity, and acceleration vectors relative to some fixed inertial reference frame.

$\vec{r}_T$ $\vec{v}_T$ $\vec{a}_T$ - Targets position, velocity, and acceleration vectors relative to the same inertial reference frame.

Define the state vector as follows:

x_1 = the target/missile relative position in the x direction ($x_1 = r_{Tx} - r_{Mx}$)

x_2 = the target/missile relative position in the y direction ($x_2 = r_{Ty} - r_{My}$)

x_3 = the target/missile relative position in the z direction ($x_3 = r_{Tz} - r_{Mz}$)

x_4 = the target/missile relative velocity in the x direction ($x_4 = \dot{x}_1 = v_{Tx} - v_{Mx}$)

x_5 = the target/missile relative velocity in the y direction ($x_5 = \dot{x}_2 = v_{Ty} - v_{My}$)

x_6 = the target/missile relative velocity in the z direction ($x_6 = \dot{x}_3 = v_{Tz} - v_{Mz}$)

$\dot{x}_4$ = the target/missile relative acceleration in the x direction ($\dot{x}_4 = a_{Tx} - a_{Mx}$)

$\dot{x}_5$ = the target/missile relative acceleration in the y direction ($\dot{x}_5 = a_{Ty} - a_{My}$)

$\dot{x}_6$ = the target/missile relative acceleration in the z direction ($\dot{x}_6 = a_{Tz} - a_{Mz}$)

Thus we have a linear model describing the engagement.

$$\begin{aligned} \dot{x}_1 &= x_4 \\ \dot{x}_2 &= x_5 \\ \dot{x}_3 &= x_6 \\ \dot{x}_4 &= a_{T_x} - a_{M_x} \\ \dot{x}_5 &= a_{T_y} - a_{M_y} \\ \dot{x}_6 &= a_{T_z} - a_{M_z} \end{aligned} \tag{1}$$

ASSUMPTION 1

Let $a_{Tx} = a_{Ty} = a_{Tz} = 0$. This means that the target has constant velocity in both magnitude and direction.

If the control vector, $\underline{u}$, is defined to be the missile acceleration and it is assumed that target acceleration is zero then Equation (1) can be written in state space form such that

$$\dot{\underline{x}} = A\underline{x} + B\underline{u} \tag{2}$$

Where

$$A = \left[\begin{array}{c|c} 0 & I \\ \hline 0 & 0 \end{array}\right], \quad B = \left[\begin{array}{c} 0 \\ \hline I \end{array}\right]$$

Where I is an Identity Matrix with dimension 3 x 3.

And

$$\underline{x} = \begin{bmatrix} x_1 \\ x_2 \\ x_3 \\ x_4 \\ x_5 \\ x_6 \end{bmatrix} \quad \text{and} \quad \underline{u} = \begin{bmatrix} -a_{M_x} \\ -a_{M_y} \\ -a_{M_z} \end{bmatrix}$$

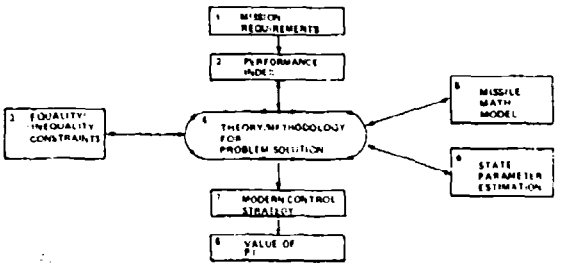

Figure 1. Major Ingredients of Modern Control Problem Formulation for Tactical Missiles

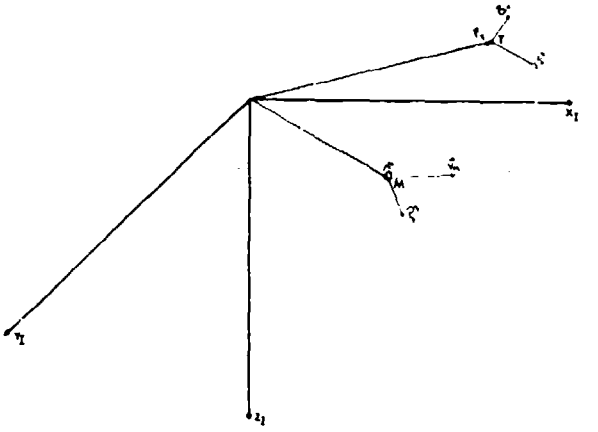

Figure 2. Missile and Target Kinematic States Relative to Inertial Reference Frame

ASSUMPTION 2

An implicit assumption was made in defining the control vector, $\underline{u}$, as the missile acceleration. This definition implies that the missile has instantaneous response and complete control over all three inertial acceleration components. Thus the missile is completely and perfectly controllable. This assumption deviates from real world tactical missiles in two areas. First, the missiles acceleration is uncontrollable in the missile body x direction because of the type of propulsion system used in these missiles. Second, the missiles' acceleration response in the body y and z (lateral and normal) is not instantaneous nor unlimited.

OPTIMAL CONTROL FORMULATION

The cost functional to be minimized is

$$J = \underline{x}^T(t_f)\mathbf{S}_f\underline{x}(t_f) + \tfrac{1}{2}\int_{t_0}^{t_f} \underline{u}^T\mathbf{R}\underline{u}\, dt \qquad (3)$$

where $\mathbf{S}_f = \begin{bmatrix} \mathbf{I} & \mathbf{0} \\ \mathbf{0} & \mathbf{0} \end{bmatrix}$ and $\mathbf{R} = \begin{bmatrix} b & 0 & 0 \\ 0 & b & 0 \\ 0 & 0 & b \end{bmatrix}$

Given the cost functional, Equation (3), and the state equation, Equation (2), the optimal control solution can be determined analytically. The solution is straight forward but tedious.

Given J and state equation (Eq 2) the Hamiltonian is constructed.

$$\mathcal{H} = \tfrac{1}{2}\underline{u}^T\mathbf{R}\underline{u} + \underline{p}^T\mathbf{A}\underline{x} + \underline{p}^T\mathbf{B}\underline{u} \qquad (4)$$

Where $\underline{p}$ is the co-state vector with dimension 6 x 1.

The necessary conditions for optimality are

$$\dot{\underline{p}} = -\frac{\partial \mathcal{H}}{\partial \underline{x}} = -A^T \underline{p} \tag{5}$$

$$0 = \frac{\partial \mathcal{H}}{\partial \underline{u}} = R\underline{u} + B^T \underline{p} \tag{6}$$

Equation (6) can be written

$$\underline{u} = -R^{-1} B^T \underline{p} \tag{7}$$

Substituting Equation (7) into Equation (2) we get

$$\dot{\underline{x}} = A\underline{x} - BR^{-1}B^T \underline{p} \tag{8}$$

From Equations (8) and (5) we get

$$\begin{bmatrix} \dot{\underline{x}} \\ \dot{\underline{p}} \end{bmatrix} = \left[\begin{array}{c|c} A & -BR^{-1}B^T \\ \hline 0 & -A^T \end{array}\right] \begin{bmatrix} \underline{x} \\ \underline{p} \end{bmatrix} \tag{9}$$

The solution to Equation (9) has the form

$$\begin{bmatrix} \underline{x}(t_f) \\ \underline{p}(t_f) \end{bmatrix} = \begin{bmatrix} F(t_f, t) \end{bmatrix} \begin{bmatrix} \underline{x}(t) \\ \underline{p}(t) \end{bmatrix} \tag{10}$$

From the boundary equations we get

$$\underline{p}(t_f) = S_f \underline{x}(t_f) \tag{11}$$

Using Equations (10) and (11), $p(t)$ can be determined analytically and applied directly to Equation (7) to find the optimal control. For this example the control solution is

$$\underline{u}(t) = \left(\frac{-3t_{go}}{3b + t_{go}^3}\right) \left[\begin{array}{c|c} I & t_{go} I \end{array}\right] \underline{X}(t) \tag{12}$$

where $t_{go} = (t_f - t)$

The theory that was used to obtain the solution assumed that t_f, final time, was specified; therefore, to insure optimality t_f must be known a priori or accurately estimated during flight.

ESTIMATION ALGORITHM

Note from the guidance law (Equation 12) that knowledge of relative position, relative velocity, and time-to-go is required for implementation. This information can be obtained from an extended Kalman Filter using line-of-sight angle and missile body acceleration measurements.

The formulation and equations that describe the filter are lengthy and rather complex, therefore, for the sake of brevity will not be given in this paper. However, a complete documentation of the filter is given in Chapter IV of (5).

Although the equations for the filter appear complex, the mechanization of the filter equations in digital code is straight/forward and easily accomplished. Further, preliminary analyses indicate that the algorithms pose no problem for mechanization in current state-of-the-art microprocessors.

ESTIMATING TIME-TO-GO

The most commonly used method for estimating time-to-go (t_{go}) is by

$$t_{go} = -R/\dot{R}$$

Where R = range-to-go

$\dot{R}$ = range rate = $\frac{dR}{dt}$

Estimating time-to-go by this method assumes that the acceleration along the line-of-sight is zero. However, this is a gross assumption in the modern air-to-air arena because of large target accelerations and most importantly large missile accelerations (nominally 30 g's).

In order to accurately compute time-to-go we must know the acceleration along the line-of-sight from present time to intercept. This acceleration is the dot product of the target/missile relative acceleration vector (a function of time) with a unit vector along the line-of-sight (also a function of time). Obviously this cannot be determined because of the uncertainty of future target maneuvers. However the missile's acceleration contributes significantly to the line-of-sight acceleration. Further the missile's axial acceleration is closely aligned to the line-of-sight for many engagements therefore it will dominantly influence the missile's contribution to the line-of-sight acceleration.

The necessity for knowledge of time-to-go arises from the theory that was used to derive the guidance law. The theory assumed that final time was fixed. Also, recall that it assumed complete control of all three missile acceleration components. These two assumptions are significant deviations from the actual tactical missile intercept problem; however, they had to be made in order to obtain a solution in closed form. In reality final time is free (within energy and physical constraints) and there is no control of missile axial acceleration. However, all is not lost. Consider the guidance law (Equation 12) written in terms of the states referenced to the missile body coordinate system and with b = 0.

$$A_{M_x} = 3\,(S_{R_x}/tgo^2 + V_{R_x}/tgo) \tag{14a}$$

$$A_{M_y} = 3\,(S_{R_y}/tgo^2 + V_{R_y}/tgo) \tag{14b}$$

$$A_{M_z} = 3\,(S_{R_z}/tgo^2 + V_{R_z}/tgo) \tag{14c}$$

Where

S_{R_x}, S_{R_y}, and S_{R_z} are the three components of the relative position vector S_R referenced to the missile body and V_{R_x}, V_{R_y}, V_{R_z} are the three components of the relative velocity vector V_R referenced to the missile body.

Since there is no control of the missile's axial acceleration, in the past Equation 14a has been completely neglected. By doing this, a considerable amount of information is not being utilized. The following time-to-go algorithm utilizes the information in Equation(14a)to solve for time-to-go and then uses the solution to time-to-go to solve for Equations(14b)and(14c).

Assuming that good information on S_R and V_R (these are obtained from the estimator) and the axial acceleration, A_{M_x}, is measurable, Equation(14a) contains only one unknown tgo. Therefore Equation(14a)can be written.

$$tgo^2 - \frac{3\,V_{R_x}}{A_{M_x}}(tgo) - \frac{3\,S_{R_x}}{A_{M_x}} = 0. \tag{15}$$

Using the Quadratic Formula, Equation(15)can be solved to obtain

$$tgo = \frac{3\,V_{R_x}}{2\,A_{M_x}} \pm \frac{1}{2\,A_{M_x}}\sqrt{9V_{R_x}^2 + 12\,S_{R_x}\,A_{M_x}} \tag{16}$$

Equation(16)has two solutions. To determine which solution is the desired solution, the constraint that

$$\lim_{S_{R_x} \to 0} \left[tgo \right] = 0$$

shall be imposed.

hith this constraint and realizing that $V_{R_X} < 0$ if the missile is closing on the target then the final solution becomes

$$tgo = \left(3\ V_{R_X} + \sqrt{9\ V_{R_X}^2 + 12\ S_{R_X}\ AMx}\right)/(2\ A_{M_X}) \qquad (17)$$

Substituting Equation (17) back into Equation (14a) the time-to-go algorithm can be rewritten to be

$$tgo = \frac{2SRx}{-V_{R_X} + \sqrt{V_{R_X}^2 + 4/3\ S_{R_X}\ A_{M_X}}} \qquad (18)$$

The advantages of this time-to-go algorithm is that it explicitly accounts for the effect of missile acceleration in estimating time-to-go: thus it provides a better estimate of time-to-go resulting in more optimal lateral and normal acceleration commands.

GUIDANCE LAW/ESTIMATOR MECHANIZATION

The guidance law and estimation algorithm are combined into a complete guidance package. The implementation of the guidance package will be done via a microprocessor based computer such that it can be integrated into the total missile system. A block diagram representation of the guidance package is given in Figure 3. The guidance package uses measurements from the seeker and missile accelerometers as inputs and provides acceleration commands to the autopilot. The figure depicts the outputs of the estimator providing information to the guidance law and time-to-go algorithm. This configuration offers great flexibility in future weapon systems because it allows for easy replacement of the guidance law or estimation algorithm or both as new techniques are developed or as new mission requirements arise.

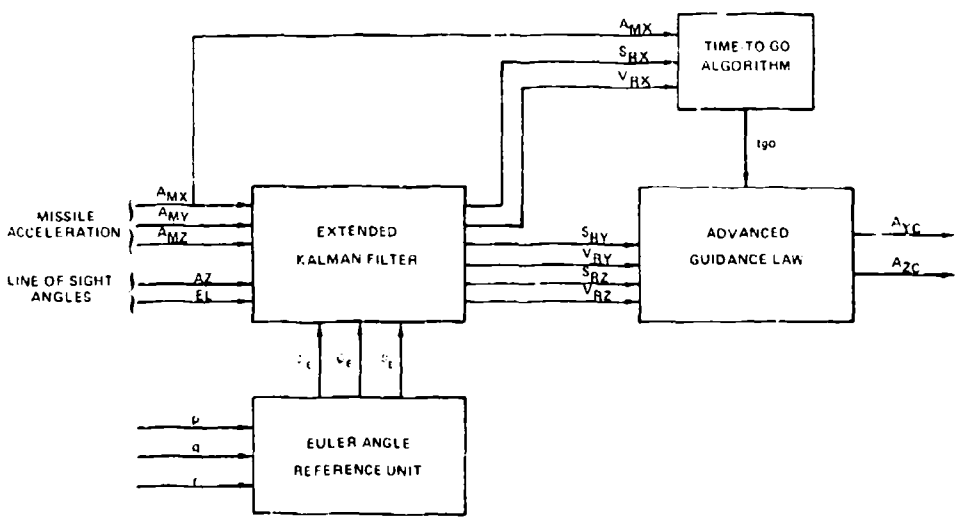

FIGURE 3. BLOCK DIAGRAM REPRESENTATION OF ADVANCED GUIDANCE PACKAGE

In implementing the guidance/estimation algorithms consideration must be given for the coordinate systems to which the input/output data is referenced. The seeker measurements are with reference to the seeker, the accelerometer measurements and acceleration commands are referenced to the missile body and the guidance state vector is referenced to inertial coordinates. By utilizing measurements of the missile angular rates (p, q, and r) the Euler angles relating the reference system to the missile body system can be computed. These angles are required to generate the required transformation matrices. Work is currently in progress to eliminate this need by modifying the guidance equations to allow mechanization in missile body coordinates.

EVALUATION

The most economical and effective method to evaluate any guidance algorithm is to implement it in a detailed simulation of a missile system and perform simulated missile fly-outs against realistic target models. This was accomplished in the analysis of the guidance package presented in this paper.

The guidance package was implemented in a six-degree-of-freedom (6-DOF) missile simulation of a conceptual short range air-to-air missile. The simulation contains detailed nonlinear math models of the major missile subsystems including the seeker, autopilot, or stability augmentation system, and, propulsion systems; realistic noise

models of the on-board sensors and seeker measurements; detailed aerodynamic models of missile airframe characteristics; and the models that describe the missiles' equations of motion. Additionally, the simulation contains a three-degree-of-freedom target model which incorporates a "smart" target nine "g" evasive maneuver algorithm.

In order to establish a baseline, proportional navigation along with well designed low-pass filters for smoothing the seeker measurements was implemented in the simulation and evaluated under the same conditions as the advanced guidance package. The navigation gain was optimized to minimize miss distance.

To evaluate and compare the two guidance techniques (proportional navigation and the advanced guidance package), numerous Monte Carlo analyses were performed for a large number of engagement conditions. To accomplish this, over 2000 fly-outs per guidance algorithm were accomplished with the aid of a digital computer. This comprehensive analysis allowed the generation of effective launch envelopes. The effective launch envelope defines the geometric region in space from which the missile can be launched and a mean miss distance of ten feet or less be obtained. A further constraint was imposed in that the standard deviation of the miss distance had to be less than the mean miss distance. This additional constraint translates into a high confidence factor of the Monte Carlo analysis. A minimum of ten Monte Carlo runs was accomplished for each launch condition. If the results appeared to be sensitive to the noise distribution then further Monte Carlo runs were conducted until the percent change in the standard deviation was within acceptable limits.

The missile and target were co-altitude (3.05 kilometers) at launch and were co-speed at launch (.9 Mach). The target performed its evasive out-of-plane maneuver algorithm when the range became less than or equal to 1.83 kilometers.

The effective launch envelopes are depicted in Figures 4 and 5. Figure 4 shows the case for 0° off-boresight angle (the off-boresight angle defines the angle between the initial line-of-sight vector and the initial missile velocity vector, therefore 0° off-boresight means the missile was launched directly at the target). Figure 5 shows the launch envelope for 40° off-boresight launches where the missiles' velocity vector lagged the line-of-sight vector by 40°. This is considered a worst case launch condition for the missile. The polar plots of the launch envelopes in Figures 4 and 5 depict launch range versus aspect angle (the angle between the initial line of sight vector and the targets velocity vector at launch). For instance a 0° off-boresight, 0° aspect angle launch condition would be a tail-on shot; a 0° off-boresight, 180° aspect angle launch condition would be a head-on shot; and a 40° off-boresight, 90° aspect angle launch condition would be a beam shot where the targets velocity vector would be perpendicular to the line-of-sight and the missiles velocity vector would lag the line-of-sight by 40°.

It should be noted again that both guidance algorithms (proportional navigation and the advanced guidance) used passive seeker information, however, proportional navigation only used the filtered measurements of line-of-sight rate, whereas the advanced guidance package used line-of-sight angle and missile acceleration measurements as inputs to the estimator which provided estimates of relative range and relative velocity.

As can easily be seen from Figures 4 and 5, the advanced guidance law significantly out-performed the proportional navigation law, especially in the close-in arena. Considering that this was accomplished without additional sensor devices is a significant achievement in missile guidance development.

CONCLUSIONS AND RECOMMENDATIONS

The results of this effort have clearly shown that the use of Optimal Control and Estimation Theory for deriving advanced tactical missile guidance concepts can yield extremely high performance guidance algorithms. Further, this can be done without increasing the hardware requirements of the missile system.

These concepts also offer the potential for decreasing the sensor accuracy specifications without degradating the total system performance. This could result in effective low-cost weaponry. However, there is a limit to this process and no studies have yet been pursued to fully explore this potential. This type of study could be extremely beneficial to the Air Force.

It has also been shown in recent studies that these techniques are applicable to solving guidance problems for fixed (strapdown) seekers. More studies in the future are needed to pursue this potentially high pay-off technology.

Thus far only the development of terminal guidance laws has been accomplished via Optimal Control and Estimation. It is feasible that equivalent performance improvements can be made in other tactical missile subsystem technology areas such as mid-course guidance for beyond visible range missiles, propulsion system design especially in areas where partial thrust control is possible such as in pulse motors and Ramjets, and in autopilot design. The application of Optimal Control and Estimation to these areas needs to be fully explored.

In terms of mechanization, future work needs to be accomplished in thoroughly defining the on-board computer requirements for realization of the algorithms. Although these algorithms appear to be implementable in microprocessors and solvable in real time, the Air Force will not be able to fully determine the potential pay-off of these algorithms until this task is explicitly accomplished.

It should also be noted that the guidance algorithm presented in this paper is the most simplistic of all the algorithms developed in this research program. Other more sophisticated and more complex algorithms have been developed. These higher order algorithms offer the potential for further missile performance improvements that will be necessary to meet future mission requirements. Trends in digital hardware technology indicate that it will be practical to mechanize even the most sophisticated of these algorithms in future air-to-air missiles.

In conclusion, Optimal Control and Estimation Theory, combined with modern digital technology offer the potential for the development of high performance, moderate cost tactical weapons in the next generation of missiles.

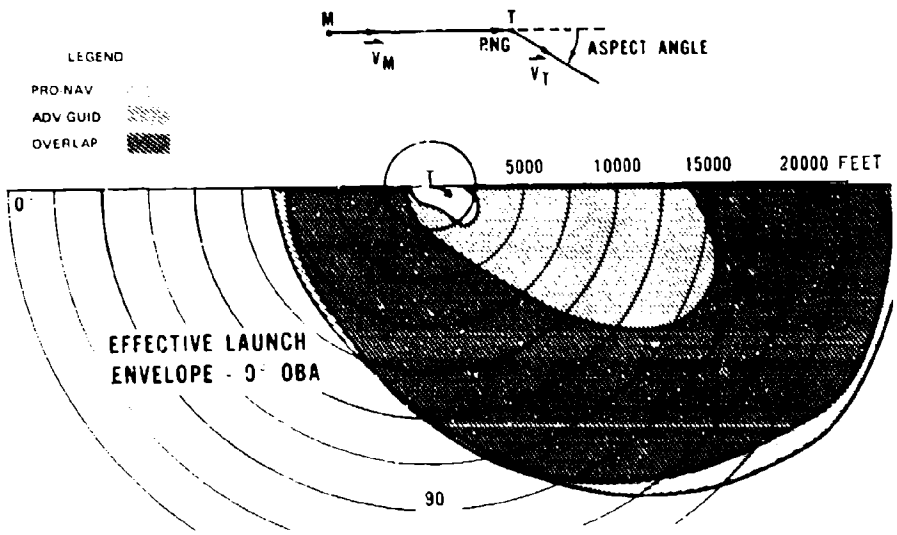

Figure 4. Effective Launch Boundaries for Pro-Nav and Advanced Guidance 0° Off-Boresight Angle

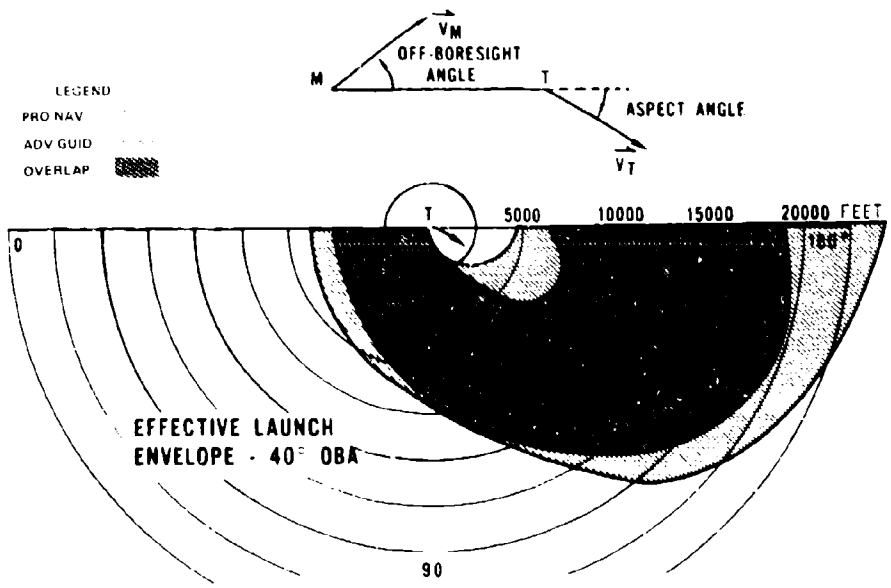

Figure 5. Effective Launch Boundaries for Pro-Nav and Advanced Guidance - 40° Off-Boresight Angle

REFERENCES

1. Youngblood, J. N. "Optimal Linear Guidance of Air-to-Air Missiles", AFATL-TR-78-12, February 1978

2. Fiske, P.H., "Advanced Digital Guidance and Control Concepts for Air-to-Air Tactical Missiles", AFATL-TR-77-130, November 1977

3. Gupta, N.K., "Tactical Missile Guidance and Control Law Methodology", AFATL-TR-80-20, March 1980

4. Anderson, G. M., "Guidance and Control Law Methodology", AFATL-TR-79-86, October 1979

5. Sammons, J.M., et al, "Development and Comparison of Optimal Filters", AFATL-TR-79-87, October 1979

6. Riggs, T.L., "Linear Optimal Guidance for Short Range Air-to-Air Missiles," Proceedings of NAECON 1979, Volume II, pages 757-764, May 1979

DEVELOPMENT TESTING AND FLIGHT CERTIFICATION TESTING OF TERMINALLY GUIDED SUBMISSILES

by

Jerrel G. Bland, H. Dennis Ulrich, Kenneth L. Wismer,
W. Dean Clingman and Cynthia K. Gronewold

BOEING AEROSPACE COMPANY
P. O. Box 3999
Seattle, Washington 98124

SUMMARY

The segments of an example Terminally Guided Submissile (TGSM) tactical mission are examined to identify those guidance and control modes employed in performing the mission. Special control problems resulting from drop testing from helicopter carrier vehicles are also identified to further define the elements of the test problem. Boeing's development test program for TGSM vehicles is then described, including descriptions of our terminal guidance laboratory facilities. Additional detail is given on the laboratory configurations for testing TGSM's using both IR and millimeter wave (MMW) seekers.

Development of the real time Hardware-In-The-Loop (HITL) TGSM simulation is then summarized along with those problems addressed through the use of the HITL simulation. The final section presents some HITL simulation data generated during our Phase II Assault Breaker Program. The data is analyzed and discussed to show its utilization in evaluating TGSM performance.

LIST OF SYMBOLS AND ACRONYMS

TGSM	-	Terminally Guided Submissile
IR	-	Infra-Red
MMW	-	Millimeter Wave
HITL	-	Hardware-In-The-Loop
g	-	Acceleration Due to Gravity
A/B	-	Assault Breaker
MPS	-	Meters Per Second
TGL	-	Terminal Guidance Laboratory
GH	-	Gigahertz
RF	-	Radio Frequency
LOS	-	Line-Of-Sight
QLOS	-	Computed Pitch LOS Rate
$\dot{\sigma}_\theta$	-	Pitch LOS Rate Measured by Seeker
α'	-	Total Angle-of-Attack
RLOS	-	Computed Yaw LOS Rate
$\dot{\sigma}_\psi$	-	Yaw LOS Rate Measured by Seeker
$\dot{z}$	-	Pitch Plane Velocity
$\dot{y}$	-	Yaw Plane Velocity
δ_γ	-	Equivalent Yaw Fin Angle
$\dot{\gamma}$	-	Yaw Attitude Rate
ψ	-	Yaw Attitude Angle
δ_a	-	Equivalent Roll Fin Angle
P	-	Roll Attitude Rate
ϕ	-	Roll Attitude Angle
TABLE	-	Flight Table Pitch Gimbal Angle
TABLE	-	Flight Table Yaw Gimbal Angle

INTRODUCTION

The Terminally Guided Submissile (TGSM) is a common element to many proposed concepts for attacking second echelon armor. (Figure 1.) This paper examines an example TGSM concept some special considerations in flight testing the TGSM, Boeing's approach to TGSM development testing, including Hardware-In-The-Loop (HITL) simulation testing, and concludes by presenting some HITL simulation test data.

THE TACTICAL MISSION

The TGSM mission considered divides into four major segments which utilize combinations of Guidance and Control loops. The first segment, "A" is an attitude control mode used immediately after dispense and prior to initiating the dispersal maneuver. Segment "B" is a programmed guidance mode used to implement the desired dispersion. Segment "C" is a search and acquisition mode which is functionally identical to Segment "A". Segment "D" is the final terminal guidance mode used to intercept the target.

These segments are depicted on Figure 2 and are further defined in the following paragraphs in the order employed.

Attitude Control Prior to Dispersal - Segment "A"

This is the initial function employed upon release or launch from an example carrier vehicle. It may be attitude rate control only, referenced to the launch or release attitude, or it may be integrated attitude rate referenced to a pre-set desired attitude such as horizontal or vertical. The TGSM considered employs a pre-set "vertical" reference attitude initialized from the carrier reference system just prior to launch. Accumulated attitude error is thus a function of the initialization error, the drift rate in the TGSM attitude rate sensors, and the elapsed time since initialization. Acceleration sensitive drifts may also be significant depending on the acceleration or "g" loads imposed during the launch sequence. Attitude rate control is exercised immediately following clearance of the TGSM control fins as the missile is launched or dispensed and the fins snap into extended position. A short time is allowed for the TGSM flight path to stabilize and to clear the carrier vehicle before activating the programmed attitude profile to implement the desired dispersal maneuver.

Programmed Guidance for TGSM Dispersal - Segment "B"

The desired TGSM dispersal pattern for our example is executed by rolling each vehicle to a prestored angle and then activating a prestored pitch plane attitude profile designed to terminate at a specific attitude and velocity. Initial Assault Breaker "seekerless" TGSM testing utilized this guidance mode with a programmed series of roll, pitch, and yaw maneuvers to verify the flight control system and the aerodynamic model.

Terminal Guidance - Segment "D"

Completion of the programmed guidance maneuver is followed by activation of the seeker start search program which is terminated at "acquisition" (segment "C"). Proportional guidance is then utilized to home on the acquired target. Guidance gain and response time are a compromise designed to achieve the minimum miss distance commensurate with the seeker angle tracking noise and the requirement for adequate stability margins in the autopilot control loops.

SPECIAL DROP TEST CONSIDERATIONS

The control problem can be further complicated for certain types of TGSM testing, especially helicopter borne drop tests as was used for testing the Phase II Assault Breaker (AVID) TGSMs. For the Boeing TGSM tests, dynamic pressure varied from a low near "0" with the initial 9 meters-per-second (mps) launch velocity to a high of over 1.5×10^6 grams/meter^2 at the over 150 mps velocity at impact. The result was a requirement for a compensating gain schedule to maintain near constant control effectiveness throughout the drop test mission. Maintaining adequate stability margins thus required a very close match between the predicted velocity-time profile used to establish the prestored gain schedule, and the range of actual velocity-time profiles that may exist in a "real world" drop test.

THE DEVELOPMENT TEST PROGRAM

The criteria for success in a TGSM test program is closely related to the demonstrated accuracy in impacting the target. For shaped charge warhead devices, a miss - no matter how small - is of little value in killing the hard targets of interest. Demonstrating the required accuracy with the least number of TGSM rounds thus requires a high level of confidence in the models used for predicting TGSM performance. These accuracy requirements apply to the individual TGSM subsystem models, the target and the target background model, the flight environment model, and the initial or launch conditions model. The target and target background models, especially for real world battlefield flight environments is an area where the data base is still very limited. Both the Assault Breaker and WASP programs have utilized tower and captive flight tests to expand this data base; however, additional testing is still required for adverse weather and battlefield environments.

For this paper, our concern is primarily one of guidance performance. We therefore assume that target acquisition has occurred and we examine those tests required to refine or verify the subsystem models in order to finalize the guidance and control loop parameters. Utilization of these models and parameters in terminal guidance simulations provides the guidance performance predictions and parameter sensitivities required to predict miss distance. At Boeing these are "All Computational" or "AL Comp" simulations utilizing mathematical models entirely. Such simulations are formulated early in a program and are continually refined as wind tunnel tests are completed and individual components of subsystem hardware are designed and the hardware is available for model verification. As this occurs, the test program enters what we call the Hardware-In-The-Loop (HITL) test phase.

HITL SIMULATION TESTING

HITL simulation testing employs a versatile "real time" simulation with appropriate target and missile motion simulators to accurately duplicate the seeker-target dynamic interaction and the missile rotational dynamics. Target radiation is provided at the proper frequency or wave length and with the appropriate dynamics and signature characteristics for the TGSM target seeker being tested. Tests are performed using hardware substitutions for different subsystem mathematical models until the final flight certification testing which utilizes the entire TGSM unit as shown on Figure 3. These tests are performed in Boeing's Terminal Guidance Laboratory (TGL) shown on Figures 4 and 5.

Terminal Guidance Laboratory (TGL)

Target simulators in the TGL provide dynamically and spectrally valid target signatures for seekers operating in the Infra-Red (IR) and Optical domain, the 2 to 12 gigahertz (GHz) region of the Radio Frequency (RF) spectrum, and the millimeter wave (MMW) region (passive only - 94 to 169 GHz). For this paper, TGSM test considerations are restricted to sensors utilizing IR and passive MMW seekers. Both types were evaluated during Boeing's Phase II Assault Breaker program and will be evaluated during the current WASP program. Figure 5 shows the MMW test facility used for the passive MMW seeker tests.

Since the seeker impact on guidance accuracy is primarily a function of the angle and angle rate tracking noise during the final phase of flight, MMW target simulation facilities were developed first for the passive mode which is employed by both Boeing Assault Breaker and WASP MMW seekers for this phase of flight. Both seekers were developed by the Sperry Company and utilize an initial active mode for better target discrimination and longer acquisition range; however, increasing glint noise at close range with the active mode forces a switchover to passive operation which provides a much lower noise level during the crucial final homing.

While dynamic MMW target simulation for the active MMW seekers is desirable, Boeing's facility ... providing this capability is still in the design stage and is not scheduled for completion until late 1981.

Missile motion is simulated in the TGL with a three-axes dynamic flight simulator built by the Carco Electronics Company. The flight table portion of this simulator is shown on Figure 3 with the entire Boeing Assault Breaker TGSM mounted for test.

Figure 6 shows the varian -72 computer complex which implements the simulation equations in real time and interfaces with the different laboratory simulators, the instrumentation and recording equipments, the TGSM being tested, and the operators console.

Laboratory Configuration and Operation for HITL Simulation Testing

HITL simulation testing utilizes the TGL facilities to excite the TGSM subsystems with external forces and radiation which is designed to closely match the external stimulus that would be encountered in an actual flight.

Figure -7 depicts the TGL configuration for testing an IR seeker guided TGSM. In this configuration, laser radiation at the proper wave length is reflected by the two-axes mirror onto a spherical screen. The increasing angle subtended by the target with decreasing range is simulated with the spot size controller. Computed relative range and velocity drives the spot size controller while computed flight path rotation rate drives the two-axes mirror. Detected motion of the target spot by the table mounted IR seeker generates line-of-sight (LOS) rate signals which are input to either a flight control system model, or the TGSM flight control system hardware. Either measured or computed fin angle signals are input to the aerodynamic model which outputs pitch, yaw, and roll signals to the three-axis flight table and mirror and spot size controller signals for flight path rotation and range closure. The subsystem computer models are programmed to duplicate the known subsystem dynamic responses, as well as deviations from these "mean" characteristics to account for unknowns and to do parametric studies for system optimization. External seeker noise can be input with the two-axes mirror, or electrically input and summed with the seeker output signals. Different seeker blind ranges can be simulated by turning of the laser at different simulated ranges. The simulation is initiated at some programmed range and velocity which are misaligned by various angular amounts to examine the effects of target acquisitions at different ranges and over some band of search angles. Each run is terminated when the computed range vector goes through "0". Target miss distance and various simulation parameters are recorded and used to evaluate the TGSM being tested.

The facility shown in Figure -9 is used for testing TGSM's using MMW target seekers. For this facility, simulated target radiation is generated with an array of gas discharge tubes which are programmed to provide the same apparent target motion and growth with range closure as in the IR facility. Figure -8 depicts the laboratory configuration for testing TGSM's with MMW target seekers. The IR and MMW simulation functions are identical except for those associated with controlling the target simulator. Figure -9 shows a MMW seeker mounted in the MMW laboratory flight table.

The capabilities and constraints of the IR and MMW target simulators are shown on Figure -10.

HITL Simulation Development

The initial Hardware In-The-Loop (HITL) testing consisted of open loop modeling tests on the major functional components which are the autopilot, fin actuator, rate sensors and seeker (Figure 11). After each hardware subassembly was flown in the loop with the others simulated in software, the subassemblies were added one at a time until the entire missile was flown in the hardware-in-the-loop simulation.

These initial subassembly tests consisted of taking sufficient open loop test data to obtain the transfer function for the assembly. The transfer function was then implemented in software that would run in real time. After all subassemblies were modeled or sufficient design data was available to generate a model, the real time simulation was generated using aerodynamic data taken in wind tunnel tests and the model data generated for each subassembly. By using design data to generate preliminary models for hardware-in-the-loop simulation software, the software program development progressed in parallel with the hardware and was ready when the hardware was available. As each flight configured hardware subassembly became available, closed loop test data was generated to develop a more realistic model.

The resulting closed-loop models were then used to update the computer simulation, which was then used to evaluate the effect of the updated model on system performance. To obtain adequate performance, system gains, bandwidths and dead zones were first adjusted in the system software model which ultimately required TGSM hardware or software modifications prior to the final flight certification HITL simulation test. As each piece of hardware was added in the loop, the optimization process was repeated until all hardware was flown in the loop for the final optimization. This final optimization involved repeated simulation runs to examine guidance accuracy and stability for the expected range of drop test conditions.

After each actual TGSM drop test the flight data was reviewed and, if required, the hardware or software was modified as well as the software for the HITL simulation. The optimization process is continual as better modeling data becomes available and the hardware matures.

Some of the problems addressed by hardware-in-the-loop testing of terminally guided submissiles are:

1. Seeker control loop optimization
2. Seeker output filter optimization
3. Guidance filter optimization
4. Autopilot software compatability
5. Autopilot hardware inadequacies
6. Seeker software/hardware inadequacies
7. Actuator dead band and nonlinearities

Discovered hardware inadequacies can sometimes be compensated for by software and thus keep hardware changes to a minimum. This occurred a number of times during the Phase II Assault Breaker HITL testing.

The following section presents example hardware-in-the-loop test data taken in Boeing's Terminal Guidance Laboratory prior to some of our Phase II Assault Breaker TGSM drop tests.

HITL Simulation Results

Figure 12 is a top level block diagram of our example TGSM guidance and control loop. Initial HITL testing of the integrated TGSM utilizes the entire missile to examine the stability of the autopilot attitude control loop, first for the "attitude hold" mode used during segment "A" and finally for the terminal homing mode during segment "D". Figure 13 is a time plot of the four fin angles from launch to ground impact as well as the six discretes used to sequence TGSM events or record subsystem status. A study of the discretes shows that the run is initiated with the "start gyro" discrete, followed by the "launch" discrete which activates the TGSM digital autopilot program. These first two discretes are input through the TGSM umbilical cable and would be generated by the launch control system on the helicopter. The "launch" discrete would activate the launch mechanism.

The stored program allows a short time for the TGSM to clear the launcher before firing the squib which punctures the "actuator gas" bottle and activates the control system. For HITL testing, this discrete supplies actuator gas through an external port into the fin actuator system. However, a limited number of HITL tests were performed with "live" gas bottle squibs thus using the on-board actuator gas supply.

The "seeker search" discrete is delayed to permit a buildup of vertical velocity and dynamic pressure sufficient for the required maneuverability. A two stage "seeker lockon" is used to ensure solid target tracking prior to closing the guidance loops. A drop out of the "seeker lockon" discrete just prior to the "end of the run" signifies that the seeker lost track on the target just prior to ground impact. This "break lock" condition near impact is not uncommon as the angle subtended by the target expands exponentially near impact. Examining "miss distance" sensitivity to the range where "break lock" occurs is an example of the kind of trade studies permitted with the HITL simulation.

Fin activity for the run depicted on Figure 13 was relatively well behaved. During the initial flight with low dynamic pressure, larger fin angles were required to maintain attitude control. As dynamic pressure built up, this fin angle activity reduced in magnitude until the "lock-on" transient when the guidance loops were closed. Once this transient was passed, fin activity again settled down, but not to as low a value even though dynamic pressure continued to rise. This is due to the "angle rate tracking noise" on the guidance signals from the seeker. The somewhat larger angles on Fin-1 and Fin-3 just prior to impact implies a combination "pitch-yaw" maneuver since the missile is roll stabilized to a "0" roll angle which bisects the angle between the control fins.

Figure 14 is a time plot of the three rate gyro outputs which register the attitude rates resulting from the fin angle history shown on Figure 13. The rates follow a similar pattern to that exhibited by the fin angles except for the roll axis. Here due to the low moment of inertia, even small fin angles produce significant roll rate activity. Of equal or greater concern would be any large roll rate transients that might occur at launch when the low dynamic pressure results in minimal control authority. This concern requires that close attention be paid to the design of the launch mechanism on the carrier helicopter as well as the proposed tactical carrier vehicle.

The major portion of HITL testing to evaluate attitude control loop stability can be performed without the target seeker hardware. This can be accomplished with either "shorted" seeker inputs or a noise generator input to simulate seeker noise effects. However, to evaluate homing performance or TGSM impact accuracy requires first the seeker hardware for extensive open-loop testing, second a validated real-time software simulation for all TGSM subsystems but the seeker, and third, the entire integrated TGSM vehicle for final flight certification to achieve a desired impact accuracy or "miss distance".

The open-loop seeker tests are designed to determine or verify the seeker transfer function. The parameters of interest are the frequency response and tracking limits, the linearity or stability of the scale factors for the guidance signals, the bias and angle rate tracking noise on these signals, the sensitivity of these signals to temperature, TGSM attitude rate or acceleration, cross-coupling between seeker output signals for the two axis, and seeker blind range and its variation with the environment or target/background combination. HITL testing provides only limited data on blind range variations or output signal sensitivity to temperature or acceleration. However, it does permit an evaluation of the "miss distance" results from such variations.

Well designed seekers generally satisfy most of the homing requirements which are normally identified in the subsystem or interface specification. Exceptions to this are the angle rate tracking noise and both cross-coupling and attitude rate or motion coupling into the guidance signals. This latter parameter tends to be well-controlled for spinning dish or stabilized platform seekers, but can be large for body referenced or strapdown seekers.

High cross-coupling values are often measured during initial seeker testing. Normally the HITL simulation facilities permit an accurate measurement of this coupling which can usually be reduced by compensation.

Angle rate tracking noise is generally the defining parameter which limits the achievable TGSM homing performance. Figure 15 is a measured sample of angle rate tracking noise plotted as a power spectral density. These curves closely parallel the seeker frequency response and show a sharp cut-off in the region of 15 to 20 hertz. Utilization of these signals for TGSM guidance would further limit the pass band by adjusting the guidance filter downward until a further decrease increased the miss distance.

Such a guidance filter optimization is carried out using the seeker hardware and the validated real-time software simulation for the remaining TGSM subsystems. These "closed loop" seeker tests examine the extremes of maneuverability requirements resulting from both large target off-set angles and minimum acquisition range or homing time. The resulting combination of guidance gain and filter response is designed to provide an acceptable miss distance for the aggregate of conditions and uncertainties in the test or tactical mission.

FLIGHT CERTIFICATION

Optimization of the guidance and control parameters during the HITL closed-loop seeker tests is followed by flight certification testing utilizing the entire integrated TGSM vehicle. Figures 16, 17, 18 and 19 are examples of such flight certification data. Figure 16 is a time plot of both the computed pitch line-of-sight (LOS) rate (QLOS) and the measured pitch LOS rate ($\dot{\sigma}_\theta$) from the seeker. Also shown are the total angle-of-attack (α) and the resulting pitch plane velocity ($\dot{z}$). Figure 17 presents the computed yaw LOS rate (RLOS) and the measured yaw LOS rate ($\dot{\sigma}_\psi$) from the seeker. The yaw plane velocity ($\dot{y}$) resolved from the total angle-of-attack (α) is also plotted on Figure 17. Figure 18 is a time plot of the Equivalent Yaw Fin Angle (δ_γ), the resulting yaw attitude rate (γ), the integrated yaw attitude angle (ψ), and the Equivalent Roll Fin Angle (δ_β). Figure 19 presents time plots for the resulting roll rate (P), the integrated roll angle (ϕ), and the pitch (θ table) and yaw (ψ table) gimbal angles from the three axis flight table where the TGSM is mounted.

An examination of these HITL simulation data plots shows similar behavior to the fin angle and rate gyro data presented on Figures 13 and 14. The computed roll rate (P) is a close match to the measured gyro roll rate. The measured gyro yaw rate and the computed yaw rate (r) are also closely matched, including the lock-on transient which originates on the seeker yaw LOS rate signal ($\dot{\sigma}_\psi$) shown on Figure 17. While the computed signals "RLOS" and "QLOS" are not used in this simulation mode, they do provide an indication of proper seeker operation. A comparison between the computed and measured LOS rate signals also shows the significant modulation resulting from the angle rate tracking noise as shown on Figure 15. While this noise is producing rather large roll rate oscillations, it is no more than 15% of maximum rate, and the resulting miss distance is acceptable. Reducing either the autopilot or guidance gain would reduce the roll oscillations, but would increase the miss distance. Increasing the gains might reduce the miss distance but the roll oscillations would increase and further reduce the roll loop stability margins. This would increase the risk that a combination of vehicle parameter uncertainties, operating conditions, and a noise spike on the LOS rate signal could drive the roll loop into instability and loss of control thus greatly greatly increasing the miss distance.

CONCLUSIONS

The use of real time HITL simulations for development and flight certification testing of TGSM vehicles provides a versatile tool for evaluating both the subsystem components as well as the integrated vehicle.

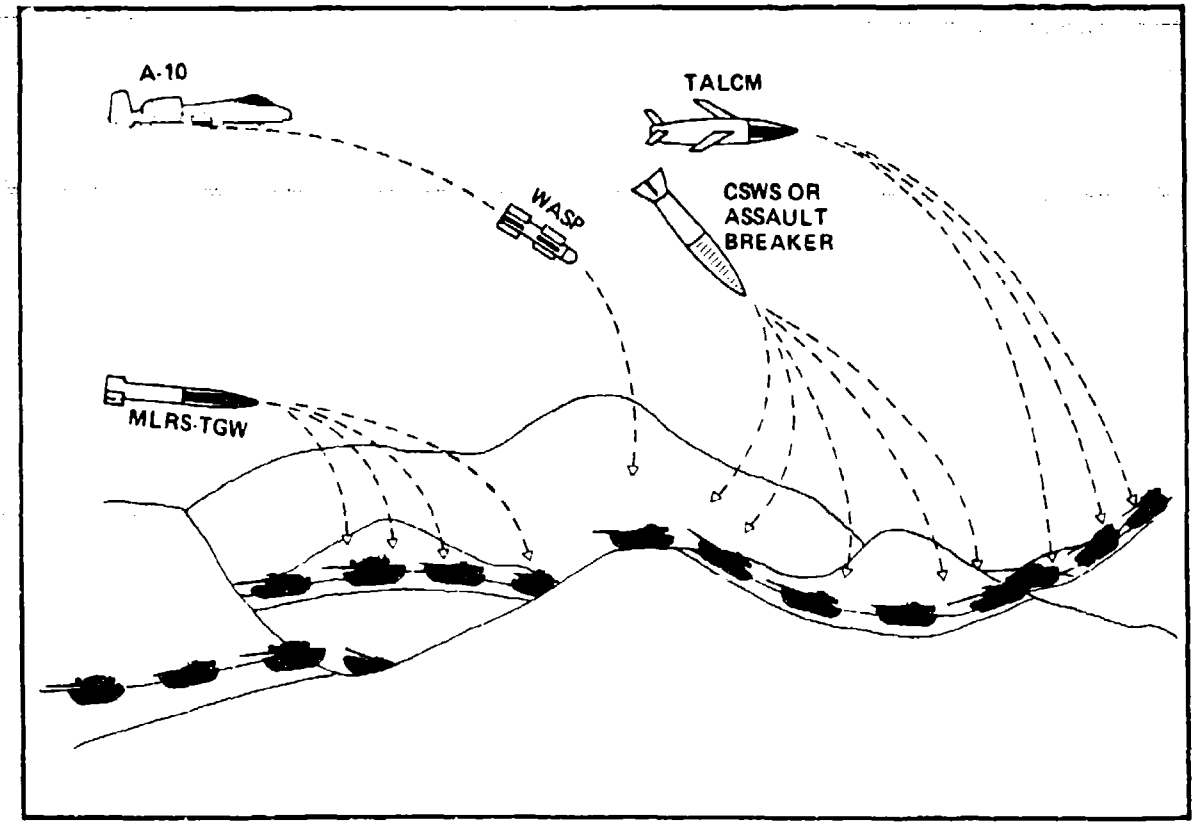

Figure 1. Terminally Guided Submissile Carriers

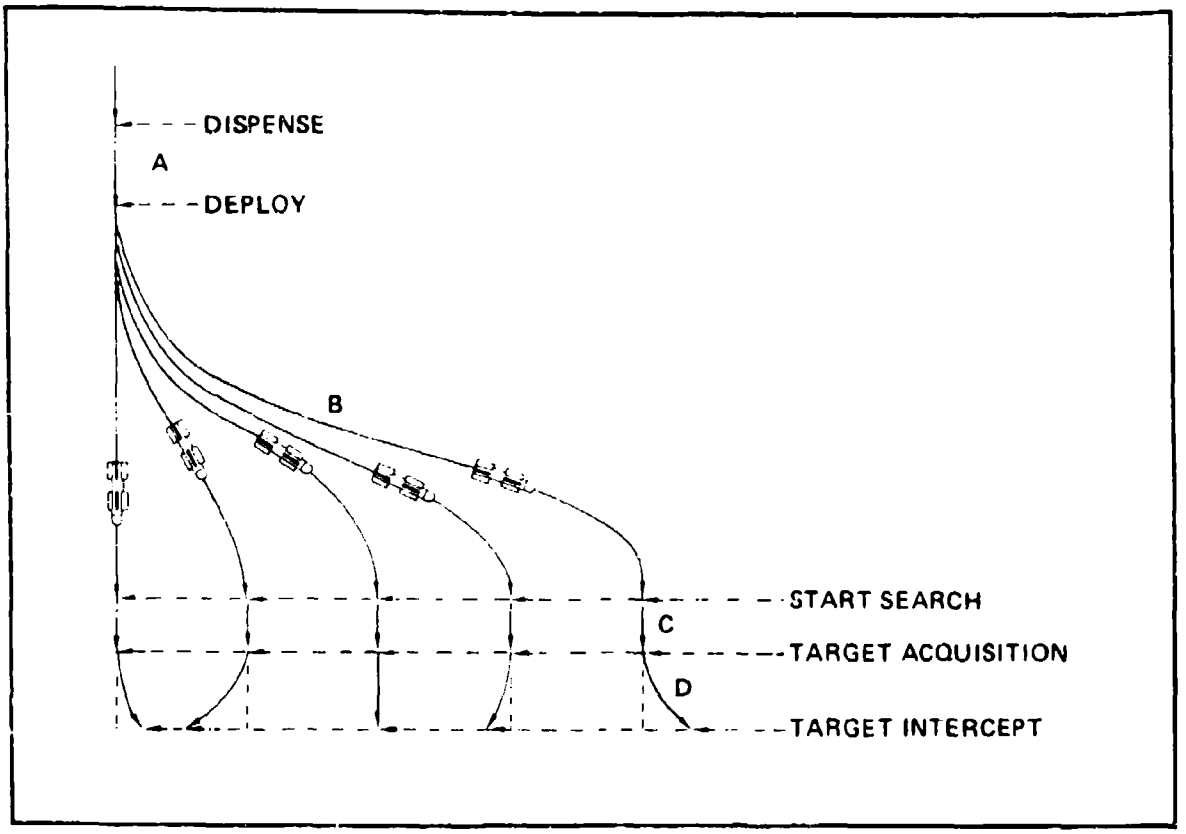

Figure 2. Operating Sequence

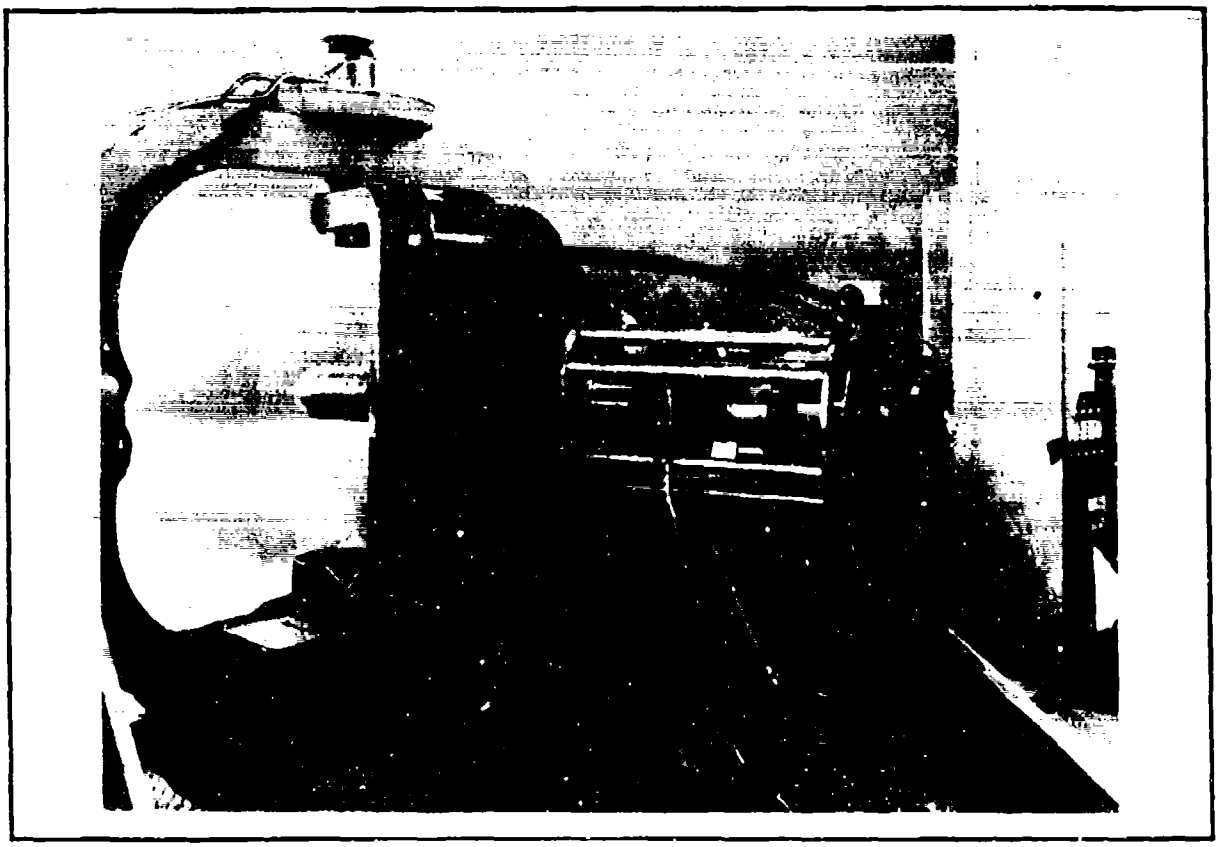

Figure 3. Dynamic Flight Simulator With TGSM

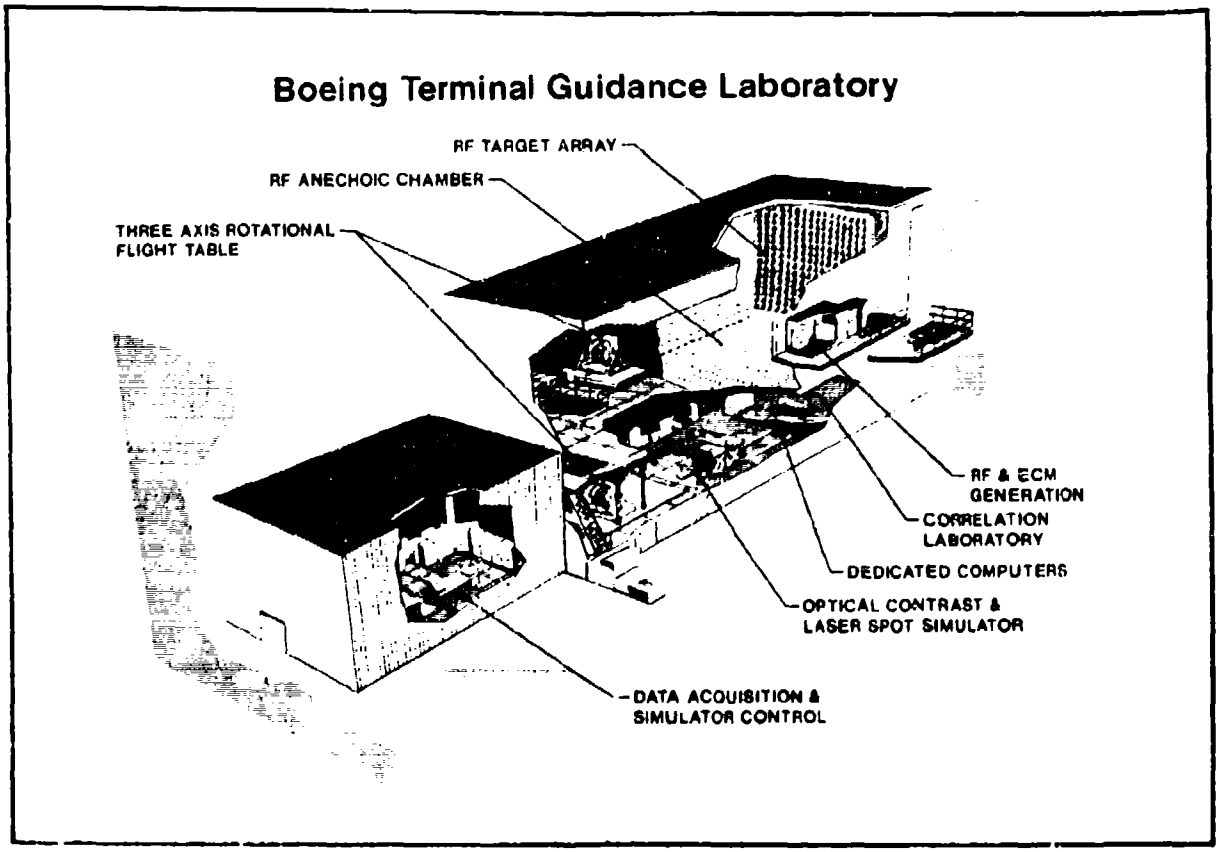

Figure 4. Boeing Terminal Guidance Laboratory

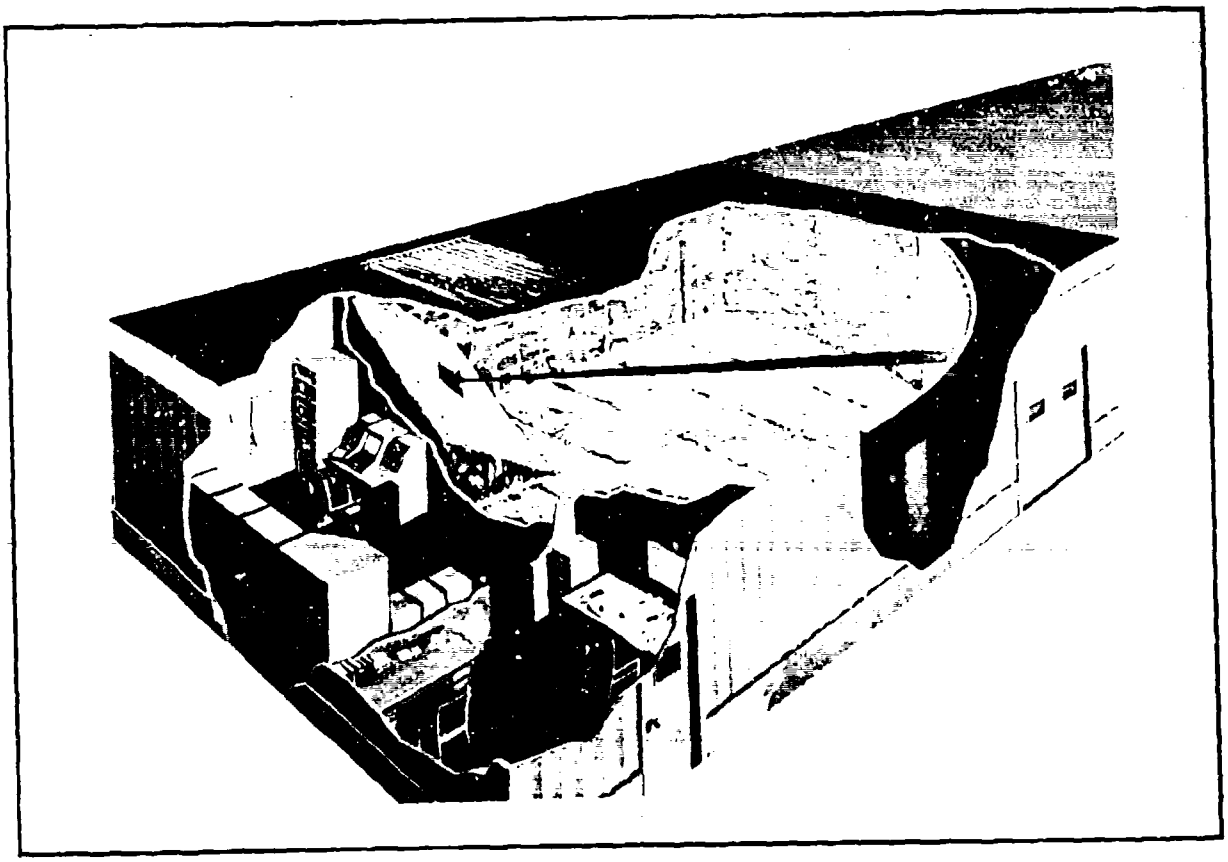

Figure 5. Millimetre Wave Test Facility

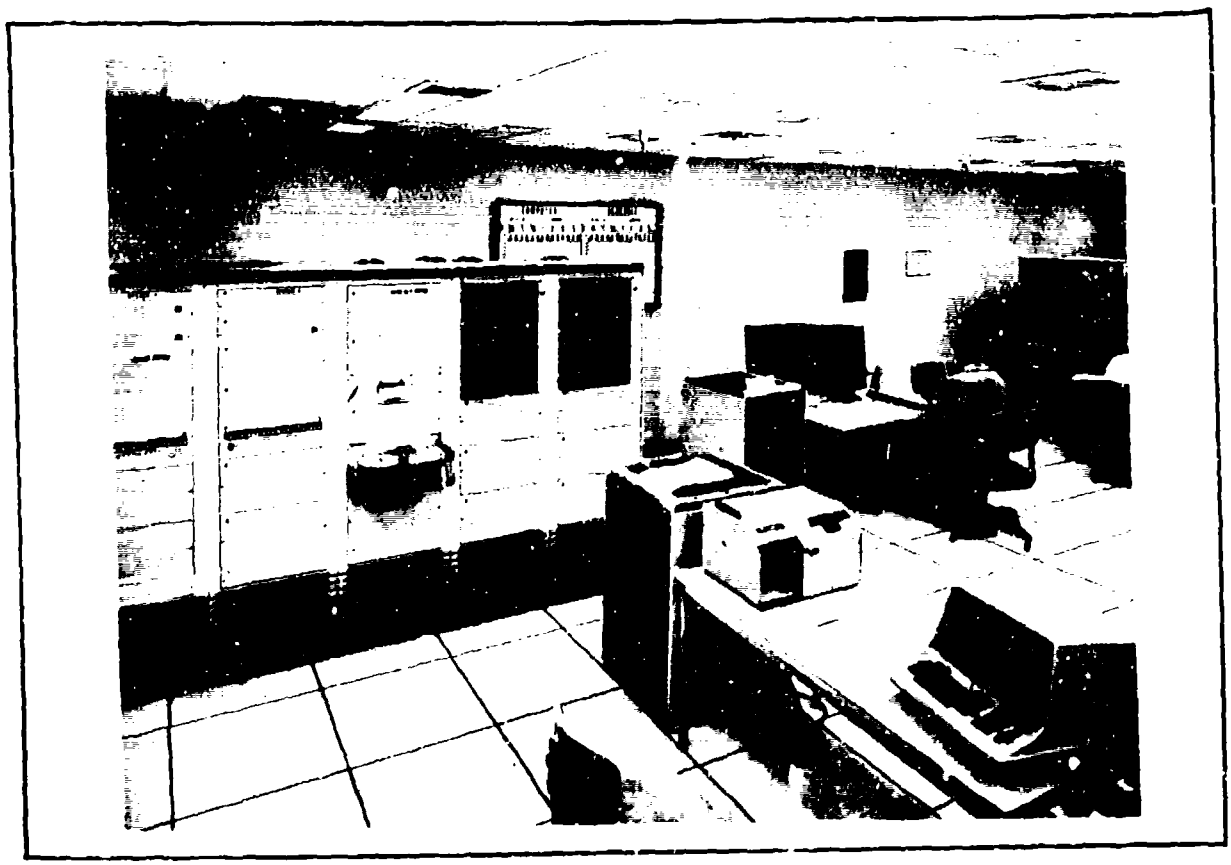

Figure 6. Varian-72 Simulation Computer Complex

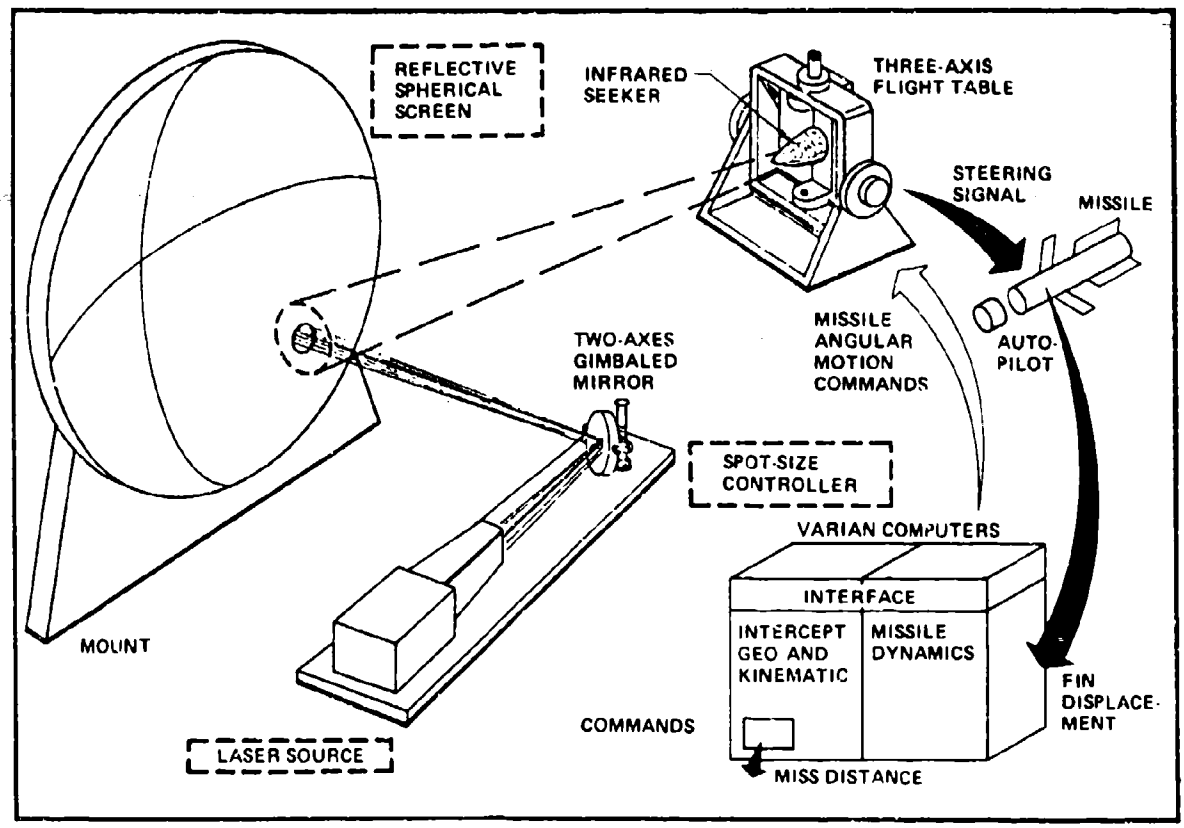

Figure 7. Hardware-in-the-Loop Simulation for Testing Infrared Seeker-Guided TGSM's

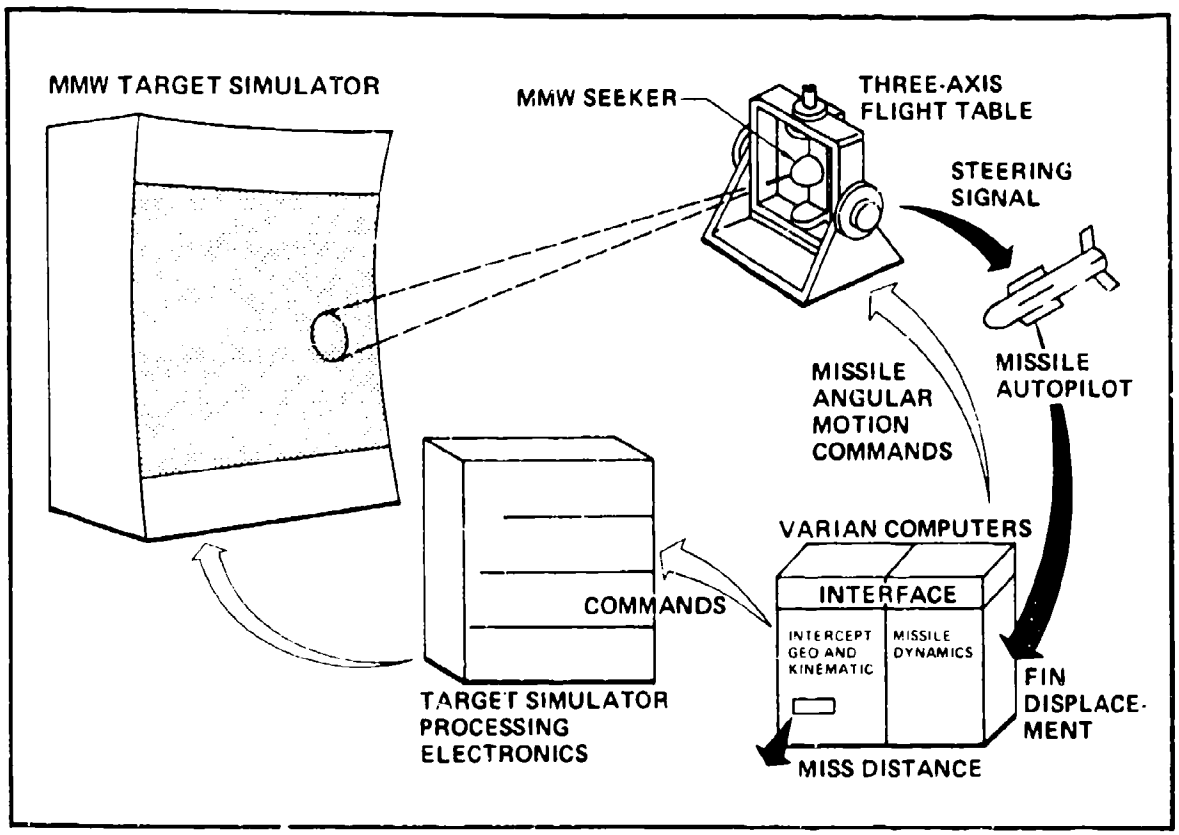

Figure 8. Hardware-in-the-Loop Simulation for Testing MMW Seeker-Guided TGSM's

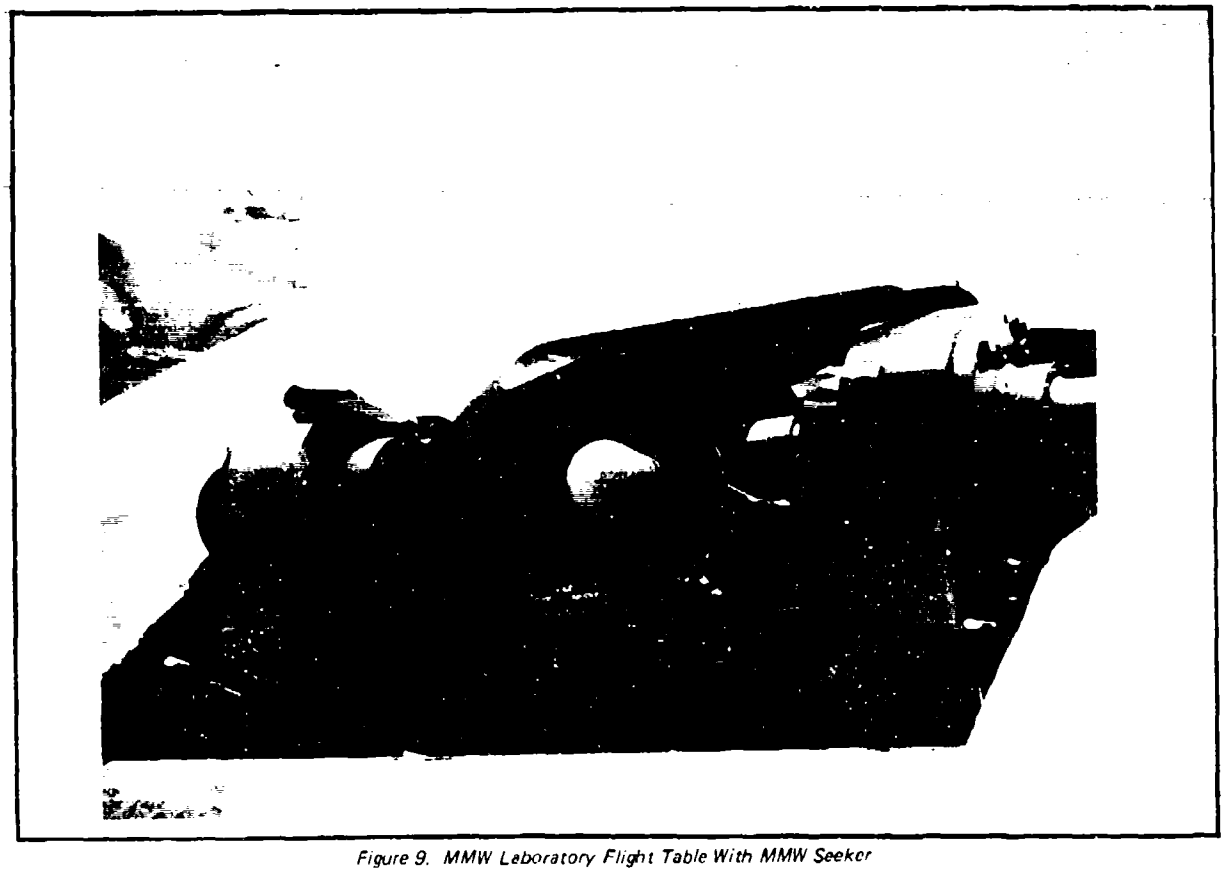

Figure 9. MMW Leboratory Flight Table With MMW Seeker

	IR	MMW
Chamber size	N/A	30 x 30 x 13 ft
Array or screen size	8-ft diameter with 15-ft radius of curvature	10 ft x 8 ft (curved)
Number of elements	N/A	1,280 (3-in centers) (40 x 30)
Resolution cell size	1 mrad	0.6 deg
Sensor-to-array distance	15 ft	22 ft
Array or screen size (angular)		
Horizontal	±15 deg	±12.8 deg
Elevation	±15 deg	±10.3 deg
Bandwidth or radiometric temperature range	5.4μ and 10.6μ wavelength	100K to 320K
Temperature control	±1°K	±1°K
Sky opening	N/A	10 x 10 ft
Flight table	3-axis	3-axis

Figure 10. Millimetre-Wave and IR Target Simulator Facilities (Capabilities and Constraints)

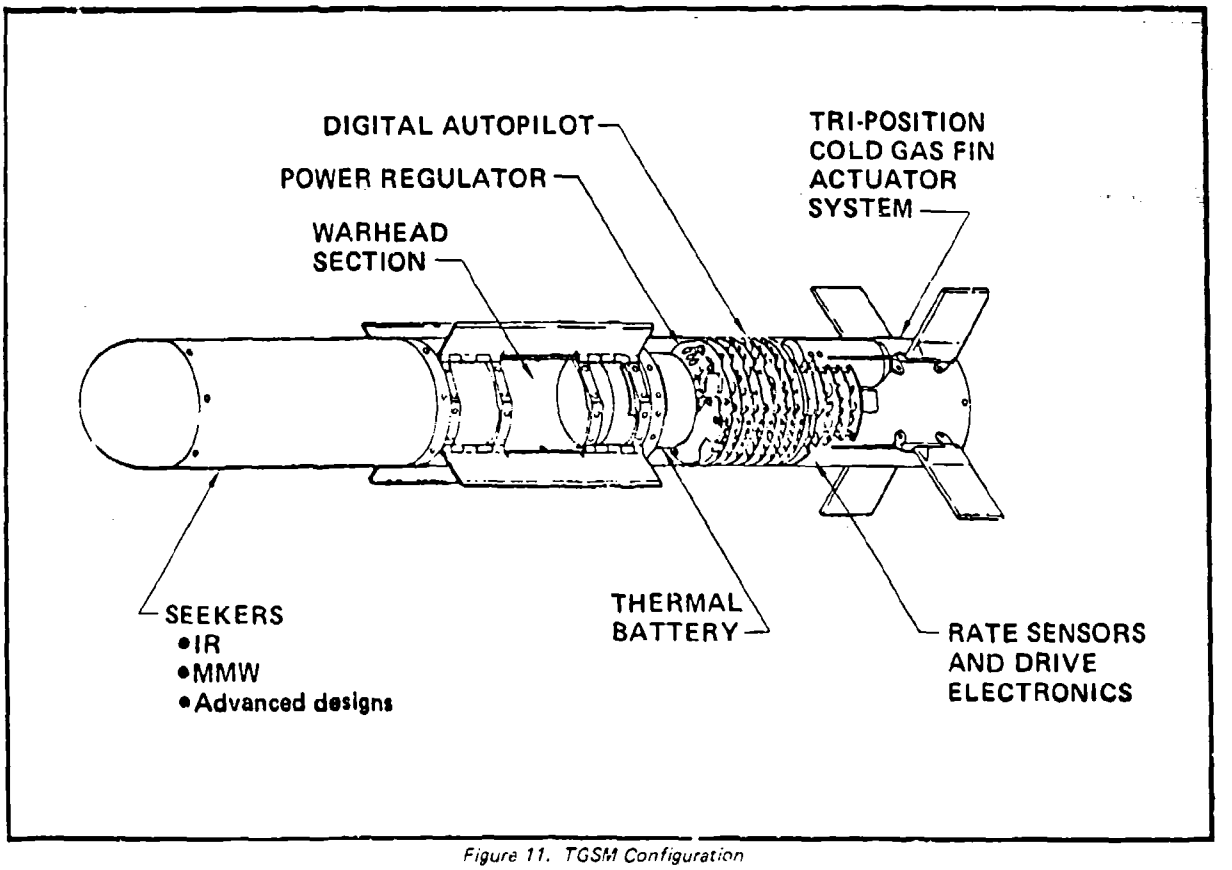

Figure 11. TGSM Configuration

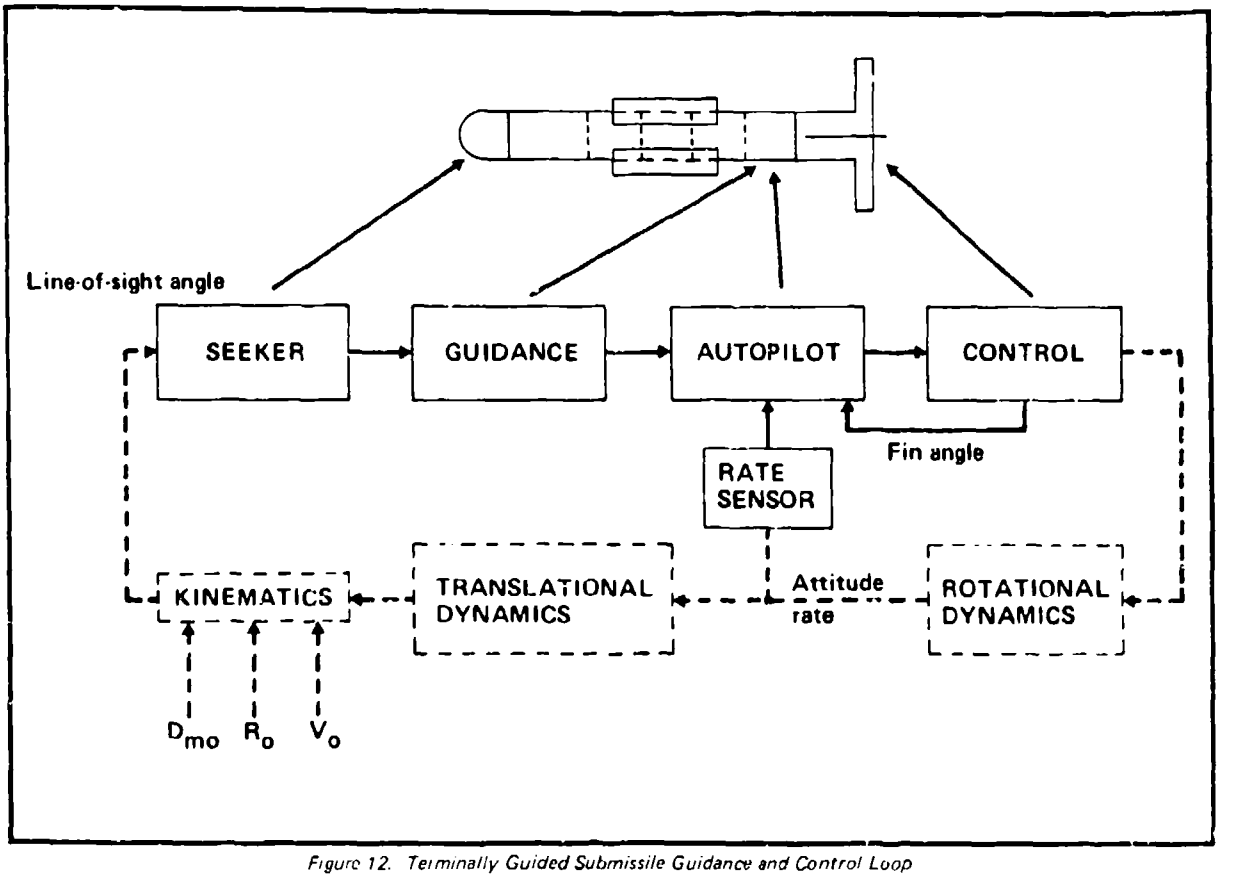

Figure 12. Terminally Guided Submissile Guidance and Control Loop

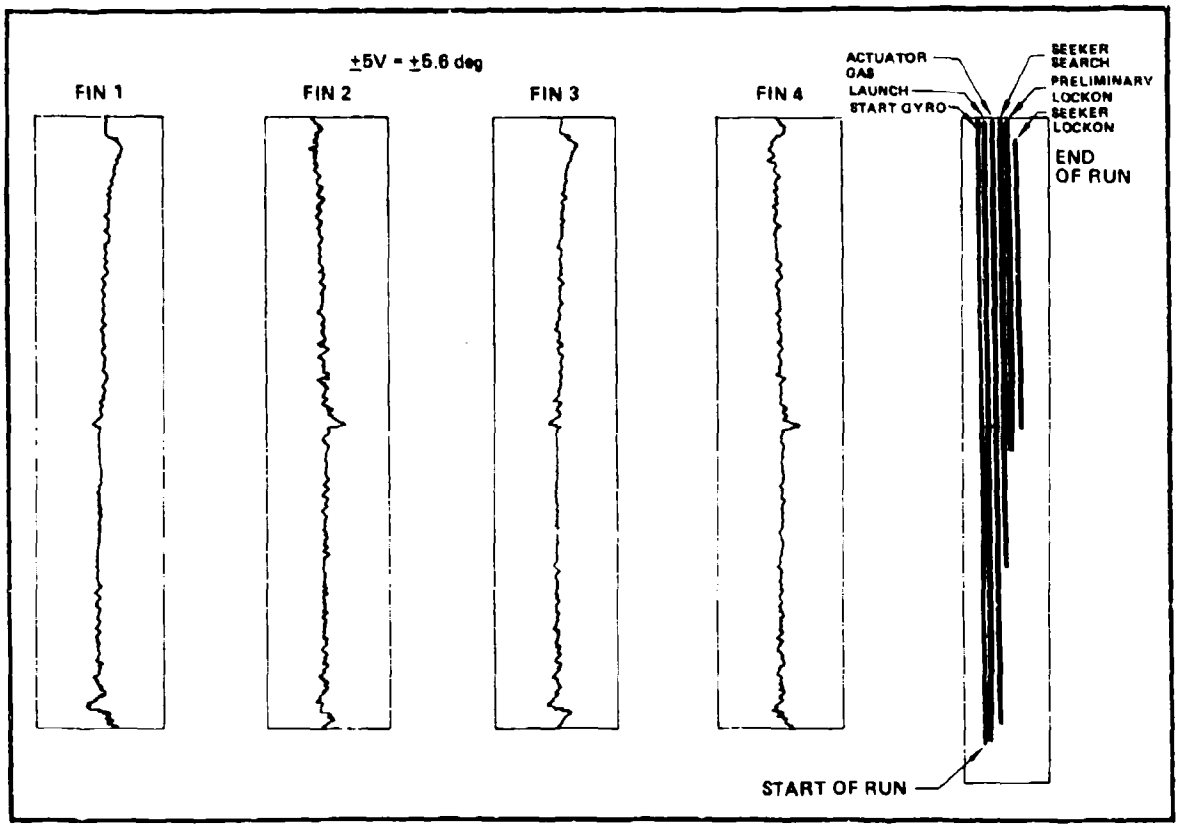

Figure 13. Hardware-in-the-Loop Test Data

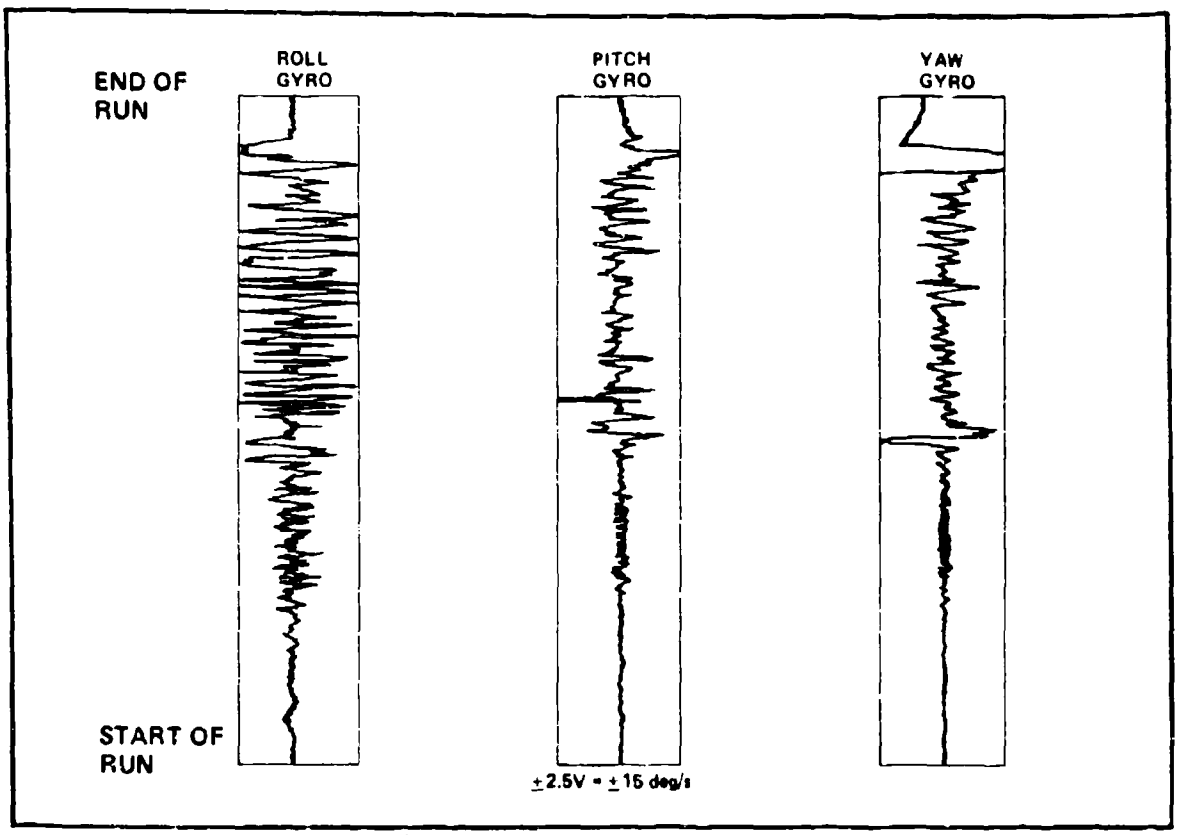

Figure 14. Hardware-in-the-Loop Test Data

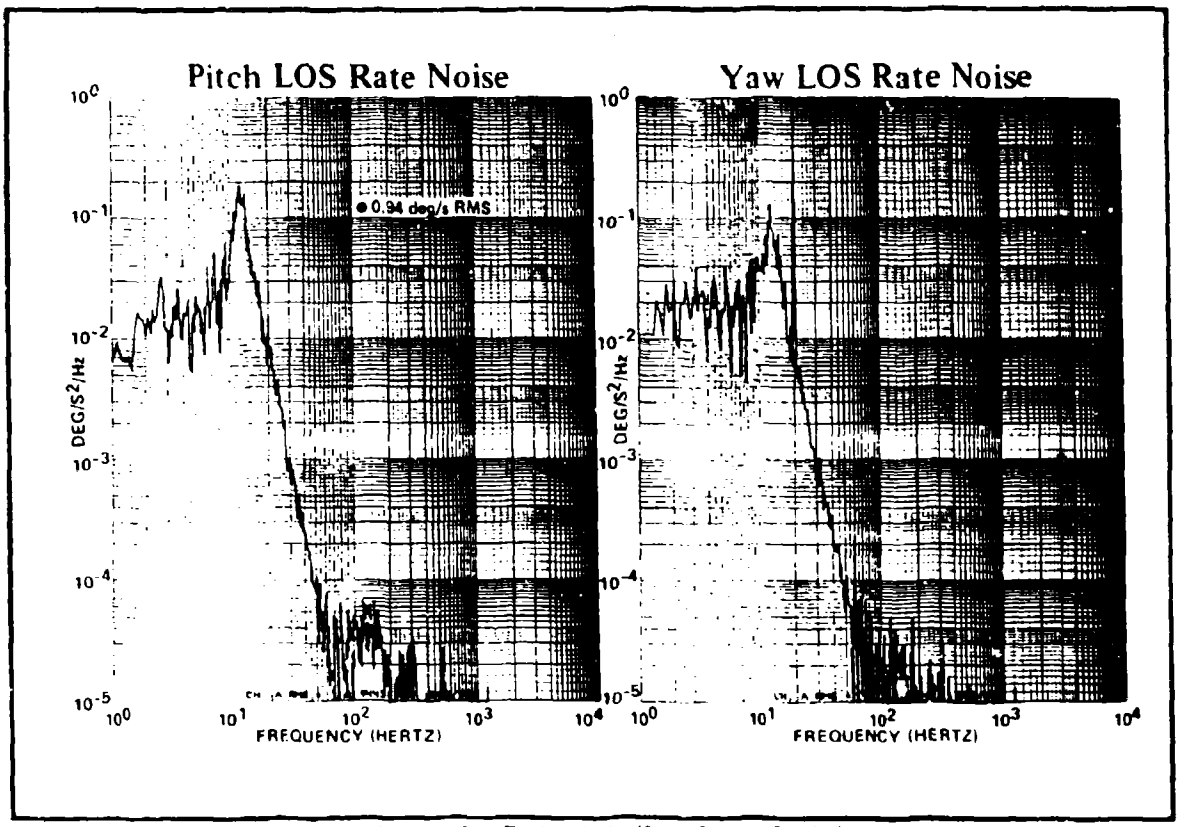

Figure 15. Angle Rate Tracking Noise (Power Spectral Density)

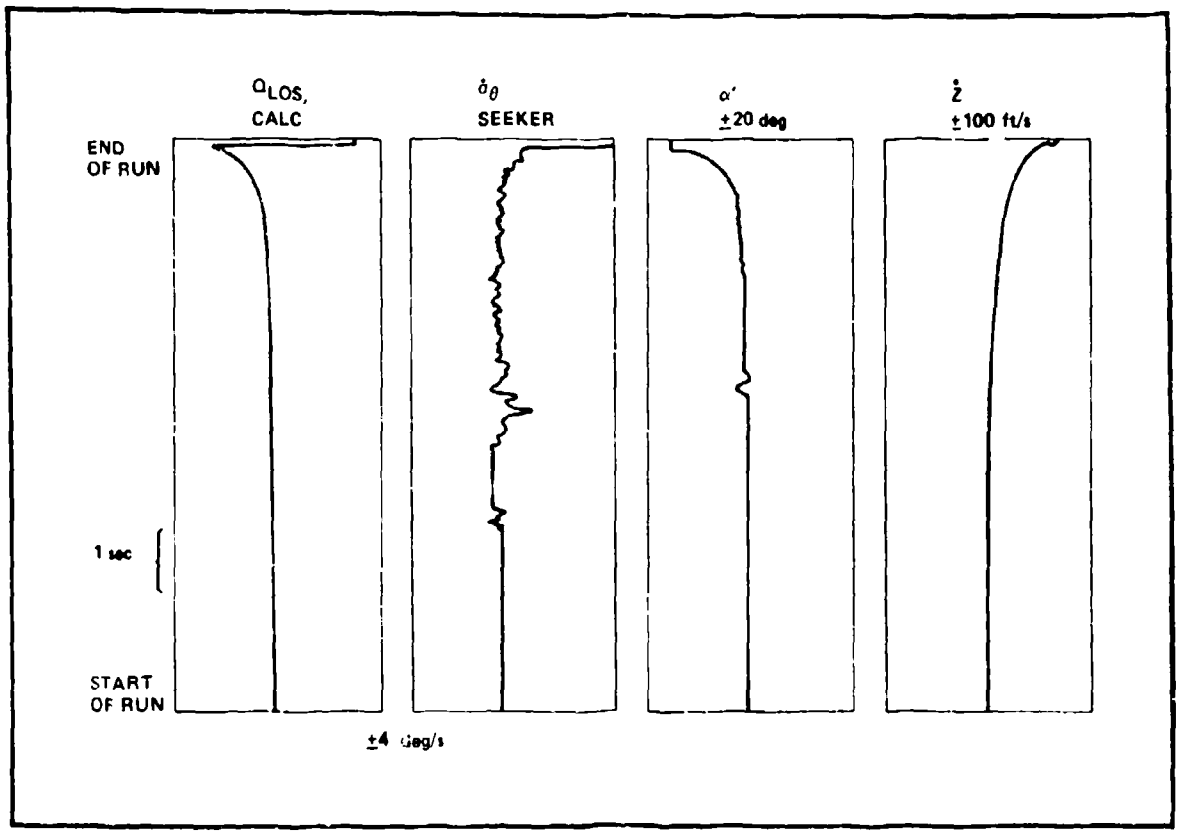

Figure 16. Hardware-in-the-Loop Test Data

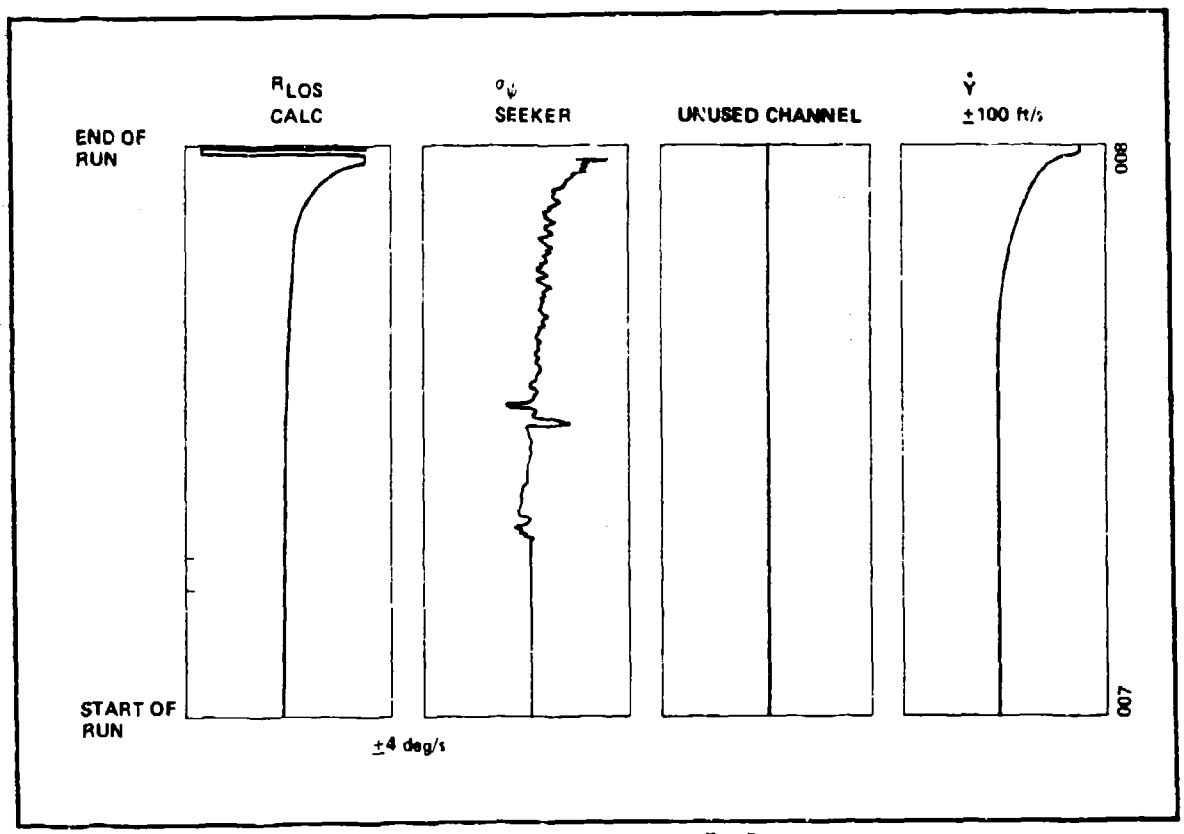

Figure 17. Hardware-in-the-Loop Test Data

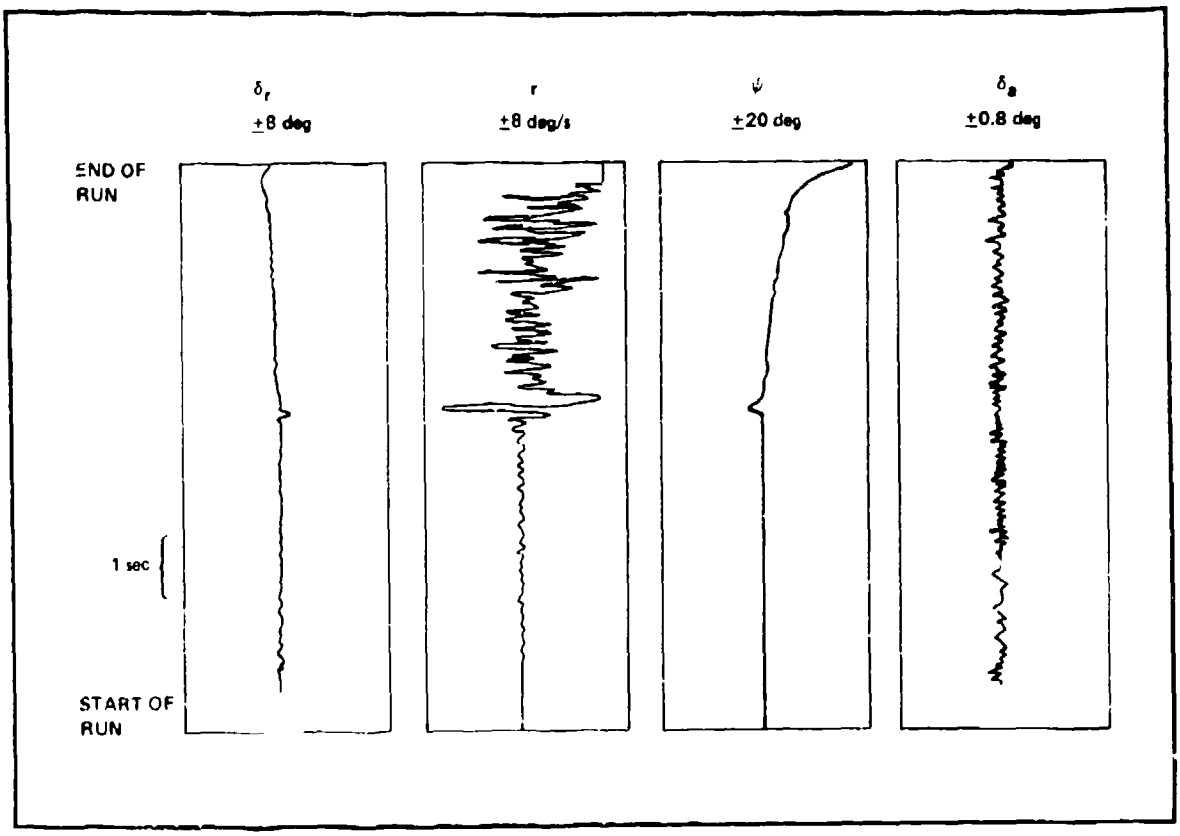

Figure 18. Hardware-in-the-Loop Test Data

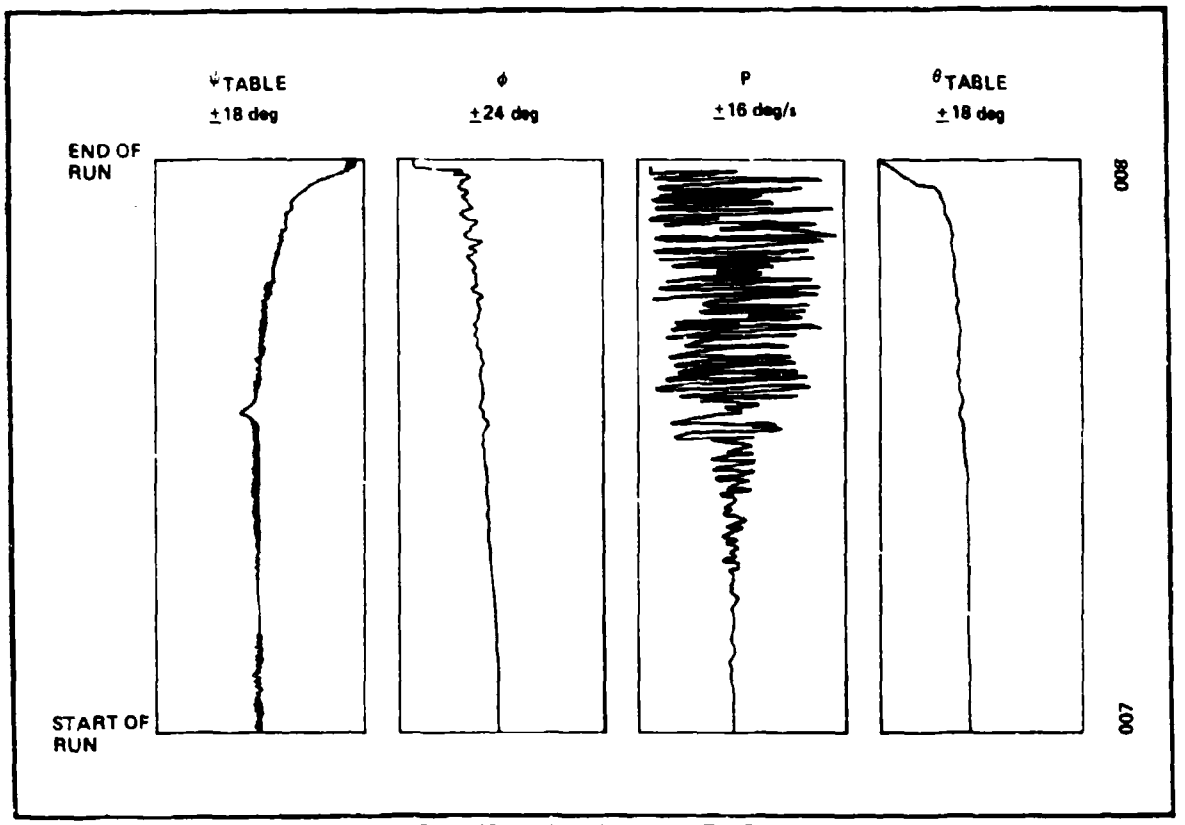

Figure 19. Hardware-in-the-Loop Test Data

CLUTTER MODEL VALIDATION FOR MILLIMETER WAVE (MMW) SEEKERS

by

R.Salemme
Air Force Armament Laboratory/DLMT
Eglin Air Force Base, Florida 32542
(904) 882-3344

and

D.Bowyer and R.Merritt
Systems Control, Inc.
P.O. Box 156
Shalimar, Florida 32579
(904) 862-5988

ABSTRACT

In the development of millimeter wave (MMW) seekers for tactical weapons applications, a high fidelity simulation of the seeker, the targets, and the clutter background can greatly facilitate hardware development and can help to predict results from seeker flight tests. In order to develop this high fidelity simulation, much information on the nature of the clutter background must be obtained to ensure a valid simulation. The purpose of this paper is to discuss the way in which the clutter background is being modeled in the MMW seeker simulation currently under development by Systems Control, Inc. (SCI) under contract to the Air Force Armament Laboratory (AFATL) and to discuss the clutter measurement data which are required in order to validate these clutter models.

In the clutter modeling process, an empirical approach is used in which deterministic map data are used to establish homogeneous terrain subareas. These subareas are then represented, statistically, with a spatial distribution for the median clutter backscatter from each cell and a temporal distribution for the scintillation around this median. In addition, a spatial correlation is applied to the median backscatter for adjacent cells. To validate these clutter models, the primary method is to use the statistics which are derived from measurement data over a variety of different terrain types to verify the statistics in the clutter model. An alternate method is to compare the actual seeker output from flight tests over a specific test site to the output of a simulation of this same test flight. The requirement for validated clutter models has led to the establishment of an extensive clutter measurements program by AFATL. The requirements for this measurements program have been established based on the clutter parameters which must be validated and projected flight configurations of tactical seekers which are currently under development.

1.0 INTRODUCTION

The Soviet military threat in Eastern Europe requires that NATO forces be prepared for armed conflict at any time of the day or night during all seasons of the year. The environmental conditions which exist for lengthy periods of time in that area of the world make it highly desireable that weapon systems possess adverse weather capabilities. Current radar guided weapons have the desired adverse weather characteristics, but do not have the accuracy required for tactical weapons. Laser and other optical guidance seekers have excellent resolution and accuracy, but exhibit poor adverse weather characteristics. During recent years improving resolution and accuracy for tactical weapons under adverse weather conditions have resulted in significant interest in the development of Millimeter-Wave (MMW) terminally guided seekers for use against armored targets. These very high radio frequency systems have potential for improved resolution with reduced size and weight relative to radar seekers presently in the operational inventory, while maintaining excellent adverse weather penetrability not found in optical systems.

To support the development of MMW, air-to-surface weapons, the Air Force Armament Laboratory (AFATL) has sponsored a program with Systems Control, Inc. of Palo Alto, Ca to develop a detailed detection simulation of MMW

seekers, targets, and background clutter. This simulation allows the weapon system designer the flexibility to investigate current and future MMW sensor and signal processing techniques without the expense of a hardware development and test program.

It is recognized, however, that any simulation is limited by the degree to which it can be validated with experimental or flight test data. The purpose of this paper is to describe the MMW seeker models, the data which is being used to validate these models, and the validation results which have been obtained to date. The primary data source for validation of target and background models is radar terrain signature measurements. AFATL is presently planning an extensive MMW signature measurement program to obtain the necessary data to complete the modeling activity. In general, the measurement community has been criticized for collecting data that is of little or no use to the user (modeling) community. To ensure that the required types, quantity, and quality of measurement data are collected to support the modeling task, modeling personnel have been integrated into the signature measurement programs. These personnel have provided inputs ranging from site selection to data calibration, as well as the data reduction and cataloging of signature measurements. The Signature Measurement program will be discussed in a later section.

The detection simulation under development is partitioned into three major models: Terrain, Seeker Data Stream, and Seeker Processing Models. The Terrain Model allows the construction of a seeker-independent clutter map consisting of terrain types of various shapes. The map is divided into resolution cells (pixels) corresponding to the highest resolution that any of the seekers to be evaluated can achieve. For each pixel, random clutter is generated from the distribution associated with the terrain type to which the pixel belongs. Targets and false targets can be strategically placed on the map. The Seeker Data Stream Model filters the terrain clutter map to achieve the seeker resolution of interest. The trajectory is specified and the missile and seeker are set into motion over the map. As the seeker sweeps back and forth over the terrain map, a simulated data stream is generated emulating the seeker detector output. The Seeker Processing Model filters and thresholds the detector output from the Seeker Data Stream Model in a manner consistent with the logic employed by the seeker being simulated. Whenever the processed data satisfies all the seeker target criteria a detection is declared. It then determines which detections are targets and which are false alarms and keeps track throughout the simulated flight.

2.0 CLUTTER MODEL DEVELOPMENT

In order to simulate the detection of hard targets (such as tanks) in a clutter background by a Millimeter-Wave (MMW) seeker, an accurate representation of that clutter background is required. The main thrust of this paper is a description of the approach which was taken in modeling the clutter[1], with a clear definition of the assumptions made, and a discussion of the work accomplished to validate these assumptions.

2.1 Terrain Modeling Approach

The techniques for representing clutter in a MMW seeker detection simulation can be divided into three basic approaches:

Deterministic clutter maps (real data)

Empirical clutter maps (real terrain features with statistical subareas)

Statistical clutter maps.

The deterministic clutter maps, since they are real data, provide the highest fidelity source of input to the MMW seeker detection simulation. Because these models are actual data they provide an excellent baseline to compare seeker system performance, or provide a validation tool for the more flexible statistical models. However, these maps impose the limitation that the seeker simulation must be run at the same parameters (such as depression angle, range, and flight path) as those for which the original clutter data were taken. This limits the amount of parametric performance studies which can be done.

The empirical clutter map is one in which real terrain edge features such as tree lines, small patches of woods, roads, etc., are modeled deterministically (real data), and the clutter within the major subareas is represented statistically. An example of an empirical clutter map is the hard target sitting in a grassy field next to a lake (Fig.1). The advantage to this type of model is that parametric simulation runs can easily be made, and the results can be validated with real data. An example of this is shown in Section 3.

The statistical clutter maps are the same as the empirical clutter maps except that the terrain subarea edge features are totally generated statistically. This technique has the advantage of being easier to produce on the computer, however, it cannot be validated against actual data from a specific terrain area. Also, simulation of seeker performance against specific terrain discontinuities such as tree lines (perpendicular or parallel to the flight path) or roads, is not feasible. The total statistical process results in purely random boundaries not representative of the actual features.

2.2 Clutter Statistics

In the MMW seeker detection simulation being developed, an empirical terrain clutter map is used as the input.

For this type of model, the assumption is made that each subarea can be generated independently, with the statistics representative of the type of terrain being modeled. Each subarea is assumed to be homogeneous; that is, the statistics within a subarea are the same for the entire subarea.

The clutter map is generated as an array of clutter resolution elements (pixels). The radar backscatter coefficient for each pixel in a subarea is assumed to be a random sample from a Rayleigh distribution, representing the temporal fluctuation (scintillation) of each clutter resolution cell. The mean backscatter coefficient for each pixel is, in turn, assumed to be a random sample from a log-normal distribution, representing the spatial fluctuation of the average clutter level within a given homogeneous area. In addition, it is assumed that the spatial clutter statistics are not independent from pixel to pixel, that is, the mean backscatter coefficient for adjacent pixels is correlated. This spatial correlation is assumed to have the form of a 1/f spatial power spectrum.

Based on these assumptions, which are obtained from early clutter signature measurements programs[2], the clutter map can be generated, on a subarea-by-subarea basis, as shown in Figure 2. Each of the filtered, Gaussian clutter samples, represented by the density function

$$P(X) = (1/\sqrt{2\pi}\sigma) \exp(X^2/2\sigma^2)$$

are then transformed by the expression

$$y = 10^{X/10}$$

to produce, log-normally distributed clutter which is characterized by the density function

$$P(y) = 10 \log(e)/(y\sqrt{2\pi}\sigma) \exp(-(10 \log(y) - \mu)^2/2\sigma^2).$$

This non-linear transformation causes some distortion of the 1/f spatial power spectrum, however, it has been shown[3], to a first approximation, that this distortion is negligible.

For each of the spatial clutter samples in the clutter map, a temporal fluctuation, or scintillation, must be introduced. For a narrow-band transmit waveform this fluctuation is characterized by a Rayleigh density function given by

$$P(X) = (X/\sigma^2) \exp(-X^2/2\sigma^2)$$

where σ is determined by the sample from the log-normal distribution discussed above.

For those seekers in which a wideband transmit waveform is processed non-coherently to reduce the amount of scintillation, the assumption is made that the temporal statistics are the average of a number of Rayleigh random variables. Using the central limit theorem, it can be shown that this statistic can be approximated with a Gaussian random variable with the appropriate mean backscatter coefficient and with the variance reduced by the number of degrees of freedom in the frequency averaging waveform.

3.0 CLUTTER MODEL VALIDATION

Although the assumptions described in Section 2, concerning the MMW clutter backscatter statistics, are based on previous measurements; only recently has any attempt been made to validate these assumptions using data at MMW frequencies[4]. Currently this validation is being performed using two different approaches. One of these is to directly estimate the appropriate statistics of clutter backscatter from MMW backscatter data taken by Lincoln Laboratory at 16 GHz in an earlier program[5]. The other validation approach is to compare the output of a seeker simulation, flown against a specific target area, to the output of an actual seeker from a captive flight test. The results of these two approaches are discussed in Sections 3.1 and 3.2, respectively.

3.1 Model Validation with 16 GHz Clutter Backscatter Data

The data described in this section of the paper were gathered over the Stockbridge test site near Rome, NY. This site was configured as shown in the map of Figure 3, with the wooded areas represented by the cross-hatched areas, and identifiable point targets represented with a number.

The data were gathered with a 16 GHz radar operated by Lincoln Laboratory. This is a pulsed radar with a range resolution (using pulse compression) of 8.85 M and a PRF of 4 KHz (typically). The total pulse-to-pulse agile bandwidth of the radar is 500 MHz covered in 32 steps. The antenna produces a fan beam which is electronically steered in azimuth, with a 0.33 degree azimuth beamwidth and a 26 degree elevation beamwidth.

The data are gathered by flying the radar at an altitude of 530 meters and rapidly sweeping the beam, in azimuth, across those areas to be mapped. The resulting video signal is then sampled every 10 meters in range and every

0.25 degree in azimuth to produce clutter maps in the format shown in Figure 4. This is a map of clutter reflectivity, γ, which is the clutter backscatter coefficient divided by the sine of the depression angle ($\sigma_0/\sin\phi$). The reflectivity values for these maps have been averaged over the 32 frequency samples, and the high RCS values are shown as the dark areas on the map. The depression angle for these scenes range from 21 degrees at the long ranges, to 50 degrees at the short ranges.

Amplitude statistics of the radar reflectivity, γ, have been computed for several different subsets of these clutter maps. At this time, only the spatial statistics have been estimated; that is, the reflectivity in dB from each pixel has been averaged over all 32 frequencies to obtain an estimate of the mean reflectivity for that cell. Then the cumulative distributions have been computed for these mean reflectivities. The cumulative density function for this average for different pixels is then plotted on Gaussian probability paper as a function of γ in dB. Examples of these distribution functions are shown in Figures 5 and 6, for woods and grass respectively. With the assumption that much of the clutter fluctuations due to independent frequency samples have been removed with the averaging process, these curves then represent the spatial clutter statistics. The reason for plotting the cumulative density function on Gaussian paper is to determine the qualitative goodness of fit to a log-normal distribution, represented by a straight line on these plots. The median γ (in dB), μ, and the standard deviation of the $\log\gamma$ values (in dB), σ, for these areas are shown on the curves.

From the plots of the cumulative density function, (Figures 5 and 6) it can be seen that most of the data appears to fit a log-normal distribution. For some of the data analyzed, the high end of the curve flattens out. It is unclear at this point why, but this effect might be attributed to a few large scatterers, or "point targets", within the supposedly homogeneous area which was chosen for analysis. Follow-on analysis using controlled terrain areas will be conducted to resolve this issue. Also, a reduction in the slope on the low end of some of the curves, as shown in Figure 6, is typical of sensor noise effects being the predominant factor; however, approximate calculations of expected signal-to-noise ratio (SNR) for this sensor indicates that it should not be noise limited for the values of backscatter coefficient shown on these curves. Fortunately, the low end of the curves is not of great interest to clutter modeling for target-in-clutter systems because it is only the largest clutter values that tend to be detected as false targets.

Work which remains to be done is to calculate a quantitative "goodness-of-fit" of the data to the log-normal distribution as well as others, such as the Weibull distribution. Also, the frequency scintillation statistics about the frequency mean can be estimated, by forming histograms for the 32 frequency samples for each pixel, and then averaging histograms over a number of pixels in a given homogeneous area.

In addition to computing the amplitude statistics of the clutter, the spatial correlation of the clutter was estimated by computing the spatial power spectrum of the reflectivity ( ). Frequency averaging was performed to remove as much scintillation as possible. Reflectivity, not log-reflectivity, was used in this analysis, and, for simplicity, the overall mean spatial reflectivity was subtracted from the mean reflectivity for each clutter cell before the spectrum was computed.

Examples of the spatial power spectrum for the wooded subarea whose statistics are shown in Figure 5 are shown in Figures 7 and 8. These are the azimuth and range "slices", respectively, from the two-dimensional spatial power spectrum of the clutter. Also shown on these curves are plots of the FT spectrum which was assumed for the clutter models described in Section 2. It can be seen that for the azimuth slice, this is a good assumption; while, for the range slice, it is not. For this reason, more work remains to be done in validating the clutter spatial correlation for MMW clutter backscatter. AFATL is planning an extensive clutter background measurement program which will be discussed in a later section. Analysis of the data collected during this program should allow the confirmation of these assumptions.

3.2 Model Validation with MMW Seeker Test Data

The second approach to clutter model validation which has been used on this program is to compare the simulated seeker output for a specific terrain area to the actual seeker output for a captive flight test over the same terrain area. The clutter and seeker parameters in the model were then varied, parametrically, until the simulated and real data matched.

One of the terrain areas chosen for this validation process was a specific site on Range B-70 at Eglin AFB, FL. This site is represented schematically in the map of Figure 1. These features are used to generate an empirical clutter map, and these clutter data are processed through a simulated seeker to obtain a processed output in a format which is the same as seeker flight test data. The outputs of the model and the seeker data are displayed in the form of three-dimensional clutter maps as shown in Figures 9 and 10, for the seeker and the model respectively. These plots represent a range-azimuth plot of the seeker (or model) output for a single scan of the antenna across the target area.

The plots of Figure 9 and 10 are representative of the end of the validation procedure, after it was determined that clutter backscatter coefficients of -15 dBsm/m^2 for grass and -30 dBsm/m^2 for the lake were required to match the outputs with a log standard deviation of 1.5 dB. These validation results are predicated on the assumption that the clutter density function for the various terrain types is known, so that the statistics are not validated in this process. The parameters which can be varied (and partially validated) are the median and log-standard deviation of the different types of clutter, and the spatial correlation functions. In addition, this validation procedure helps to separate the seeker dependent terms such as receiver noise and calibration uncertainties, from the clutter-dependent effects.

4.0 BACKGROUND/TARGET MEASUREMENT PROGRAM

To provide additional clutter background data necessary to complete the validation of the MMW terrain models, the AFATL is conducting an extensive airborne, MMW radar signature measurement program. The objective is to obtain high resolution, well calibrated MMW target and background signature measurement data which will support design and development of advanced MMW seekers and target acquisition algorithms; this will be accomplished, through the use of the measurement data, to ensure a thorough understanding of targets and clutter characteristics as they apply to the modeling and analysis task.

4.1 Measurement Data Requirements

The requirement is to collect enough data to allow characterization of clutter background returns. The major background types to be collected are:

- Forest
- Plowed fields
- Rocky fields
- Grass
- Smooth, terrain
- Rolling terrain
- Rugged Terrain
- Roadsides
- Embankments
- Tree lines
- Single and small groups of trees
- Natural false targets

The measurement program calls for the collection of 200 scenes in which homogeneous background areas of the required types can be found. Those kinds of false targets expected in operational scenarios, such as fences, railroad tracks, bridges, farm houses etc., will be included. In addition, measurement data will be collected to establish seasonal and weather effects.

4.2 Measurement Locations

The primary thrust of the MMW seeker development is an antiarmor, European battlefield scenario. Measurement locations were chosen to match European climate and topographical features. The program calls for MMW measurements at one site in the continental United States (CONUS) and two sites in Europe. During the European deployment both MMW and Infrared (IR) measurements will be collected concurrently.

The Northeastern United States has been identified to replicate climate and topography (plains, mountains, river systems, and vegetation, including soft and hardwood forests as well as pastoral and agricultural lands) found in Europe. Fort Drum, NY has been selected as the CONUS measurement site. It is located North of Watertown, NY in the Northeast region of the Continental United States. Fort Drum and the local area satisfy all the factors considered, except the spatial distribution of background types found in East/West European border areas. However, it is unlikely that any other CONUS site would be better in this regard.

Two measurement sites have been selected in Europe. One in the Northeast German plain and the other in the mid to Southeast region. Meppen near the Netherlands border has been selected as the Northern German plain site. Landsberg located approximately 50 km from Munich has been selected as the test site that is characteristic of the more hilly Southeastern region of Germany.

4.3 Measurement Parameters

The background/target signature measurements will be collected using two active (radar) sensors operating in the frequency regions of 35 and 94 GHz. These radar sensors will be installed in an airborne platform (DHC-7A Caribou). The aircraft will be flown at low speed along a race-track course. Both sensors will be pointed at some fixed depression angle out of the rear cargo door and simultaneous 35 GHz and 94 GHz measurements will be made. The pencil beam antenna will be scanned in azimuth to illuminate a swath on the ground which will be 100 meters wide. The scene is developed by bush-broom scanning, using the motion of the aircraft, to collect data along a 2500 - 7500 meter scene. Due to the 100 meter measurement scene width constraint, some data will be collected from adjacent swaths to provide data for mosaicing to form larger terrain maps. Sensor data and pointing information will be digitally recorded as the sensor scans the scene. In addition to the natural clutter, calibration corner reflectors, bench marks, and man-made targets of interest will be placed in the scene. A ground truth van will be located near the target area to collect meteorological data.

Measurement data will be collected at 12, 30 and 75 depression angles. Expected resolution area (3 dB, two-way) determined from radar beam footprint size (beam limited) for a constant slant range is given in Table 1.

Both radars sequentially transmit linear and circular polarization, and receive parallel and cross polarization. The polarization is switched fast enough so that for each pass all polarization information is available. The 35 GHz radar sensor has a total bandwidth of 512 MHz covered in 16 steps of 32 MHz each. In addition, the transmit waveform can be swept in frequency across the 512 MHz band. The 94 GHz sensor operates only in a wideband noise mode for either band limited (50 MHz) or wideband (240 MHz) operation. Both radar sensors operate primarily in a noncoherent mode; however, the 35 GHz system can also operate coherently to gather data applicable to MTI analysis.

TABLE 1

Sensor Resolution

94 GHz System

Depression Angle	*Resolution Area*
75	3.6 M^2
30	6.9 M^2
12	16.6 M^2

35 GHz System

Depression Angle	*Resolution Area*
75	18.5 M^2
30	35.7 M^2
12	28.1 M^2 (4 M range gating)

4.4 Data Reduction

Raw data collected in the field will be processed to reduced form and put in a computerized data base at Eglin AFB for use by Governmental and DoD contractor personnel. Reduced data is defined as scaled, calibrated data which outside developers can use with high confidence and minimum data explanation.

In order to ensure the quality of the data, a fairly extensive set of data checks and calibration procedures have been established. During the data collection flights and immediately after each flight (post-flight), quick-look data analysis will be accomplished. Data monitoring equipment will be employed on the aircraft for real time monitoring of the digitally recorded header records, system noise measurements, apparent signal-to-noise ratio, and the quality of the measurment data.

The radar calibration approach calls for both sensor and in-scene calibration. Each channel (amplitude and phase, for each polarization) will be calibrated prior to and after each mission. This will be accomplished by recording an internal reference signal and returns from calibrated reference corner reflectors placed in a special array on the flight line. In addition to the sensor calibration, additional aids will be provided in the scene for data calibration. To serve this purpose an array of calibration corner reflectors will be placed just before and/or after the data collection ground scene. This array includes 29 reflectors with five different RCS values. It is expected that processing of the in-scene reference array data, combined with the pre- and post-flight calibration, will result in absolute measurement data accuracy of better than ± 3 dB.

Due to aircraft motion, the spatial distribution of the data is skewed. Using inertial information from the on-board inertial navigation system, and in-scene optical bench mark data, the digital background measurement data will be corrected.

All of the clutter data will be analyzed before it is cataloged to produce, in addition to clutter maps, the mean and variance of the spatial and temporal clutter distributions, and the spatial correlation function. These parameters will be computed for each identifiable, homogeneous subarea in the clutter array. There will be a data set generated for each frequency, depression angle, polarization, and scene type. These analyzed data will be entered into the data base.

4.5 Measurements Data Base

To organize and make available to the user community the MMW target and background signature measurement data, AFATL is developing a computerized data base. Currently the data base exists for infrared (IR) data and is currently being expanded to include MMW data. The Target and Background Information Library System (TABILS) is a computerized directory allowing other Services, DoD Agencies and contractor personnel requiring MMW or IR measurement data access to the AFATL data base. The TABILS directory system allows easy identification of specific unique data by the user. Measurement data can be identified by target or background type, frequency, polarization, data bandwidth, seasonal or meteorological characteristics. This directory is accessible through remote computer terminal to the Eglin AFB Math Laboratory. After required data have been identified through TABILS, users request the desired data. A digital tape will then be generated and sent to the requester.

5.0 SUMMARY

The Air Force Armament Laboratory has sponsored the development of MMW seeker, target and terrain models. These analytical tools are being used to evaluate current and future seeker system designs for the purpose of advancing MMW technology in the area of antiarmor applications. The key to flexible, realistic simulations are accurate statistical clutter backscatter models. Based on qualitative work accomplished to date, it appears that the spatial cumulative density

function fits a log-normal distribution. The spatial correlation function has a 1/f spectrum for an azimuth slice of the data, but qualitatively this does not appear to be a good assumption for a corresponding range slice. The data which will be available over the next year from the terrain background signature measurements program will greatly facilitate the development of realistic terrain models.

REFERENCE

1. Smith, F.W. Pearce, H.M. — *Millimeter Wave Target/Background Modeling*, Eighth DARPA/Tri-Service Millimeter Wave Conference, 3--5 April 1979.

2. Currie, et al. — *Radar Millimeter Backscatter Measurement, Vol.I. Snow and Vegetation*, AFATL-TR-77-92, Georgia Institute of Technology, July, 1977.

3. — *Millimeter Wave Modeling and Analysis, Interim Report*, Systems Control, Inc., January, 1980.

4. Vote, F.W. — *Tactical Target/Clutter Signature Studies at Ku/Ka Bands*, Eighth DARPA/Tri-Service Millimeter Wave Conference, 3--5 April, 1979.

5. Stovall, R.E. — *Ku-Band Ground Clutter Data*, MIT/LL Report, November, 1978.

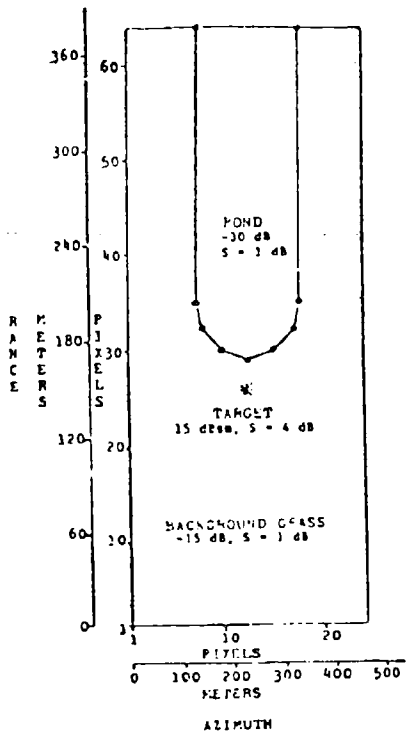

Fig.1 Clutter map features

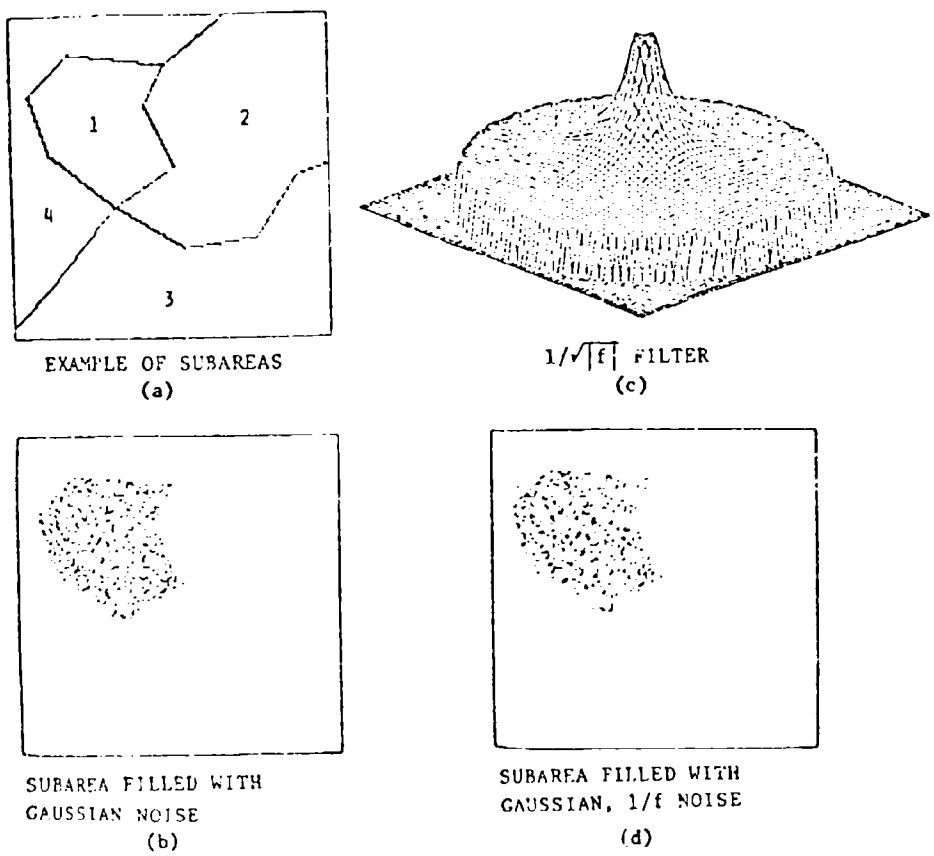

Fig.2 Empirical clutter map generation

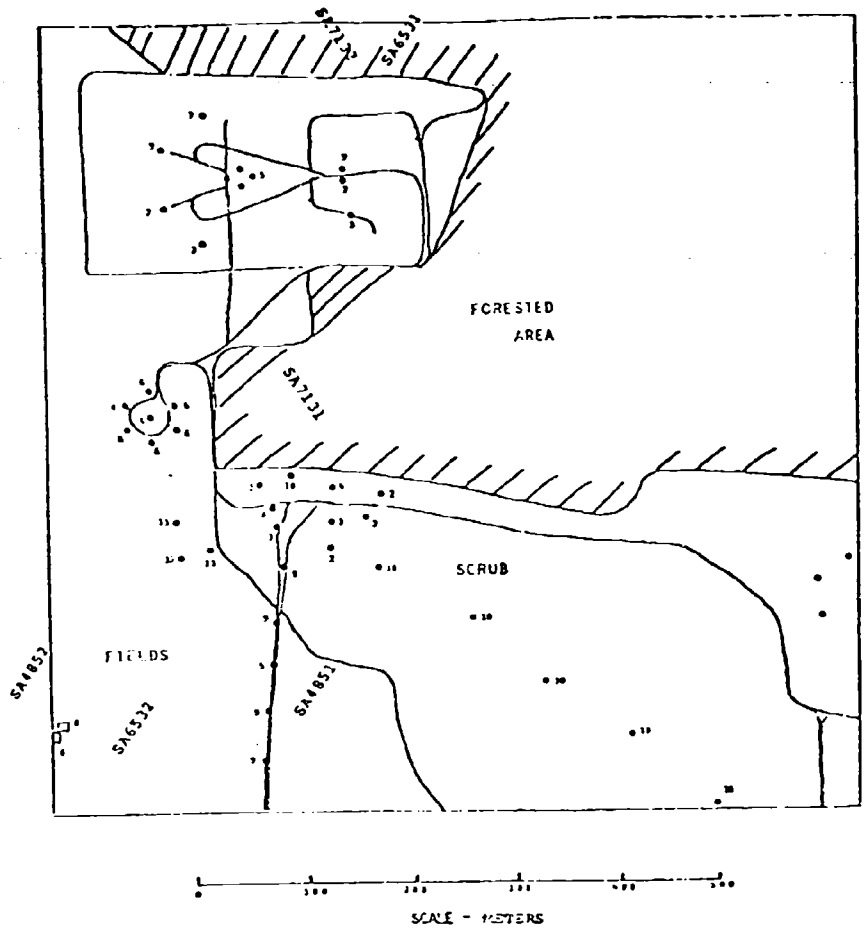

Fig.3 Stockbridge target array

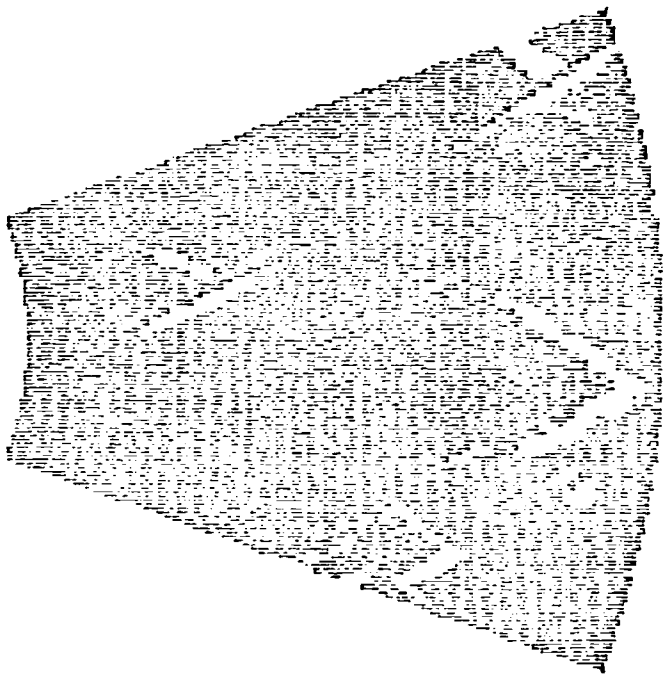

Fig.4 Clutter map for one snapshot of the stockbridge array

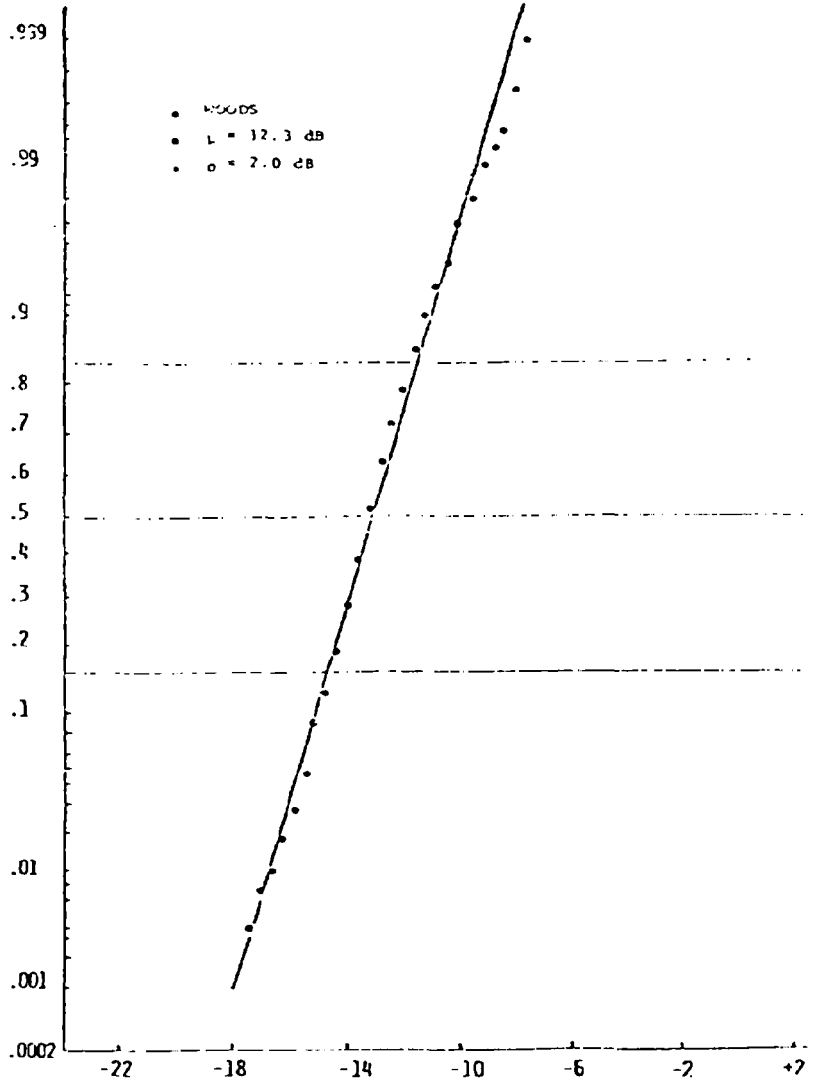

Fig.5 Cumulative distribution for wooded subarea

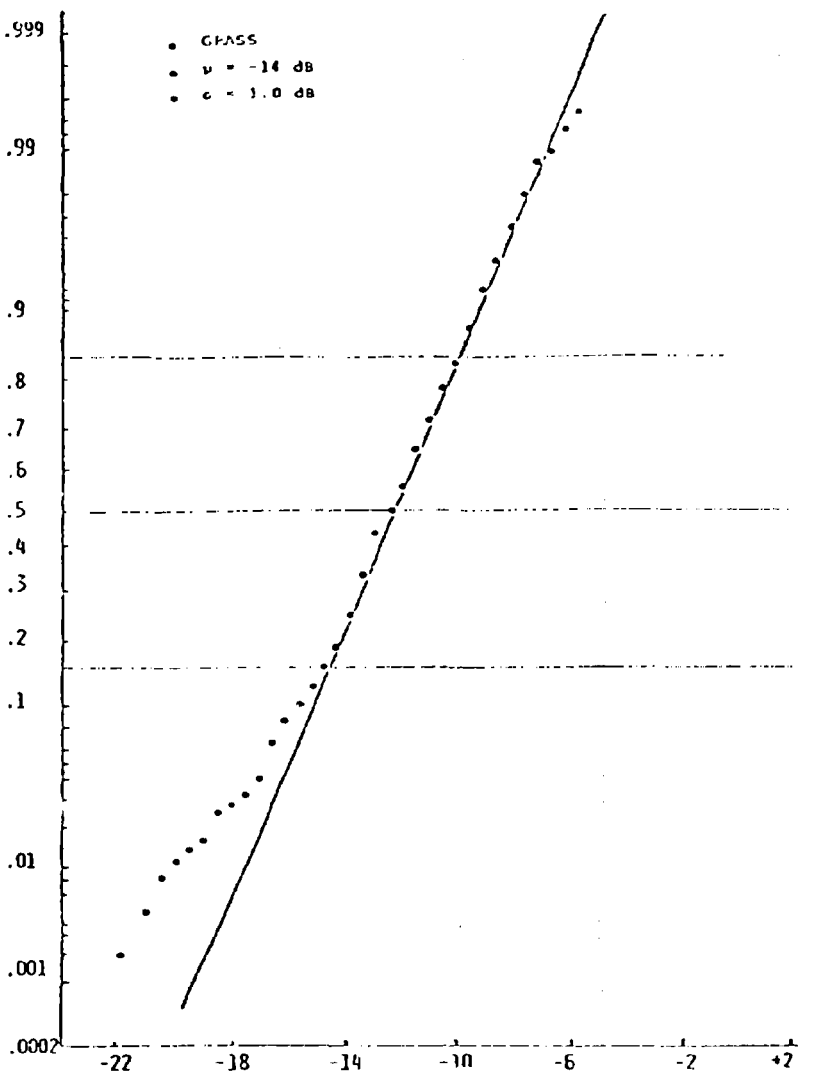

Fig.6 Cumulative distribution for grassy subarea

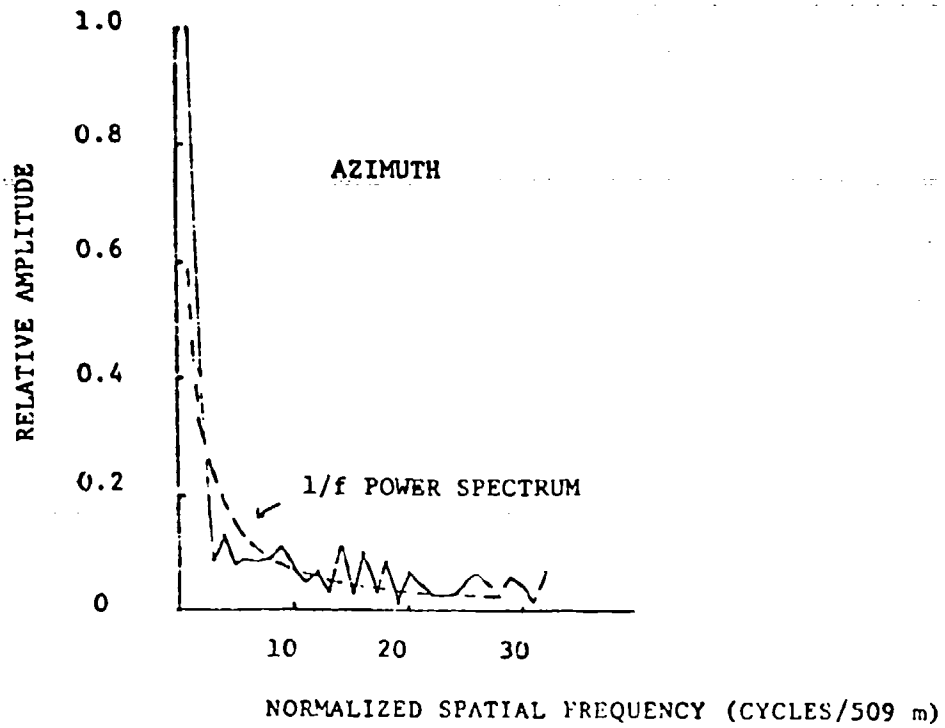

Fig.7 Spatial power spectrum for wooded subarea (azimuth dimension)

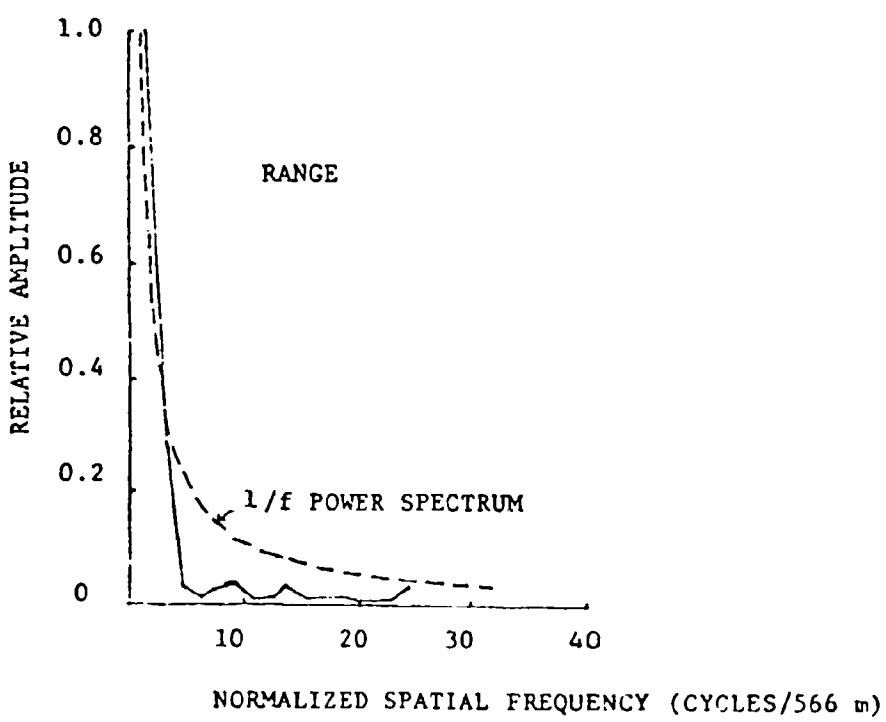

Fig.8 Spatial power spectrum for wooded subarea (range dimension)

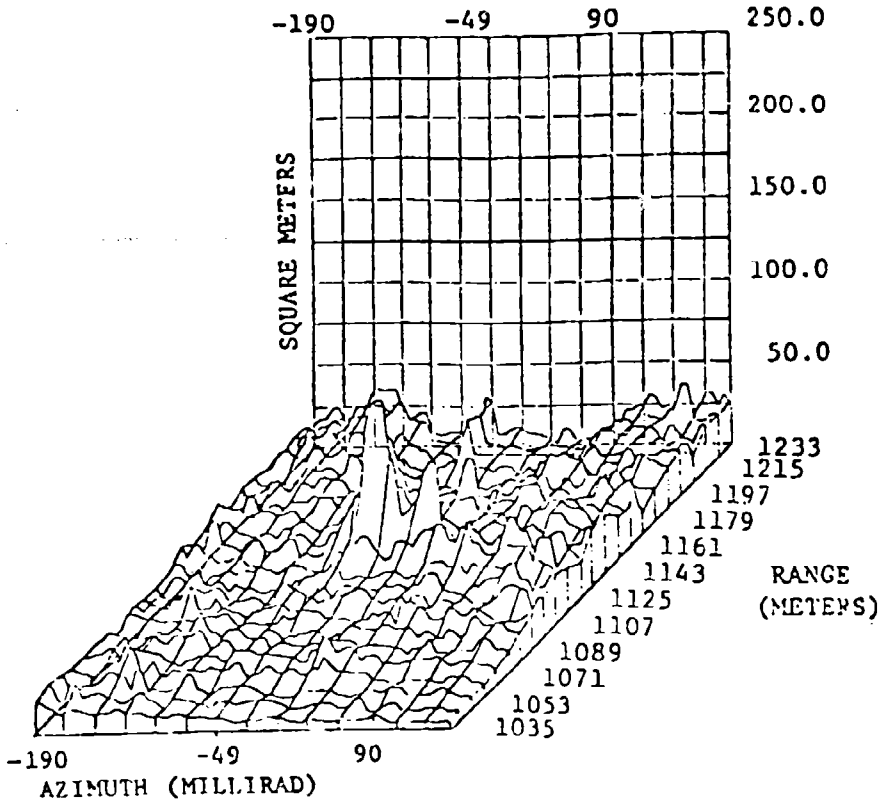

Fig.9 Seeker clutter map output

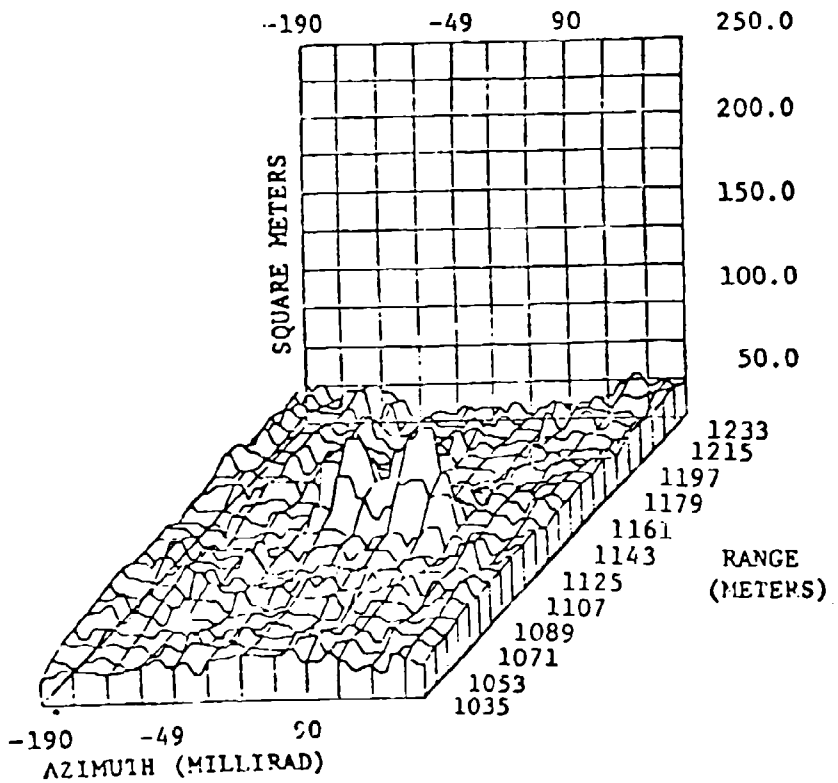

Fig.10 Simulated seeker clutter map output

REPORT DOCUMENTATION PAGE

1. Recipient's Reference	2. Originator's Reference	3. Further Reference	4. Security Classification of Document
	AGARD-CP-292	ISBN 92-835-1370-3	UNCLASSIFIED

5. Originator Advisory Group for Aerospace Research and Development
North Atlantic Treaty Organization
7 rue Ancelle, 92200 Neuilly sur Seine, France

6. Title

GUIDANCE AND CONTROL ASPECTS OF TACTICAL AIR-LAUNCHED MISSILES

7. Presented at the Guidance and Control Panel Symposium held at Eglin Air Force Base, Florida, USA - 6/9 May 1980.

8. Author(s)/Editor(s)	9. Date
Various	October 1980
10. Author's/Editor's Address	**11. Pages**
Various	154

12. Distribution Statement This document is distributed in accordance with AGARD policies and regulations, which are outlined on the Outside Back Covers of all AGARD publications.

13. Keywords/Descriptors

Seekers
Guidance
Control
Human factors
Testing

14. Abstract

The proceedings include papers presented at a symposium of the Guidance and Control Panel held at Eglin Air Force Base, Florida, USA -- 6/9 May 1980.

Twenty six papers were presented on the following topics:

- Operational requirements
- System considerations
- Air-to-surface guided weapons technology
- Air-to-air guided weapons technology
- Tactical guided weapons evaluation techniques.

AGARD Conference Proceedings No.292
Advisory Group for Aerospace Research and Development, NATO
GUIDANCE AND CONTROL ASPECTS OF TACTICAL AIR-LAUNCHED MISSILES
Published October 1980
154 pages

The proceedings include papers presented at a symposium of the Guidance and Control Panel held at Eglin Air Force Base, Florida, USA - 6/9 May 1980.

Twenty six papers were presented on the following topics:

- Operational requirements
- System considerations
- Air-to-surface guided weapons technology
- Air-to-air guided weapons technology
- Tactical guided weapons evaluation techniques.

ISBN 92-835-1370-3

AGARD Conference Proceedings No.292
Advisory Group for Aerospace Research and Development, NATO
GUIDANCE AND CONTROL ASPECTS OF TACTICAL AIR-LAUNCHED MISSILES
Published October 1980
154 pages

The proceedings include papers presented at a symposium of the Guidance and Control Panel held at Eglin Air Force Base, Florida, USA - 6/9 May 1980.

Twenty six papers were presented on the following topics:

- Operational requirements
- System considerations
- Air-to-surface guided weapons technology
- Air-to-air guided weapons technology
- Tactical guided weapons evaluation techniques.

ISBN 92-835-1370-3

AGARD-CP-292

Seekers
Guidance
Control
Human factors
Testing

AGARD Conference Proceedings No.292
Advisory Group for Aerospace Research and Development, NATO
GUIDANCE AND CONTROL ASPECTS OF TACTICAL AIR-LAUNCHED MISSILES
Published October 1980
154 pages

The proceedings include papers presented at a symposium of the Guidance and Control Panel held at Eglin Air Force Base, Florida, USA - 6/9 May 1980.

Twenty six papers were presented on the following topics:

- Operational requirements
- System considerations
- Air-to-surface guided weapons technology
- Air-to-air guided weapons technology
- Tactical guided weapons evaluation techniques.

ISBN 92-835-1370-3

AGARD-CP-292

Seekers
Guidance
Control
Human factors
Testing

AGARD

NATO OTAN

7 RUE ANCELLE · 92200 NEUILLY-SUR-SEINE

FRANCE

Telephone 745.08.10 · Telex 610176

DISTRIBUTION OF UNCLASSIFIED AGARD PUBLICATIONS

AGARD does NOT hold stocks of AGARD publications at the above address for general distribution. Initial distribution of AGARD publications is made to AGARD Member Nations through the following National Distribution Centres. Further copies are sometimes available from these Centres, but if not may be purchased in Microfiche or Photocopy form from the Purchase Agencies listed below.

NATIONAL DISTRIBUTION CENTRES

BELGIUM
Coordonnateur AGARD – VSL
Etat-Major de la Force Aérienne
Quartier Reine Elisabeth
Rue d'Evere, 1140 Bruxelles

CANADA
Defence Science Information Services
Department of National Defence
Ottawa, Ontario K1A 0K2

DENMARK
Danish Defence Research Board
Østerbrogades Kaserne
Copenhagen Ø

FRANCE
O.N.E.R.A. (Direction)
29 Avenue de la Division Leclerc
92320 Châtillon sous Bagneux

GERMANY
Fachinformationszentrum Energie
Physik, Mathematik GmbH
Kernforschungszentrum
D-7514 Eggenstein-Leopoldshafen 2

GREECE
Hellenic Air Force General Staff
Research and Development Directorate
Holargos, Athens

ICELAND
Director of Aviation
c/o Flugrad
Reykjavik

ITALY
Aeronautica Militare
Ufficio del Delegato Nazionale all'AGARD
3 Piazzale Adenauer
Roma/EUR

LUXEMBOURG
See Belgium

NETHERLANDS
Netherlands Delegation to AGARD
National Aerospace Laboratory, NLR
P.O. Box 126
2600 A.C. Delft

NORWAY
Norwegian Defence Research Establishment
Main Library
P.O. Box 25
N-2007 Kjeller

PORTUGAL
Direcção do Serviço de Material
da Força Aérea
Rua da Escola Politécnica 42
Lisboa
Attn: AGARD National Delegate

TURKEY
Department of Research and Development (ARGE)
Ministry of National Defence, Ankara

UNITED KINGDOM
Defence Research Information Centre
Station Square House
St. Mary Cray
Orpington, Kent BR5 3RE

UNITED STATES
National Aeronautics and Space Administration (NASA)
Langley Field, Virginia 23365
Attn: Report Distribution and Storage Unit

THE UNITED STATES NATIONAL DISTRIBUTION CENTRE (NASA) DOES NOT HOLD STOCKS OF AGARD PUBLICATIONS, AND APPLICATIONS FOR COPIES SHOULD BE MADE DIRECT TO THE NATIONAL TECHNICAL INFORMATION SERVICE (NTIS) AT THE ADDRESS BELOW.

PURCHASE AGENCIES

Microfiche or Photocopy

National Technical
Information Service (NTIS)
5285 Port Royal Road
Springfield
Virginia 22161, USA

Microfiche

Space Documentation Service
European Space Agency
10, rue Mario Nikis
75015 Paris, France

Microfiche

Technology Reports
Centre (DTI)
Station Square House
St. Mary Cray
Orpington, Kent BR5 3RF
England

Requests for microfiche or photocopies of AGARD documents should include the AGARD serial number, title, author or editor, and publication date. Requests to NTIS should include the NASA accession report number. Full bibliographical references and abstracts of AGARD publications are given in the following journals

Scientific and Technical Aerospace Reports (STAR)
published by NASA Scientific and Technical
Information Facility
Post Office Box 8757
Baltimore/Washington International Airport
Maryland 21240, USA

Government Reports Announcements (GRA)
published by the National Technical
Information Services, Springfield
Virginia 22161, USA

Printed by Technical Editing and Reproduction Ltd
Harford House, 7–9 Charlotte St, London W1P 1HD

ISBN 92-835-1370-3